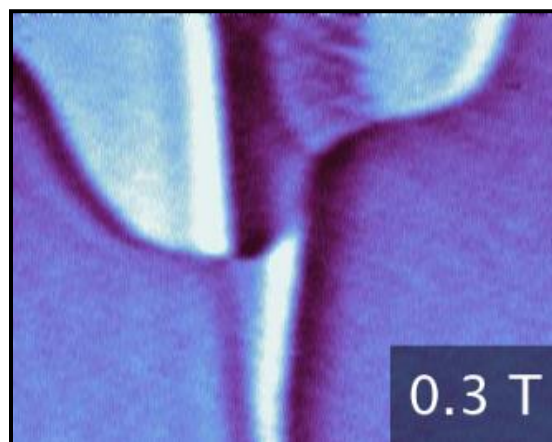
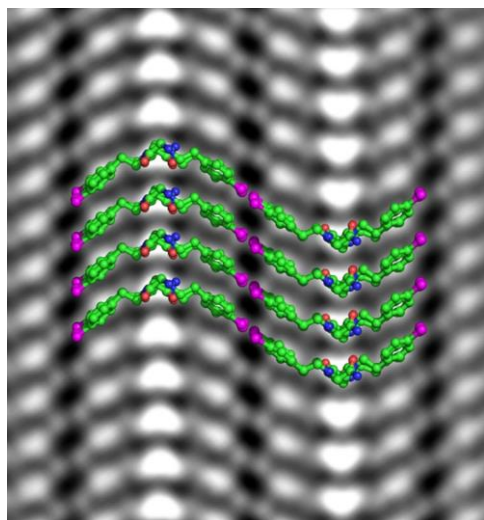
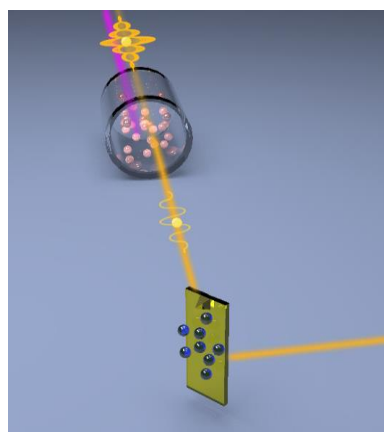
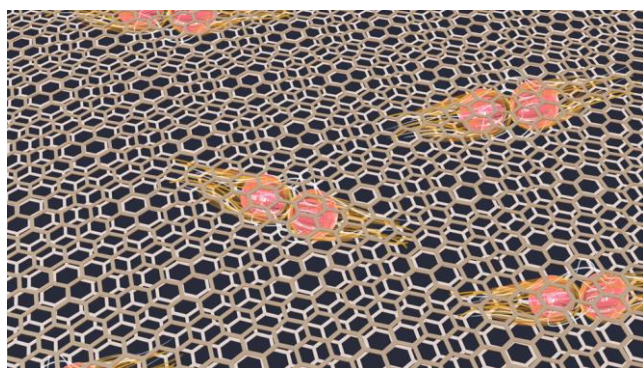


Electron and Scanning Probe Microscopies

2020 Principal Investigators' Meeting



Zoom Virtual Meeting, Anywhere USA
October 20-21, 2020



U.S. DEPARTMENT OF
ENERGY

Office of
Science

Office of Basic Energy Sciences
Materials Sciences and Engineering Division

On the Cover

- Top Left: *Superconductivity in a Stack of Two Twisted Atomic Sheets of Carbon.* Twisting two graphene sheets at a magic angle forms a moiré pattern. Superconductivity emerges in this lattice for a range of electron concentrations. Researchers have used a scanning tunneling microscope to visualize electrons with high spatial resolution in this material and to show that entanglement of electrons caused by their interaction is at heart of its novel properties. Work published in *Nature* **572**, 101 (2019).
Courtesy: Ali Yazdani, Princeton University
- Top Right: *Quantum Microscopies with Squeezed Light.* Researchers have recently provided a proof-of-principle demonstration of quantum-enhanced readout of the displacement of an atomic force microscope microcantilever with a squeezed optical readout field. Work published in *Phys. Rev. Lett.* **124**, 230504 (2020).
Courtesy: Ben Lawrie, Oak Ridge National Laboratory
- Bottom Left: *First Real Space Images of Atoms in a Synthetic Polymer.* Individual bromine atoms in a synthetic polypeptoid crystal were directly imaged using cryogenic transmission electron microscopy. Work published in *Proc. Natl. Acad. Sci.* **116**, 22491 (2019).
Courtesy: Nitash Balsara, Lawrence Berkeley National Laboratory
- Bottom Right: *Robust A-type Order and Spin-Flop Transition on the Surface of Antiferromagnetic Topological Insulator.* Cryogenic magnetic force microscopy image was taken at 0.3 T magnetic field perpendicular to the sample surface. Research results provide key ingredients for understanding the electronic properties of the antiferromagnetic topological insulator MnBi_2Te_4 . Work published in *Phys. Rev. Lett.* **125**, 037201 (2020).
Courtesy: Weida Wu, Rutgers University

This document was produced under contract number DE-SC0014664 between the U.S. Department of Energy and Oak Ridge Associated Universities.

The research grants and contracts described in this document are supported by the U.S. DOE Office of Science, Office of Basic Energy Sciences, Materials Sciences and Engineering Division.

Foreword

This volume comprises the scientific content of the 2020 Electron and Scanning Probe Microscopies Principal Investigators' (PIs) Meeting sponsored by the Materials Sciences and Engineering Division (MSED) in the Office of Basic Energy Sciences (BES) of the U. S. Department of Energy (DOE). The meeting, held on October 20–21, 2020, is the 8th biennial meeting in the Electron and Scanning Probe Microscopies area organized by BES. This year the meeting format is virtual due to the challenging situation facing all of us this year. The purpose of the meeting is to bring together researchers funded in this core research area, to facilitate the exchange of new results and research highlights, to foster new ideas and collaborations among the participants, and to discuss how to advance electron and scanning probe microscopy, spectroscopy, and associated theoretical tools, in order to address forefront scientific challenges. The meeting also affords BES program managers an opportunity to assess the state of the entire program collectively on a periodic basis, to chart future directions and to identify new programmatic needs.

The Electron and Scanning Probe Microscopies Core Research Activity supports basic research that addresses grand science challenges using advanced electron and scanning probe microscopy and spectroscopy techniques to understand the atomic, electronic, and magnetic structures and properties of materials. This activity also supports the development of new methods and techniques to advance basic science and materials characterizations for energy applications. Topical areas highlighted in this year's meeting include: ultrafast diffraction and real-time microscopy, quantum materials, quantum information science and advanced imaging, in-situ microscopy of energy materials, data science and theory, and new microscopy and spectroscopy methods. This year we are utilizing discussion panels in this virtual format to give PIs the opportunity to confer the status of the field, and to identify challenges, opportunities, and future directions for the microscopy community.

I thank all of the meeting attendees for their active participation and for sharing their ideas and new research results. Special thanks go to all session moderators. I am grateful to my BES colleagues, Helen Kerch, Mick Pechan, Athena Sefat, Michael Sennett, and Lane Wilson, for participating in the meeting and co-moderating the relevant sessions. My sincere thanks also go to Teresa Crockett in MSED and Linda Severs and Tia Moua at the Oak Ridge Institute for Science and Education for their excellent work providing all the logistical support for the meeting.

Jane G. Zhu
Program Manager, Electron and Scanning Probe Microscopies
Division of Materials Sciences and Engineering, Basic Energy Sciences
Office of Science
U. S. Department of Energy

Table of Contents

Agenda	ix
 Laboratory Projects	
<i>The Discovery of New Properties in Layered Ferroelectrics through the Synergistic Combination of Scanning Probe Microscopy and Theory</i> Nina Balke, Petro Maksymovych, Rama Vasudevan, and Albina Borisevich	3
<i>Atomic Resolution Electron Microscopy of Soft Matter</i> Nitash Balsara, Xi Jiang, Andrew Minor, Ronald Zuckermann, and David Prendergast	8
<i>Developing Cryogenic Electron Microscopy for Energy Storage Materials</i> Yi Cui, Wah Chiu, Jen Dionne, and Paul McIntyre	13
<i>Spin Physics and Nanoscale Probes of Quantum Materials</i> David Goldhaber-Gordon, Marc Kastner, Hari C. Manoharan, and Joseph Orenstein	18
<i>Direct Probing Charge and Spin Behaviors in Ferroics</i> Myung-Geun Han, Joseph Garlow, and Yimei Zhu	21
<i>Understanding and Controlling Entangled and Correlated Quantum States in Confined Solid-State Systems Created via Atomic Scale Manipulation</i> Stephen Jesse, Ondrej Dyck, Andy Lupini, Mina Yoon, and Prineha Narang	26
<i>Learning the Physics and Chemistry of Materials from Structural STEM Data</i> S.V. Kalinin, M.F. Chisholm, C.T. Nelson, A.R. Lupini, and M.P. Oxley	31
<i>Nanoscale Quantum and Classical Sensing for Superconducting and Topological Quantum Information</i> Ben Lawrie, Eugene Dumitrescu, Gabor Halasz, Matt Brahlek, Chengyun Hua, and Petro Maksymovych	36
<i>Atomic and Mesoscopic Phenomena in Quantum Systems with Broken Translational Symmetry</i> M. P. Oxley, A. R. Lupini, C. T. Nelson, M. F. Chisholm, and S. V. Kalinin	41
<i>Emergent Behavior in Nanoscale Functional Heterostructures</i> Amanda K. Petford-Long, Saidur Bakaul, Charudatta Phatak, and Suzanne G. E. te Velthuis	46

<i>Structure and Electron Dynamics in Photoexcited CDW Materials using MeV Ultrafast Electron Probes</i> Jing Tao, Jun Li, and Zhixiu Liang	51
<i>Liquid Cell Electron Microscopy: Heterogeneity and Fluctuations at Solid-Liquid Interfaces</i> Haimei Zheng, Peter Ercius, Emory Chan, and Lin-Wang Wang	56
<i>Unraveling Electron, Spin and Lattice Correlations using Advanced Electron Microscopy</i> Yimei Zhu, Lijun Wu, Junjie Li, Jing Tao, Xuewen Fu, and Tatiana Konstantinova	62
 University Grant Projects	
<i>Quantitative Interpretation of milli-eV Spatially Resolved EELS Mapping</i> P. E. Batson	69
<i>Data-Science Enabled, Robust and Rapid MeV Ultrafast Electron Diffraction Instrument System to Characterize Materials Including for Quantum and Energy Applications</i> Sandra Biedron and Manel Martínez-Ramón	74
<i>Infrared Nano-Spectroscopy of Plasmonic Materials with High-Resolution STEM-EELS</i> Jon P. Camden and David J. Masiello	76
<i>Non-zero Transverse Resistance in Zero Magnetic Field in $Al_2O_x/SrTiO_3$ Two-Dimensional Electron Gases: Evidence for Spatially Varying Magnetism near the Quantum Paraelectric Transition</i> Venkat Chandrasekhar	81
<i>Structural Complexity and Photocatalytic Functionality: Carbon Nitride Systems</i> Peter A. Crozier	86
<i>Real-Time Measurements of Complex Transition Metal Oxide Nanostructure Growth</i> Michael A. Filler and Frances M. Ross	91
<i>Molecular and Materials Energetics Visualized with Femtosecond TEM</i> David J. Flannigan	96
<i>Magneto-Thermal Microscopy of Complex Topological Spin Textures</i> Gregory D. Fuchs	101
<i>Development of a Coherent Spin-Magnon Interface Between Quantum Spins and a High-Q Organic Based Magnet</i> Gregory D. Fuchs, Daniel C. Ralph, Ezekiel Johnston-Halperin, and Michael E. Flatté	105

<i>Multimodal Hyperspectral Scanning Probe Microscopy for Understanding Low Dimensional Perovskite Semiconductors</i> David S. Ginger	110
<i>Tuning Exchange Interactions at the Atomic Scale in 2D Magnet / Semiconductor Heterostructures</i> Jay A. Gupta, Roland Kawakami, and Michael E. Flatté	115
<i>Emergent Phenomena in Ferroelectric/van der Waals Heterostructures</i> Xia Hong	120
<i>Sub-picometer Precision Imaging of 2D Materials Enabled by Deep Learning</i> Pinshane Y. Huang and Bryan K. Clark	124
<i>Mesoscopic Imaging of Electronic Landscape in Complex Materials</i> Keji Lai	128
<i>Nematic Transitions in Iron Pnictide Superconductors Imaged with a Quantum Gas</i> Benjamin Lev	133
<i>Interfacial Superconductivity in Epitaxial Single Layer FeTeSe/SrTiO₃</i> Lian Li	137
<i>Probing Dynamic Phase Changes and Interfaces with Cryogenic and In Situ Analytical Electron Microscopy</i> Ying Shirley Meng	142
<i>Atomic Electron Tomography: Determining the 3D Structure of Crystal Defects and Amorphous Materials at the Single-Atom Level</i> Jianwei (John) Miao	146
<i>Magnetic Imaging of Topological Phases of Matter</i> Katja C. Nowack	151
<i>Probing the Atomic Scale Structure and Electronic Properties of Ferroelectric Interfaces</i> Xiaoqing Pan	155
<i>Combining Microscopy and Quantum Calculations to Unveil Nanostructure Properties</i> Sokrates T. Pantelides	160
<i>Nano-Optical Imaging, Spectroscopy, and Control of Quantum Materials</i> Markus B. Raschke	165
<i>Exploring Energy Conversion and Non-Equilibrium Carrier Distributions at the Nanoscale via Novel Scanning Probe Approaches</i> Pramod Reddy and Edgar Meyhofer	169

<i>Symmetry-Breaking Mechanism and Metastable States in Charge-Ordered Systems Probed using Femtosecond Electron Diffraction and Spectroscopy</i> Chong-Yu Ruan	173
<i>Electronic Properties of Organic Photovoltaic Systems under Mechanical Stress</i> Santiago D. Solares and Hanning Chen	177
<i>Probing Quantum Materials with Quantitative STEM</i> Susanne Stemmer	181
<i>Intrinsic Topological Superconductors for Next-Generation Quantum Systems</i> Susanne Stemmer, Leon Balents, Stephen Wilson, and Andrea Young	185
<i>Exploring and Embracing Heterogeneity in Atomically Thin Energy Materials</i> Peter Sutter and Eli Sutter	189
<i>Dielectrics under Extreme Electric Fields: In Situ Studies on Nanoscale Mechanisms</i> Xiaoli Tan and Geoff Brenneka	194
<i>Probing Majorana States in Topological-Superconductor Proximity Systems</i> Stuart Tessmer, Dale Van Harlingen, and Alex Levchenko	199
<i>Tools for and Applications of 4D STEM to Functional Materials</i> Paul M. Voyles and Dane Morgan	204
<i>Visualizing Emergent Phenomena in Topological and Quantum Materials</i> Weida Wu	209
<i>Machine Learning-Enabled Advanced Electron Tomography for Resolving Chemical Inhomogeneity and Materials Dynamics</i> Huolin Xin	213
<i>Transport and Imaging of Mesoscopic Phenomena in Novel Low-Dimensional Materials</i> Amir Yacoby and Pablo Jarillo-Herrero	215
<i>Probing Correlated Superconductors and Their Phase Transitions on the Nanometer Scale</i> Ali Yazdani	219
<i>Spin-Polarized Scanning Tunneling Microscopy and Spectroscopy of Iridium-Oxides</i> Ilija Zeljkovic	224
<i>Emerging Functionality in Transition-Metal Compounds Driven by Spatial Confinement</i> Jiandi Zhang	228

Author Index	237
Participant List	239

AGENDA

2020 Electron and Scanning Probe Microscopies
Principal Investigators' Meeting
Zoom Virtual Meeting, Anywhere, USA
October 20–21, 2020

Note: All Times Below are Eastern!

Tuesday October 20, 2020

10:50 – 11:00 a.m. Log-in to Zoom and “settle in.” Having trouble? Call 865-368-6930

Session I: Welcome and Division and ESPM Program Updates

- 11:00 – 11:10 [Welcome and Materials Sciences and Engineering Division Update](#)
Andy Schwartz, Acting Division Director, MSED, DOE-BES
- 11:10 – 11:25 [Welcome and Electron and Scanning Probe Microscopies Program Update](#)
Jane Zhu, Program Manager, ESPM, DOE-BES

Session II: Ultrafast Diffraction and Real-Time Microscopy

Moderators: Lane Wilson (DOE-BES) and David Flannigan (UMN)

- 11:25 – 11:40 [Nano-optical Imaging, Spectroscopy, and Control of Quantum Materials](#)
Markus Raschke, University of Colorado
- 11:40 – 11:55 [Structure and Electron Dynamics in Photoexcited CDW Materials using MeV Ultrafast Electron Probes](#)
Jing Tao, Brookhaven National Laboratory
- 11:55 – 12:30 [Panel Discussion](#)
David Flannigan, Chong-Yu Ruan, Yimei Zhu, Greg Fuchs, Frances Ross, Markus Raschke, Jing Tao
- 12:30 – 1:00 Break (Lunch or Coffee)

Session III: Quantum Materials

Moderators: Mick Pechan (DOE-BES) and Susanne Stemmer (UCSB)

- 1:00 – 1:15 [Probing Correlated Superconductors and Their Phase Transitions on the Nanometer Scale](#)
Ali Yazdani, Princeton University
- 1:15 – 1:30 [Spin Physics and Nanoscale Probes of Quantum Materials](#)
David Goldhaber-Gordon, SLAC and Stanford University
- 1:30 – 1:45 [Unraveling Electron, Spin and Lattice Correlations using Advanced Electron Microscopy](#)
Yimei Zhu, Brookhaven National Laboratory
- 1:45 – 2:00 [Visualizing Emergent Phenomena in Topological and Quantum Materials](#)
Weida Wu, Rutgers University
- 2:00 – 2:45 [Panel Discussion](#)
Susanne Stemmer, Keji Lai, Lian Li, Venkat Chandrasekhar, Amir Yacoby, Jiandi Zhang, Ali Yazdani, David Goldhaber-Gordon, Yimei Zhu, Weida Wu
- 2:45 – 3:15 Break (Coffee or Lunch)

Session IV: Quantum Information Science and Advanced Imaging

Moderators: Athena Sefat (DOE-BES) and Ben Lawrie (ORNL)

- 3:15 – 4:00 Short talks (7 minutes for each speaker)
Ben Lawrie, Oak Ridge National Laboratory
Benjamin Lev, Stanford University
Gregory Fuchs, Cornell University
Stephen Jesse, Oak Ridge National Laboratory
Susanne Stemmer, University of California Santa Barbara
Amir Yacoby, Harvard University
- 4:00 – 4:50 [Panel Discussion](#)
- 4:50 – 5:00 Close-out, Day 1

Wednesday October 21, 2020

10:50 – 11:00 a.m. Log-in to Zoom and “settle in.” Having trouble? Call 865-368-6930

Session V: In -Situ Microscopy of Energy Materials

Moderators: Michael Sennett (DOE-BES) and Peter Crozier (ASU)

- 11:00 – 11:15 [Probing Dynamic Phase Changes and Interfaces with Cryogenic and In Situ Analytical Electron Microscopy](#)
Shirley Meng, University of California San Diego
- 11:15 – 11:30 [Atomic Resolution Electron Microscopy of Soft Matter](#)
Nitash Balsara, LBNL and UC Berkeley
- 11:30 – 11:45 [Developing Cryogenic Electron Microscopy for Energy Storage Materials](#)
Yi Cui, SLAC and Stanford University
- 11:45 – 12:00 [Liquid Cell Electron Microscopy: Heterogeneity and Fluctuations at Solid-Liquid Interfaces](#)
Haimei Zheng, Lawrence Berkeley National Laboratory
- 12:00 – 12:30 [Panel Discussion](#)
Peter Crozier, David Ginger, Peter Sutter, Jon Camden, Shirley Meng, Nitash Balsara, Yi Cui, Haimei Zheng
- 12:30 – 1:00 Break (Lunch or Coffee)

Session VI: Data Science, Theory, and New Developments in Methods & Instrumentation

Moderators: Helen Kerch (DOE-BES) and Paul Voyles (Wisconsin)

- 1:00 – 1:15 [Learning the Physics and Chemistry of Materials from Structural STEM Data](#)
Sergei Kalinin, Oak Ridge National Laboratory

- 1:15 – 1:30 [Atomic Electron Tomography: Determining the 3D Structure of Crystal Defects and Amorphous Materials at the Single-Atom Level](#)
Jianwei (John) Miao, University of California, Los Angeles
- 1:30 – 1:45 [Exploring Energy Conversion and Non-Equilibrium Carrier Distributions at the Nanoscale via Novel Scanning Probe Approaches](#)
Prمود Reddy, University of Michigan
- 1:45 – 2:00 [Probing the Atomic Scale Structure and Electronic Properties of Ferroelectric Interfaces](#)
Xiaoqing Pan, University of California, Irvine
- 2:00 – 2:45 [Panel Discussion](#)
Paul Voyles, Sok Pantelides, Pinshane Huang, Mark Oxley, Phil Batson, Sergei Kalinin, John Miao, Pramod Reddy, Xiaoqing Pan
- 2:45 – 3:15 Break (Coffee or Lunch)

Session VII: Magnetic Imaging and 2D Materials

Moderators: Jane Zhu (DOE-BES) and Katja Nowack (Cornell)

- 3:15 – 3:30 [Emergent Behavior in Nanoscale Functional Heterostructures](#)
Amanda Petford-Long, Argonne National Laboratory
- 3:30 – 3:45 [Tuning Exchange Interactions at the Atomic Scale in 2D Magnet / Semiconductor Heterostructures](#)
Jay Gupta, Ohio State University
- 3:45 – 4:00 [The Discovery of New Properties in Layered Ferroelectrics through the Synergistic Combination of Scanning Probe Microscopy and Theory](#)
Nina Balke, Oak Ridge National Laboratory
- 4:00 – 4:40 [Panel Discussion](#)
Katja Nowack, Ilija Zeljkovic, Stuart Tessmer, Xia Hong, A. Petford-Long, Jay Gupta, Nina Balke
- 4:40 – 5:00 *Close out*
Jane Zhu, Program Manager, ESPM, DOE-BES

LABORATORY PROJECTS

The discovery of new properties in layered ferroelectrics through the synergistic combination of scanning probe microscopy and theory

Nina Balke, Petro Maksymovych, Rama Vasudevan, Albina Borisevich

Oak Ridge National Laboratory

Keywords: Ferroelectrics, piezoelectrics, atomic force microscopy, electron microscopy

Research Scope

Polarization of materials is at the heart of many applications in energy and information technology often based on the possibility to control phenomena through externally applied forces. The action of electric field, in particular, enacts both linear and non-linear dielectric responses creating rich phenomenology of dipolar glasses, paraelectrics, relaxors, antiferroelectrics, and ferroelectrics. In this FWP we will pursue how new and unexpected properties can emerge through the coupling of or transition between distinct polar behaviors, including the possibilities to change polar material properties on demand between states of materials which typically do not co-exist. One way to realize this is the stabilization of out of equilibrium polar phases, often confined to interfaces or surfaces due to broken symmetry, but which are topologically protected. Of fundamental interest are not only intrinsic but also extrinsic polar phenomena which are associated with polar properties introduced by ionic defects which can be controlled via chemical modification routes. The project goal can only be achieved through the fundamental understanding of polar properties and how to transform them on multiple length scales from the atomic to micrometer scale properties which requires the development of new probing methodologies and integrated microscopic approaches. Specifically, we aim to explore (a) polar transitions based on order-disorder phenomena in ferroelectric ion conductors such as CuInP_2S_6 , (b) the coupling of intrinsic and extrinsic polar properties, for example the coupling of intrinsic polarization with oxygen vacancies in BaTiO_3 and (c) the creation of new functionality at boundaries of dissimilar polar properties such as the enhancement of electromechanical and electrical properties of ferroelectric-antiferroelectric interfaces.

Recent Progress

In the concurrence period, we achieved unprecedented insight into ferroic material properties of layered ferroelectric crystals through the combination of atomic force and electron microscopy (AFM and STEM, respectively) with density functional theory predictions in collaboration with project DE-FG02-09ER46554 (Pantelides, Vanderbilt University). This enabled the discovery of new polar phases and new functionality which is based on the intricate interplay of ferroic and ionic phenomena. Through the synergistic combination of experiment and theory, we developed interpretable SPM as next cycle in technique development and expanded the information content which can be extracted from SPM measurements which can be compared to a multitude of complimentary characterization techniques for a truly integrated microscopy approach.

The family of layered thio- and seleno-phosphates has gained attention as possible control dielectrics for the rapidly growing family of 2D and quasi-2D electronic materials. Here, we are exploring the piezoelectric and ferrielectric properties of CuInP_2S_6 (CIPS) which is a layered crystal featuring van der Waals (vdW) gaps where the Cu and In displacement are responsible for the observed ferrielectricity (Fig. 1a).¹ The local mapping of the effective piezoelectric constant d along the z-direction using quantitative AFM (Figure 1b) reveal an unusual contrast – four distinct

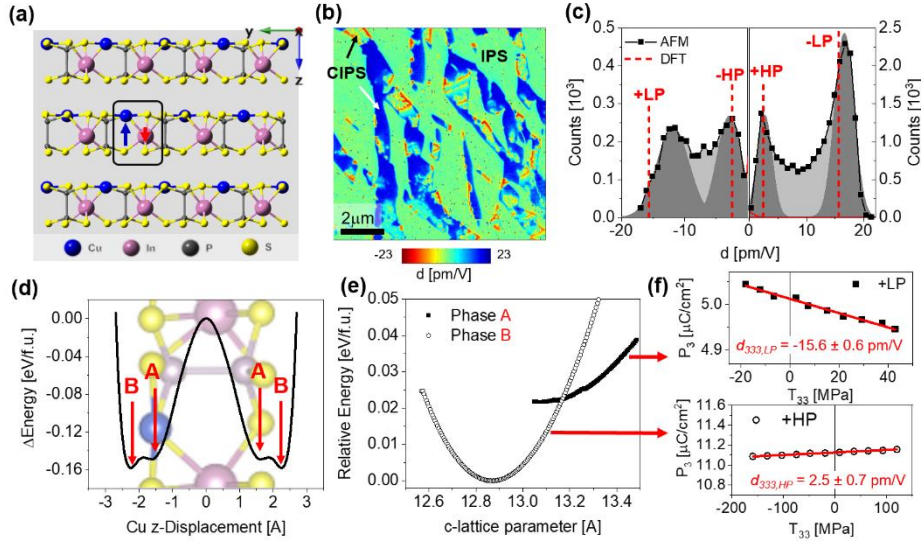


Figure 1: (a) The layered structure of CIPS. (b) Quantified piezoelectric constant map measured by PFM at room temperature. (c) Histogram of the measured values of the CIPS phase with Gaussian function fits around the four distinct maxima.

Dotted lines depict the theoretically predicted values of the four polarization states. (d) Change in energy versus the polarization extracted from the displacement of Cu. (e) Energy calculation for the polar phase described by the Cu residing in the layer (A) or vdW gap (B). (f) Theoretical polarization-stress curves along the z-direction around the zero-stress state for the LP and HP phase.

while structural very similar to each other, the polar properties of the two phases vary greatly. When the Cu occupies the position in the vdW gap, the polarization doubles from ~ 5 to $\sim 11 \mu\text{C}/\text{cm}^2$ (therefore, the two phases are termed low and high polarization states, LP and HP) and the piezoelectric constant changes from $-15.6 \text{ pm}/\text{V}$ to $2.5 \text{ pm}/\text{V}$, respectively. Most notable, the predicted values match the experimentally measured ones very closely (see Fig. 1c) which verifies the theoretical results and provides the first experimental evidence for the existence of the HP phase.

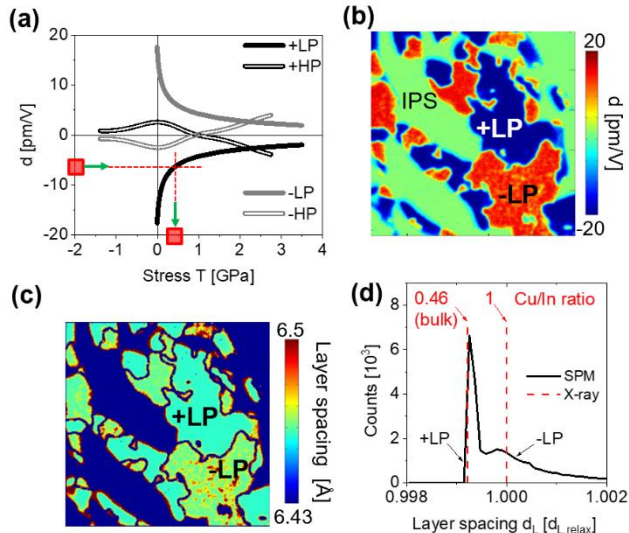


Figure 2. (a) Stress-dependent piezoelectric constant for all polarization states as calculated from DFT. (b) Map of local piezoelectric constant as obtained by AFM and (c) after conversion to layer spacing map through comparison with DFT. (d) Comparison of local layer spacing with published X-ray measurements.

signal levels which indicate complex piezoelectric properties (Fig. 1c). The experiments could be interpreted with the addition of density functional theory (DFT) calculations which show the existence of four stable position for the polar Cu displacement within layers (site A) or in the van-der-Waals gap (site B) which forms a quadruple energy well (Fig. 1d). This is due to the existence of two polar phases whose energy landscapes overlap strongly (Fig. 1e). Interestingly,

The excellent match between experiment and theory allows to extract an enhanced information content from AFM measurements. DFT reveals that the quadruple-well is highly tunable by strain and, therefore, the piezoelectric properties depend on stress (Fig. 2a).

This allows for the opportunity to assign a polarization state to the experimental value of piezoelectric constant (Fig. 2b) and extract also values for polarization, stress, strain, c-lattice parameter, and layer spacing (Fig. 2c) which is based on the correlations between these properties as described by theory.² This new level of insight is difficult to detect on AFM length scales of 10's of nm with other techniques and allows for the direct comparison to other techniques which measure layer spacing such as X-ray (Fig. 2d). We found that in a region with only +LP and -LP domains, the +LP domain is strained as expected from bulk measurements and the local Cu/In composition, whereas the oppositely oriented -LP domain shows a relaxed layer spacing above the bulk value according to comparison with published X-ray data (Fig. 2d).

The polarization-direction dependent strain relaxation is highly unusual and can be traced back to asymmetric surface relaxation observed by DFT due to the asymmetric Cu position for +LP and -LP surfaces. The -LP domain relaxes stronger than the +LP domain (Fig. 3a) which is consistent with the experimental observation (Fig. 2d). In addition to surface contributions, local strain states may vary throughout the bulk. Therefore, we performed STEM on CIPS cross-section and found extended defects in the layering (Fig. 3b,c) which results in strong local variations of strain tensor components (Fig. 3d).³ The nature of the defects can be described as topological defects such as edge dislocations where an additional CIPS layer is inserted and abruptly terminates, as well as domain walls and kinks with high areal density (Fig. 3e). We find evidence for nanodomains that span multiple layers and observe that the presence of the defects is weakly correlated with the presence of domain boundaries. These studies confirm the rich nature of defect structures in layered materials and suggest opportunities for their future study beyond the traditional single-layer paradigm

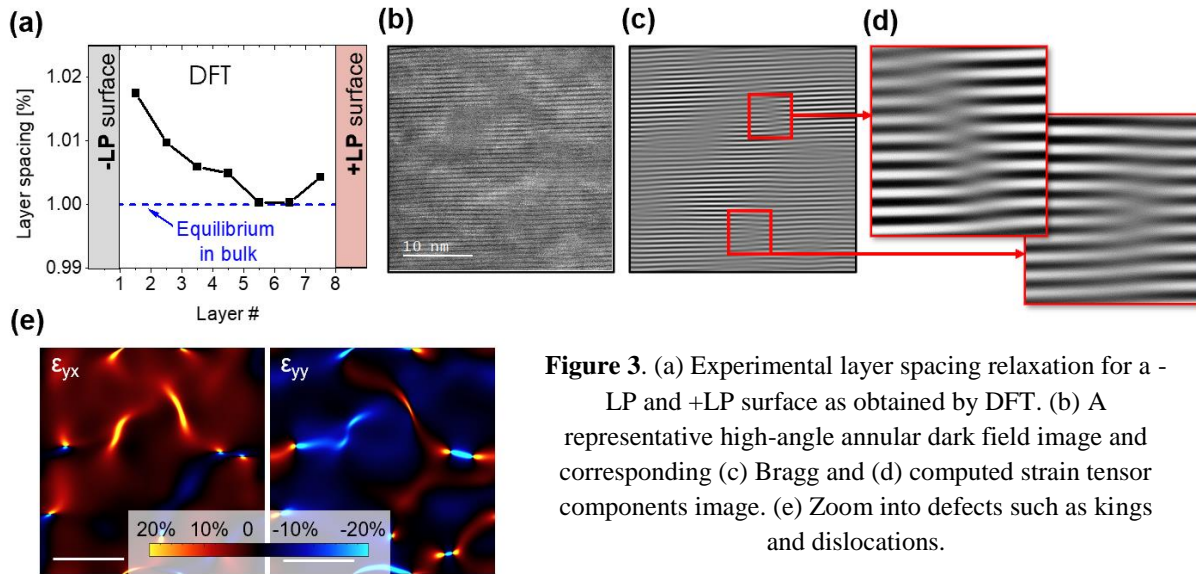


Figure 3. (a) Experimental layer spacing relaxation for a -LP and +LP surface as obtained by DFT. (b) A representative high-angle annular dark field image and corresponding (c) Bragg and (d) computed strain tensor components image. (e) Zoom into defects such as kinks and dislocations.

With the enhanced understanding of piezoelectric and ferrielectric properties of CIPS and the link to polarization through theory, we can begin to explore polarization switching in CIPS. We found that out of all four possible polarization states, only two participate in the switching process. Locally, we can identify areas showing a pure polarization reversal, a phase change, or both (Fig. 4a). Out of all observed hysteresis loop, one is standing out which shows a transition between +HP and -HP states (orange curve in Fig. 3a). The corresponding polarization loop shows an unusual polarization alignment against the applied electric field (Fig. 4b). This can be explained

by a field-driven Cu motion across the vdW gap, the first fundamental step of ionic conduction, which results in a polarization reversal which does not happen in traditional ferroelectric materials. We have demonstrated that it is possible to isolate the Cu transition across the vdW gaps reversibly on local scales resulting in inverse polarization loops that exhibit two negative slopes constituting a negative capacitance (NC) regime where $dP/dE < 0$ (Fig. 4c). This interplay of ionic and polar properties enables stable NC during polarization switching, unlike transient NC methods based on ferroelectric circuits. This innovation offers a pathway towards new designs for efficient computing based on intrinsic material properties without the need for additional circuitry.

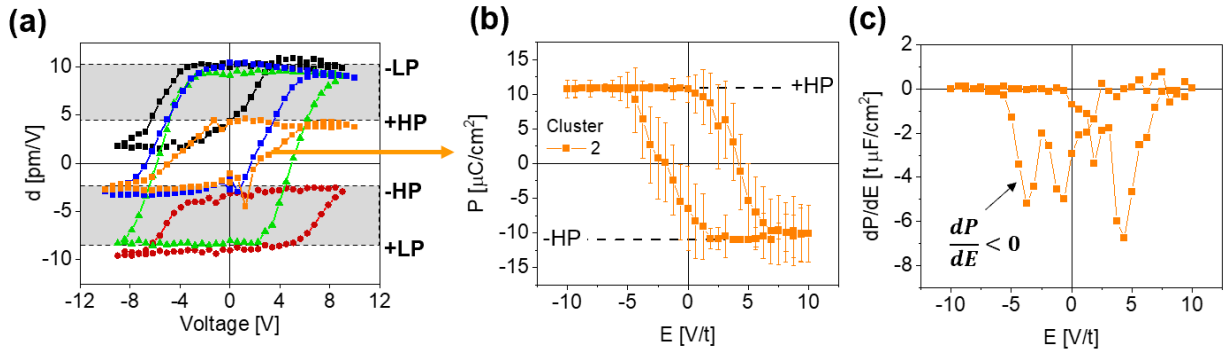


Figure 4. (a) Characteristic piezoelectric constant hysteresis loops observed in different regions of CIPS. (b) Corresponding polarization loop extracted for the orange curve in (a) by comparing experimental and theoretical values. (c) Derivative of polarization curve in (b).

Future Plans

In the future, we will explore the interplay of ferroic and ionic material properties with the goal to modify the ferroelectric properties on demand. This will be done at the nanoscale and the microscale to establish a road map how the unusual local phenomena can be harnessed on larger length scales. We will explore the role of voltage pulses to introduce Cu disorder to transition from the ferroelectric to the paraelectric state controllably and reversibly. In this process, the role of interfaces and surfaces are of fundamental interest since they need to be able to accommodate Cu. We also plan to continue and further develop our integrated experiment-theory approaches to better understand the fundamental ferroelectric and ion conducting properties of CIPS.

References

1. J. A. Brehm, S. Neumayer, L. Tao, A. O'Hara, M. Chyasnachichus, M. A. Susner, M. A. McGuire, S. V. Kalinin, S. Jesse, P. Ganesh, S. T. Pantelides, P. Maksymovych, and N. Balke, *Tunable quadruple-well ferroelectric van-der-Waals crystals*, Nat. Mater. **19**, 43-48 (2020).
2. S.M. Neumayer, J.A. Brehm, L. Tao, A. O'Hara, P. Ganesh, S. Jesse, M.A. Susner, M.A. McGuire, S.T. Pantelides, P. Maksymovych, N. Balke, *Local Strain and Polarization Mapping in Ferrielectric Materials*, ACS Appl. Mater. Interfaces **12**, 38546-38553 (2020).
3. R. Vasudevan, S.M. Neumayer, M.A. Susner, M.A. McGuire, S.T. Pantelides, P. Maksymovych, D.N. Leonard, N. Balke, A. Borisevich, *Domains and topological defects in layered ferroelectric materials*, ACS Appl. Nano Mater. **3**, 8161-8166 (2020).
4. S.M. Neumayer, L. Tao, A. O'Hara, J. Brehm, M. Si, P.-Y. Liao, T. Feng, S.V. Kalinin, P. D. Ye, S.T. Pantelides, P. Maksymovych, N. Balke, *Alignment of polarization against an electric field in van der Waals ferroelectrics*, Phys. Rev. Applied **13**, 064063 (2020).
5. S.M. Neumayer, L. Tao, A. O'Hara, M.A. Susner, M.A. McGuire, P. Maksymovych, S.T. Pantelides, N. Balke, *The concept of negative capacitance in ionically conductive van-der-Waals ferroelectrics*, Adv. Energy Mater. doi.org/10.1002/aenm.202001726 (2020).

Publications (10 most relevant)

1. S. M. Neumayer, E. A. Eliseev, M. A. Susner, A. Tselev, B. J. Rodriguez, J. A. Brehm, S. T. Pantelides, G. Panchapakesan, S. Jesse, S. V. Kalinin, M. A. McGuire, A. N. Morozovska, P. Maksymovych, and N. Balke, “Giant negative electrostriction and dielectric tunability in a van der Waals layered ferroelectric”, *Phys. Rev. Mater.* **3**, 024401 (2019).
2. J. A. Brehm, S. Neumayer, L. Tao, A. O’Hara, M. Chyasnovich, M. A. Susner, M. A. McGuire, S. V. Kalinin, S. Jesse, P. Ganesh, S. T. Pantelides, P. Maksymovych, and N. Balke, *Tunable quadruple-well ferroelectric van-der-Waals crystals*, *Nat. Mater.* **19**, 43-48 (2020).
3. S.M. Neumayer, J.A. Brehm, L. Tao, A. O’Hara, P. Ganesh, S. Jesse, M.A. Susner, M.A. McGuire, S.T. Pantelides, P. Maksymovych, N. Balke, *Local Strain and Polarization Mapping in Ferrielectric Materials*, *ACS Appl. Mater. Interfaces* **12**, 38546-38553 (2020).
4. K.P. Kelley, Y. Ren, A. Morozovska, E. Eliseev, Y. Ehara, H. Funakubo, T. Giamarchi, N. Balke, R.K. Vasudevan, Y. Cao, S. Jesse, S. V. Kalinin, *Dynamic manipulation in Piezoresponse Force Microscopy: creating non-equilibrium phases with large electromechanical response*, *ACS Nano* **14**, 10569 (2020).
5. R.R. Vasudevan, S.M. Neumayer, M.A. Susner, M.A. McGuire, S.T. Pantelides, P. Maksymovych, D.N. Leonard, N. Balke, A. Borisevich, *Domains and topological defects in layered ferroelectric materials*, *ACS Appl. Nano Mater.* **3**, 8161-8166 (2020).
6. S.M. Neumayer, M. Susner, M. McGuire, S.T. Pantelides, S. Kalnaus, P. Maksymovych, N. Balke, *Experimental investigation of ferroelectric behavior in van der Waals layered materials under in-plane strain*, *IEEE Transactions on Ultrasonics, Ferroelectrics, and Frequency Control*, **10.1109/TUFFC.2020.3007290** (2020).
7. S.M. Neumayer, L. Tao, A. O’Hara, J. Brehm, M. Si, P.-Y. Liao, T. Feng, S.V. Kalinin, P. D. Ye, S.T. Pantelides, P. Maksymovych, N. Balke, *Alignment of polarization against an electric field in van der Waals ferroelectrics*, *Phys. Rev. Applied* **13**, 064063 (2020).
8. Dziaugys, K. Kelley, J.A. Brehm, A. Puretzky, T. Feng, S. Neumayer, M. Chyasnovich, E.A. Eliseev, J. Banys, Y. Vysochanskii, F. Ye, B. Chakoumakos, M. A. McGuire, S.V. Kalinin, G. Panchapakesan, S.T. Pantelides, N. Balke, A.N. Morozovska, P. Maksymovych, *Piezoelectric domain walls in van der Waals ferrielectric $\text{CuInP}_2\text{Se}_6$* , *Nat. Comm.* **11**, 3623 (2020).
9. K. P. Kelley, L. Li, Y. Ren, Y. Ehara, H. Funakubo, S. Somnath, S. Jesse, Y. Cao, R. Kannan, R. K. Vasudevan, and S. V. Kalinin. “Tensor factorization for elucidating mechanisms of piezoresponse relaxation via dynamic piezoresponse force spectroscopy,” *npj Comp. Mater.* **6**, 113 (2020).
10. S.M. Neumayer, L. Tao, A. O’Hara, M.A. Susner, M.A. McGuire, P. Maksymovych, S.T. Pantelides, N. Balke, *The concept of negative capacitance in ionically conductive van-der-Waals ferroelectrics*, *Adv. Energy Mater.* **doi.org/10.1002/aenm.202001726** (2020).

Atomic Resolution Electron Microscopy of Soft Matter

Nitash Balsara^{1,3}, Xi Jiang¹, Andrew Minor^{2,4}, Ronald Zuckermann², David Prendergast²

¹Materials Sciences Division and ²Molecular Foundry, Lawrence Berkeley National Laboratory, Berkeley, CA 94720; ³College of Chemistry and ⁴Department of Materials Science and Engineering, University of California, Berkeley, CA 94720

Keywords: Electron microscopy, atomic-scale, soft materials

Research Scope

The goal of our program is to produce images of soft materials with atomic resolution using electron microscopy. The proposed work is inherently challenging because soft materials are unstable under the electron beam. Our work encompasses both cryogenic transmission electron microscopy (cryo-EM) and four-dimensional scanning transmission electron microscopy (4D-STEM). Our experiments were conducted on crystalline nanostructures formed by self-assembly of amphiphilic peptoid molecules in water and the organic semiconductor molecules in thin films. Molecular dynamics simulations are used to characterize thermal fluctuations and disorder, and this information is convoluted with the contrast transfer function of the microscope used in experiments to obtain theoretical images. We demonstrate the application of our techniques to imaging the crystalline structure of peptoid membrane at the atomic level and establish structure–property relationships in organic systems using techniques previously only available for hard materials. These methodologies that we have developed will be extended to a wide variety of soft materials.

Recent Progress

A fundamental challenge in materials science is to understand the atomic-level structures of nanoarchitectures assembled from synthetic polymers. Here, we synthesized a family of sequence-defined polypeptoids that form free-floating crystalline 2-dimensional nanosheets, in which not only individual polymer chains and their relative orientations, but also atoms in nanosheets were directly observed using the cryo-EM. These atomic details are inaccessible by conventional scattering techniques. Using the feedback between sequence-controlled synthesis and atomic imaging, we observed how the nanosheet structure responds to chemical modifications at the atomic-length scale [1]. These atomic-level insights open the door to the design of bioinspired nanomaterials with more precisely controlled structures and properties.

Figure 1 A shows the chemical structure of a nearly monodisperse diblock polypeptoid comprising a hydrophobic poly-N-(2-phenylethyl)glycine (pNbrpe) block with bromine atoms at the para position phenylethyl side chains and a hydrophilic poly-N-2-(2-(2-methoxyethoxy) ethylglycine) (pNte). The self-assembly of this material in water results in the formation of

molecularly thin sheets of the crystalline hydrophobic pNbrpe chains stabilized by dissolved pNte chains [2,3]. The sheets were divided into $87 \times 87 \text{ \AA}$ boxes and analyzed using the Relion software package [4,5]. Every box in the nanosheet obtained from this peptoid belonged to the same class which is shown in Figure 1B. The averaging technique works extremely well when very few classes are needed. The antiparallel V-shaped motif was obtained in this system. At the ends of each side chain is a bright dot that represents the projection view of three bromine atoms in a column. It is clear that in some polymers, we can identify individual atoms if the atom is heavy enough. Moving forward, we will exploit this molecular construct to further our understanding of atomic self-assembly in soft materials. We are using molecular dynamics to understand the role of steric effects and polarity on the organization of polymeric chains. In the system shown in Figure 1C, the bromine atom is constrained to like a fixed distance away from the benzene ring due to a covalent bond.

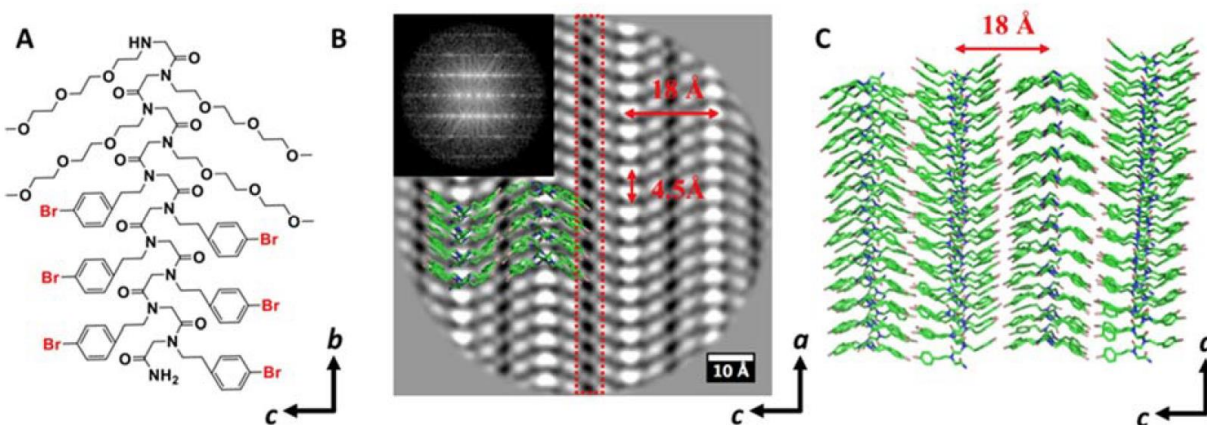


Figure 1. **A.** Chemical structure of polypeptoid block copolymer. **B.** Averaged image. The Fourier transform of the image is shown in the inset. The rows of small dots at the end of side chains represent bromine atoms. One such row is outlined in a dotted red box. **C.** MD simulations showing the expected locations of individual Br atoms.

The present study on the investigation of polypeptoid crystal structures at the atomic level is not only a significant advance in soft material imaging but also in enabling the future design of biomimetic nanomaterials with more precisely controlled structures and properties.

In addition to the direct imaging of atoms in synthetic polymers using cryo-EM, 4D-STEM was used to study the structural ordering at the level of individual defects and nanoscale domains in films of organic semiconductors. 4D-STEM uses a focused electron beam that is rastered across an electron transparent sample and at each scan position a diffraction pattern is acquired (Figure 2A). The individual convergent beam electron diffraction (CBED) patterns provide comprehensive information regarding structure, orientation, localized lattice strain, and other material properties. We refer to this technique as 4D-STEM since it involves a 2-dimensional scanned area where at each point a 2-dimensional diffraction pattern is acquired (Figure 2B and C).

In our initial studies of soft materials using 4D-STEM we have focused on organic semiconductor molecular thin films. As their electronic properties depend highly on their crystallographic geometry, organic semiconductors exemplify the need for improved understanding of the link between structural and functional properties across a multitude of length scales. They are thus ideally suited for study by electron microscopy methods. We have imaged the nanocrystalline structure of an organic molecular thin film using 4D-STEM with a spatially localized probe (~ 2 nm) as shown in Figure (Figure 2D and E). Our technique revealed previously unknown structural features, such as grain overlapping through the thickness of the thin film, and information about the local crystal structure and its variations (Figure 2D and E). While a sample cast from a single solvent exhibited a liquid-crystal structure with crystalline orientations varying smoothly over all possible rotations, the addition of a co-solvent induced pronounced segmentation of the structure characterized by the emergence of sharp grain boundaries and overlapping domains. Our results demonstrated the power of 4D-STEM to provide insight into the structure of functional organic solids and show how structure-property relationships can be visualized in organic systems using techniques previously only available for hard materials such as metals and ceramics.

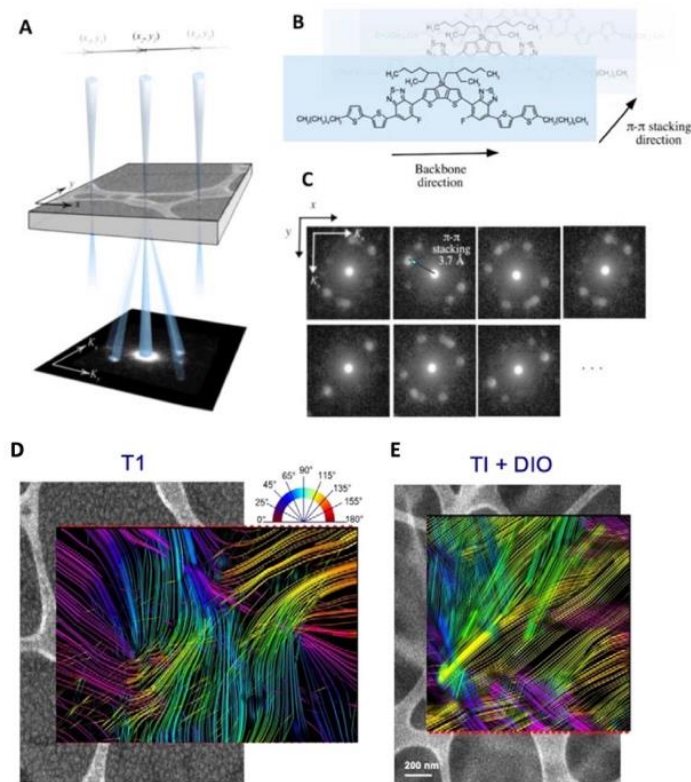


Figure 2. **A.** Schematic of the 4D-STEM technique. Rastering the convergent beam enables detection of a full diffraction pattern for each (x, y) , with a step size large enough to prevent the beam from damaging the yet unsampled neighboring positions. **B.** Illustration of π - π stacking of p-DTS(FBTTh₂)₂ (named T1). **C.** 4D-STEM data from a sample containing T1. Comparison of grain morphology between p-DTS(FBTTh₂)₂ drop cast without solvent (T1) in **D** and with solvent (T1 + DIO) in **E**. 4D-STEM images show the continuity of lattice orientations.

To summarize, we have developed imaging methods based on both transmission and scanning transmission electron microscopy to study crystalline, and liquid crystalline soft matter at unprecedented spatial resolution.

Future Plans

The atomic-scale imaging of polypeptoid crystalline membrane has been demonstrated in previous study where the individual bromine atoms were able to be identified with 1.5 Å resolution. The protocols for the cryo-EM 2-D imaging and the imaging processing has been established. This has the potential to open the door to resolving individual atoms without the resorting to a model. Atomic-scale 3-D reconstruction of the polypeptoid crystalline membrane wherein all of the crystals are identical are still challenging due to issues related to the presence of local heterogeneity of tilting geometry of unit cells in a tilted crystal. We are working on algorithms to identify, average and reconstruct over such collections of tilted images with fidelity.

4D-STEM has shown the ability to provide local spatial information of lattices and grains in organic thin films. This method will be extended to a wide variety of soft materials, in particular the functional diblock copolymers with semicrystalline blocks which serve as solid electrolyte in battery, such as the polystyrene-*b*-polyethylene oxide (PS-*b*-PEO). The effect of salt on the crystalline structures in the PEO domain as functions of concentration, temperature and spatial distribution can be revealed using 4D-STEM in future study.

References

1. S Xuan, X Jiang, R.K. Spencer, N.K. Li, D Prendergast, N.P. Balsara and R.N. Zuckermann, “Atomic-level engineering and imaging of polypeptoid crystal lattices”, *Proc. Natl. Acad. Sci.* 116, pp. 22491- 22499, (2019)
2. Sun, J.; Jiang, X.; Lund, R.; Downing, K. H.; Balsara, N. P.; Zuckermann, R. N. Self-assembly of crystalline nanotubes from monodisperse amphiphilic diblock copolypeptoid tiles. *P Natl Acad Sci USA* 2016, 113 (15), 3954-3959.
3. Greer, D. R.; Stolberg, M. A.; Kundu, J.; Spencer, R. K.; Pascal, T.; Prendergast, D.; Balsara, N. P.; Zuckermann, R. N. Universal Relationship between Molecular Structure and Crystal Structure in Peptoid Polymers and Prevalence of the *cis* Backbone Conformation. *J Am Chem Soc* 2018, 140 (2), 827-833.
4. Li, X. M.; Mooney, P.; Zheng, S.; Booth, C. R.; Braunfeld, M. B.; Gubbens, S.; Agard, D. A.; Cheng, Y. F. Electron counting and beam-induced motion correction enable near-atomic-resolution single-particle cryo-EM. *Nat Methods* 2013, 10 (6), 584.
5. Scheres, S. H. RELION: implementation of a Bayesian approach to cryo-EM structure determination. *Journal of structural biology* 2012, 180 (3), 519-30.
6. O. Panova, C. Ophus, C.J. Takacs, K.C. Bustillo, L. Balhorn, A. Salleo, N.P. Balsara and A.M. Minor, “Diffraction imaging of nanocrystalline structures in organic semiconductor molecular thin films”, *Nature Materials*, 18, pp. 860–865. (2019)

Publications

A. Publications primarily funded

1. S Xuan and R.N. Zuckermann, “*Diblock copolypeptoids: a review of phase separation, crystallization, self-assembly and biological applications*”, *J. Mater. Chem. B* 8, pp. 5380-5394 (2020).
2. S Xuan and R.N. Zuckermann, “*Engineering the atomic structure of sequence-defined peptoid polymers and their assemblies*”, *Polymer*, 202, pp. 122691 (2020).
3. S Xuan, X Jiang, R.K. Spencer, N.K. Li, D Prendergast, N.P. Balsara and R.N. Zuckermann, “*Atomic-level engineering and imaging of polypeptoid crystal lattices*”, *Proc. Natl. Acad. Sci.* 116, pp. 22491-22499, (2019)
4. O. Panova, C. Ophus, C.J. Takacs, K.C. Bustillo, L. Balhorn, A. Salleo, N.P. Balsara and A.M. Minor, “*Diffraction imaging of nanocrystalline structures in organic semiconductor molecular thin films*”, *Nature Materials*, 18, pp. 860–865. (2019)
5. X. Jiang, R.K. Spencer, J. Sun, C. Ophus, R.N. Zuckermann, K.H. Downing, N.P. Balsara, “*Resolving the Morphology of Peptoid Vesicles at the One Nanometer Length-Scale using Cryogenic Electron Microscopy*”, *Journal of Physical Chemistry B*, 123, pp. 1195–1205, (2019)
6. X. Jiang, S.T. Xuan, J. Kundu, D. Prendergast, R.N. Zuckermann, N.P. Balsara, “*Effect of processing and end groups on the crystal structure of polypeptoids studied by cryogenic electron microscopy at atomic length scales*”, *Soft Matter*, 15, pp. 4723-4736. (2019)
7. D.R. Greer, M.A. Stolberg, S. Xuan, X. Jiang, N.P. Balsara, R.N. Zuckermann, “*Liquid-Crystalline Phase Behavior in Polypeptoid Diblock Copolymers*”, *Macromolecules*, 51, pp. 9519–9525. (2018).
8. X. Jiang, D.R Greer, J. Kundu, C. Ophus, A.M. Minor, D. Prendergast, R.N. Zuckermann, N.P. Balsara, K.H. Downing. “*Imaging Unstained Synthetic Polymer Crystals and Defects on Atomic Length-scales using Cryogenic Electron Microscopy*”, *Macromolecules*, 51, pp. 7794-7799, (2018).

B. Collaborative Publications:

1. K.W. Gao, X Jiang, Z.J. Hoffman, G.K. Sethi, S Chakraborty, I Villaluenga, N.P. Balsara, “*Optimizing the monomer structure of polyhedral oligomeric silsesquioxane for ion transport in hybrid organic–inorganic block copolymers*” *Journal of Polymer Science* 58, pp. 363-371 (2020)
2. D Devaux, I Villaluenga, X Jiang, Y.H. Chang, D.Y. Parkinson, N.P. Balsara “*Lithium-Sulfur Batteries with a Block Copolymer Electrolyte Analyzed by X-ray Microtomography*”, *Journal of The Electrochemical Society*, 167, 060506, (2020)
3. S Chakraborty, X Jiang, Z.J. Hoffman, G.K. Sethi, C Zhu, N.P. Balsara, I Villaluenga “*Reversible Changes in the Grain Structure and Conductivity in a Block Copolymer Electrolyte*”, *Macromolecules* 53, pp. 5455-5464, (2020)
4. H.J. Oh, M.S. Aboian, M.Y.J. Yi, J.A. Maslyn, W.S. Loo, X. Jiang, D.Y. Parkinson, M.W. Wilson, T, Moore, C.R. Yee, G.R. Robbins, F.M. Barth, J.M. DeSimone, S.W. Hetts, N.P. Balsara, “*3D Printed Absorber for Capturing Chemotherapy Drugs before they Spread through the Body*”, *ACS Central Science*, 5, pp. 419-427, (2019)
5. X Li, WS Loo, X Jiang, X Wang, M.D. Galluzzo, K.I. Mongcopa, A.A. Wang, N.P. Balsara, B.A. Garetz “*Confined versus Unconfined Crystallization in Block Copolymer/Salt Mixtures Studied by Depolarized Light Scattering*”, *Macromolecules* 52, pp. 982-991, (2019)
6. Marcus Gallagher-Jones, Colin Ophus, Karen C. Bustillo, David R. Boyer, Ouliana Panova, Calina Glynn, Chih-Te Zee, Jim Ciston, Kevin Canton Mancina, Andrew M. Minor, Jose A. Rodriguez, “*Nanoscale mosaicity revealed in peptide microcrystals by scanning electron nanodiffraction*”, *Communications Biology*, 2, article number 26, (2019)

Developing Cryogenic Electron Microscopy for Energy Storage Materials

Yi Cui^{1,5}, Wah Chiu^{2,3,4}, Jen Dionne¹ and Paul McIntyre^{1,6}

Affiliations:

¹Department of Materials Science and Engineering, Stanford University, Stanford, CA 94305. ²Department of Bioengineering, Stanford University, Stanford, CA 94305. ³Department of Microbiology and Immunology, Stanford University School of Medicine, Stanford, California 94305, USA. ⁴Photon Science, SLAC National Accelerator Laboratory, 2575 Sand Hill Road, Menlo Park, California 94025, USA. ⁵Stanford Institute for Materials and Energy Sciences, SLAC National Accelerator Laboratory, 2575 Sand Hill Road, Menlo Park, California 94025, USA. ⁶Stanford Synchrotron Radiation Laboratory, SLAC National Accelerator Laboratory, 2575 Sand Hill Road, Menlo Park, California 94025, USA.

Keywords: cryo-EM, energy storage, battery

Research Scope

In the past decade, the development of cryo-EM technology by structural biologists have enabled near-atomic resolution imaging of sensitive biomolecules in their native state.^{1,2} Cui and Chiu labs collaborated to adopt this technique for materials science and have demonstrated breakthrough results on first atomic resolution imaging of sensitive energy materials.³⁻⁵ These first-ever images of sensitive energy materials illustrate the potential impact cryo-EM could have on energy research, opening up a wealth of research opportunities to investigate previously unknown aspects of battery operation. Our central focus is to develop and leverage innovations in cryo-EM to uncover and understand the fundamental processes governing battery operation and failure. Such dynamic processes span the entire battery architecture bridging materials and interfaces at the cathode, electrolyte, and anode, which underlie the development of advanced battery materials. Driven by important yet unanswered scientific problems across multiple length and time scales, we will pursue advances in cryo-EM to stabilize sensitive materials and interfaces in their equilibrium and metastable intermediate states. The development of cryo-EM for battery research will enable new discoveries in the short-term, while establishing cryo-EM as a foundational technique at the frontier of future energy research both within and beyond battery materials.

Recent Progress

We leveraged the cryo-EM methods to resolve several important yet unanswered scientific questions among the battery community. The rich information and fundamental findings of batteries at nanoscale in native state provide a clear understanding of crucial failure mechanisms in batteries and introduce new discoveries in energy science.

Fluorinated Species in Battery Solid-Electrolyte Interphases:

The stability of lithium batteries is tied to the physicochemical properties of the solid-electrolyte interphase (SEI). Owing to the difficulty in characterizing this sensitive interphase, the nanoscale distribution of SEI components is poorly understood.

Here, we use cryogenic scanning transmission electron microscopy

(cryo-STEM) to map the spatial distribution of SEI components across the metallic Li anode. We reveal that LiF, an SEI component widely believed to play an important role in battery passivation, is absent within the compact SEI film (~15 nm); instead, LiF particles (100–400 nm) precipitate across the electrode surface. We term this larger length scale as the indirect SEI regime. On the basis of these observations, we conclude that LiF cannot be a dominant contribution to anode passivation nor does it influence Li⁺ transport across the compact SEI film. We refine the traditional SEI structure derived from ensemble-averaged characterizations and nuance the role of SEI components on battery performance.

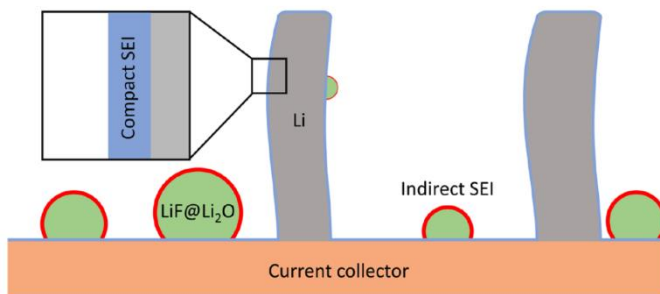


Figure 1. Schematic of the SEI structure derived from cryo-EM

Metal Dissolution Impact on Solid-Electrolyte Interphase:

Dissolution of transition metals from high-voltage cathodes and their incorporation into the solid-electrolyte interphase (SEI) of carbonaceous anodes drastically reduces the lifetime of Li-ion batteries. The effects of dissolved transition metals on the performance of carbonaceous anodes are well characterized; however, the impact on Li-metal anode performance and the SEI is rarely considered. Here, we use cryogenic electron microscopy to reveal the impact of dissolved Ni on the SEI formation process on Li-metal. A link between Ni incorporation into the SEI and the failure of Li-metal

batteries is established. We find that Ni is reduced into its metallic state and incorporates as small clusters into the SEI, locally changing the chemistry and nanostructure of the SEI. These chemical and nanostructure changes locally modify the Li-ion and electron transport properties of the SEI, accelerating electrolyte decomposition, increasing formation of “dead” Li, and ultimately causing failure.

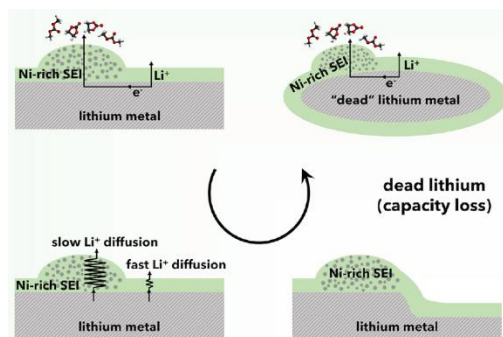


Figure 2. Schematic of Ni impurities in Lithium metal SEI

Cathode Electrolyte Interphase in Lithium Batteries: Cathode electrolyte interphase (CEI), the intimate coating layer formed on the positive electrode, has long been thought to be critical for high performance of the positive electrode. However, many aspects of CEI remain unclear. This originates from the lack of effective tools to characterize structural and chemical properties of these sensitive interphases at nanoscale. Here, we develop a protocol to preserve the native state and directly visualize the interface on the positive electrode using cryogenic electron microscopy (cryo-EM). We find that under normal operation conditions, there does not exist an intimate

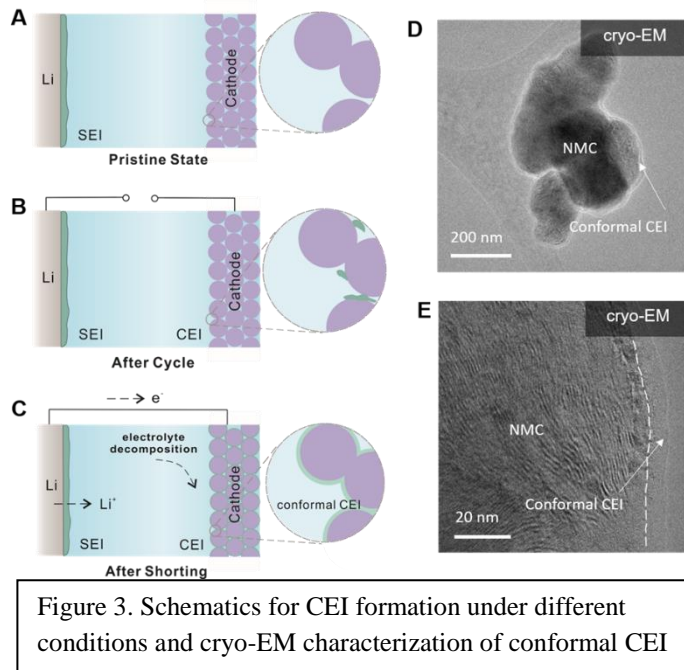


Figure 3. Schematics for CEI formation under different conditions and cryo-EM characterization of conformal CEI

coating layer at the single-particle level in commercial carbonate-based electrolyte. However, we found that upon brief external electrical shorting between anodes and cathodes, a solid-electrolyte interphase (SEI), which usually forms at the anode surface, could form on cathodes, and be electrochemically converted into a stable, conformal CEI in situ. The conformal CEI helps improve Coulombic efficiency and overall capacity retention of the battery. This generates a different perspective of the CEI in commercial carbonate-based electrolytes than previously understood.

Future Plans

We aim to develop protocols and devices to reveal the atomic structure and chemistry in batteries spanning multiple time and length scales. We will develop methods to do macroscopic cryogenic cross-sectioning of full-cell batteries for EM study and correlate the nanoscale structures with macroscale phenomena inside the real full cells. This will allow us to map the battery across different length scales. We will also develop *operando*-freezing protocols and devices to capture the transient states of batteries. By freezing the battery while applying the bias, we would have temporal resolution of what is inside a working battery. These protocols and devices will be applicable to various high energy battery materials and systems beyond lithium.

Preparing sectioned macroscale samples for cryo-EM imaging: We aim to develop efficient cryo-sectioning protocols for sample preparations for battery research. Towards complete understanding of nanoscale processes that occur during battery operation, direct observation and analysis of macroscale batteries is required, along with correlation of the nanoscale structure and chemistry to electrochemical performance of real full cells. We plan to explore two different cryogenic sectioning techniques to prepare thin samples: cryo-ultramicrotome and cryo-focused-

ion beam. Preparation of cells at different states of charge and lifetime enable a wholistic understanding of the physicochemical evolution and aging of the battery.

Development of *operando* freezing capabilities for electrochemical devices: We aim to design, engineer, and build an electrochemical plunge-freezing apparatus with optimized freezing protocols that can capture short-lived intermediates present during battery operation. To facilitate rapid temperature quenching, we will develop a model battery architecture that is suitable for fast temperature quenching. We will plunge freeze the cell while applying bias and manually disassembled inside the cryogen. This *operando*-freezing protocols and first-generation device would allow us to investigate important research questions, such as SEI formation kinetics at early timescales, transient distribution of electrolyte components during battery operation, etc.

High resolution imaging of sensitive battery materials beyond Li metal: We aim to reveal the atomic structure and chemistry of sensitive battery materials beyond Li metal. In principle, materials that are weakly bound (lower melting point) and less conductive (both electronically and thermally) are more susceptible to damage by the electron beam. This can make high-resolution imaging of other high energy battery materials (e.g. Na metal anode, S cathode) more challenging, even at cryogenic temperatures. Moreover, it is important to define and quantify electron beam damage for each materials system so that standard protocols and metrics of “stability” can be established.

References

1. W. Chiu and K.H. Downing. *Editorial Overview: Exciting Advances in CryoEM Herald a New Era in Structural Biology*, *Curr Opin Struct Biol* **46**, iv–viii (2017).
2. A. Merk, A. Bartesaghi, S. Banerjee, V. Falconieri, P. Rao, M. Davis, R. Pragani, M. Boxer, L.A. Earl, J. Milne and S. Subramaniam. *Breaking Cryo-EM Resolution Barriers to Facilitate Drug Discovery*, *Cell* **165**, 1698–1707 (2016).
3. Y. Li, Y. Li, A. Pei, K. Yan, Y. Sun, C. Wu, L. Joubert, R. Chin, A.L. Koh, Y. Yu, J. Perrino, B. Butz, S. Chu and Y. Cui. *Atomic structure of sensitive battery materials and interfaces revealed by cryo–electron microscopy*, *Science* **358**, 506–510 (2017).
4. Y. Li, W. Zhou, Y. Li, W. Huang, Z. Zhang, G. Chen, H. Wang, G. Wu, N. Rolston, R. Vila, W. Chiu and Y. Cui. *Unravelling Degradation Mechanisms and Atomic Structure of Organic-Inorganic Halide Perovskites by Cryo-EM*. *Joule* **3**, 2854–2866 (2019).
5. Y. Li, K. Wang, W. Zhou, Y. Li, R. Vila, W. Huang, H. Wang, G. Chen, G. Wu, Y. Tsao, H. Wang, R. Sinclair, W. Chiu and Y. Cui. *Cryo-EM Structures of Atomic Surfaces and Host-Guest Chemistry in Metal-Organic Frameworks*. *Matter* **1**, 428–438 (2019).

Publications

1. W. Huang, H. Wang, D.T. Boyle, Y. Li and Y. Cui, *Resolving Nanoscopic and Mesoscopic Heterogeneity of Fluorinated Species in Battery Solid-Electrolyte Interphases by Cryogenic Electron Microscopy*, *ACS Energy Lett.* **5**, 1128-1135 (2020).

2. Y. Li, Y. Li, W. Huang, W. Chiu, Y. Cui, *Opportunities for cryogenic electron microscopy in materials and nano science*, ACS Nano **14**, 9263–9276 (2020).
3. R. A. Vila, W. Huang, and Y. Cui, *Nickel impurities in the solid-electrolyte interphase of lithium metal anodes revealed by cryogenic electron microscopy*, Cell Rep Phys Sci, (2020). (In Press)
4. Z. Zhang, J. Yang, W. Huang, H. Wang, W. Zhou, Y. Li, Y. Li, J. Xu, W. Huang, W. Chiu, and Y. Cui, *Cathode Electrolyte Interphase in Lithium Batteries Revealed by Cryogenic Electron Microscopy*, (Matter, In Review)
5. D. T. Boyle, W. Huang, H. Wang, Y. Li, H. Chen, Z. Yu, Z. Bao, and Y. Cui, *Corrosion of Lithium Metal Anodes During Storage and its Nanoscopic Origins*” (submitted)
6. K. Sytwu, M. Vadai, F. Hayee, D. K. Angell, A. Dai, J. Dixon, and J. Dionne, *Driving energetically-unfavorable dehydrogenation dynamics with plasmonics* (Science, In Review).

Spin Physics and Nanoscale Probes of Quantum Materials

David Goldhaber-Gordon¹, Marc Kastner¹, Hari C. Manoharan¹, Joseph Orenstein²

¹ *Stanford Institute for Materials and Energy Sciences, SLAC National Accelerator Laboratory & Department of Physics, Stanford University;* ² *Lawrence Berkeley National Laboratory & Department of Physics, University of California, Berkeley*

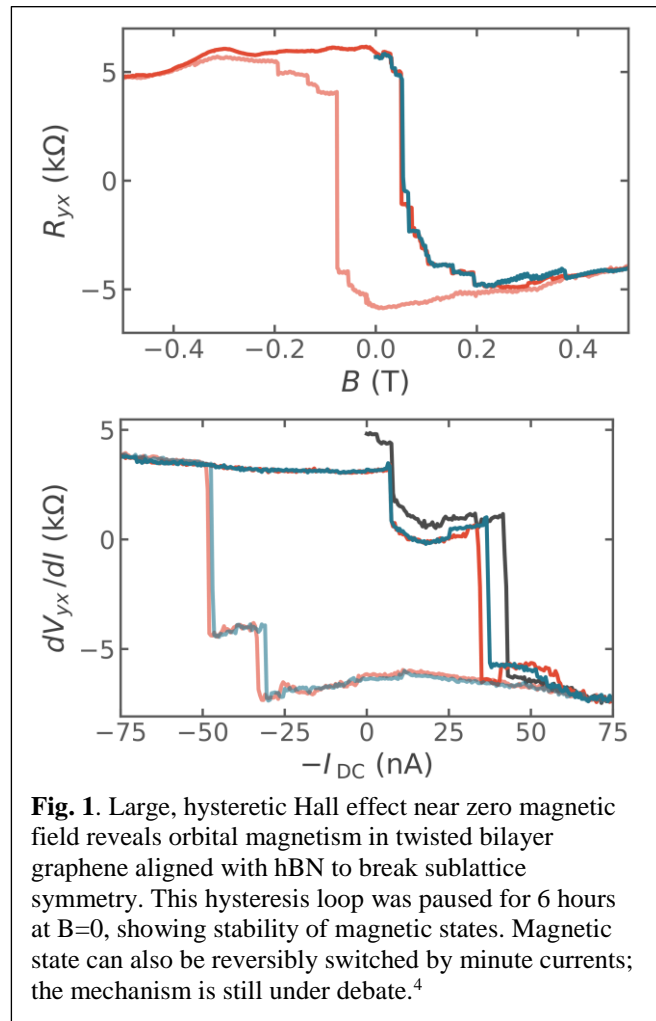
Keywords: Magnetism, Topological Insulator, 2D Materials, Local Probes, Spectroscopy

Research Scope

The Spin Physics and Nanoscale Probes of Quantum Matter FWP, co-located at SIMES/SLAC and LBNL, has the vision of assembling a world-class collaboration to fabricate and characterize material systems, in which electron spin plays an essential role in giving rise to emergent phenomena, such as topological order and exotic quasiparticles. In particular, the FWP focuses on the discovery of new states of quantum matter and novel physical effects associated with spin, isospin, and electronic degrees of freedom. The overarching goal of the research team is to observe and manipulate these quantum states at microscopic to mesoscopic scales, and to use the resulting insights to design and identify transformative quantum materials with tailored functionality.

Recent Progress

Quantum Anomalous Hall. Studies on two-dimensional electron systems in a strong magnetic field first revealed the quantum Hall (QH) effect, a topological state of matter featuring a finite Chern number and chiral edge states. Haldane later theorized that Chern insulators with integer QH effects could appear in lattice models with complex hopping parameters even at zero magnetic field. Such behaviors have now been experimentally seen in both magnetically doped 3D chalcogenide-based topological insulator thin films and graphene-based moiré systems. We have been studying both of these, and exploring their possibilities, similarities, and differences. Specifically, we discovered perhaps the first orbital ferromagnet¹ (also a Chern insulator, as beautifully verified by Andrea Young et al.²) at zero external magnetic field, in twisted bilayer graphene aligned with hexagonal boron nitride. With Feng Wang, we also showed that the ABC-trilayer graphene/hexagonal boron nitride (ABC-TLG/hBN) moiré superlattice also displays a correlated Chern insulator.³ These states are highly electrically tunable.



This has also been a period of technique and infrastructure development as our FWP has refocused on new experimental problems and the tools needed to address them. The teams of **Goldhaber-Gordon** and **Kastner** have entirely rebuilt a scanning gate microscope operating at dilution refrigerator temperatures to reduce electrical and vibrational noise, and have begun to probe electron flow in graphene-based heterostructures with engineered bandstructure. **Manoharan** has developed a novel scanning electrometer based on monitoring the frequency shift of a single vibron THz excitation in a molecule on the tip of an STM. Over controlled substrates, this probe has demonstrated a sensitivity of $\pm 0.001e$ while imaging otherwise hidden charge fluctuations in a surface 2D electron gas. **Orenstein** has designed and installed a new scanning optical cryostat, with polarization-preserving and magneto-optic capabilities. Its lower base temperature ($< 1.7\text{K}$) has been planned to support probing the nature of magnetic states in graphene-based moiré systems and spin liquid candidates, in collaboration with **Goldhaber-Gordon** and **Kastner**.

Future Plans

We will focus on magnetism in 2D materials, especially moiré-induced flat bands, as well as junctions between superconductors and other electronic phases (topological insulators, magnets, etc.) In trying to understand and manipulate such systems, **Orenstein** will perform THz spectroscopy⁵ and time-resolved Kerr effect measurements on the same samples **Manoharan** and **Goldhaber-Gordon** probe by scanning tunneling spectroscopy, atomic force microscopy, and other more specialized scanning probe microscopies, and **Goldhaber-Gordon** and **Kastner** by transport and RF studies. **Goldhaber-Gordon** will pattern samples, following design ideas from all team members. **Orenstein** will map magnetization patterns and correlate them with potential drops measured with those other techniques. **Kastner** will work with the other investigators to plan, guide, and interpret experiments.

References

1. Aaron L. Sharpe, Eli J. Fox, Arthur W. Barnard, Joe Finney, Kenji Watanabe, Takashi Taniguchi, M. A. Kastner, and David Goldhaber-Gordon, Emergent ferromagnetism near three-quarters filling in twisted bilayer graphene. *Science* 365 (6453), 605 (2019).
2. Guorui Chen, Aaron L. Sharpe, Eli J. Fox, Ya-Hui Zhang, Shaoxin Wang, Lili Jiang, Bosai Lyu, Hongyuan Li, Kenji Watanabe, Takashi Taniguchi, Zhiwen Shi, T. Senthil, David Goldhaber-Gordon, Yuanbo Zhang, and Feng Wang, Tunable correlated Chern insulator and ferromagnetism in a moiré superlattice. *Nature* 579 (7797), 56 (2020).
3. M. Serlin, C. L. Tschirhart, H. Polshyn, Y. Zhang, J. Zhu, K. Watanabe, T. Taniguchi, L. Balents, and A. F. Young, Intrinsic quantized anomalous Hall effect in a moiré heterostructure, *Science* 367, 900 (2020)/
4. Wen-Yu He, David Goldhaber-Gordon, and K. T. Law, Giant orbital magnetoelectric effect and current-induced magnetization switching in twisted bilayer graphene. *Nat. Commun.* 11, 1650 (2020).
5. Liang Wu, A. Little, E. E. Aldape, D. Rees, E. Thewalt, P. Lampen-Kelley, A. Banerjee, C. A. Bridges, J.-Q. Yan, D. Boone, S. Patankar, D. Goldhaber-Gordon, D. Mandrus, S. E. Nagler, E. Altman, and J. Orenstein, Field evolution of magnons in $\alpha\text{-RuCl}_3$ by high-resolution polarized terahertz spectroscopy, *Phys. Rev. B* 98, 094425 (2018).

Publications

1. Liang Wu, A. Little, E. E. Aldape, D. Rees, E. Thewalt, P. Lampen-Kelley, A. Banerjee, C. A. Bridges, J.-Q. Yan, D. Boone, S. Patankar, D. Goldhaber-Gordon, D. Mandrus, S. E. Nagler, E. Altman, and J. Orenstein, Field evolution of magnons in α -RuCl₃ by high-resolution polarized terahertz spectroscopy, *Phys. Rev. B* 98, 094425 (2018).
2. E. J. Fox, I. T. Rosen, Yanfei Yang, George R. Jones, Randolph E. Elmquist, Xufeng Kou, Lei Pan, Kang L. Wang, D. Goldhaber-Gordon, Part-per-million quantization and current-induced breakdown of the quantum anomalous Hall effect, *Phys. Rev. B* 98, 075145 (2018).
3. Ilan T. Rosen, Indra Yudhistira, Girish Sharma, Maryam Salehi, M. A. Kastner, Seongshik Oh, Shaffique Adam, and David Goldhaber-Gordon, Absence of strong localization at low conductivity in the topological surface state of low-disorder Sb₂Te₃, *Phys. Rev. B* 99, 201101 (2019).
4. Aaron L. Sharpe, Eli J. Fox, Arthur W. Barnard, Joe Finney, Kenji Watanabe, Takashi Taniguchi, M. A. Kastner, and David Goldhaber-Gordon, Emergent ferromagnetism near three-quarters filling in twisted bilayer graphene. *Science* 365, 605 (2019).
5. Guorui Chen, Aaron L. Sharpe, Eli J. Fox, Ya-Hui Zhang, Shaoxin Wang, Lili Jiang, Bosai Lyu, Hongyuan Li, Kenji Watanabe, Takashi Taniguchi, Zhiwen Shi, T. Senthil, David Goldhaber-Gordon, Yuanbo Zhang, and Feng Wang, Tunable correlated Chern insulator and ferromagnetism in a moiré superlattice. *Nature* 579, 56 (2020).
6. J. Figgins, L. S. Mattos, W. Mar, Y. T. Chen, H. C. Manoharan, and D. K. Morr, Quantum engineered Kondo lattices. *Nat. Commun.* 10, 5588 (2019).
7. Monica Allen, Yongtao Cui, Eric Yue Ma, Masataka Mogi, Minoru Kawamura, Ion Cosma Fulga, David Goldhaber-Gordon, Yoshinori Tokura, and Zhi-Xun Shen, Visualization of an axion insulating state at the transition between 2 chiral quantum anomalous Hall states, *Proceedings of the National Academy of Sciences* 116, 14511 (2019).
8. Maja D. Bachmann, Aaron L. Sharpe, Arthur W. Barnard, Carsten Putzke, Markus König, Seunghyun Khim, David Goldhaber-Gordon, Andrew P. Mackenzie, and Philip J. W. Moll, Supergeometric electron focusing on the hexagonal Fermi surface of PdCoO₂, *Nature Comm.* 10, 5081 (2019).
9. Guorui Chen, Aaron L. Sharpe, Patrick Gallagher, Ilan T. Rosen, Eli J. Fox, Lili Jiang, Bosai Lyu, Hongyuan Li, Kenji Watanabe, Takashi Taniguchi, Jeil Jung, Zhiwen Shi, David Goldhaber-Gordon, Yuanbo Zhang, and Feng Wang, Signatures of tunable superconductivity in a trilayer graphene moiré superlattice, *Nature* 572, 215 (2019).
10. Wen-Yu He, David Goldhaber-Gordon, and K. T. Law, Giant orbital magnetoelectric effect and current-induced magnetization switching in twisted bilayer graphene. *Nat. Commun.* 11, 1650 (2020).

Direct Probing Charge and Spin Behaviors in Ferroics

Myung-Geun Han, Joseph Garlow and Yimei Zhu
Department of Condensed Matter Physics and Materials Science
Brookhaven National Laboratory, Upton, NY 11973

Keywords: Multiferroics, Topological defects, Skyrmions, *In situ* TEM, Domain switching dynamics

Research Scope

The focus of this research task under the FWP Number MA-015-MACA is to study charge and spin behavior and their ordering, especially those related topological defects, including ferroic domain walls, vortices and chiral textures in ferroelectric and ferromagnetic systems under external stimuli to unveil the underlying physical principles that control emergent macroscopic functionalities. The research areas include 1) intriguing electronic or magnetic phenomena at domain walls and interfaces, and 2) understanding topological natures and switching pathway of charge and spin textures under external stimuli. We utilize *in situ* electron microscopy to study dynamics and functionalities of topological defects across phase transitions under external electric/magnetic fields under controlled cooling or heating. The research areas of ultrafast electron microscopy and instrumentation as well as electronic inhomogeneities are covered by a separate abstract.

Recent Progress

In the last two years, our research focus was mainly on manipulation of domain walls and topological defects in various ferroic systems using *in situ* TEM methods.

Deterministic electric-field control of ferroelastic and ferroelectric domain walls

Electric field-control of ferroelastic domain switching is a key to achieve large electromechanical responses. However, in epitaxial thin films, ferroelastic switching is profoundly suppressed due to substrate clamping. In the study of a bilayered PZT

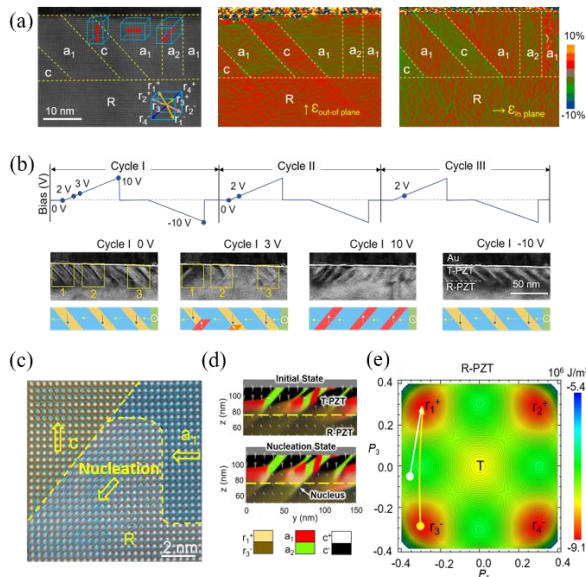


Fig. 1. (a) High-angle annular dark-field scanning transmission electron microscopy image of the T/R-PZT bilayer and corresponding out-of-plane/in-plane strain maps obtained by geometrical phase analysis. Polytwin domains with in-plane (a_1 and a_2) and out-of-plane (c) polarizations are observed in the T-PZT layer. (b) In situ bright-field TEM images obtained in the course of three cycles of voltage sweep, showing reproducible ferroelastic domain switching in the T-PZT layer. Schematics of domain structures are shown below each images. Note that the orientation of the c/a domain walls is rotated by 90° . (c) Atomic-resolution image showing the nucleation site near the interface. The Zr/Ti atomic displacements (blue arrows) and polarization (yellow arrows) are overlaid. (d) Simulated domain structures at initial state and nucleation state. (e) Energy landscape highlighting the preferred switching paths.

heterostructure, we show the reproducible ferroelastic domain switching in and elucidate its fundamental switching mechanism^[1]. The bilayer consisting of two polymorphs, tetragonal $\text{PbZr}_{0.2}\text{Ti}_{0.8}\text{O}_3$ (T-PZT) and rhombohedral $\text{PbZr}_{0.55}\text{Ti}_{0.45}\text{O}_3$ (R-PZT), was grown on SrTiO_3 . Geometric phase analysis shows typical c/a polydomain (polytwin, 90° domains) structures in the T-PZT layer and monodomain state in the R-PZT layer. Our *in situ* TEM experiment shows ferroelastic domain switching induced by external electric fields in a deterministic manner (i.e., the c/a domain wall orientation is rotated by 90°) and the nucleation occurs at the triple junction where the T/R-PZT interface meets the c/a domain wall). Phase-field simulation confirms the triple junction as the prominent nucleation sites, reducing the length of switching path on energy landscape and lowers the energy barrier. This ferroelectric-interface engineering approach presents a viable path towards thin film electromechanical devices with high performance potentials.

Topologically nontrivial spin structures in two-dimensional materials

The recent discovery of ferromagnetic order in two-dimensional (2D) materials provides an additional degree of freedom in engineering 2D heterostructures and devices for quantum information science. We show that topologically nontrivial magnetic-spin states, skyrmionic bubbles, can be realized in exfoliated insulating 2D van der Waals $\text{Cr}_2\text{Ge}_2\text{Te}_6$ (CGT)^[2]. Due to the competition between dipolar interactions and uniaxial magnetic anisotropy, hexagonally packed nanoscale bubble lattices emerge by cooling with magnetic field applied along the out-of-plane

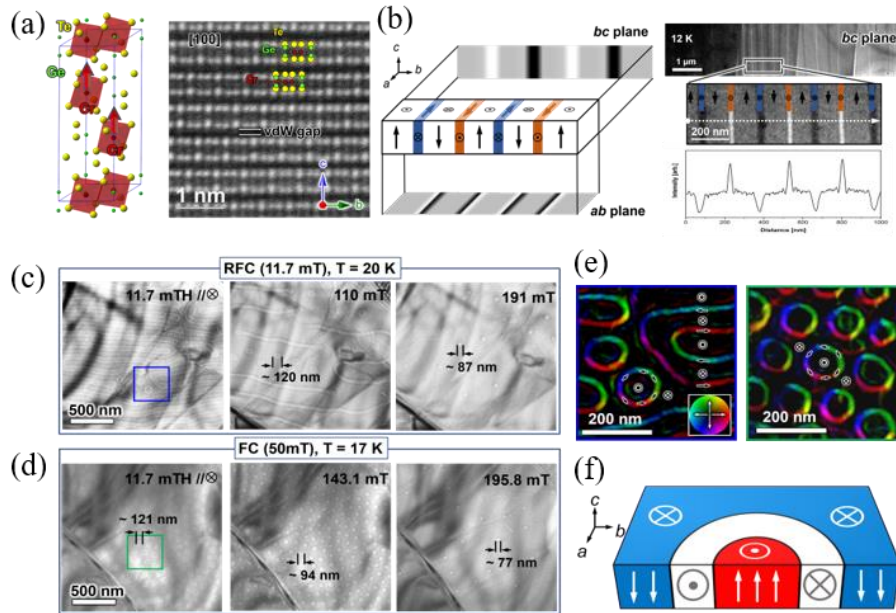


Fig. 2. (a) Schematic of crystal structure showing Cr spin arrangement and atomic resolution STEM image. (b) orientation-dependent magnetic contrast due to strong anisotropy along the c -axis, and thickness-dependent domain population, demonstrating the intrinsic magnetic anisotropy. Top right panel shows the four sections with 91, 133, 185, and 301 nm in thickness (from left to right). (c) Lorentz images from exfoliated CGT flakes after residual-field cooling (RFC), showing change in magnetic spin structure from stripe domains to skyrmionic bubbles. (d) Lorentz images after field-cooling (FC). Hexagonally packed skyrmionic bubble lattices are observed after FC. (e) Magnetization maps obtained by transport-intensity-equation (TIE) method from the areas indicated with blue and green boxes in the Lorentz images. (f) Schematic of spin structure.

direction. Our observations of homochiral skyrmionic bubbles provide a new avenue for designing 2D-material based novel quantum states. CGT is a ferromagnetic insulator with a band gap of ~ 0.74 eV, a strong uniaxial anisotropy with an easy axis perpendicular to the ab plane, rendering it a promising platform to realize skyrmionic bubbles. We found that stripe domains spontaneously develop below $T_c \sim 64$ K in thin samples, demonstrating strong intrinsic perpendicular anisotropy. Due to the competition between dipolar interactions and uniaxial magnetic anisotropy, hexagonally

packed nanoscale bubble lattices emerge by field cooling with magnetic field applied along the out-of-plane direction. Despite the lack of symmetry breaking the Dzyaloshinskii-Moriya interaction (DMI), skyrmionic bubble lattices in CGT are single-chiral, in contrast to other skyrmionic bubbles with random chirality reported in centrosymmetric magnets. Our observation of topologically nontrivial homochiral skyrmionic bubbles in exfoliated vdW materials provides a new avenue for novel quantum states in atomically thin insulators for magneto- electronic and quantum devices.

In order to better and quantitatively understand complex topological spin textures, we developed a methodology combining Fresnel propagator simulations with tilt-series Lorentz phase microscopy, which allows us to characterize three-dimensional spin textures, especially in multilayer films, beyond the small defocus limit for Lorentz imaging^[3]. We also systematically studied skyrmion dynamics in insulating multiferroic Cu_2OSeO_3 and their collective control by in-situ cryo-Lorentz phase microscopy. We investigated helical-skyrmion phase transitions as function of temperature, magnetic field, Te-doping, and sample thickness. Two novel phenomena in chiral spin textures were observed: anisotropic scaling and skyrmion channeling with a fixed-Q state^[4]. This results provide a viable way toward controlled manipulation of skyrmion lattices, envisaging chirality-controlled skyrmion flow circuits and enabling precise measurement of emergent electromagnetic induction and topological Hall effects in skyrmion lattices.

Future Plans

Expanding our study on charge-spin-lattice interactions to quantum regimes, we will study topological charge and spin textures and their emergent phenomena under magnetic and/or electric fields at low temperatures.

Electric-field/current control of magnetic skyrmions

Using our custom-designed electrical biasing liquid-helium cooling holder we will study electric field and current effects on topological spin textures in chiral and 2D magnets, which can greatly broaden the research scope in quantum materials. Insulating Cu_2OSeO_3 is an ideal platform to achieve electric field control of skyrmion lattices due to its magnetoelectric coupling arising from magnetism-induced inversion symmetry breaking (i.e., a type-II multiferroic). Our preliminary study shows that the helicity of skyrmions can be reversed by external electric fields (Fig.3c). However, such helicity reversal would require a sign change of DMI vector, that is locked by underlying crystal structure. We will focus on revealing underlying physical origin for the helicity reversal behavior observed in our preliminary experiments to shed lights on electric-field control of chiral spin textures.

In addition, we will also study electric current effects on skyrmionic bubbles in ferromagnetic Kagome metal Fe_3Sn_2 . We have experimentally confirmed the skyrmionic bubble lattices in this system that is directly coincided with the thermopower anomaly. Based on our preliminary results shown in Fig. 3g, we found the stability of skyrmionic bubbles is dramatically affected by electric current. We will explore further these electrical current effects on skyrmionic bubbles focussing on their topological Hall effects. Last, but not least, we will directly image radio-frequency-excited magnons in skyrmion lattices at the picosecond time scale using our tunable electron beam pulser system^[5]. Our study will provide viable controlling knobs over skyrmions and their lattices in both phase and temporal domains.

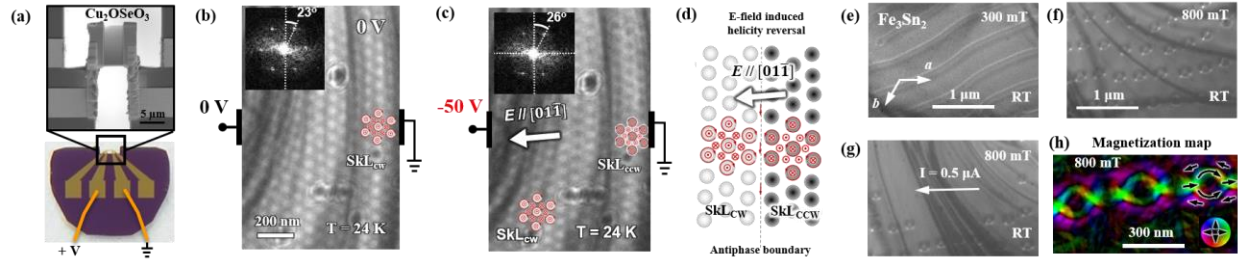


Fig. 3. Electric field/current control of topological spin textures. (a) A TEM-ready device sample prepared by focused ion beam connected to the Au electrodes for *in situ* electrical biasing at liquid-helium temperature. (b) A Lorentz TEM image taken under an external magnetic field (~ 93 mT) along the viewing direction at $T = 24$ K showing a single chiral skyrmion lattice with clockwise in-plane spin rotation sense (SkL_{cw}). (c) Lorentz TEM image obtained with -50 V applied showing helicity reversal behavior (i.e., formation of skyrmion lattice with counter clockwise in-plane spin rotation, SkL_{ccw}) near the electrical ground (top right). Insets in b and c are Fourier transforms of SkLs. (d) A schematic showing antiphase boundary separating two skyrmion lattices with opposite in-plane spin rotation. (e) A Lorentz TEM image under 300 mT showing stripe domains in the ab plane of Fe_3Sn_2 at room temperature. (f) Skyrmionic bubble lattices formed with increasing external magnetic field (800 mT). (g) Electric-current-induced destabilization of skyrmionic bubble. (h) A magnetization map reconstructed by the TIE method.

Polarization switching pathway in two-dimensional ferroelectrics

Electrically switchable macroscopic polarization in 2D van der Waals materials has been extensively studied thanks to their unique platforms to study fundamental electronic and structural ordering phenomena in low dimensions beyond conventional interfacial strain engineered thin films. Recently, ferroelectric switching has been demonstrated in Weyl semimetals WTe_2 and MoTe_2 with broken inversion and time-reversal symmetry. Exploring the domain structures in these polar Weyl semimetals is important because their topologically nontrivial band structures, such as Weyl points and Fermi-arc connectivity, can be manipulated via domain structures. Furthermore, orientation and/or emergent phenomena and functional properties can be harnessed in domain walls where broken inversion symmetry is restored. Combining atomic imaging and *in situ* electrical biasing in TEM, we will investigate complex phase and ferroelectric domain-wall configurations in 2D ferroelectric materials to understand their polar nature and switching pathways.

References

- [1] Y. Zhang, M.-G. Han, J. Garlow, Y. Tan, F. Xue, L.-Q. Chen, N. Valanoor, and Y. Zhu, *Deterministic ferroelastic domain switching in ferroelectric bilayers*, Nano Lett. **19**, 5319-5326 (2019).
- [2] M.-G. Han, J. Garlow, Y. Liu, H. Zhang, D. DiMarzio, D. Jariwala, P. Cedomir, and Y. Zhu, *Topological magnetic spin textures in exfoliated two-dimensional van der Waals $\text{Cr}_2\text{Ge}_2\text{Te}_6$* , Nano Lett. **19**, 7859-7865 (2019).
- [3] J. A. Garlow, P. D. Pollard, M. Beleggia, D. Tanmay, H. Yang, and Y. Zhu, *Quantification of mixed Bloch-Néel topological spin textures stabilized by the Dzyaloshinskii-Moriya interaction in Co/Pd multilayers*, Phys. Rev. Lett. **122**, 237201, 1-6 (2019).
- [4] M.-G. Han, J. Garlow, L. Camacho, Y. Kharkov, G. Vats, K. Kisslinger, K. Kato, O. Sushkov, C. Ulrich, Y. Zhu, T. Söhnel, and J. Seidel, *Scaling, rotation and channeling behavior of helical and skyrmion phases in thin films of Te-doped Cu_2OSeO_3* , Sci. Adv. **6**, eaax2138 (2020).
- [5] X. Fu, E. Wang, Y. Zhao, A. Liu, E. Montgomery, V. J. Gokhale, J. J. Gorman, C. Jing, J. W. Lau, Y. Zhu, *Laser-free ultrafast electron microscopy of electromagnetic wave dynamics*, Sci. Adv., **6** eabc3456 (2020).

Publications

(10 most relevant)

1. Y. Zhang, Y. Tan, D. Sando, L.-Q., Chen, N. Valanoor, Y. Zhu, and M.-G. Han, *Controlled nucleation and stabilization of ferroelectric domain wall patterns in epitaxial (110) bismuth ferrite heterostructures*, Adv. Funct. Mater. (in press).
2. Q. Du, M.-G. Han, Y. Liu, W. Ren, Y. Zhu, and C. Petrovic, *Room-temperature skyrmion thermopower in Fe_3Sn_2* , Adv. Quantum Technol. 2000058 (2020)
3. R. Peng, K. Zou, M.-G. Han, S. Albright, C. Lau, H. C. Xu, Y. Zhu, F. J. Walker, and C. H. Ahn, *Picoscale structural origins of superconductivity in monolayer $FeSe/SrTiO_3$* , Sci. Adv. **6**, eaay4517 (2020).
4. M.-G. Han, J. Garlow, L. Camacho, Y. Kharkov, G. Vats, K. Kisslinger, K. Kato, O. Sushkov, C. Ulrich, Y. Zhu, T. Söhnle, and J. Seidel, *Scaling, rotation and channelling behavior of helical and skyrmion phases in thin films of Te-doped Cu_2OSeO_3* , Sci. Adv. **6**, eaax2138 (2020).
5. M.-G. Han, J. Garlow, Y. Liu, H. Zhang, D. DiMarzio, D. Jariwala, P. Cedomir, and Y. Zhu, *Topological magnetic spin textures in exfoliated two-dimensional van der Waals $Cr_2Ge_2Te_6$* , Nano Lett. **19**, 7859-7865 (2019).
6. J. A. Garlow, P. D. Pollard, M. Beleggia, D. Tanmay, H. Yang, and Y. Zhu, *Quantification of mixed Bloch-Néel topological spin textures stabilized by the Dzyaloshinskii-Moriya interaction in Co/Pd multilayers*, Phys. Rev. Lett. **122**, 237201, 1-6 (2019).
7. S. Lee, A. B. Georgescu, A. T. Lee, G. Fabbri, M.-G. Han, Y. Zhu, J. W. Freeland, A. S. Disa, Y. Jia, M. P. M. Dean, F. J. Walker, S. Ismail-Beigi, and C. H. Ahn, *Strong orbital polarization in a cobaltate-titanate oxide heterostructure*, Phys. Rev. Lett. **123**, 117201, 1-7 (2019).
8. P. Zhou, L. Chen, Y. Liu, I. Sochnikov, M.-G. Han, A. T. Bollinger, X. He, Y. Zhu, I. Bozovic, and D. Natelson, *Pair tunneling in $La_{2-x}Sr_xCuO_4$ junctions above the critical temperature*, Nature **572**, 493-496 (2019).
9. Y. Zhang, M.-G. Han, J. Garlow, Y. Tan, F. Xue, L.-Q. Chen, N. Valanoor, and Y. Zhu, *Deterministic ferroelastic domain switching in ferroelectric bilayers*, Nano Lett. **19**, 5319-5326 (2019).
10. X. Chen, X. Zhang, M.-G. Han, L. Zhang, Y. Zhu, X. Xu, and X. Hong, *Magnetotransport anomaly in room temperature ferrimagnetic $NiCo_2O_4$ thin films*, Adv. Mater. **31**, 1805260 (2019).

Understanding and Controlling Entangled and Correlated Quantum States in Confined Solid-state Systems Created via Atomic Scale Manipulation

**Stephen Jesse, Ondrej Dyck, Andy Lupini, Mina Yoon - Oak Ridge National Laboratory
Prineha Narang - Harvard University**

Keywords: Scanning Transmission Electron Microscopy, Atomic manipulation, Confined quantum systems, 2D materials for quantum

Research Scope

Success of quantum information science requires the capability to tailor and control minute interactions in coupled quantum states, protect them from perturbations, establish connections to the macroscopic world, and understand their behavior at a fundamental level. Here we address these challenges by utilizing the atomically focused electron beam of a scanning transmission electron microscope (STEM) to manipulate the local atomic structure and chemistry in low-dimensional materials to build and understand quantum systems from the bottom up. Our experimental efforts integrate with multifaceted predictive theory to interpret measurements and guide materials choices and atomic scale design. This includes developing novel theoretical frameworks that model non-equilibrium processing in quantum optical centers and spin systems, their behavior within resonant cavities, and their interactions with the local environment. We aim to create, enhance, and stabilize entangled and correlated states through direct control over dopant and vacancy position and material geometry to locally tune bandgaps, electronic wavefunctions, and phonon modes, and to provide the conditions under which topological effects emerge. A key enabling aspect of this work leverages recent successes in enhancing STEM as a platform for atomic scale manipulation with the goal of scaling this up to allow fabrication of an array of defects with designed patterns. We are developing and applying these novel capabilities to control the insertion and motion of multiple dopants in low-dimensional materials to form arrays that can act as quantum centers or, according to recent theoretical predictions, can transform the material locally to imbue it with robust topologically isolated edge-states. Through this work, we will directly address open questions in the materials physics of atomic scale solid-state quantum systems by eliciting direct control of matter at the atomic scale.

Recent Progress

The focus of this project is to rationally design, controllably synthesize, characterize, and build new understanding about the quantum optical, magnetic, and electronic properties of specified local atomic scale defects and arrays of defects in suspended 2D materials systems. Recent progress has demonstrated expanding capabilities to controllably create a variety of dopant-defect complexes within the STEM and examine their properties from both experimental and theoretical standpoints. These are summarized below:

1. Controlled Insertion of Single and Heteroatomic Dopant Systems and the Role of Local Atomic Configuration and Strain. A key capability toward the fabrication of devices that harness

the quantum properties of matter at atomic scales is the ability to create structural units from a few atoms that exhibit desirable functional properties. These properties are largely dictated by the local atomic structure which is derived from bonding and chemistry. Here we demonstrate the ability to use STEM to controllably insert a wide variety of dopants [8] (Cr, Ti, Fe, Ag, Co, Ni, Si, and Pt), modulate their local bonding and defect structure (and in so doing, establish which configurations are stable), and predict properties of these systems. Figure 1 a)-c) give a visual depiction of the insertion process where the e-beam is used to eject a C atom from the lattice and an adatom sputtered from nearby source material attaches to the defect site. Leveraging theoretical insights, we drive the structural evolution of the defect through continued e-beam irradiation and use first principles theory to deepen our understanding about the energetics of the observed transformations and the emergent physical properties of the formed structures. Figure 1 d) shows an example summary of this process for a Cr defect evolving from occupation of a single vacancy to a double and then triple vacancy and predict how local arrangement and strain can tune band gaps and introduce magnetic properties [7]. We have concurrently screened candidate structures across the

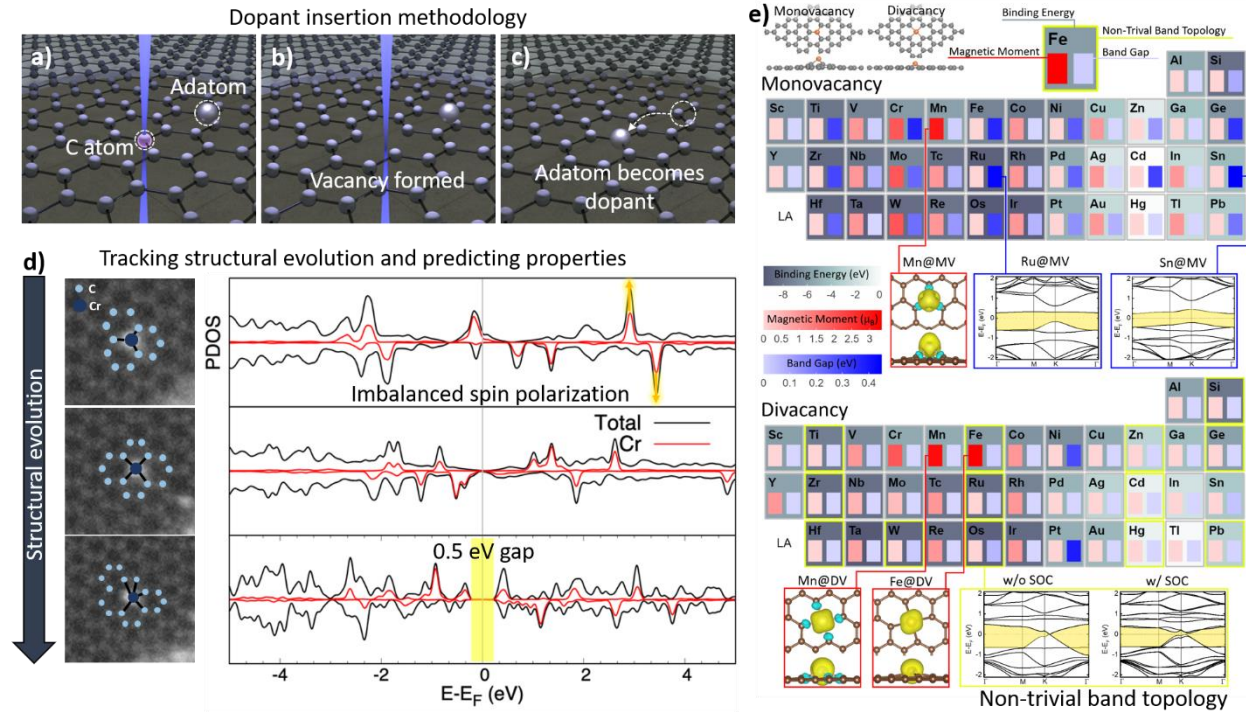


Figure 1: Summary of e-beam-directed doping, structural evolution, and theoretical screening. a)-c) Schematic diagrams illustrating the e-beam-directed doping process where a C atom is ejected from the graphene lattice and replaced with an atom sputtered from nearby source material. d) shows a summary of a three-fold coordinated Cr dopant in graphene evolving under e-beam irradiation. The calculated partial density of states (PDOS) is shown in the right-hand panel. e) Graphical summary of the methodical search through dopant structures in graphene. Dopants at monovacancies and divacancies were considered. Each tile includes color coding for the calculated binding energy, magnetic moment and band gap. Yellow highlights indicate non-trivial band topology. Structural configurations showing large magnetic moments and large band gaps are more closely shown in the call-out boxes. An example of the band topology is shown for Os.

periodic table using first principles theory to search for dopant-structures with desirable properties. Figure 1 e) shows a summary of these results where binding energies, magnetic moments, electronic band gaps, and band topology were examined for both monovacancy and divacancy dopant configurations. While single point defects, like dopants attached to mono, di, or trivacancy lattice sites, provide a sizeable property landscape to explore, more complicated structures involving several atoms and differing atomic species have been demonstrated as amenable to STEM-based synthesis (PtSi, NiSi, and AgSi) [2]. This expands the field of structural possibilities factorially. Direct observation of the structure enables and helps to guide development theoretical models to examine the properties and synthesis pathways closely.

2. Prediction of Defect Interactions for Emitter, Spin, and Topological Systems. As our ability to synthesize specific defect arrangements expands, theory and modeling developments have been directed toward predicting how *interactions* between defects in 2D materials can be leveraged to induce desirable quantum behaviors and thus provide a roadmap for experimental STEM-based atomic scale synthesis targets. As one example, a new strategy is proposed to explore various quantum phases [i.e., quantum spin Hall insulators, quantum anomalous Hall insulators (QAHI), 2D magnetic Weyl semimetals, and 2D ferromagnetic semiconductors] and to achieve a topological quantum material that is stable at a high temperature. Results show that it is possible engineer the magnetic ordering as well as the band topology of 2D post-transition metal systems by simply applying strain on a substrate [6]. QAHI are a highly promising class of quantum materials in spintronic and quantum computational devices because of their incredibly precise quantization and their robustness against defects along spin-polarized edge electron channels. Realization of the high-temperature QAH effect has been hindered by the difficulty of simultaneously controlling both magnetization and spin-orbit coupling (SOC). Thus, it is of great significance to discover new QAHI with both larger SOC gaps and higher ferromagnetic critical

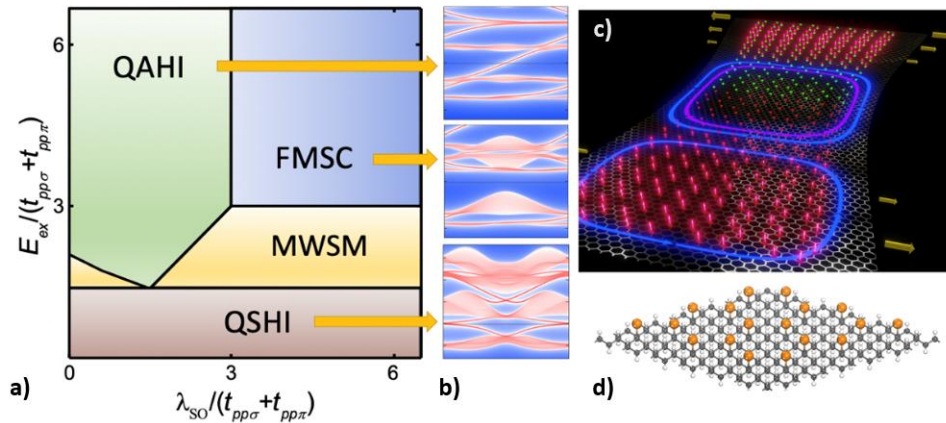


Figure 2: We propose a new realistic strategy to engineer topological and magnetic properties of 2D hexagonal lattices consisting of post-transition metals. a) Versatile quantum phases, including quantum anomalous Hall insulators, quantum spin Hall insulators, 2D magnetic Weyl semimetals, and 2D ferromagnetic semiconductors, can be achieved by simply changing local strain. b) shows corresponding band structure. c) shows a conceptual diagram illustrating how strain can be used to control magnetic and topological properties. d) shows the atomic configurations of 2D Sn on graphane

temperature. This work represents an important scientific advancement and impact because it realizes the first magnetic post-transition metal systems and high-temperature QAHI in terms of both materials and design principles. Figure 2d shows the atomic configurations of 2D Sn on graphane. The phase diagram in Figure 2a, based on the Tight-binding (TB) Hamiltonian, delineates different quantum phases in the phase space of λ_{SO} (spin-orbit coupling) and E_{ex} (magnetic exchange interaction) scaled by the TB hopping parameters. Band structures that represent each phase are shown in Figure 2b.

Parallel work has focused on understanding emission from coupled defect pairs. Scalable quantum systems require deterministic entangled photon pair sources. Recent results [9] demonstrate a scheme that uses a dipole-coupled defect pair to deterministically emit polarization-entangled photon pairs. Based on this scheme, we predict spectroscopic signatures and quantify the entanglement with physically realizable system parameters and describe how the Bell state fidelity and efficiency can be optimized by precisely tuning transition frequencies. A defect-based entangled photon pair source would offer numerous advantages including flexible on-chip photonic integration and tunable emission properties via external fields, electromagnetic environments, and defect selection. Related work [4] has shown how modulating local phonon properties can tune photon-mediated qubit-qubit interactions. Here, optically active qubits of differing excitation energies are mutually coupled via a dispersive interaction with a shared mode of an optical cavity. By acoustically modulating the qubit excitation energies it is shown that, in fact, it is possible to tune to resonance a preselected pair of qubits and thus open a communication channel between them. This method potentially enables fast (approximately ns) and parallelizable on-demand control of many physical qubits and provides suggestions for experimental paths to verifications of these concepts will be used to guide experimental aspects of this project.

Future Plans

We are currently developing novel means to introduce atomic species to the surface of graphene and other 2D materials by in-situ evaporation within the STEM. This involves integrating local heaters/evaporators into the sample holder as well as using laser sources to evaporate material that can then be integrated into the sample. If successful, this will greatly simplify atomically precise doping and enable introduction of different elements over a predetermined array of locations. Previous work has focused primarily on modifications of graphene and future work will be directed towards establishing similar capabilities on wider classes of 2D materials including WSe₂, WS₂, and WTe₂ as they show promise for hosting quantum emitters and exhibiting useful topological states. We will also begin both in-situ and ex-situ measurements of quantum properties of synthesized defects. Theory and modelling efforts will continue to explore new promising materials-defect systems and focus on systems that have been demonstrated experimentally including magnetic systems in order to evaluate how magnon-mediated spin qubit interactions may break optical selection rules and understand how integrating magnetic dopants into 2D lattices may

bring about spin-interactions within neighboring dopants as a means to tune magnonic and optical properties.

Publications

1. O. Dyck, S. Jesse, N. Delby, S. V. Kalinin, and A. R. Lupini, *Variable voltage electron microscopy: Toward atom-by-atom fabrication in 2D materials*, *Ultramicroscopy* **211**, 112949, (2020).
2. O. Dyck, C. Zhang, P. D. Rack, J. D. Fowlkes, B. Sumpter, A. R. Lupini, S. V. Kalinin, and S. Jesse, *Electron-beam introduction of heteroatomic Pt–Si structures in graphene*, *Carbon* **161**, 750 (2020).
3. D. Ondrej, L. David, K. Songkil, J. Stephen, and S.V. Kalinin, *Direct matter disassembly via electron beam control: Electron-beam-assisted catalytic etching of graphene by nanoparticles*, *Nanotechnology* **31**, 24 (2020).
4. T. Neuman, M. Trusheim, P. Narang, *Selective acoustic control of photon-mediated qubit-qubit interactions* *Phys. Rev. A* **101** (5), 052342 (2020)
5. K. Head-Marsden, J. Flick, C. Ciccarino, P. Narang *Quantum information and algorithms for correlated quantum matter* Accepted Chemical Review
6. L. Zhang, C. Park, and M. Yoon, *Quantum phase engineering of two-dimensional post-transition metals by substrates: Toward a high-temperature quantum anomalous Hall insulator*, accepted *Nano Lett.*
7. O. Dyck, M. Yoon, A. R. Lupini, J. Swett, S. Jesse, *Atomic-scale doping of Cr in graphene to design materials from the atom up: A joint experimental and theoretical exploration*, under review Carbon.
8. O. Dyck, L. Zhang, M. Yoon, J.L. Swett, D. Hensley, C. Zhang, P.D. Rack, J.D. Fowlkes, A.R. Lupini, S. Jesse, *Doping transition-metal atoms in graphene for atomic-scale tailoring of electronic, magnetic, and quantum topological properties*, under review, *Adv. Func. Mat.*
9. D. S. Wang, T. Neuman, P. Narang. *Dipole-coupled defect pairs as deterministic entangled photon pair sources*. Under review *Phys. Rev. Lett.*
10. K. Head-Marsden, S. Krastanov, D. A. Mazziotti, P. Narang, *Capturing non-Markovian dynamics on near-term quantum computers*, *Phys. Rev. Lett.*

Learning the physics and chemistry of materials from structural STEM data

S.V. Kalinin, M.F. Chisholm, C.T. Nelson, A.R. Lupini, and M.P. Oxley

Center for Nanophase Materials Sciences, Oak Ridge National Laboratory, TN 37831

Keywords: scanning transmission electron microscopy, machine learning, ferroelectrics, quantum materials, variational autoencoders, Bayesian inference

Research Scope

Rich functionalities of quantum and strongly correlated materials emerge from the interplay between the electronic, orbital, lattice, and spin degrees of freedom that often lead to complex structural and electronic phenomena spanning atomic to mesoscopic scales. In many cases, these phenomena are associated with translational symmetry breaking, local frozen disorder, or strongly correlated disorder. However, the relevant mechanisms and roles of individual subsystems often remain unknown. Over the last decade, Scanning Transmission Electron Microscopy has emerged as a powerful quantitative probe of materials structure on the atomic level, providing high veracity information on local chemical bonding, composition, and symmetry breaking distortions. We aim to harness the power of machine learning methods to build a comprehensive picture of the chemistry and physics of quantum materials on the level of individual atomic units, including the parsimonious structural descriptors for non-periodic solids and correlative structure-property relationships, to discover the generative physical models that give rise to the observed structures and to establish associated uncertainties, and ultimately to explore the causative mechanisms operating in materials with multiple functionalities.

Recent Progress

The focus of this project is the development and implementation of STEM imaging and spectroscopic model and their application for exploration of physics and chemistry of complex materials on atomic level. Over the last two years, we have additionally explored applications of machine learning (ML) methods to transform STEM data into materials specific descriptors and further to use these to build parsimonious, generative, and causal models of materials, along with the determination of associated uncertainties. These developments for structural STEM are summarized below:

1. Bayesian crystallography: Symmetry and symmetry breaking, are the central concepts in condensed matter physics and are well defined on the macroscopic level. We explored how symmetry and elementary building blocks can be defined on the atomic level from the experimental data and show that these definitions become Bayesian in nature. We develop rotationally invariant variational autoencoders (rVAE) as an approach to analyze latent symmetries from STEM data, and demonstrate several examples for single- and multiphase materials including

$\text{Sr}_3\text{Ru}_2\text{O}_7$ and the LSMO-NiO system. We further extend this approach to explore the mechanisms of a phase transition between the trigonal prismatic and distorted octahedral phases of layered chalcogenides in the $\text{MoS}_2 - \text{ReS}_2$ system from the observed atomic positions (arXiv:2006.10001). With this information, we build a picture of the structural transition from the atomic level and determine local and global variables controlling the local symmetry breaking. In particular, we argue that the dependence of the average symmetry breaking distortion amplitude on global and local concentration can be used to separate local chemical and global electronic effects on transitions. This approach allows the exploration of atomic mechanisms beyond the traditional macroscopic descriptions, utilizing the imaging of compositional fluctuations in solids to explore phase transitions over a range of realized and observed local stoichiometries and atomic configurations.

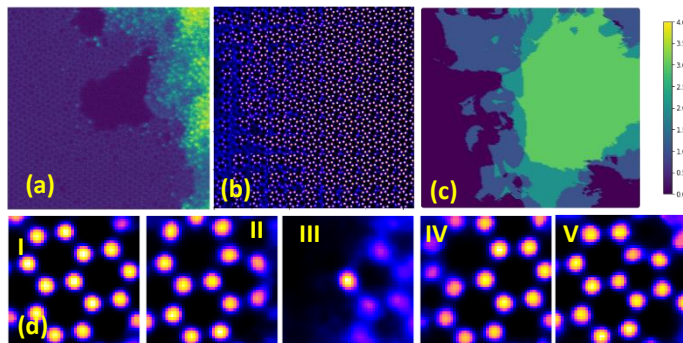


Figure 1. (a) STEM image of suspended graphene. (b) Latent space or rotational autoencoder trained on this data. (c) Number of 6-members rings adjacent to central atom (d) Several structures encoded in latent space. Note that neural network discovered molecular fragments in a fully unsupervised manner, illustrating potential of these methods to uncover physics and chemistry contained in STEM data.

2. Chemistry discovery: Structure of materials with broken long-range discrete translational symmetry including structural and dipolar glasses, spin liquids, etc. have remained one of the most fascinating areas in condensed matter physics for decades. We explore the applicability of machine learning methods, specifically rVAE and graph networks, towards the analysis of the chemical transformations in 2D materials under e-beam irradiation. We demonstrate that rVAE approach enables the effective exploration of the chemical evolution of the system based on local structural changes and may be extended to more complex systems (arXiv:2006.10267). Importantly, the rVAE allows discovery of the molecular building blocks and chemical reactions pathways in unsupervised manner, Figure 1.

3. Generative physical models: The atomic configurations visualized by STEM are directly related to the fundamental physics of the interactions giving rise to specific structures, i.e. generative models. On the mesoscale, we explore the physics of ferroelectric domain walls in

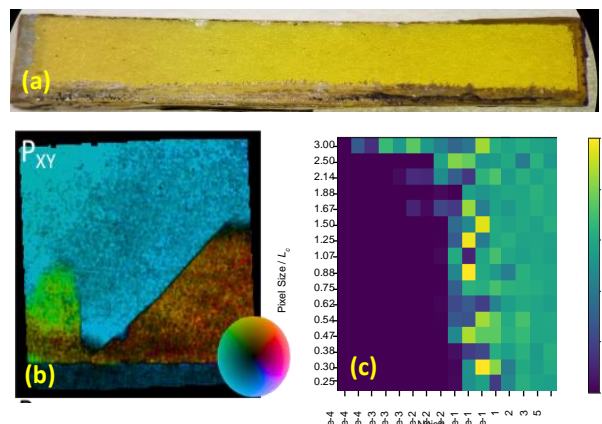


Figure 2. (a) Combinatorial library of Sm-doped BFO spans composition from ferroelectric R3c BFO to non-ferroelectric Pnma Sm-BFO, allowing to explore phase transition in composition space on atomic level. (b) Ferroelectric domains in pure BFO visualized by STEM. (c) Bayesian inference allows to establish at which resolution and noise level different models for BFO free energy can be distinguished from observational data.

BiFeO₃ using Bayesian inference analysis (arXiv:2004.09814). We demonstrate that domain wall profile shapes are ultimately sensitive to the nature of the order parameter in the material, including the functional form of the Ginzburg-Landau-Devonshire expansion, and numerical values of the corresponding parameters. The preexisting materials knowledge naturally folds into the Bayesian framework in the form of prior distributions, with different order parameters forming competing (or hierarchical) models. This inference approach both allows learning materials physics from experimental data, with associated uncertainty quantification, and establishing guidelines for instrumental development answering questions on what resolution and information limits are necessary for reliable observation of specific physical mechanisms of interest.

We further extend this approach to discrete atomistic models. Statistical distance minimization allows recovery of lattice model parameters from microscopic observations, establishes the uncertainties and reliability of such analysis in a broad parameter space, and demonstrates that reconstruction is possible well above the phase transition and in the regions of the parameter space when the macroscopic ground state of the system is poorly defined (arXiv:2004.04832, arXiv:2001.06854). This approach is general and can be further extended well beyond the lattice Hamiltonians to effectively explore parameter space of more complex off-lattice and dynamic models. We demonstrate this approach on data from a series of atomically-resolved scanning transmission electron microscopy images of Mo_xRe_{1-x}S₂ at varying ratios of Mo/Re stoichiometries, for which we propose an effective interaction model that is then used to generate atomic configurations and make testable predictions at a range of concentrations and formation temperatures. We further explore the reconstruction of atomic force fields from dynamic STEM data (arXiv:2002.05689).

4. Predictability and causative mechanisms: The knowledge of generative mechanisms is generally insufficient to understand the physics of complex materials systems with multiple competing interactions. For example, in morphotropic ferroelectrics the dopants can pin polarization; however, polarization instabilities can in turn drive cation redistribution. We explore the predictability and causality of microscopic physical mechanisms from STEM data (arXiv:2003.08575). Here, predictability of a certain effect or phenomenon is often equated with

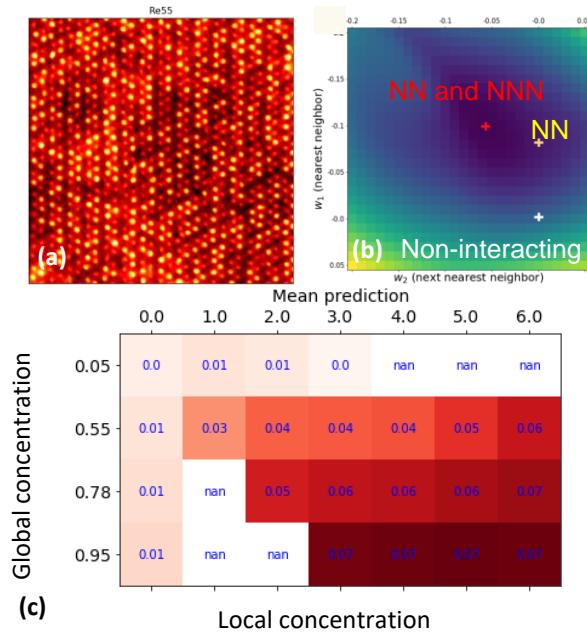


Figure 3. (a) STEM image of Re-doped MoS₂. (b) Interaction energies between Re atoms obtained from observed atomic configurations (c) Magnitude of symmetry-breaking distortion as a function of global and local composition separating the electronic and chemical effects.

the knowledge of relevant physical laws, typically understood as a functional or numerically-derived relationships between the observations and known states of the system. Correspondingly, observations inconsistent with prior knowledge can be used to derive new knowledge on the nature of the system or indicate the presence of yet unknown mechanisms. We explored the applicability of Gaussian Processing (GP) to establish predictability and uncertainty of local behaviors from multimodal observations of different groups of parameters, including the adjacent polarization values and several combinations of physical and chemical descriptors including lattice parameters, column intensities, providing an alternative to this classical paradigm. We observe that certain elements of materials domain structure including charged and uncharged domain walls and interfaces with the substrate are best predicted with specific combinations of descriptors, and this predictability and their associated uncertainties are consistent across the composition series. We further implemented the workflow for causal analysis of structural STEM data and explore the interplay between physical and chemical effects in ferroelectric perovskites across the ferroelectric-antiferroelectric phase transitions ([arXiv:2002.04245](https://arxiv.org/abs/2002.04245)). The pairwise causal criteria are used to establish the causal directions between the descriptors, ordering the data set in the causal direction. Ultimately, we believe that the causal analysis of the multimodal data will allow exploring the causal links between multiple competing mechanisms that control the emergence of unique functionalities of morphotropic materials and ferroelectric relaxors.

Future Plans

We aim to build upon our established frameworks of X-Autoencoder and encoder-decoder neural networks, where $X=\{\text{rotationally invariant, variational, etc.}\}$, and STEM data processing workflows to extract physics in systems manifesting short-range compositional/ structural/ order parameters. An exemplary case is the high susceptibility response in ferroic phase boundary/morphotropic compositions, for which we can leverage the atomic-resolution STEM combinatorial library of rare-earth (Sm) doped BiFeO_3 collected for this purpose. The principal scientific goal for this system is discovery of local parameter correlations and quantitatively bridging this with the aggregate system properties. To this end we will develop autoencoder networks to parameterize atomic STEM data, imposing known structural relationship between latent variables, as an input for statistical analysis including Bayesian inference and Gaussian process regression. From the technical standpoint this includes two significant microscopy targets: the high precision data extraction from aberrant source data (i.e. removing instrument error sources), and the unsupervised parameterization of local properties.

We further aim to extend these approaches into the Bayesian domain, which allow us to take into consideration any prior knowledge about the system and evaluate the changes in understanding of the behaviors given new experimental data. In particular, this framework allows us to systematically address questions such as: what resolution and information limits are required for observation of particular physical phenomena? Ultimately, we seek to answer questions such as: whether electronic instability due to the average Fermi level guides the development of the local atomic structure, and whether frozen atomic disorder drives the emergence of the local structural

distortions, and whether the nucleation spot of phase transition can be predicted based on observations before the transition, and what is the driving forces controlling the emergence of unique functionalities of morphotropic materials and ferroelectric relaxors?

Publications

1. M. Ziatdinov, C.T. Nelson, X. Zhang, R.K. Vasudevan, E. Eliseev, A.N. Morozovska, I. Takeuchi, and S.V. Kalinin, *Causal analysis of competing atomistic mechanisms in ferroelectric materials from high-resolution scanning transmission electron microscopy data*, npj Comp. Mat. 6, 127 (2020).
2. D. Lee, X. Gao, L. Sun, Y. Jee, J. Poplawsky, T.O. Farmer, L. Fan, E.J. Guo, Q. Lu, W.T. Heller, Y. Choi, D. Haskel, M.R. Fitzsimmons, M.F. Chisholm, K. Huang, B. Yildiz, and H.N. Lee, *Colossal oxygen vacancy formation at a fluorite-bixbyite interface*, Nature Communications, 11, 1371 (2020).
3. S. Estandia, F. Sanchez, M.F. Chisholm, J. Gazquez, *Rotational polarization nanotopologies in BaTiO₃/SrTiO₃ superlattices*, *Nanoscale* **11**, 21275 (2019).
4. M. Ziatdinov, O. Dyck, X. Li, B.G. Sumpter, S. Jesse, R.K. Vasudevan, **S.V. Kalinin**, *Building and exploring libraries of atomic defects in graphene: scanning transmission electron and scanning tunneling microscopy study*, Science Advances 5, eaaw8989 (2019)
5. M Ziatdinov, O Dyck, S Jesse, and S.V. Kalinin, *Atomic mechanisms for the Si atom dynamics in graphene: chemical transformations at the edge and in the bulk*, Adv. Func. Mat. 29, 1904480 (2019)
6. M. ZIATDINOV, **C.T. NELSON**, R.K. VASUDEVAN, D.Y. CHEN, and **S.V. KALININ**, *Building ferroelectric from the bottom up: the machine learning analysis of the atomic-scale ferroelectric distortions*, Applied Physics Letters 115, 052902 (2019)
7. A.N. Morozovska, E.A. Eliseev, C.T. Nelson, and S.V. Kalinin, *Building a free-energy functional from atomically resolved imaging: Atomic-scale phenomena in La-doped BiFeO₃*, Phys Rev. **B 99**, 195440 (2019)
8. O. Dyck, M. Ziatdinov, D.B. Lingerfelt, R.R. Unocic, B.M. Hudak, A.R. Lupini, S. Jesse, and S.V. Kalinin, *Atom-by-atom fabrication with electron beams*, Nature Materials Review 1 (2019).
9. S. Das, Y. L. Tang, Z. Hong, M. A. P. Gonçalves, M. R. McCarter, C. Klewe, K. X. Nguyen, F. Gómez-Ortiz, P. Shafer, E. Arenholz, V. A. Stoica, S.-L. Hsu, B. Wang, C. Ophus, J. F. Liu, C. T. Nelson, S. Saremi, B. Prasad, A. B. Mei, D. G. Schlom, J. Iñiguez, P. García-Fernández, D. A. Muller, L. Q. Chen, J. Junquera, L. W. Martin R. Ramesh, *Observation of room-temperature polar skyrmions* Nature 568, 368 (2019).
10. L. Vlcek, M. Ziatdinov, A. Maksov, A. Tselev, A.P. Baddorf, S.V. Kalinin, and R.K. Vasudevan, *Learning from Imperfections: Predicting Structure and Thermodynamics from Atomic Imaging of Fluctuations*, ACS Nano **13**, 718 (2019), also arXiv:1806.07475

Nanoscale quantum and classical sensing for superconducting and topological quantum information

Ben Lawrie, Eugene Dumitrescu, Gabor Halasz, Matt Brahlek, Chengyun Hua, Petro Maksymovych

Oak Ridge National Laboratory

Keywords: Quantum sensing, Vortex motion, Superconducting nanowire single photon detectors, topological quantum information

Research Scope

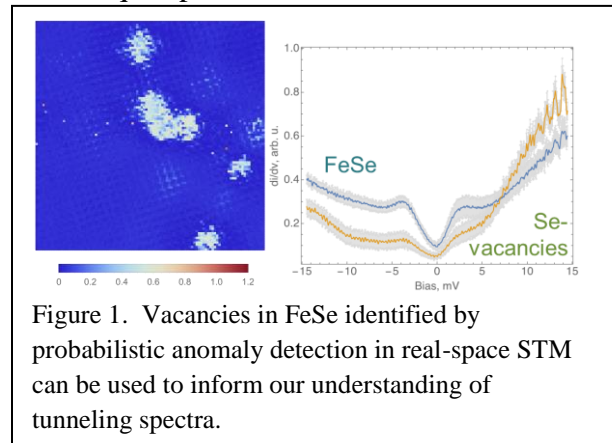
Significant progress has been made in the design of superconducting qubits in recent years, but quantum supremacy with superconducting qubit-based quantum computers remains implausible because of decoherence induced by qubit interactions with unbound Cooper pairs and low energy two-level systems, i.e., spin and charge defects. Similarly, improved control over photonic interactions with quasiparticles and vortices in superconductors will be critical to the development of next generation superconducting nanowire single photon detectors (SNSPDs), including photon-number-resolving and high T_c detectors. While a growing body of research has modeled the microscopic origins of $1/f$ noise in superconducting devices for quantum information science (QIS), there have been very limited *in situ* measurements of quasiparticle, two-level system, and vortex interactions in these prototypical quantum devices. At the same time, the detection and spatial manipulation of superconducting vortices paves a path towards the elusive task of Majorana braiding in topological superconductors—a critical step toward topological quantum computing beyond the noisy intermediate-scale quantum computing era. The overarching goal of this project is to reveal and control the fundamental nanoscale to mesoscale processes that drive qubits and quantum sensors based on topological and superconducting materials. To achieve this goal, we are addressing three research aims: (1) Develop nanoscale understanding of photon-induced vortex and quasiparticle interactions in SNSPDs for high-temperature, photon-number-resolving, single photon detectors; (2) Reveal fundamental materials limitations of superconducting qubits and resonators by understanding nanoscale interactions of quasiparticles and two-level systems; and (3) Manipulate the spatial distribution of vortex-pinned Majorana fermions in topological superconductors to enable braiding operations for topological quantum computing.

Recent Progress

Addressing our overarching goal requires a collaborative research approach that combines (1) thin film, heterostructure, and device synthesis and fabrication, (2) material and device characterization from the atomic-scale to the device-scale, and (3) analytical and numerical descriptions of superconducting quantum devices. Over the past year, we have made substantial progress in each of these areas.

Probing the ground state of unconventional superconductors We have optimized molecular beam epitaxy growth conditions for candidate topological superconductor $\text{Pd}_3\text{Bi}_2\text{Se}_2$, a strongly spin-orbit coupled superconductor that has a 2D layered Parkerite structure. A key challenge to the optimization of the intrinsic properties of high-quality ternary chalcogenides lies in the control of the elemental stoichiometry. We have found that at a sufficiently high temperature, this material can be grown in an adsorption control regime where Bi and Se are supplied in excess and the stoichiometry is controlled by the amount of Pd supplied. Excess Bi and Se evaporate due to the high vapor pressures, resulting in high-quality films that exhibit superconductivity as probed by transport and magnetization measurements. The initial thin film growth has been supported by band structure calculations, which point to the possibility of the material being topological and possibly exhibiting topological superconductivity. Because this material has a 2D structure it can be seamlessly integrated with the wide range of other 2D materials. This will enable the design and realization of novel band structures and possible spin triplet superconductivity by integration with a ferromagnet such as layered materials CrSrTe_3 or with a strongly correlated oxide such as SrRuO_3 .

New understanding of heterogeneous superconductors The characterization of superconductivity and quasiparticle and vortex dynamics in heterogeneous and nanostructured superconductors with scanning tunneling microscopy (STM) is challenging, particularly when attempting to match atomic and device-scales, thereby capturing vortex and quasiparticle effects from nanometers to tens of microns. In order to identify signatures of defects in the tunneling spectra, we have developed new unsupervised analyses of STM images of heterogeneous superconductors including FeSe and BaFe_2As_2 . Eventually these approaches will help to overcome limitations of finite acquisition time and signal to noise ratio for device-scale microscopies and provide a more comprehensive understanding of effects of disorder on electronic structure.



MilliKelvin optical microscopies Over the past year, we have developed new mesoscale optical probes for the characterization of electronic and magnetic properties at milliKelvin temperatures. In particular, we have completed the design and installation of an automated milliKelvin scanning confocal microscope and a magneto-optical Kerr effect microscope and began testing of a milliKelvin scanning NV magnetometer based on an integrated tuning fork AFM and confocal microscope installed in the same dilution refrigerator. The dilution refrigerator and milliKelvin nanopositioners were purchased and installed with LDRD funding, but the programming, design, and optimization of the automated spatially and spectrally resolved excitation and single photon detection and spectroscopy were performed as part of this FWP. Ongoing experiments are targeting mesoscale characterization of SNSPDs with scanning single photon confocal

microscopy, magneto-optical imaging of new quantum materials, and scanning laser microscopy of superconducting resonators and superconducting qubits.

Quantum Microscopies with Squeezed Light We have recently provided a proof-of-principle demonstration of quantum-enhanced readout of the displacement of an atomic force microscope microcantilever with a squeezed optical readout field¹. This work was the first to incorporate a microscope into a nonlinear interferometer so that either the squeezed light or a reference light source could interact with the microscope, thus mitigating substantial problems with laser induced heating and optical losses. Optimization of this approach could yield two orders of magnitude improvement in sensitivity for off-resonant atomic force microscopies, enabling broadband materials characterization at the nanoscale, or enabling higher speed microscopies at cryogenic temperatures.

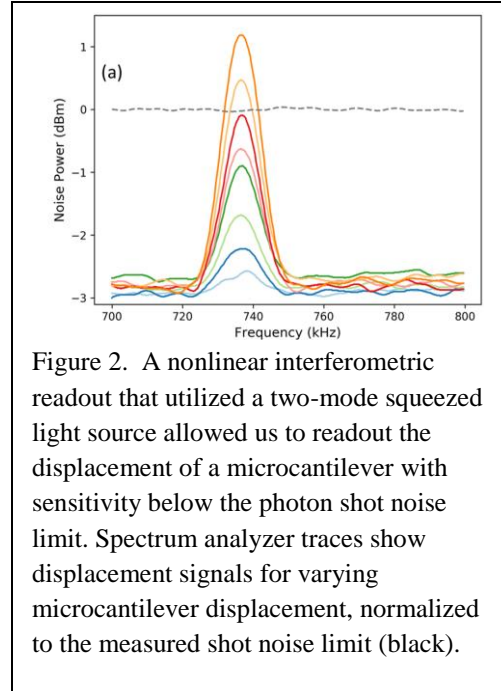


Figure 2. A nonlinear interferometric readout that utilized a two-mode squeezed light source allowed us to readout the displacement of a microcantilever with sensitivity below the photon shot noise limit. Spectrum analyzer traces show displacement signals for varying microcantilever displacement, normalized to the measured shot noise limit (black).

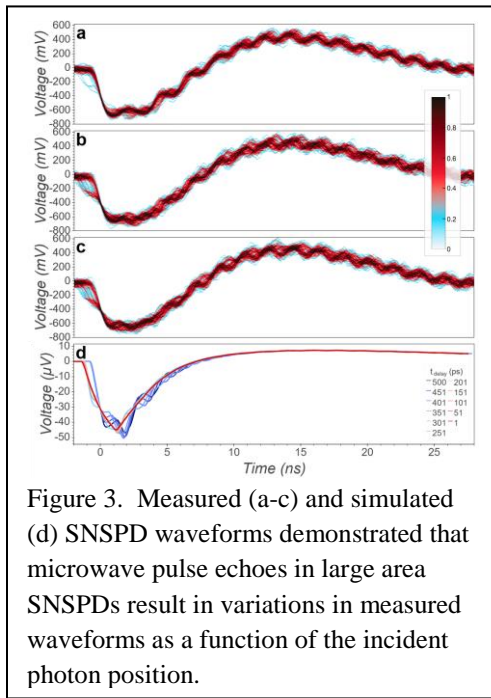


Figure 3. Measured (a-c) and simulated (d) SNSPD waveforms demonstrated that microwave pulse echoes in large area SNSPDs result in variations in measured waveforms as a function of the incident photon position.

Characterization of microwave and vortex interactions in SNSPDs at the device scale Over the past year, we have used variable spot-size excitation of SNSPDs to elucidate the effect of microwave pulse echoes on device performance, and we have characterized the SNSPD response as a function of magnetic field in order to elucidate the role of vortex dynamics in silicide-based SNSPDs². Combining dc and rf analysis of the SNSPD response in a vector magnetic field provides a fundamentally new understanding of the role of vortex dynamics in single photon detection and provides a path toward fully integrated nanophotonic quantum information science.

Robustness of Majorana zero modes to correlated disorder Majorana zero modes (MZMs) bound to superconducting vortices in 2D systems have distinct

advantages for quantum information processing because the geometry allows a greater degree of freedom in the motion of the MZMs. Notably, STM and confocal optical microscopies may be used to manipulate vortex motion and enable new paths forward for MZM braiding. While MZMs are protected against infinitesimal random disorder due to their nonlocal nature, it is important to understand the effect of experimentally plausible disorder on MZMs. We have used a combination of analytical and numerical calculations to show that disorder in a p+ip topological superconductor

is most disruptive to Majorana zero modes (and the quantum information encoded into them) when its correlation length matches the coherence length of the superconductor³.

Hybrid topological-longitudinal transmon design. We have developed the first theoretical description of a MZM coupled to a longitudinal transmon and derived phase and charge based coupling interactions for six Majorana configurations that allow parity dependent Majorana controls. We demonstrated the potential for distinguishing between parity sectors and probing quasiparticle poisoning rates and mechanisms, and we developed a charge offset scheme to preserve Majorana degeneracy, regardless of parity or spatial configuration, in the presence of capacitive coupling.

Future Plans

Over the next two years, we will bridge superconducting heterostructure synthesis and device fabrication with ongoing optical and scanning tunneling microscopies to probe and control quasiparticle, two-level-system, and vortex dynamics in superconducting devices from the nanoscale to the mesoscale. In particular, we plan to use both STM and confocal single photon microscopy to determine the fundamental constraints on current SNSPD performance and identify a path toward improved SNSPD design. We will also utilize in situ laser annealing and scanning laser microscopy to control and characterize two-level-system interactions in superconducting resonators and qubits at mK temperatures. We plan to combine angle-resolved photo-emission spectroscopy with transport measurements in lithographically patterned Little-Parks devices, and optical and scanning tunneling microscopies to characterize and manipulate Pd₃Bi₂Se₂ films. Finally, we will work toward the demonstration of scalable spatial manipulation of vortices in topological superconductors as a step toward braiding of MZMs.

References

1. R.C. Pooser, N. Savino, E. Batson, J.L. Beckey, J. Garcia, and B.J. Lawrie, *Truncated Nonlinear Interferometry for Quantum-Enhanced Atomic Force Microscopy*, Physical Review Letters, **124**, 230504 (2020).
2. C.E. Marvinney, B.E. Lerner*, A.A. Puzosky, A.J. Miller, B.J. Lawrie, *Position Sensitive Response of a Single-Pixel Large-Area SNSPD*, arXiv:2006.00126v1
3. C. Christian, E.F. Dumitrescu, G.B. Halasz, *Robustness of vortex-bound Majorana zero modes against correlated disorder* arXiv:2009.06661 (2020).

Publications

1. R.C. Pooser, N. Savino, E. Batson, J.L. Beckey, J. Garcia, and B.J. Lawrie, *Truncated Nonlinear Interferometry for Quantum-Enhanced Atomic Force Microscopy*, Physical Review Letters, **124**, 230504 (2020).
2. B. Lawrie, R. Pooser, and P. Maksymovych, *Squeezing Noise in Microscopy with Quantum Light*, Trends in Chemistry **2**, 683 (2020).

3. J. Lapano, A. R. Mazza, H. Li, D. Mukherjee, E. M. Skoropata, J. M. Ok, H. Miao, R. G. Moore, T. Z. Ward, G. Eres, H. N. Lee, M. Brahlek, *Strong spin-dephasing in a topological insulator- paramagnet heterostructure*, arXiv:2009.06827v1, Accepted in APL Materials (2020).
4. M. Brahlek, J. Lapano, J. S. Lee, *Topological Materials by Molecular Beam Epitaxy*; accepted with minor revisions by Journal of Applied Physics—Invited in the Special Issue on 2D Quantum Materials: Magnetism and Superconductivity.
5. M. Brahlek, *Criteria for realizing room temperature applications of topological materials*, arXiv 2007.02368 (2020); under review in Advanced Materials.
6. M.A. Feldman*, C.E. Marvinney, A.A. Purezky, B.J. Lawrie, *Photochromism in a Hexagonal Boron Nitride Single Photon Emitter*, arXiv:2008.05550v1, under review at Optica.
7. C.E. Marvinney, B.E. Lerner*, A.A. Purezky, A.J. Miller, B.J. Lawrie, *Position Sensitive Response of a Single-Pixel Large-Area SNSPD*, arXiv:2006.00126v1, Under review at Quantum Science and Technology.
8. C. Christian, E.F. Dumitrescu, G.B. Halasz, *Robustness of vortex-bound Majorana zero modes against correlated disorder* arXiv:2009.06661 (2020).

ERKCS89: Atomic and Mesoscopic Phenomena in Quantum Systems with Broken Translational Symmetry

4D STEM: Simulation and Quantification

Principle Investigators: M. P. Oxley, A. R. Lupini, C. T. Nelson, M. F. Chisholm, S. V. Kalinin

Center for Nanophase Materials Sciences, Oak Ridge National Laboratory, TN 37831

Keywords: STEM, CBED, Machine Learning

Sub-Program Scope

The development of high-speed cameras and direct electron detectors has led to rapid advances in the field of scanning nano diffraction, often referred to as 4D-STEM. Experimental results have improved rapidly, resulting in large data sets that can be difficult to interpret. Approaches such as ptychography recover the exit surface phase which infers information about the scattering potential. Many analysis techniques rely on reducing the large data sets by measuring the deflection of the center of mass (COM) of the convergent beam diffraction (CBED) patterns. This can be used to provide information about local structures and fields and charge densities. Both these approaches rely strongly on the phase object approximation and are thus limited to relatively thin specimens. In order to overcome these limitations, we will use machine learning techniques to analyze these large datasets. Machine learning techniques can be broadly separated into two different categories, unsupervised and supervised learning. The first is applied directly to the datasets in an attempt to reduce the dimensionality of the problem to one that can be more easily interpreted. Supervised learning requires the use of suitable training sets to train the algorithm to recognize the features of interest. This is achieved through the use of large-scale simulations of CBED patterns to generate descriptive training sets related to the material under examination. This requires a clear understanding of electron microscope parameters and accurate modelling of possible material configurations.

Recent Progress

To extract relevant physical behaviors from the 4D STEM data, it is essential that the training sets used are representative of the experimental data to avoid out of the distribution effects in ML and observational biases and confounders during physics interpretation. This means that as well as realistic structural models and accurate simulations, that microscope parameters must be correctly incorporated. It has been previously shown that the addition of a source size blur to image simulations, to account for the finite size of the electron source, is required to obtain quantitative agreement between experimental STEM images and simulations. For realistic training sets we need to include the affects of spatial incoherence on the CBED pattern itself. This requires the simulation of CBED patterns on a suitably fine spatial mesh allowing the CBED patterns to be

added in using a weighting describing the source distribution. In addition, for lower acceleration voltages, temporal incoherence must also be included by summing over a suitable range of defocus values. We have shown that this not only changes the COM distribution of the CBED patterns, but also the nature of the CBED patterns themselves¹. This is illustrated in Fig. 1 for a 60 kV

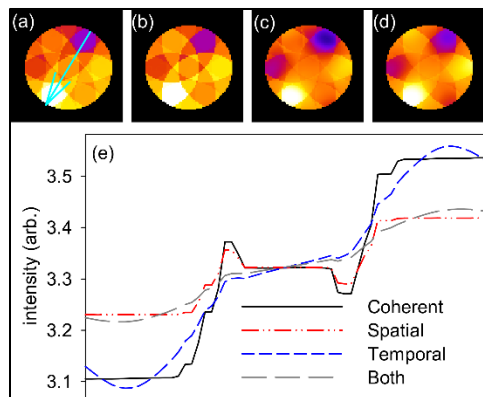


Figure 1 Simulated CBED pattern for graphene with a 60 kV probe. (a) Perfect (b) spatial incoherence (c) temporal incoherence and (d) both. A line scan (shown on (a)) through each CBED is shown in (e).

electron probe with an aperture of 30 mrad. Incident on graphene. All CBED patterns have been had their contrast adjusted to emphasize their features. Shown in (a) is a simulated CBED assuming a perfectly coherent probe. In (b) we include the effects of spatial incoherence. While the overall shape of the CBED patterns appears unchanged the overall contrast has been reduced. In (c) we show the effect of temporal incoherence. This leads to a smoothing of the CBED pattern, but no corresponding reduction in contrast. In (d) we show the effects of both temporal and spatial incoherence. To illustrate the change in contrast caused by incoherence, a line scan through the CBED patterns is shown in (e).

Obviously, the inclusion of spatial incoherence, which requires a smaller spatial grid to allow the accurate summing if CBED patterns and temporal incoherence requires the calculation of several defocus values. This greatly increases the size of the computational task. This is especially the case if large training sets are to be produced for supervised learning. In order to facilitate these calculations, we have continued to modify the μ STEM package specifically for this task. We have changed CBED output to HDF file formats and included all calculation parameters in the files. This allows parameters required for post processing data for the inclusion of incoherence to be carried out in an automated way minimizing the risk of operator error. This has been implemented on ORNL's SUMMIT supercomputer and is now routinely able to produce terabyte size training sets. As shown graphically in Fig. 2, the training sets are used to train a deep convolution neural network, using a variety of possible model parameters or structural descriptors, such as different structures and over a range of specimen thicknesses. Once trained the network is used on the experimental data returning the structural descriptors of interest. The advantage of the supervised learning approach is that our training set can include simulations for many thicknesses and so we are not limited by the phase object approximation. The phase object approximation can result in unrealistic results if COM methods are used in thicker specimens².

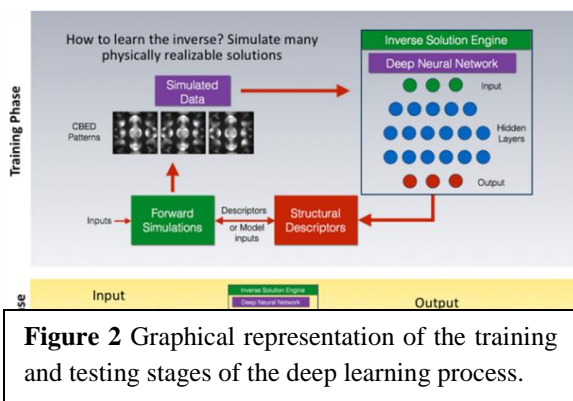


Figure 2 Graphical representation of the training and testing stages of the deep learning process.

More recently we have implemented the method of rotationally invariant variational autoencoders (rrVAE) and applied it to both simulated and experimental 4D-STEM data³. This method is designed to disentangle the general rotation of the object from other latent representations. Since much of the differences in CBED patterns are rotational as the COM moves towards the nucleus, this is ideal for the analysis of such data. This approach produces a rotational map that closely corresponds to the rotational maps found using conventional COM analysis. In addition, the latent space representations for symmetric systems closely correspond to the COM magnitude determined in the conventional manner. More interestingly, for systems that break symmetry such as graphene with vacancies and impurities, these defect exhibit strongly in some of the latent spaces. While this is early work, it suggests a more general application of this method to 4D-STEM data will be fruitful.

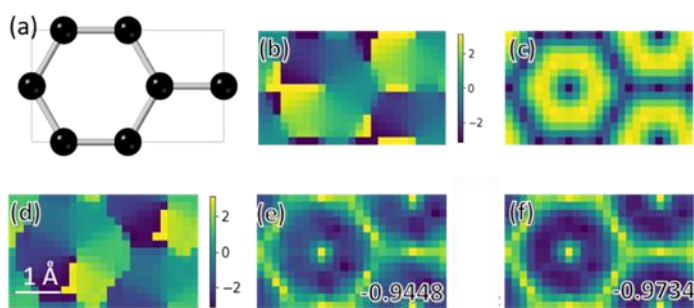


Figure 3 (a) Model structure for graphene. (b) and (c) the rotation map and magnitude calculated from the COM displacement. (d) The rotation map calculated using rrVAE. (e) and (f) the corresponding latent spaces. The Pearson r value is given in the insets.

Shown in Fig. 3 are the results of the rrVAE algorithm applied to simulated 4D-STEM data for 60 kV electrons incident on graphene. A 31 mrad probe forming aperture was used and temporal and spatial incoherence included. The model used in the multislice simulation is shown in (a). The rotation and magnitude of the COM displacement calculated from the simulated CBED patterns are shown in (b) and (c). The rotation map from the rrVAE is shown in (d). The rotation is reversed polarity

in this case. The latent spaces shown in (e) and (f) are effectively the inverse into the COM magnitude. To test the similarity of the latent spaces to the COM magnitude, we have used correlation and calculated the Pearson r coefficient. The values of close to -1 demonstrate a strong inverse linear relationship.

Future Plans

Work is underway to provide a straightforward method for applying electron densities calculated from density functional theory (DFT) to image/CBED simulations based on the quantum excitation of phonons model implemented in μ STEM. This will allow the routine simulation of training sets from structures calculated from DFT. This will be a further step in our goal to produce training sets that truly mimic experimental data.

The generation of training sets using the computational tools developed for SUMMIT is ongoing. We will initially be using this data to explore simpler modes of analysis, since restrictions have limited the ability to obtain experimental data. For example, we are investigating if it is

possible to determine the depth of its single impurity in a silicon lattice. This will have application to materials that are considered to be candidates for quantum computing.

Systems of broken translational symmetry such as the aforementioned point defects in graphene are a principle area for planned experimental deployment of the CBED trained networks like the rrVAE. We aim to extend to 3D ferroic systems where the minimum specimen thicknesses and heavy cations in of the A-site in high polarization perovskite ferroelectrics, or as required for strong spin-orbit-coupling in ferromagnetic systems, invalidate the weak phase approximation. Despite this, COM methods are utilized to characterize beam interactions with long range electromagnetic fields^{4,5}, or in the case of ferroelectrics a non-centrosymmetric space group⁶, to map the topology of the ferroic order parameter^{7,8}. For these 3D systems it may also be necessary to consider factors from the sample geometry such as sample thickness and axial tilt variations in the training. Taking perovskite ferroelectrics as a target system, our aim is for these networks to provide amongst their descriptors the quantitative spatially resolved polarization, as this is can be a known input quantity of the DFT training sets, in addition to electromagnetic fields. The interactions between complex nanoscale ferroelectric topologies and corresponding electric field distributions would allow the extraction of electrostatic energies and infer compensating charge distributions. Ideally, this would be combined with in-situ biasing to induce extrinsic ferroelectric switching, enabling the study of critical charge-evolution effects in these systems such as the freezing-in of the topology by slow-diffusion of charges.

References

1. M. P. Oxley and O. E. Dyck, *The importance of temporal and spatial incoherence in quantitative interpretation of 4D-STEM*, *Ultramicroscopy* **215**, 113015 (2020).
2. M. P. Oxley, D. Mukherjee and J. Hatchel, *Asymmetry and 4D-STEM: When the Phase Object Approximation Is Qualitatively Incorrect* *Microscopy and Microanalysis* (2020) doi:10.1017/S1431927620019807.
3. M. P. Oxley, M. Ziatdinov, O. E. Dyck, A. R. Lupini, R. Vasudevan and S. V. Kalinin, *Probing atomic-scale symmetry breaking by rotationally-invariant machine learning of multidimensional electron scattering*. Submitted to *Nature Communications*.
4. N. Shibata, S. Findlay, H. Sasaki, et al. *Imaging of built-in electric field at a p-n junction by scanning transmission electron microscopy*. *Sci Rep* **5**, 10040 (2015).
5. J.N. Chapman, P.E. Batson, E.M. Waddell, and R.P. Ferrier, *The direct determination of magnetic domain wall profiles by differential phase contrast electron microscopy*, *Ultramicroscopy* **3**, 203-214 (1978)
6. J. M. LeBeau, A. J. D'Alfonso, N. J. Wright, L. J. Allen, and S. Stemmer, *Determining ferroelectric polarity at the nanoscale*, *Applied Physics Letters* **98**, 052904 (2011)
7. Das, S., Tang, Y.L., Hong, Z. et al. *Observation of room-temperature polar skyrmions*. *Nature* **568**, 368–372 (2019).
8. T. Matsumoto, Y.G. So, Y. Kohno., H. Sawada., Y. Ikuhara, and N. Shibata, *Direct observation of $\Sigma 7$ domain boundary core structure in magnetic skyrmion lattice*, *Science Advances* **2**, 2 (2016).

Publications

1. M. P. Oxley and O. E. Dyck, *The importance of temporal and spatial incoherence in quantitative interpretation of 4D-STEM*, *Ultramicroscopy* **215**, 113015 (2020).
2. S-Z Yang, W. Sun, Y. Y. Zhang, Y Gong, M. P. Oxley, A. R. Lupini, P. M. Ajayan, M F. Chisholm, S. T. Pantelides, and W. Zhou, *Direct Cation Exchange in Monolayer MoS₂ via Recombination-Enhanced Migration*, *Phys.Rev. Lett.* **122**, 106101 (2019).
3. X. Li, O. Dyck, S. Jesse, A. R. Lupini, S. V. Kalinin and M. P. Oxley, *Structure retrieval from four-dimensional scanning transmission electron microscopy: Statistical analysis of potential pitfalls in high-dimensional data*, *Phys, Rev, E*, **100**, 023308 (2019).
4. X. Li, O. E. Dyck, M. P. Oxley, A. R. Lupini, L. McInnes, J. Healy, S. Jesse and S. V. Kalinin, *Manifold learning of four-dimensional scanning transmission electron microscopy*, *npj Computational Materials*, **5**, 5 (2019).
5. M P Oxley, J Yin, N Borodinov, S Somnath, M Ziatdinov, A R Lupini, S Jesse, R K Vasudevan and S V Kalinin, *Deep learning of interface structures from simulated 4D STEM data: cation intermixing vs. roughening*, Accepted *Mach. Learn.: Sci. Technol.* July (2020)
6. M. P. Oxley, M. Ziatdinov, O. E. Dyck, A. R. Lupini, R Vasudevan and S. V. Kalinin, *Probing atomic-scale symmetry breaking by rotationally-invariant machine learning of multidimensional electron scattering*. Submitted to *Nature Communications*.

Emergent Behavior in Nanoscale Functional Heterostructures

Amanda K. Petford-Long, Saidur Bakaul, Charudatta Phatak, Suzanne G. E. te Velthuis
Materials Science Division, Argonne National Laboratory, 9700 S Cass Avenue, Argonne,
IL 60439

Keywords: Magnetic, ferroelectric, topological structures, nanostructures, microscopy

Research Scope

We seek to understand novel emergent behavior in functional nanoscale heterostructures that show ferromagnetic, ferroelectric and resistance switching properties. A particular strength of our program is the use of 2D and 3D aberration-corrected Lorentz transmission electron microscopy and advanced scanning probe microscopy, combined with theory and simulation, to determine the quantitative parameters that control domain and transport behavior in nanostructures. We aim to obtain a fundamental understanding of the novel spin and charge distributions that are manifested in these nanoscale heterostructures by determining the governing parameters that contribute to their energy landscape, such as interfaces, geometric effects, and proximity effects between adjacent nanostructures. We further aim to understand how these spin and charge distributions can be controlled through modification of their energy landscape via external stimuli such as electric and magnetic fields, and temperature. Specific scientific challenges that we are addressing include elucidating the competing effects of curvature on chiral spin textures in ferromagnetic nanostructures, understanding the energy terms that control spin and charge transport and memristive behavior in geometrically-confined nanostructures, and the emergence of novel domain behavior in ferroelectric thin films.

Recent Progress

Free-standing ferroelectric thin films We investigated domain wall motion and quantum tunneling phenomena in epitaxial complex oxide ferroelectric films. In the first work, we showed that the domain walls in single-crystal complex oxide thin films move 2–3 orders of magnitude slower when the interfacial bonds with the heteroepitaxial substrate are broken to create a freestanding film (Figure 1a). This drastic change in domain wall kinetics does not originate from the alteration of epitaxial strain, but is correlated with structural ripples at a mesoscopic length scale and the associated flexoelectric effects induced in the freestanding films. The effects of the bond breaking on the local static ferroelectric properties, such as domain wall width and

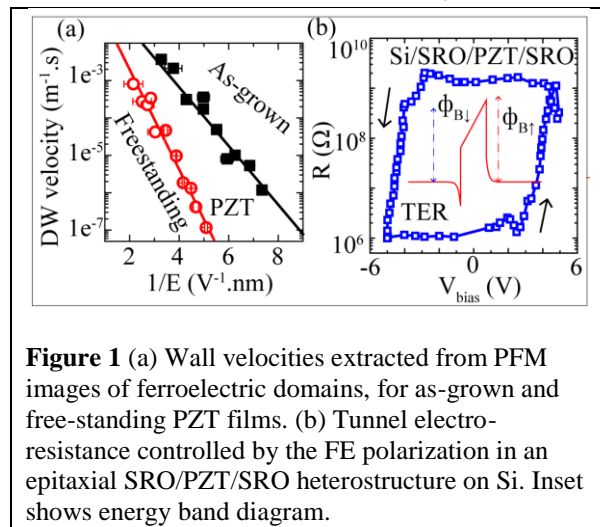
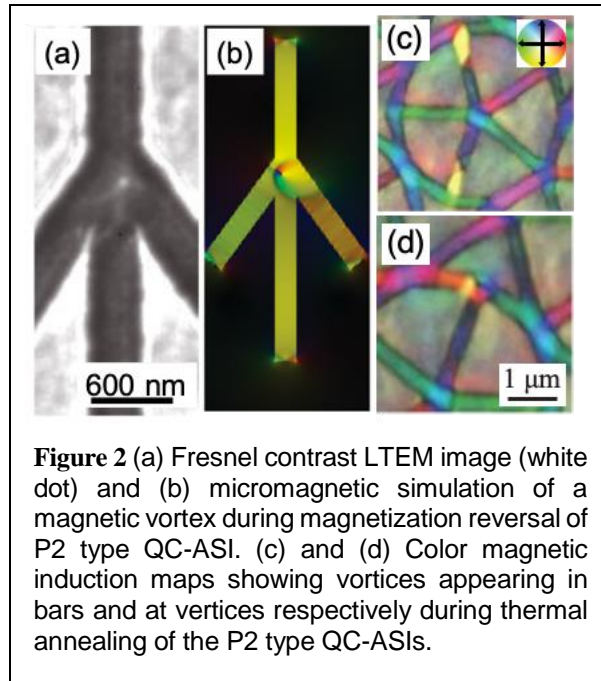


Figure 1 (a) Wall velocities extracted from PFM images of ferroelectric domains, for as-grown and free-standing PZT films. (b) Tunnel electro-resistance controlled by the FE polarization in an epitaxial SRO/PZT/SRO heterostructure on Si. Inset shows energy band diagram.

spontaneous polarization, of both the top and bottom of the freestanding films are modest and governed by the change in epitaxy-induced compressive strain. We further created freestanding metal/FE/metal heterostructures electrically integrated with silicon: such a structure cannot be created using traditional direct growth technique due to interfacial chemistry mismatch with Si. We reported quantum tunneling effects (Fig. 1b) and demonstrated that even in such a symmetric heterostructure, a polarization density asymmetry between the top and bottom layers of the ferroelectric film can develop, resulting in an asymmetric tunnel barrier that is maintained in a strain-free, freestanding state, and in memory-like behavior. This work provides a platform for our future work on ferroelectric materials.

Quasicrystalline ASIs – We have explored the effect of magnetic frustration and aperiodicity on the emergence of topologically non-trivial magnetic structures such as vortices in quasicrystalline artificial spin ices (QC-ASIs). We performed in-situ LTEM magnetization reversal, as well as in-situ thermal cooling experiments to understand their formation and motion in QC-ASI lattices patterned in Permalloy on a Penrose P2 tiling. We observed the formation of metastable vortex domain walls at vertices (Figure 2 (a)) prior to magnetization reversal of the associated vertex bars.¹ The walls do not move under application of magnetic field until they are annihilated by magnetization reversal in the associated bar. By

combining imaging and micromagnetic simulations (Fig. 2 (b)), we showed that the vortex walls are a transient state that accommodates the energy added to the QC-ASI by the applied magnetic field, as a vortex state was often lower in energy than the configurations that resulted from magnetization reversal in bars at the vertex. These transient states occur mainly in motifs with lower degeneracy. To further understand their behavior, we also performed in-situ heating and cooling experiments: the topological vortex defects in QC-ASIs form according to one of two different mechanisms depending on where in the lattice they form following thermal annealing near the Curie temperature: within the bars (Fig. 2(c)) or within the vertices (Fig. 2(d)).



The vortexes that form within the bars are topological defects that become frozen in as the magnetization in the bars fluctuates at temperatures near the Curie temperature. The vortexes that form in the vertices on the other hand, are topological defects that form as the Permalloy undergoes a second order phase transition from the paramagnetic phase to the ferromagnetic phase. Our analysis further shows that the bar defects have a strong dependence on the lattice geometry and boundary conditions of the QC-ASI lattices, namely lattices with free-

ends, or one with truncated ends. For the ultra-fast quench rates ($\sim 10^9$ K/s) that we also explored, the vertex defects can be analyzed in a broader Kibble-Zurek mechanism for topological defects.

Co nanohelices – The effect of curvilinear geometry in confined magnetic nanostructures can lead

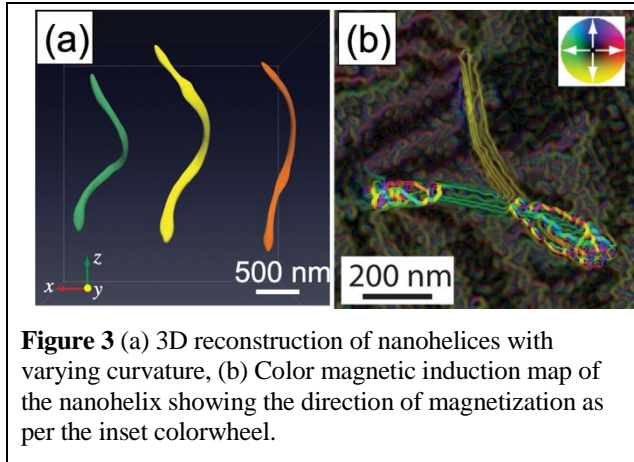


Figure 3 (a) 3D reconstruction of nanohelices with varying curvature, (b) Color magnetic induction map of the nanohelix showing the direction of magnetization as per the inset colorwheel.

to novel exchange-driven interactions such as effective anisotropy and an antisymmetric vector exchange anisotropy. We have explored this behavior by fabricating curved three-dimensional magnetic nanospirals using focused electron beam-induced deposition from a Co precursor. Using electron tomography, we determined their 3D morphology (Figure. 3(a)) and quantified the mean curvature of the helices as well as the surface curvature. We demonstrated a control

of the curvature, torsion and chirality of these nanohelices by varying the dwell time of the electron beam affecting their growth rate. We also determined their magnetic domain structure using off-axis electron holography (Figure 3(b)) which was then correlated with the geometry of the nanostructures. These results provide a pathway for understanding curvature effects on 3D magnetic domain structure.

Transport behavior in nanoscale oxide networks We explored the effect of patterning nanoscale

networks on resistance switching behavior in binary oxides, to elucidate the role of local inhomogeneities. We fabricated amorphous TiO_2 into a 2D honeycomb lattice containing periodic voids (Figure 3(a)). Using a combination of transport measurements, impedance spectroscopy and electron holography, we investigated the interplay of quantum confinement effects and resistive switching behavior in the films. The patterned film does not undergo resistive switching, but it

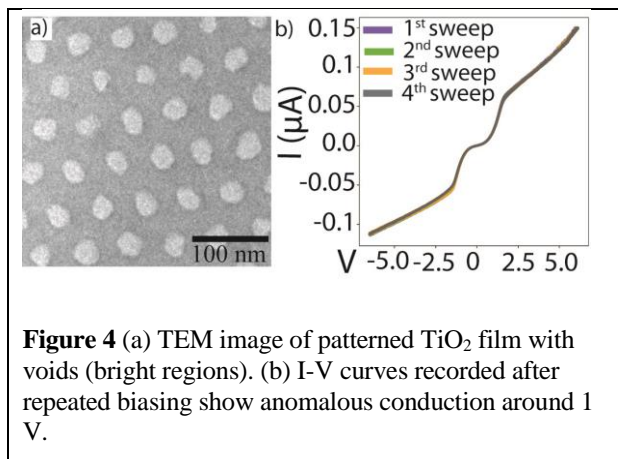


Figure 4 (a) TEM image of patterned TiO_2 film with voids (bright regions). (b) I-V curves recorded after repeated biasing show anomalous conduction around 1 V.

does show sub-Ohmic transport behavior at applied bias <5 V, and an anomalous conduction window around 1 V applied bias. Within the anomalous conduction window, the patterned film is more conductive than the unpatterned film. Using electron holography, we determined that electric fields near the voids in the patterned film suppress the resistive switching. Combining our experimental data with modeling, we propose the origin of the anomalous conduction window to be quantum confinement and the formation of the current density filaments. These results provide insights into the role of confinement effects on electronic transport properties of thin films, which can be harnessed for memristive and neuromorphic applications.

Future Plans

As of October 2020, Suzanne te Velthuis will be joining our program at the 20% level, bringing expertise in magneto-optical Kerr effect (MOKE) microscopy, which complements the other techniques used in our program, with respect to both spatial and temporal sensitivity.

Topological Defects in Ferromagnetic Nanostructures We are exploring ways to create artificial pinning landscapes that will lead to controlled creation of skyrmions whose effect on magneto-transport we can then explore. To date we have explored the formation of room temperature skyrmions in various systems, including Ni₂MnGa and Pt/Co/W multilayer thin films. In the former case, the skyrmions are stabilized due to competition between dipolar, exchange, and domain wall energy whereas in the latter case, the interfacial Dzyaloshinskii-Moriya interaction (DMI) plays a dominant role. Going forward, we will combine these two approaches by using Ga ion implantation to create artificially-patterned confined regions in multilayer films with interfacial DMI in order to create controlled skyrmion textures. We will then explore their transport behavior under applied electric currents via spin-transfer torques and spin-orbit torques.

Artificial spin ices We are extending our studies of ASIs to explore the influence of increasing lattice heterogeneity on the energy terms that drive the emergence of long- and short-range order. In particular, we will explore the influence of lattice order ranging from periodic to quasicrystalline to random on the spin interactions and resulting magnetic order and magnetization reversal behavior in the ASIs. We will also continue our exploration of the transport of magnetic solitons across connected ASIs to understand the effect of their chirality and winding number on the magnetoresistance of the lattices. Furthermore, the control of magnetic order in ASIs by creating antiferromagnetically-coupled islands at each lattice site, coupled either within the plane or vertically, will be investigated. By controlling the inter-island spacing, the coupling strength between paired islands can be tuned, resulting in additional magnetic frustration effects. Due to the degeneracy of the system, several quasi-ordered states are possible, and we will explore the transition between such states either using thermal excitation or external magnetic field protocols.

Ferroelectric materials: We will continue working on freestanding ferroelectric materials to understand their properties and the correlations among various electromechanical and electronic transport phenomena. In particular, we will explore how the ferroelectric order parameter and related phenomena evolve in freestanding materials as the strain changes from zero to beyond the conventional limit (~1%). In addition, we will work to understand the local electromagnetic and piezoresponse behavior in binary ferroelectric materials such as HfO₂. We will investigate the interplay between ferroelectric and ferromagnetic order parameters in multiferroic systems in order to gain a common understanding of how local inhomogeneities effect the local energy landscape and thus domain wall behavior.

Publications

1. V. Brajuskovic, A. Addi, C. Phatak, A. K. Petford-Long, *Observation of transient states during magnetization reversal in a quasicrystal artificial spin ice*, Phys. Rev. B **98**, 094424 (2018).
2. R. Agarwal, Y. Sharma, S. Chang, K. C. Pitike, C. Sohn, S. M. Nakhmanson, C. G. Takoudis, H. N. Lee, R. Tonelli, J. Gardner, J. F. Scott, R. S. Katiyar, S. Hong, *Room-temperature relaxor ferroelectricity and photovoltaic effects in tin titanate directly deposited on a silicon substrate*, Phys. Rev. B **97**, 054109 (2018).
3. C. Phatak and A. Petford-Long, *Direct evidence of topological defects in electron waves through nanoscale localized magnetic charge*, Nano Lett. **18(11)**, 6989–6994 (2018).
4. W. Jiang, S. Zhang, X. Wang, C. Phatak, Q. Wang, W. Zhang, M.B. Jungfleisch, J.E. Pearson, Y. Liu, J. Zang, X. Chang, A. Petford-Long, A. Hoffmann, S.G.E. te Velthuis, *Quantifying chiral exchange interaction for Néel-type skyrmions via Lorentz transmission electron microscopy*, Phys. Rev. B **99**, 104402 (2019).
5. X. Xu, Y. Liu, J. Wang, D. Isheim, V. P. Dravid, C. Phatak, and S. M. Haile, *Variability and origins of grain boundary electric potential detected by electron holography and atom-probe tomography*, Nat. Mater. **19**, 887-893 (2020).
6. F. Barrows, V. Brajuskovic, A. K. Petford-Long, C. Phatak, *Emergent magnetic ordering and topological frustration in quasicrystal artificial spin ices*, Phys. Rev. B **99(9)**, 094424 (2019).
7. S. Bakaul, J. Kim, S. Hong, M.J. Cherukara, T. Zhou, L. Stan, C. R. Serrao, S. Salahuddin, A. Petford-Long, D. Fong, M. Holt, *Ferroelectric domain wall motion in freestanding single-crystal complex oxide thin film*, Advanced Materials **32(4)**, 1907036 (2020)
8. M. Abuwasib, C. R. Serrao, L. Stan, S. Salahuddin, S. Bakaul, *Tunneling electroresistance effects in epitaxial complex oxides on silicon*, Applied Physics Letters **116**, 032902 (2020).
9. C. Phatak, C. S. Miller, Z. Thompson, E. B. Gulsoy, A. K. Petford-Long, *Curved three-dimensional cobalt nanohelices for use on domain wall device applications*, ACS Appl. Nano Mater. **3**, 6009–6016 (2020).
10. F. Barrows, X. Xu, S. Haile, C. Phatak, and A. K. Petford-Long, *Electron Holography Investigation of Resistive Switching CeO₂/STO Nanocolumns*, Microscopy and Microanalysis, 1-3, (2020) doi:10.1017/S143192762001991

Structure and electron dynamics in photoexcited CDW materials using MeV ultrafast electron probes

Jing Tao (PI), Jun Li and Zhixiu Liang
Condensed Matter Physics and Materials Science Division,
Brookhaven National Laboratory, Upton, NY 11973

Keywords: Ultrafast electron diffraction, charge density wave, non-equilibrium process

Research Scope

This Early Career Award project (ended in July 2020) aimed to sharpen the understanding of the quantum entanglement between charge and lattice degrees of freedom in correlated materials and quantum materials by probing structural dynamics of non-equilibrium states using MeV ultrafast electron diffraction (UED). In the study of 2D material 1T-TaSeTe with charge-density-wave (CDW) structures, on one hand we have achieved simultaneous observations of both electron and lattice dynamics, revealing the dephasing and correlation behavior between the two upon photoexcitation by measuring CDW reflections at various scattering angles. On the other hand, the intensity analysis of Bragg reflections on the UED results from 1T-TaSeTe led to the discovery of an unexpected lattice distortion, indicating a sublattice manipulation by photoexcitation. Emboldened by the established capabilities of UED methods, quantitative interpretations of charge-lattice interactions become possible for far-from-equilibrium phenomena. The knowledge gained from this project on CDW dynamics and mechanisms of a few 2D dichalcogenides and correlated materials using UED is complementary to and will be strengthened by other ultrafast techniques, theoretical modeling, first-principle calculations and data-science methods.

Recent Progress

Concurrent probing of both electron and lattice dynamics in CDW 1T-TaSeTe using UED

It has been technically challenging to concurrently probe the electrons and the lattices in materials during non-equilibrium processes, allowing their correlations to be determined [1, 2]. Limited by technical difficulties, the electron dynamics and lattice evolution in a material during non-equilibrium processes are commonly investigated by discrete methods, for instance, angle-resolved photoemission spectroscopy for electron dynamics and x-ray diffraction for lattice dynamics. Correlating the observations of the different experimental methods requires careful synchronization, however, is often an insurmountable problem due to the distinct nature of the probes and the different experimental and material conditions employed.

Here, by quantifying the reflections in a single set of UED patterns, we demonstrate it is possible to determine the subtle behavior in the temporal characteristics (the measurement of t_c in Fig. 1(b)) of the diffraction intensity as a function of scattering angles. This roots in the electron scattering principle of the change in scattering power from the valence electrons and nucleus screened by the core-electrons as the scattering angle changes (Fig. 1(a)). With the help of dynamic models and theoretical calculations, the UED results qualitatively depict the dynamic processes of both the electron and lattice simultaneously, manifesting an advantage of electron scattering in related applications (Fig. 1(c)). This novel approach opens the door to studying quantum effects

that arise from electron-lattice dephasing in next-generation optoelectronic, spintronic and photovoltaic devices.

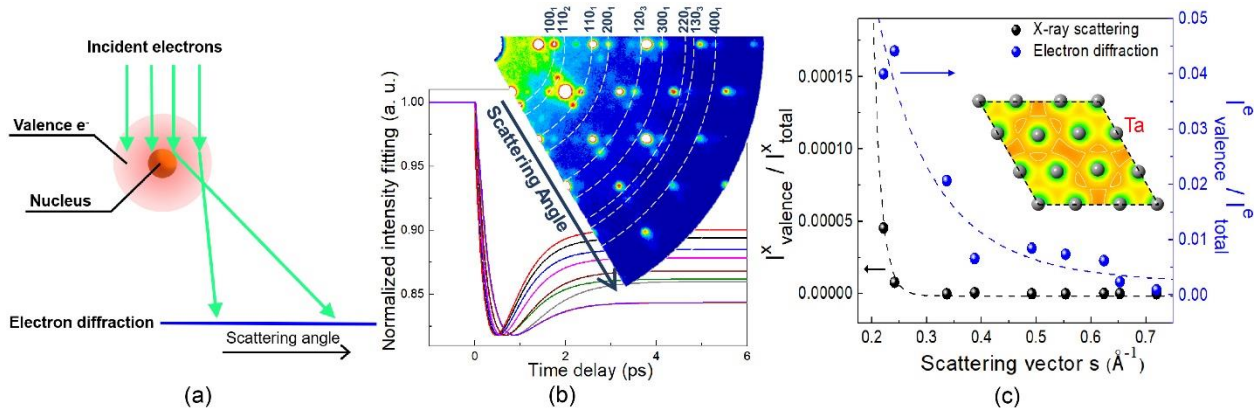


Figure 1. (a) Schematic of electron scattering principles indicates the diffraction intensity sensitivity to valence electrons at a small scattering angle and to nuclei positions at a large scattering angle. (b) In 1T-TaSeTe material, CDW superlattice reflection (SLR) intensity vs. time plots were measured at multiple scattering angles from an UED pattern, plot curves as double-exponential fitting of the data. Each measurement shows a fast intensity drop and a slow recovery turning at a cusp point t_c . Values of t_c are clearly seen to become larger as the scattering angle increases, which can be attributed to the probe with different sensitivities to valence electrons and nuclei. (c) Structure factors of the CDW state were calculated for both electron and x-ray scattering, corresponding to the measured SLRs, based on valence charges and total charges of Ta and Se atoms calculated by DFT, showing measurable intensities scattered from valence charges from electron diffractions. The dashed lines are guides to the eye. The inset shows the calculated charge density distribution of the Ta plane (Ta atoms are shown) in 1T-TaSe₂.

Probing lattice dynamics with intra-unit-cell spatial resolution in CDW 1T-TaSeTe using UED

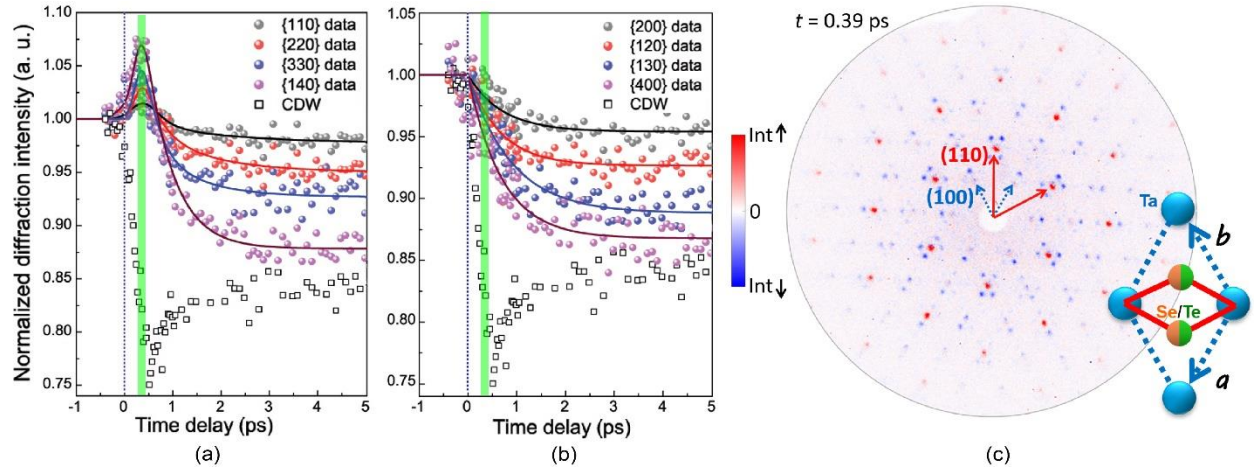


Figure 2. (a) Normalized intensity change of four Type-1 Bragg peaks as a function of delay time. The highest intensities are reached at ~ 400 fs for all the Type-1 Bragg peaks. (b) Normalized intensity change of four Type-2 Bragg peaks as a function of delay time. In contrast to Type-1, the intensities fall off right after the photoexcitation. Solid lines in (a) and (b) are eye guides for the measurements. For comparison, black boxes in (a) and (b) are CDW SLR (120_3). (c) An intensity difference map is shown at ~ 400 fs, with color scale bar presented on the left. The $\{100\}$ Bragg peaks (blue dashed arrows) correspond to the unit cell of the material (a crystal model on the right), while the Type-1 Bragg peaks (red indicated by $\{110\}$ arrows) form a sublattice frame in the reciprocal space, suggesting an intra-unit-cell distortion (see the red diamond in the crystal model) at the delay time.

Understanding of the charge-lattice interactions highly relies on the measurement accuracy of the lattice order during the dynamic processes. Due to technical limitations such as multiple scattering, the characterizations of lattice distortion and modulations of the unit-cell have often been simplified in the UED data analysis, which might introduce errors in the interpretation of driving mechanisms. For example, in a few dichalcogenides with CDW the dominance of the metal-atom (such as Ta and Ti) dynamics over the nonmetal-anion (such as S, Se and Te) is evident from the enhanced Bragg diffraction peak intensities at hundreds of fs [3]. However, we discover two types of the intensity change in Bragg peaks in CDW 1T-TaSeTe upon photoexcitation, as depicted in Fig. 2(a) and 2(b). At ~ 400 fs, a sublattice is formed, i.e., in the reciprocal space Bragg peaks with a periodicity larger than that of unit-cell reflections show independent intensity changes (Fig. 2(c)). This strongly suggests the existence of an intra-unit-cell distortion in the material and, more specifically, the atomic displacements of Se/Te with respect to Ta atoms. The dominance of the nonmetal-anion dynamics revealed here represents a new kind of laser manipulation of lattice distortion and unveil potentials to create quantum states with novel intra-unit-cell orders.

Future Plans

The ECA program of the PI (Jing Tao) ended at the end of July, 2020, and the PI joined the research group of Electron Microscopy and Nanostructure (Yimei Zhu as the PI and group leader) at BNL. Hence the future plans proposed here are incorporated in the proposed works under Zhu's FWP Number MA-015-MACA.

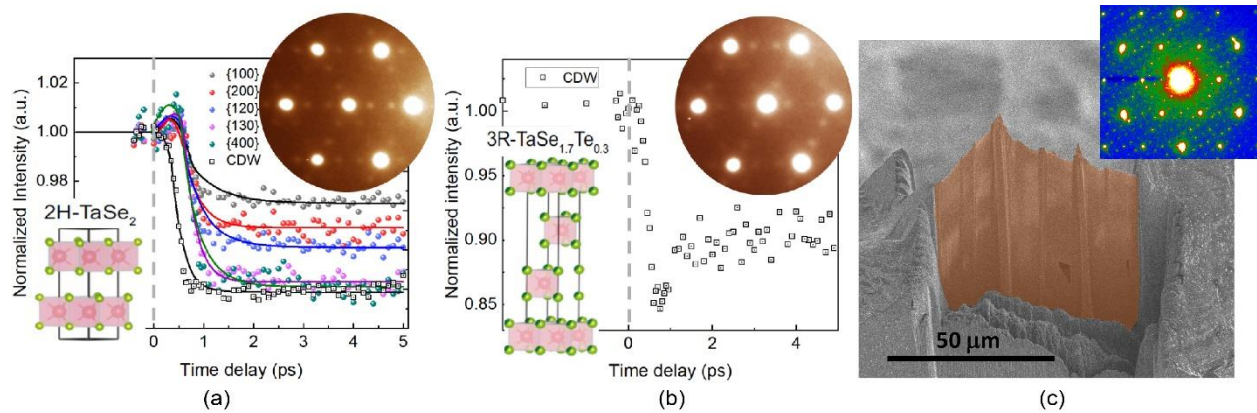


Figure 3. (a) Normalized intensity change of five Bragg peaks as a function of delay time in 2H-TaSe₂. All Bragg peaks were measured to have enhanced intensities at ~ 500 fs followed by intensity decreasing. Black boxes are CDW SLRs for comparison and help to align with time zero. (b) Normalized intensity change of a CDW reflection as a function of delay time in 3R-TaSe_{1.7}Te_{0.3}. The bottom-left insets in (a) and (b) are crystal models, while the top-right insets are UED patterns obtained at the temperature of 30 K so the CDW SLRs are clearly shown. (c) A SEM photograph of single-crystal Cu₂S UED sample with an electron diffraction pattern obtained in TEM, showing a monoclinic single-crystal phase of the sample at room temperature.

To further understand the key mechanisms postulated for the CDW formation, including Fermi surface nesting and electron-phonon coupling, we plan to study a series of CDW materials with different but related crystal structures using UED and pump-probe techniques. Preliminary UED results were obtained from 2H-TaSe₂ and 3R-TaSe_{1.7}Te_{0.3} (materials from Robert Cava at Princeton Univ.) with CDW SLRs and preliminary measurements are shown in Fig. 3(a) and 3(b). At the current stage, we found that the physical properties and the observed structural dynamics

of 2H-TaSe₂ encompass drastically different characteristics in comparison to the previously studied 1T-TaSeTe material, which may arise from their electronic structures and phonon dispersion relationships. During photoexcitation with a photon energy of 1.55 eV, preliminary DFT calculations indicate that three t_{2g} orbitals of Ta and strongly hybridized Se orbitals in 1T-TaSeTe could be responsible for electron excitation and relaxation, while only one t_{2g} orbital of Ta in 2H-TaSe₂ can be found to involve in the process, suggesting electron redistribution among available orbitals in some CDW materials as a possible mechanism. Moreover, phonon dispersion relationships and phonon populations in these materials will also be calculated using DFT methods (in collaboration with Weiguo Yin at BNL) and structural dynamics will be probed by other synchrotron x-ray based ultrafast techniques (in collaboration with Ian Robinson and Mark Dean at BNL) to benefit from multimodal approaches for comprehensive interpretations of the underlying physics.

In addition to the study of CDW materials, structural dynamics in other correlated materials, such as CrI₃ with intriguing spin-lattice coupling [4] (in collaboration with Cedimir Petrovic at BNL) and Cu₂S with unconventional charge-lattice interactions [5], will be investigated as well to reveal the roles of competing degrees of freedom in materials' functionalities and to explore the hidden quantum phases with laser manipulation. Specifically, preliminary UED pump-probe data at various temperatures have been acquired from CrI₃, and a single-crystal Cu₂S UED sample has been successfully prepared for UED pump-probe experiments (Fig. 3(c)) with dedicated sample preparation approaches. Furthermore, we plan to engage in the research activities using data-science methods such as trained artificial neural networks for robust and rapid UED data analysis (in collaboration with Sandra Biedron at Univ. of New Mexico).

References

1. Z. Tao, T.-R. T. Han, S. D. Mahanti, P. M. Duxbury, F. Yuan, C.-Y. Ruan, K. Wang, and J. Wu, *Decoupling of structure and electronic phase transitions in VO₂*, Phys. Rev. Lett. **109**, 166406 (2012).
2. T. Konstantinova, J. D. Rameau, A. H. Reid, O. Abdurazakov, L. Wu, R. Li, X. Shen, G. Gu, Y. Huang, L. Rettig, I. Avigo, M. Ligges, J. K. Freericks, A. F. Kemper, H. A. Dürr, U. Bovensiepen, P. D. Johnson, X. Wang, and Y. Zhu, *Nonequilibrium electron and lattice dynamics of strongly correlated Bi₂Sr₂CaCu₂O_{8+δ} single crystals*, Sci. Adv. **4**, eaap7427 (2018).
3. M. Eichberger, H. Schäfer, M. Krumova, M. Beyer, J. Demsar, H. Berger, G. Moriena, G. Sciaini, and R. J. Dwayne Miller, *Snapshots of cooperative atomic motions in the optical suppression of charge density waves*, Nature **468**, 799-802 (2010).
4. M. A. McGuire, H. Dixit, V. R. Cooper, and B. C. Sales, *Coupling of Crystal Structure and Magnetism in the Layered, Ferromagnetic Insulator CrI₃*, Chem. Mater. **27**, 612-620 (2015).
5. J. Tao, J. Chen, J. Li, L. Mathurin, J.-C. Zheng, Y. Li, D. Lu, Y. Cao, L. Wu, R. J. Cava, and Y. Zhu, *Reversible structure manipulation by tuning carrier concentration in metastable Cu₂S*, PNAS **114**, 9832 (2017).

Publications (10 most relevant)

1. J. Li, J. Li, K. Sun, L. Wu, R. Li, J. Yang, X. Shen, X. Wang, H. Luo, R. J. Cava, I. K. Robinson, X. Jin, W.-G. Yin, Y. Zhu, and J. Tao, *Concurrent probing of electron-lattice dephasing induced by photoexcitation in 1T-TaSeTe using ultrafast electron diffraction*, Phys. Rev. B **101**, 100304 (R) (2020).
2. S. Guo, R. D. Zhong, W. Wang, J. Tao, D. R. Ni, R. J. Cava, *K₃Ir₂O₆ and K_{16,3}Ir₈O₃₀, Low-Dimensional Iridates with Infinite IrO₆ Chains*, J. Am. Chem. Soc. **142**, 5389 (2020).
3. L. T. Nguyen, M. Abeykoon, J. Tao, S. Lapidus, R. J. Cava, *Long-range and local crystal structures of the Sr_{1-x}Ca_xRuO₃ perovskites*, Phys. Rev. Mater. **4**, 034407 (2020).

4. T. Konstantinova, L. Wu, M. Abeykoon, R. J. Koch, A. F. Wang, R. K. Li, X. Shen, J. Li, J. Tao, I. A. Zaliznyak, C. Petrovic, S. J. L. Billinge, X. J. Wang, E. S. Bozin, and Y. Zhu, *Photoinduced dynamics of nematic order parameter in FeSe*, Phys. Rev. B **99**, 180102, 1-6 (2019).
5. Y. Liu, J. Li, J. Tao, Y. Zhu, and C. Petrovic, *Anisotropic magnetocaloric effect in $Fe_{3-x}GeTe_2$* , Sci. Rep. **9**, 13233, 1-8 (2019).
6. Y. Liu, L. Wu, X. Tong, J. Li, J. Tao, Y. Zhu, and C. Petrovic, *Thickness-dependent magnetic order in CrI_3 single crystals*, Sci. Rep. **9**, 13599, 1-8 (2019).
7. F. O. von Rohr, A. Ryser, H. Ji, K. Stolze, J. Tao, J. J. Frick, G. R. Patzke, and R. J. Cava, *The $h-Sb_xWO_{3+2x}$ oxygen excess antimony tungsten bronze*, Chem.-Eup. J. **25**, 8, 2082-2088 (2019).
8. Wang, W.; Sun, K.; Oey, Y. M.; Cava, R. J.; Wu, L.; Zhu, Y.; Yu, R. and Tao, J., *Smectic and nematic phase modulations and transitions under electron beam in $Tb_2Cu_{0.83}Pd_{0.17}O_4$* , Phys. Rev. Mater. **3**, 093601, 1-7 (2019).
9. Z. Wang, R. Jin, L. Wu, J. Tao, A. B. Karki, J. Y. Pan, Y. Zhu, and E. W. Plummer, *Atomically imaged crystal structure and normal-state properties of superconducting $Ca_{10}Pt_4As_8((Fe_{1-x}Pt_x)_2As_2)_5$* , Phys. Rev. B **100**, 094103 1-8 (2019).
10. J. Li, S. Cheng, L. Wu, J. Tao, Y. Zhu, *The effect of scanning jitter on geometric phase analysis in STEM images*, Ultramicroscopy **194**, 167 (Nov 2018).

Liquid Cell Electron Microscopy: Heterogeneity and Fluctuations at Solid-Liquid Interfaces

Principal Investigators: Haimei Zheng¹, Peter Ercius², Emory Chan², Lin-Wang Wang¹

¹Materials Sciences Division, Lawrence Berkeley National Laboratory, Berkeley, CA 94720

²The Molecular Foundry, Lawrence Berkeley National Laboratory, Berkeley, CA 94720

Keywords: Liquid cell electron microscopy, *in situ* transmission electron microscopy, solid-liquid interfaces, nucleation and growth, materials structural transformations

Research Scope

The overarching goal of this program is to develop and utilize the advanced *in situ* liquid cell transmission electron microscopy (TEM) to elucidate how atomic level heterogeneity and fluctuations at solid-liquid interfaces determine the physical and chemical properties and processes of materials, with a focus on nucleation and precipitation/dissolution in liquids or at solid-liquid interfaces. Liquid cell TEM enables invaluable insights into the underlying mechanisms of nucleation, growth and many other material transformation processes critical to novel materials discovery and the function of energy devices. The development of advanced instrumentation for imaging and chemical identification through liquids with atomic resolution provides transformative opportunities for investigation of nucleation and materials dynamic phenomena in a liquid solution or at solid-liquid interfaces that are at the frontiers of basic energy science.

Recent Progress

1. Liquid cells development

We develop novel liquid cells, which allow high resolution imaging of materials dynamic phenomena in liquids with TEM. Progress has been made in the development of ultra thin liquid cells with two-dimensional materials as membrane. For example, MoS₂ liquid cells were made through a novel polymer-free MoS₂ transfer process, where the MoS₂ membrane was a functional substrate as well as the membrane window (**Fig. 1**)¹. A facile membrane transfer process was created to produce clean MoS₂ membranes with a high yield. We found that three monolayers (~2 nm) thick MoS₂ membranes are ideal. A MoS₂ liquid cell may consist of a MoS₂ membrane on one side and graphene on the other side. *In situ* TEM with these MoS₂

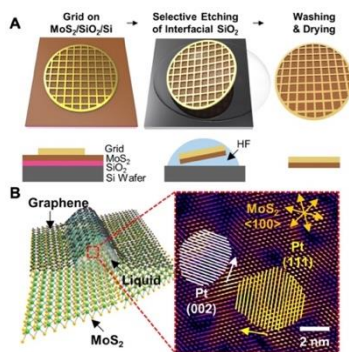


Fig. 1. Development of MoS₂ liquid cells allowing the *in situ* study of 2D heterostructures. (A) Schematic illustration of polymer-free transfer process of MoS₂. (B) With the development of MoS₂ liquid cells for TEM, the growth of Pt nanocrystals on MoS₂ through Van der Waals interactions was revealed through direct observation.

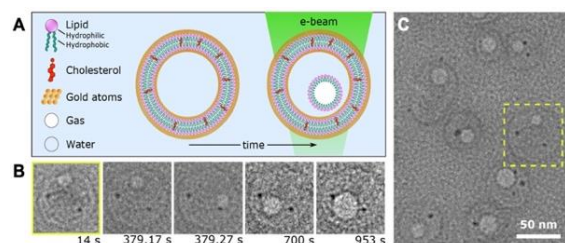


Fig. 2. (A) Liposome nanoreactors. (B) TEM micrograph of POPC:cholesterol liposomes encapsulating nanobubbles in a TEM liquid cell. (C) Nanobubble diffusion and growth over time in the liposome outlined in (B).

imaging (**Fig. 2**).² We successfully imaged these gold-coated liposomes in both graphene liquid cells (GLCs) and carbon film liquid cells at electron dose rates as high as $700 \text{ e}/\text{\AA}^2 \cdot \text{s}$.

These liposome nanoreactors allowed us to visualize nanoscale reactions confined in zeptoliter volumes with 0.1 s resolution. Specifically, the electron-beam-induced radiolysis of water produces 9-60 nm bubbles that evolve selectively inside the liposomes. The dynamic behavior of nanobubbles inside lipid vesicles in a TEM has been captured. These results suggest that liposomes are a viable platform for controlling and imaging nanoscale reactions *in situ*.

In addition, we have also made other types of liquid cells by modifying the existing liquid cells, including carbon-film liquid cells through a much more facile fabrication process than graphene liquid cell fabrication; electrochemical liquid cells with patterned electrodes.

2. Nucleation, growth and structural transformations of materials

We have made significant progress in imaging and understanding of nucleation, growth and structural transformations of materials with liquid cell TEM. A variety of systems have been investigated, which address a series of important scientific questions. For example, *what are the intermediates during materials transformations between two stable states? How are concentration fluctuations correlated to the structural ordering in liquid solution? What are the effects of*

liquid cells revealed that Pt nanocrystals grow on MoS_2 through Van der Waals interactions and hetero-epitaxy. Our development of MoS_2 liquid cells opens the opportunity to study the growth of many nanoscale heterostructures.

We have also developed nanoreactors based on lipid vesicles. We synthesized liposomes of 1-palmitoyl-2-oleoyl-phosphatidylcholine (POPC) and cholesterol (35-60 nm diameter), then coated them with gold to enhance their stability during

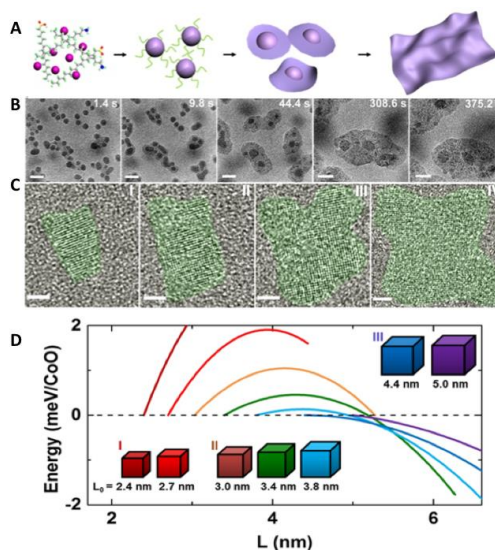


Fig. 3. Growth and transformations of cobalt oxide and cobalt nickel oxide nanocrystals into 2D nanosheets. (A) A schematic illustration of the evolution from 3D nanoparticles to 2D nanosheets in a molecular precursor solution. (B) Cobalt nickel oxide nanoparticle formation and transformation into 2D nanosheets. Scale bars are 10 nm. (C) High resolution image of a cobalt oxide nanoparticle transforms into a 2D nanosheet. Scale bars are 2 nm. (D) The energy evolution of cobalt oxide during the 3D-to-2D transition. Total energy evolution of the cobalt oxide system as a function of spreading particle size (L).

surface ligand passivation on solution growth processes? How does the nucleation respond to an external stimulus, e.g. an electric bias?

For example, we recently studied the formation of transition metal oxide (cobalt oxide, cobalt nickel oxide and nickel oxide) nanosheets using liquid cell TEM.³ The advanced imaging through liquids with high spatial and temporal resolution provided an opportunity for us to uncover the atomic pathways of 2D nanostructure formation that involve 3D nanoparticle intermediates and 3D-to-2D transformations (**Fig. 3**). Density functional theory (DFT) calculations are used to elucidate the driving force for the 3D-to-2D transformations. We conducted *ab initio* calculation and the results show that 3D-to-2D transformations are governed by the competition between the negative surface energy and the positive edge energy. Revealing of the 2D growth involving 3D-to-2D transformations represents a significant advance in the study of 2D materials growth mechanisms. Such a growth pathway is different from 2D nanosheet formation through oriented attachment of the primary 3D nanocrystals and the “soft template”-assisted growth of 2D nanostructure. Our study provides critical new insights into the design and synthesis of 2D nanocrystals for various applications, such as catalysis, sensing, and many other surface-enhanced applications.

3. Dynamic phenomena at electrode-electrolyte interfaces

Electrochemical liquid cells have been developed for the study of nanoscale electrochemical processes. Direct observations of electrochemical reactions with the simultaneous structural/chemical analysis were achieved. The mechanisms of a wide range of electrochemical processes have been unveiled.

Compared to commercial liquid cells, our development of electrochemical cell TEM offers significant advantages for the study of electrochemical processes related to battery applications. Using the commercial liquid electrolyte used in lithium-ion batteries, we have studied Li/Na metal plating and stripping, and solid–electrolyte interphase (SEI) formation at the nanoscale. For example, a recent study showed a remarkable leap in the capability of liquid phase TEM in revealing spatially resolved SEI chemistry on lithium nanograin deposits (**Fig. 4**).⁴ It has

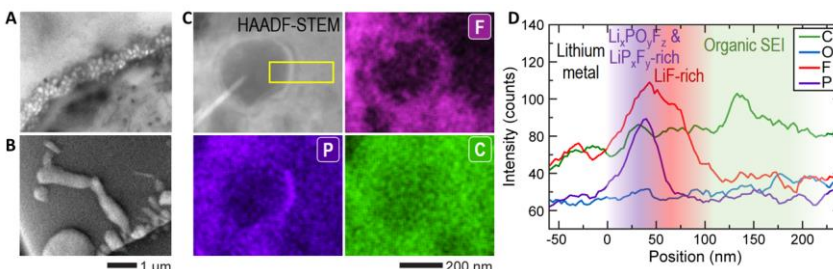


Fig. 4. Electrochemical liquid cell TEM study of lithium electro-deposition. (A,B) *in situ* TEM images of lithium nanogranules formed in a liquid cell with a cationic polymer film coated electrodes and lithium dendrites grown in a bare liquid cell. (C) High-angle annular dark-field scanning TEM (STEM) image and corresponding STEM-energy dispersion x-ray (EDX) elemental maps of an *in situ* grown lithium nanogranule showing spatially resolved solid-electrolyte interphase chemistry. (D) EDX line-scan profile of the lithium nanogranule corresponding to the marked region in the HAADF-STEM image in (C). Plots show both P and F signals are the most intense near the lithium nanogranule surface. P was concentrated in the 0–50 nm inner layer, while F was more broadly distributed in the 0–100 nm layer of the SEI. A slightly higher concentration of C and O was found 100–200 nm above the nanogranule surface.

been a great challenge to study SEI and lithium growth due to the experimental difficulties originating from the vulnerability to air or moisture exposure in post-processing. This work reported the *in situ* observation of the suppression of lithium dendritic growth arising from a cationic polymer coating. By correlating the lithium growth and the SEI chemistry, the mechanisms of lithium dendrite suppression through modification SEI chemistry have been uncovered.

The study of electrochemical phenomena using liquid cell TEM requires low dose imaging and carefully control of electron beam effects. The success opens many opportunities to the study of electron beam sensitive materials and their dynamic structural transformations.

4. Electron beam effects

The molecular dissociation and damage caused by electron beam illumination is a significant issue.

Radiolysis ionization under electron beam illumination induces dissociation and damage of organic and biological molecules. To understand the atomistic mechanism of radiolysis damage, our team developed a systematic procedure based on real-time time-dependent density functional theory (rt-TDDFT) for simulating the radiolysis damage processes of molecules; this procedure can describe the ionization cross sections of the electronic states and the fast dissociation processes caused by hot carrier cooling and the Auger decay on deep levels.⁵ For the radiolysis damage of C₂H₆O₂, our simulation unexpectedly showed that there is strong competition among three different dissociation paths, including fast dissociation caused by nonadiabatic cooling of the hot carrier; fast dissociation caused by Auger decay, which induces double ionization and Coulomb explosion; and slow dissociation caused by increased kinetic energy. As the energy of the incident electron beam changes, the time scales of these dissociation paths and their relative contributions to the molecule damage change significantly. These simulation results explain the measured mass spectra of the C₂H₆O₂ dissociation fragments and also provide clear competition mechanisms for blocking these dissociation paths in the TEM imaging of organic and biological materials.

Future Plans

We plan to continue our development of novel liquid cells that will enable unprecedented control over the chemical reactions, with electric biasing capabilities and various temperature control. We will develop/employ advanced image detection and image processing techniques. In addition, understanding and controlling of electron beam effects is essential for the future program success. With the new generation of liquid cells, advanced imaging and theoretical calculation, we will be able to achieve atomic imaging, understanding and further controlling of dynamic phenomena at solid-liquid interfaces.

References

1. J. Yang, M. K. Choi, Y. Sheng, J. Jung, K. Bustillo, T. Chen, S.W. Lee, P. Ercius, J. H. Kim, J. H. Warner, E. M. Chan, H. Zheng “*MoS₂ liquid cell electron microscopy through clean and fast polymer-free MoS₂ transfer.*” *Nano Letters* **19**, 1788-1796 (2019).
2. S. B. Alam, J. Yang, K. C. Bustillo, C. Ophus, P. Ercius, H. Zheng, E. M. Chan, “*Hybrid nanocapsules for in situ TEM imaging of gas evolution reactions in confined liquids*” *Nanoscale* doi.org/10.1039/D0NR05281G (2020).
3. J. Yang, Z. Zeng, J. Kang, C. Czarnik, X. Zhang, C. Ophus, C. Yu, K. Bustillo, M. Pan, J. Qiu, L. W. Wang, H. Zheng, “*Formation of two-dimensional transition metal oxide nanosheets with nanoparticles as intermediates.*” *Nature Materials* **18**, 970–976 (2019).
4. S. Lee, J. Shangguan, J. Alvarado, S. Betzler, S. J Harris, M. M Doeff, H. Zheng, “*Unveiling the mechanisms of lithium dendrite suppression by cationic polymer film induced solid electrolyte interphase modification.*” *Energy & Environmental Science* **13**, 1832-1842 (2020).
5. Z. Cai, S. Chen, L. W. Wang, “*Dissociation path competition of radiolysis ionization-induced molecule damage under electron beam illumination*” *Chemical Sciences* **10**, 10706 (2019).

Publications from Program

1. S. B. Alam, J. Yang, K. C. Bustillo, C. Ophus, P. Ercius, H. Zheng, E. M. Chan, “*Hybrid nanocapsules for in situ TEM imaging of gas evolution reactions in confined liquids*” *Nanoscale* doi.org/10.1039/D0NR05281G (2020).
2. Z. Zeng, P. Barai, S. Lee, J. Yang, X. Zhang, W. Zheng, Y. Liu, K. C Bustillo, P. Ercius, J. Guo, Y. Cui, V. Srinivasan, H. Zheng “*Electrode roughness dependent electrodeposition of sodium at the nanoscale.*” *Nano Energy* **72**, 104721 (2020).
3. S. Lee, J. Shangguan, J. Alvarado, S. Betzler, S. J Harris, M. M Doeff, H. Zheng, “*Unveiling the mechanisms of lithium dendrite suppression by cationic polymer film induced solid electrolyte interphase modification.*” *Energy & Environmental Science* **13**, 1832-1842 (2020).
4. Z. Cai, S. Chen, L. W. Wang, “*Dissociation path competition of radiolysis ionization-induced molecule damage under electron beam illumination*” *Chemical Sciences* **10**, 10706 (2019).
5. J. Yang, Z. Zeng, J. Kang, C. Czarnik, X. Zhang, C. Ophus, C. Yu, K. Bustillo, M. Pan, J. Qiu, L. W. Wang, H. Zheng, “*Formation of two-dimensional transition metal oxide nanosheets with nanoparticles as intermediates.*” *Nature Materials* **18**, 970–976 (2019).
6. Y. Wang, X. Peng, A. Abelson, P. Xiao, C. Qian, L. Yu, C. Ophus, P. Ercius, L. W. Wang, M. Law, H. Zheng, “*Dynamic deformability of individual PbSe nanocrystals during superlattice phase transitions.*” *Science Advances* **5**, eaaw5623 (2019).
7. Z. Yin, S. Betzler, T. Sheng, Q. Zhang, X. Peng, J. Shangguan, K. Bustillo, J. Li, S. Sun, H. Zheng, “*Real time TEM observation of facet dependent pseudo-photocatalytic behavior of TiO₂ nanorods for water splitting.*” *Nano Energy* **62**, 507-512 (2019).

8. J. Yang, M. K. Choi, Y. Sheng, J. Jung, K. Bustillo, T. Chen, S.W. Lee, P. Ercius, J. H. Kim, J. H. Warner, E. M. Chan, H. Zheng “*MoS₂ liquid cell electron microscopy through clean and fast polymer-free MoS₂ transfer.*” Nano Letters **19**, 1788-1796 (2019).
9. Q. Zhang, G. Gao, G. Gao, Y. Shen, X. Peng, J. Shangguan, Y. Wang, H. Dong, K. Bustillo, L. W. Wang, L. Sun, H. Zheng, “*Anomalous shape evolution of Ag₂O₂ nanocrystals modulated by surface adsorbates during electron beam etching*” Nano Letters **19**, 591-597 (2019).
10. X. Peng, A. Abelson, Y. Wang, C. Qian, J. Shangguan, Q. Zhang, Lei Yu, Z. Yin, W. Zheng, K. Bustillo, X. Guo, H. Liao, S. Sun, M. Law, H. Zheng, “*In situ TEM study of the degradation of PbSe nanocrystals in air.*” Chemistry of Materials **31**, 190-199 (2019).

Unraveling Electron, Spin and Lattice Correlations using Advanced Electron Microscopy

Yimei Zhu, Lijun Wu, Junjie Li, Jing Tao, Xuewen Fu and Tatiana Konstantinova
Department of Condensed Matter Physics and Materials Science
Brookhaven National Laboratory, Upton, NY 11973

Keywords: Electron microscopy instrumentation, Electron-spin correlation, Electronic heterogeneities, Ultrafast and non-equilibrium, and Quantum materials

Research Scope

The goal of this FWP (MA-015-MACA) is to study property-sensitive nanoscale structure, defects and interfaces of technologically important materials, such as high-temperature superconductors, transition-metal oxides, ferroelectric and spintronic films, and other energy related materials. We develop and implement advanced electron microscopy methods and instrumentation at required spatiotemporal resolution to reveal atomic disorder, electronic inhomogeneity, and transient dynamics of these materials. We focus on three research themes: 1) Heterogeneities, 2) Non-equilibrium and ultrafast phenomena and 3) Advanced characterization tools. The study of ferroelectric and ferromagnetic materials and charge and spin ordering/switching in theme 1 is covered by a separate abstract.

Recent Progress

In the past two years we have made significant progress in advancing the frontier of electron microscopy instrumentation and methods, notably the design of a compact, low-cost imaging-lens system for quadrupole multiplets for MeV ultrafast electron microscopy and the development of laser-free electron pulser for frequency-tunable stroboscopic ultrafast electron microscopy, which earned us several R&D innovation awards. We've also made great strides on materials research, unraveling several long-standing puzzles regarding charge-lattice and spin-lattice correlations, topological phenomena and interfaces, including interface enhanced superconductivity in quantum materials. Our research covered energy materials as well, particularly to understand ionic-transport mechanisms in low-dimensional oxides in responding to DOE-BES' calls on national energy security. We refer our research outcomes to the publications listed at the end of this abstract.

Heterogeneities. Heterogeneity recognizes that the functionalities of quantum materials often arise from the presence of spatial symmetry breaking, through the spontaneous appearance of degrees of freedom. Our research in this area has been focused on the study of electronic inhomogeneity, spatially resolved symmetry breaking in charge and spin order, for instance in ferroelectric, ferromagnetic and multiferroic systems (see the separate abstract). Moreover, we observe, manipulate and control the local orders by applying external stimuli to reveal competing order of charge, orbital, spin and lattice, as well as their fluctuation, instability and interactions. For instance to understand the tenfold increase in the superconducting transition temperature in one unit-cell FeSe on SrTiO₃ substrate over the bulk FeSe we developed, for the first time, the atomic resolution 10K low temperature imaging and energy-loss spectroscopy capabilities and compared the observations with that of room temperature (Fig.1) along with Hall transport measurements of the same samples^[1]. Our objective is to correlate crystal structure and electronic structure, especially their local symmetry breaking due to the presence of defects and interfaces, with overall properties of wide range quantum materials.

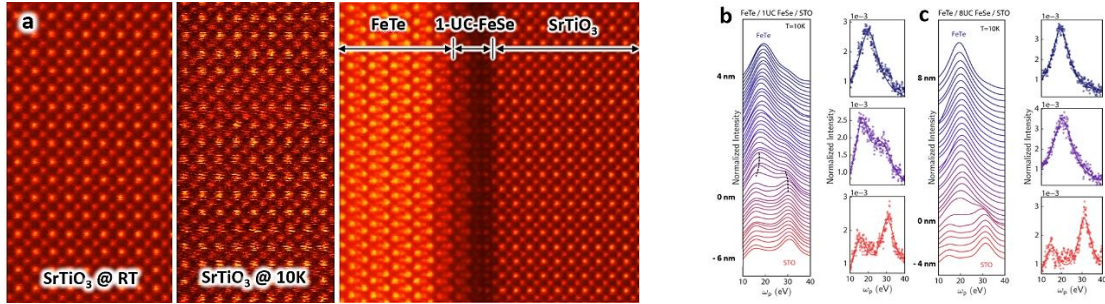


Fig.1 (a) STEM images at room temperature and 10K. The right panel shows the heterostructure of the 10-unitcell (UC) capping layer FeTe on 1UC-FeSe grown on SrTiO₃ for interface enhanced superconductivity. (b-c) Valence EELS across the interfaces at 10K from (b) FeTe/1UC-FeSe/STO, and (c) FeTe/8UC-FeSe/STO. Black dashed lines in (b) indicate a redshift in plasmon peaks near the FeSe/STO interface [1].

Non-equilibrium and ultrafast phenomena. In the area of ultrafast research we focused on electron-lattice interaction dynamics in high-T_c cuprate and FeSe superconductors [2,3]. We combine ultrafast electron diffraction (UED) with synchrotron x-ray pair-distribution-function (PDF) analysis. We probed the lattice interactions in FeSe with electronic degrees of freedom and focus on the nematicity, a common thread of unconventional superconductors. We show photoexcitation leads to a surprising enhancement of the high-symmetry crystalline order as a result of a suppression of low-symmetry local lattice distortions, signatures of nematic fluctuations. The distortions are present at temperatures below and above the nematic phase transition, as corroborated by PDF and TEM analyses. Nonequilibrium lattice behavior of FeSe reveals two distinct time scales of nematic response to photoexcitation, corresponding to diffusive and percolative dynamics of nematic fluctuations respectively [3].

Advanced characterization tools. The development and deployment of advanced imaging capabilities supported by this FWP is at the forefront of the field, especially in the area of ultrafast electron microscopy instrumentation. In the past two years, our main activities include: 1) the design of a compact quadrupole-based multiplets imaging system for a home-built MeV-ultrafast electron microscope; and 2) the development, installation and optimization of the Laser-Free Electron Pulsar (LFEP) (Fig.2) that can be retrofit to commercial electron microscopes with pulsed beams for stroboscopic ultrafast electron microscopy without requiring expensive fs lasers.

These activities earned us the 2019 R&D100 Award and the 2019 and 2020 Microscopy Innovation Award and several patents. We studied for the first time the GHz electromagnetic wave propagation dynamics [4] in a RF micro-electromechanical system, revealing the transient oscillating electromagnetic field, time-resolved polarization, amplitude, and nonlinear local field enhancement.

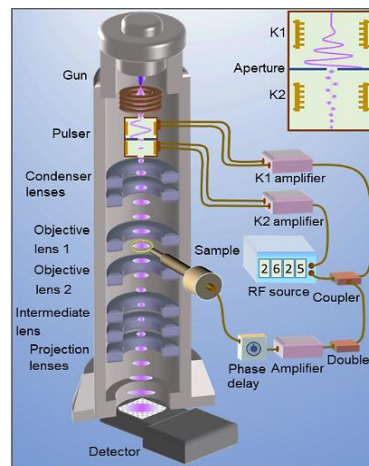


Fig.2 Schematic of the Laser-Free Electron Pulsar showing the integration of a RF-pulsar system a frequency-doubler, and a delay-control RF circuit for the sample excitation. The Pulsar consists of two traveling-wave metallic comb stripline elements: the modulator K1 and the demodulator K2, with a chopping aperture between them. K1 sweeps the continuous electron beam across the chopping aperture to create two electron pulses in each RF cycle, while K2 compensates the K1-induced transverse momentum on the pulses to further rectify the shape of the chopped beam. The Pulsar is inserted between the gun and the condenser lens. Since there is no modification of the microscope its original performance is not compromised [4].

Future Plans

We will continue to focus our three research themes: Heterogeneities, Non-equilibrium and

ultrafast phenomena and Advanced characterization tools, to understand electron-spin-lattice correlations in quantum and energy materials. Below are some proposed activities.

Mapping valence electron distribution based on multipole refinement using 4D-STEM is an area we would like to explore. Valence electrons are electrons involved in chemical bonding that determine materials' functionality. The ability to accurately measure valence electron distribution is at the heart of condensed matter physics and materials science research. The advancement in aberration correction and detector technology opened a door to various applications using 4D-STEM, which generates a diffraction pattern for each scanning position within a crystal unit-cell and produces incredible amounts of data in momentum space. Currently 4D-STEM analysis relies on the center-of-mass of the diffraction patterns in electric field and charge density mapping. It only derives the total projected charge density and is limited to phase objects (extremely thin samples). Recently, we developed a new analytical method to accurately map aspherical valence electron distributions with atom-centered multipolar functions formalism using the whole 4D-STEM dataset [5]. We demonstrate that the method is sensitive not only to the miniscule charge transfer, but also to the atomic site symmetry and aspherical electron orbitals. The process and outcome of the refinement is much more robust and reliable than quantitative convergent beam electron diffraction (QCBED).

We propose to map aspherical valence-electron distribution in MgB_2 , MoS_2 , MoTe_2 and other topological 2D materials (Fig.3). We believe the proposed method can revolutionize the way electron and x-ray diffraction is implemented for valence electron mapping. In the past two decades the PIs supported by the FWP have gained tremendous expertise in charge-density and valence-electron mapping using QCBED in strongly correlated electron systems. However, QCBED is not suitable for defects, as the local strain significantly degrades the information in diffraction patterns. With the probe smaller than the unit-cell in 4D-STEM the approach should in principle work for defects and interfaces. Machine Learning will be incorporated in handling the full dataset.

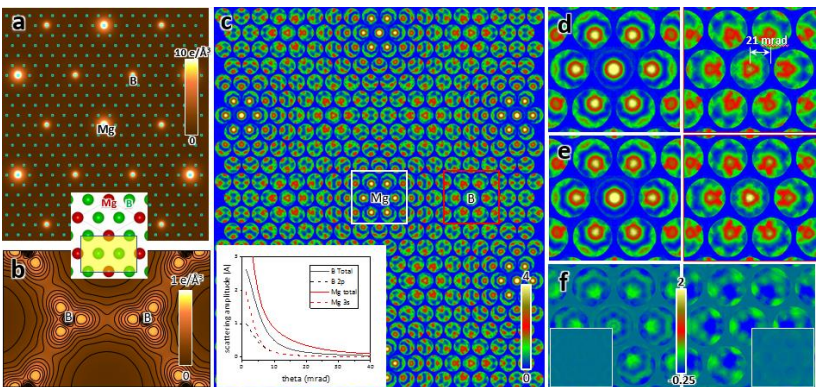


Fig.3 Projected total electron density (a) and valence electron density (b) of MgB_2 superconductor calculated using multiple density formalism with 1 electron transfer from Mg to B. (c) Calculated 4D-STEM pattern showing site symmetry for 10nm thickness. The inset plots scattering amplitude vs angle. (d) Magnified area in (c) around Mg (left column) and B site (right column). (e) Same scan positions as in (d) but calculated based on the Independent Atom Model. (f) Intensity difference between (d) and (e). Insets show intensity difference for 1nm thickness, which is negligibly small [5].

Photoinduced topological phase transitions and GHz electrical excitations is one of our focuses in ultrafast research. Studies of the topological aspects of electronic band structure and the emergent phases governed by topological and chiral protection reveal unusual electronic quasiparticles of Weyl, Dirac, and other exotic types with novel properties valuable for technological applications. Of particular interest is the engineering of new phases of matter using ultrafast external stimuli, such as photonic and electronic excitations, to observe, manipulate and control materials' functionality. Recently, we started to work on ZrTe_5 , a weak topological insulator, to uncover how a transient 3D Dirac chiral semimetal state can be optically induced by

a fs-laser pulse (Fig.4). We propose to further investigate the coherent atomic displacements in ZrTe_5 and related systems to identify phonon modes that can be manipulated, including the energy-selective tuning of the band structure by populating particular modes using THz photons in collaboration with researchers at SLAC. Photoinduced transitions in the nontrivial topological band structures of layered Dirac/Weyl materials such as $(\text{R,A})\text{MnBi}_2$ and $(\text{R,A})\text{MnSb}_2$ (R: rare-earth, A: alkaline-earth) will be also studied.

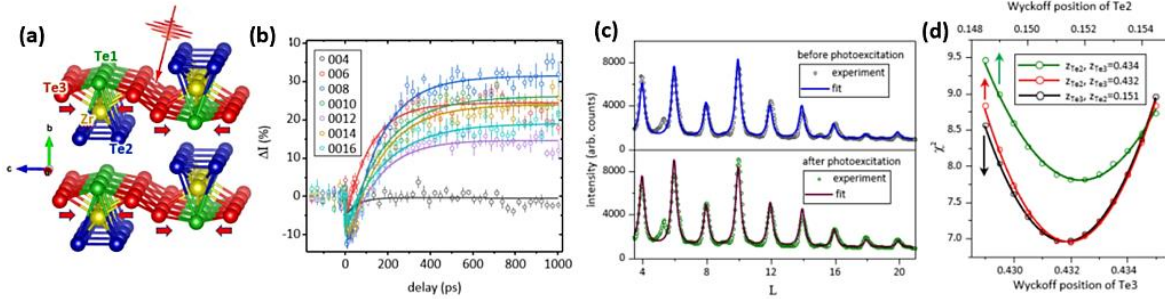


Fig.4 Probing photoinduced dynamics of ZrTe_5 . (a) Crystal structure. (b) Photoinduced intensity change of (00l) Bragg peaks as a function of time delay. (c) Measured intensity profiles (open circles) of the (00l) reflections before (top) and after (bottom) photoexcitation. (d) Goodness of fit (χ^2) as a function of the Wyckoff position of Te3 and Te2 to determine the photoinduced displacement. χ^2 reaches a minimum ($\chi^2 = 7.0$) for $z_{\text{Te}2}=0.151$ and $z_{\text{Te}3}=0.432$. The movement of Te3 leads to the insulating bandgap closing in the photoexcited transient state in ZrTe_5 .

Another class of materials we propose to study is the 2D systems with intriguing charge-density-wave (CDW), such as Te-stabilized $\text{TaSe}_{2-x}\text{Te}_x$ exhibiting polytypism in its crystal structures (1T, 2H and 3R etc) associated with various crystal symmetries (trigonal, hexagonal and rhombohedral etc). We will focus on the phonon evolution through lattice dynamics upon photoexcitation using the time-resolved crystallography approach we developed and to map momentum-dependent diffuse scattering and to quantitatively trace atomic motions. We also plan to use LFEP (Fig.2) to study electric current/field induced Mott insulator-metal transition, which is a hallmark quantum phenomenon and currently receiving considerable attentions due to the potentially new physics involved and the possible applications in microelectronics. Similarly, switching and breathing dynamics of topological chiral spin-textures under excitation, such as magnetic vortex and skyrmions will be of great interest for GHz electric excitations. Study of wave propagation^[4] of acoustically actuated nanomechanical magnetoelectric antennas and sensors based on ferromagnetic/piezoelectric heterostructures has also been planned. Antenna miniaturization has been an open challenge for decades and has the potential for portable wireless communication systems and radars on mobile platforms.

References

- [1] Zhao, W., et al., *Direct imaging of electron transfer and its influence on superconducting pairing at FeSe/SrTiO₃ interface*, *Sci. Adv.* **4**, eaao2682 (2018); Andrejevic, N. et al., *Spectroscopic Signatures of Interfacial Coupling in Single-Layer FeSe on SrTiO₃*, arXiv 1908.05648 (2019).
- [2] Konstantinova, T.; Rameau, J. D.; Reid, A. H.; Abdurazakov, O.; ... and Zhu, Y., *Non-equilibrium electron and lattice dynamics of strongly correlated Bi₂Sr₂CaCu₂O_{8+δ} single crystals*, *Sci. Adv.* **4**, eaap7427 (2018).
- [3] Konstantinova, T.; Wu, L.; Abeykoon, M.; Koch, R. J.; Wang, A. F.; Li, R. K.; Shen, X.; Li, J.; Tao, J.; Zaliznyak, I. A.; Petrovic, C.; Billinge, S. J. L.; Wang, X. J.; Bozin, E. S. and Zhu, Y., *Photoinduced dynamics of nematic order parameter in FeSe*, *Phys. Rev. B* **99**, 180102 (R) (2019).
- [4] Fu, X.; Wang, E.; Zhao, Y.; Liu, A.; Montgomery, E.; Gokhale, V. J.; Gorman, J. J.; Jing, C.; Lau, J. W.; Zhu, Y., *Laser-free ultrafast electron microscopy of electromagnetic wave dynamics*, *Science Advances*, **6** eabc3456 (2020).
- [5] Wu, L.; Meng, Q.; and Zhu, Y., *Mapping valence electron distributions with multipole density formalism using 4D-STEM*, *Ultramicroscopy* **219**, 113095 (2020).

Publications

(10 most relevant, total journal articles supported by this FWP: 96, Sept. 2018 - Aug. 2020)

For full list of publications, see <https://www.bnl.gov/cmpmsd/tem/publications/>

1. S. Deng, L. Wu, H. Cheng, J. C. Zheng, S. Cheng, J. Li, W. Wang, J. Shen, J. Tao, J. Zhu, and Y. Zhu, *Charge-lattice coupling in hole-doped $\text{LuFe}_2\text{O}_{4+\delta}$: the origin of second-order modulation*, Phys. Rev. Lett. **122**, 126401, 1-6 (2019).
2. X. Fu, E. Wang, Y. Zhao, A. Liu, E. Montgomery, V. J. Gokhale, J. J. Gorman, C. Jing, J. W. Lau, Y. Zhu, *Laser-free ultrafast electron microscopy of electromagnetic wave dynamics*, Sci. Adv., **6** eabc3456 (2020).
3. J. A. Garlow, P. D. Pollard, M. Beleggia, D. Tanmay, H. Yang, and Y. Zhu, *Quantification of mixed Bloch-Néel topological spin textures stabilized by the Dzyaloshinskii-Moriya interaction in Co/Pd multilayers*, Phys. Rev. Lett. **122**, 237201 (2019).
4. J. W. Lau, K. B. Schliep, M. B. Katz, V. J. Gokhale, J. J. Gorman, C. Jing, A. Liu, Y. Zhao, E. Montgomery, H. Choe, W. Rush, A. Kanareykin, X. Fu, and Y. Zhu, *Laser-free GHz stroboscopic transmission electron microscope: Components, system integration, and practical considerations for pump-probe measurements*, Rev. Sci. Instrum. **91**, 021301 (2020).
5. T. Konstantinova, L. Wu, M. Abeykoon, R. J. Koch, A. F. Wang, R. K. Li, X. Shen, J. Li, J. Tao, I. A. Zaliznyak, C. Petrovic, S. J. L. Billinge, X. J. Wang, E. S. Bozin, and Y. Zhu, *Photoinduced dynamics of nematic order parameter in FeSe*, Phys. Rev. B **99**, 180102(R) 1-6 (2019).
6. Q. Meng, G. Xu, H. Xin, E. A. Stach, Y. Zhu, and D. Su, *Quantification of charge transfer at the interfaces of oxide thin films*, J. Phys. Chem. A **123**, 21, 4632-4637 (2019).
7. W. Wan, F. R. Chen, and Y. Zhu, *Design of compact ultrafast microscopes for single- and multi-shot imaging with MeV electrons*, Ultramicroscopy **194**, 143-153 (Nov 2018).
8. L. Wu, Q. Meng, and Y. Zhu, *Mapping valence electron distributions with multipole density formalism using 4D-STEM*, Ultramicroscopy **219**, 113095 (2020).
9. W. Zhang, D.-H. Seo, T. Chen, L. Wu, M. Topsakal, Y. Zhu, D. Lu, G. Ceder, and F. Wang, *Kinetic pathways of ionic transport in fast charging lithium titanate*, Science **367**, 1030-1034 (2020).
10. P. Zhou, L. Chen, Y. Liu, I. Sochnikov, A. T. Bollinger, M.-G. Han, Y. Zhu, X. He, I. Bozovic, and D. Natelson, *Electron pairing in the pseudogap state revealed by shot noise in copper oxide junctions*, Nature **572**, 7770, 493-496 (2019).

***UNIVERSITY GRANT
PROJECTS***

Quantitative Interpretation of milli-eV Spatially Resolved EELS Mapping

P.E. Batson

Department of Physics and Astronomy

Rutgers, The State University of New Jersey

136 Frelinghuysen Road, Piscataway, NJ 08854

batson@physics.rutgers.edu

Research Scope

The long term Goal of this project is to develop spatially resolved EELS to better understand the *spatial* and *time* dependence of charge density excitations in nanoscale structures on time scales that range from atto-seconds for core excitations through femto-seconds for electronic processes and finally pico-seconds for vibrational modes. In prior funding periods, we have begun to calculate this information using a Kramers-Kronig transformation of EELS data to reveal the phase of spectral peaks, which define the timing of excitations within the sample relative to each other. The main difficulty is to extract consistent information from imprecise and incomplete experimental data. Ultimately, access to this information will enable rational design of nanostructures to collect, convert, transport, utilize, and store energy. In Fig. 1, we show how a keV electron passing an edge of a nanoscale MgO cube maps a projection of the cube response on a screen below [1]. Ultimately, the work described here is aimed at learning how to obtain data that is sufficiently complete and accurate to calculate maps of specimen behavior in space and time.

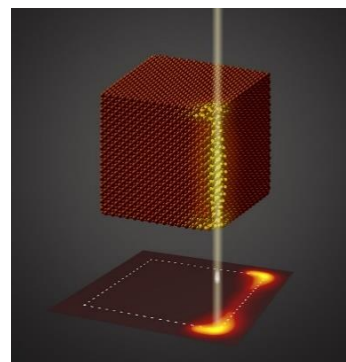


Fig. 1. A keV electron passing the edge of an MgO cube creates a phonon polariton pinned to the edge, and a map is displayed below.

During the past two years, we have collaborated in several projects to improve our understanding of EELS in the 10 meV – 1 KeV ranges using the monochromated Nion microscope. In the milli-eV range, we are working out rules for obtaining a Phonon Density of States (PDOS) from bulk scattering (Batson). In the few hundred meV range, we are investigating carrier plasmons in a doped semi-conductor, Indium Tin Oxide (ITO) (HB Yang), looking at surface, interface and bulk plasmons to infer how they might constrain and modify bulk transport behavior. In a metal-insulator system, we are looking at Rabi coupling of metal surface plasmons to insulator surface polaritons (Lagos, Batson, Botton). Jumping to the core losses, above 100 eV or so, a high energy resolution and collection efficiency is needed to obtain decay processes. To this end, we have been comparing high resolution EELS in the Nion microscope with some data from the 1990's obtained with the VG Microscope Wien Filter spectrometer. The agreement in overall core loss shapes are encouraging, even at the 0.1eV level (Yeh, Yang, Batson).

Spatially Resolved Bulk Phonon Density of States - Batson, Lagos, Yang, Yeh

Obtaining acoustic phonon intensities using an Angstrom sized electron probe is new to science. In the past, these excitations have been accessible only to inelastic neutron and x-ray scattering, both also governed by the dynamical form factor $S(\mathbf{q}, \omega)$ with differing pre-factors. During the

past two years we have created rigorous spectral processing that creates a single scattering vibrational intensity with a clean removal of the unscattered beam down to a little better than 10 meV. Next we remove a systematic term in $1/\text{energy}$ for the acoustic vibrational modes [2], and finally remove the temperature dependent Bose statistical factor that reflects the Principle of Detailed Balance. Fig. 2. shows this numerical processing for SiC. It includes Acoustic (TA, LA), and Optical (TO, LO) Phonon modes. The last panel (upper right) includes a theoretical PDOS [3]. There is also an apparent signal from a surface vibrational mode on the carbon terminating face of the SiC at 12 meV (arrow) [4].

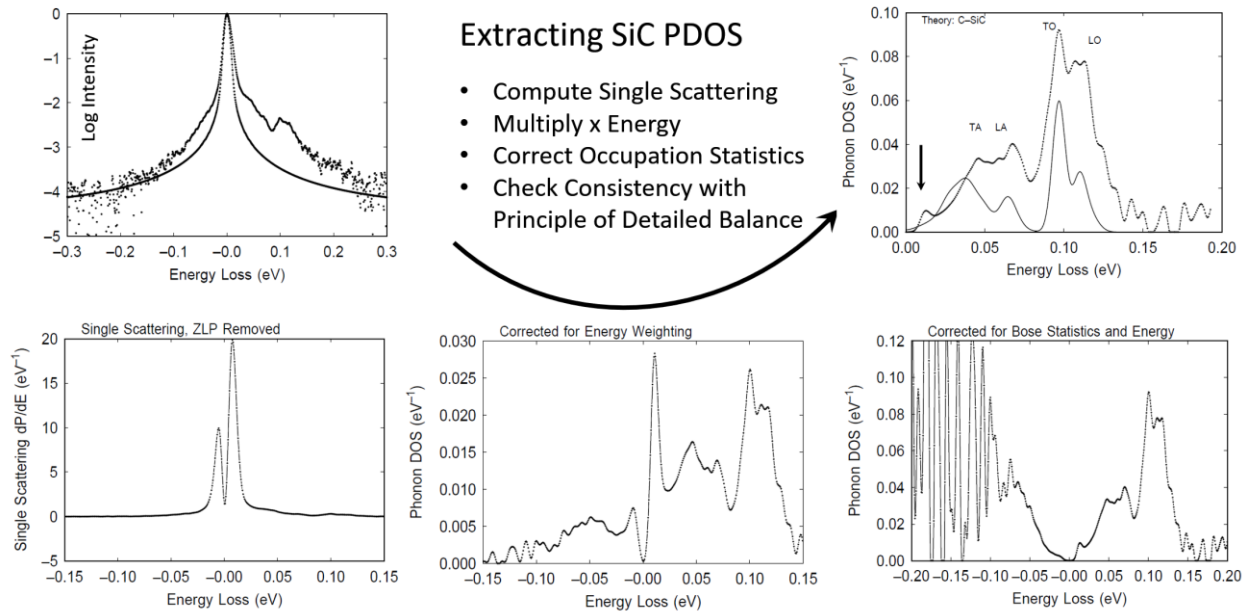


Fig. 2. Processing used to derive a bulk Phonon Density of States: Fit Zero Loss with bulk scattering in transmission. Normalize area, equal to incident beam current. Use a log deconvolution to obtain single scattering. Correct acoustic scattering for a $1/\text{energy}$ strength of impact scattering cross section. Remove Bose Occupation Statistics, checking for consistency with Detailed Balance. This appears to work down to a limit of about $\frac{1}{2}$ the FWHM of the ZLP.

Carrier Plasmon Behavior in Indium Tin Oxide – H. Yang, P.E. Batson, E. Garfunkel

In Figs. 3 and 4 we summarize the bulk and surface *Carrier* plasmons in $\text{Sn}:\text{In}_2\text{O}_3$. Electrons donated by the Sn dopant occupy a shallow conduction band and respond to external fields like a metal having a low electron density, immersed within a large background dielectric function imposed by the Indium Oxide valence electrons. In ITO the Carrier bulk plasmon is near 950 meV (arrows), and surface plasmons lie in the 400-800 meV range. Experimental results are compared with theory in Figures 3c,d. Near a specimen edge, surface plasmons are reflected, creating standing waves on the ITO film that interact with the KeV electron beam, allowing their behavior to be mapped in Fig. 4. The general behavior, shown here, will be discussed together with detailed changes near defects and grain boundaries that allow a determination of the local carrier density and likely mobility from the bulk plasmon characteristics. This work is important to the long term goal, because it also connects low intensity electronic behavior to high intensity phonon losses in the energy range immediately below, evidenced by the large scattering intensity below 100 meV in Fig. 3c,d. This work is currently under review.

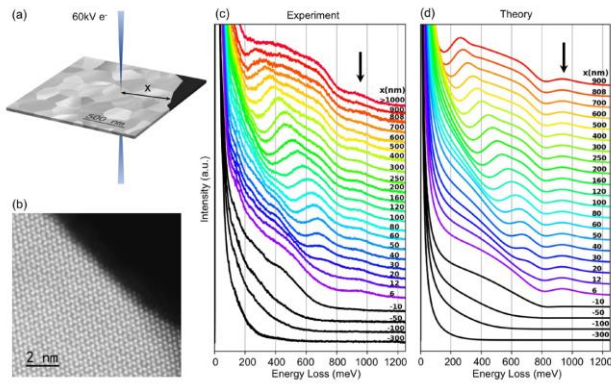


Fig. 3. ITO experiment: a) Scattering geometry at distance x , from specimen edge. b) ADF sample structure. c) Bulk (colors) and alioof (black) spectra include carrier polaritons and bulk (arrow) plasmon spectra. d) Theory.

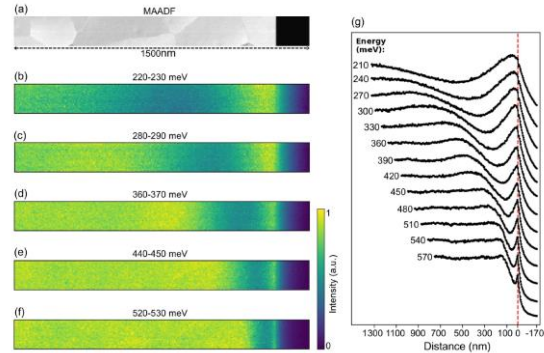


Fig. 4. Area mapping for several energy windows capture carrier surface polariton interference behavior on the top/bottom of the thin specimen, bounded on the right by the ITO-vacuum edge.

Plasmon – Phonon Coupling – M.J. Lagos, P.E. Batson, G. Botton

Placing two rod-like antennas of aluminum and amorphous silica in a parallel configuration, with the aluminum infrared plasmon response tuned to coincide with the “cavity” vibrational response of the silica antenna, should produce Rabi splitting [5], with the appearance of new quasi-particles

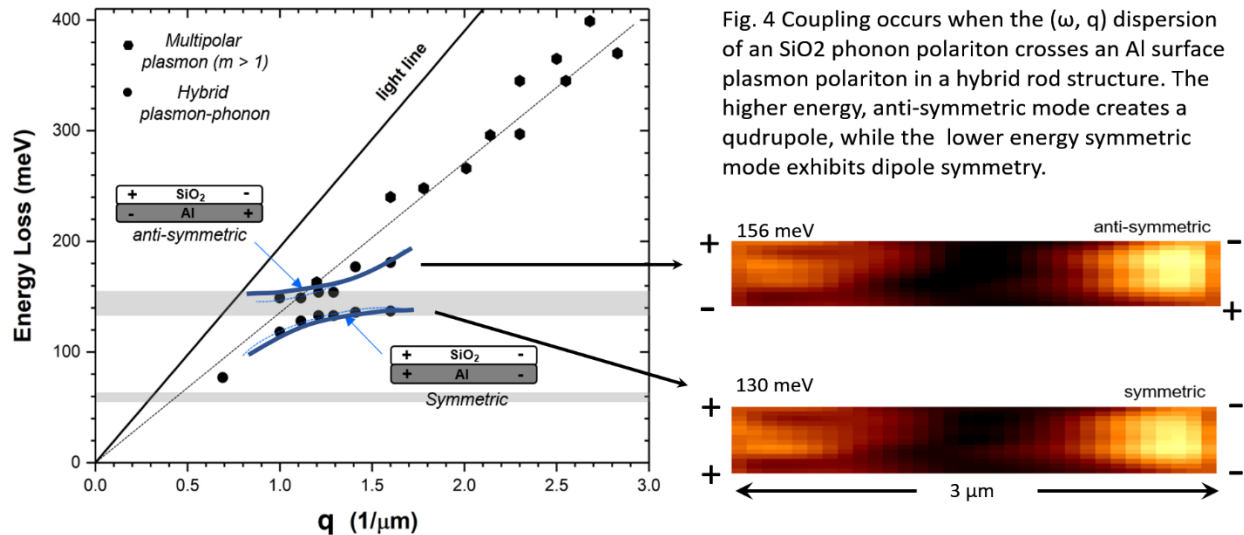


Fig. 4 Coupling occurs when the (ω, q) dispersion of an SiO₂ phonon polariton crosses an Al surface plasmon polariton in a hybrid rod structure. The higher energy, anti-symmetric mode creates a quadrupole, while the lower energy symmetric mode exhibits dipole symmetry.

having complimentary symmetry. In a collaboration with McMaster University, we have achieved this behavior using 3 μm length rods, recording both EELS spectra and imaging with a range of rod lengths, to evaluate the regimes of weak and strong coupling. The spectral results showed true Rabi splitting involving plasmon-phonon coupling, with typical spectra showing two peaks separated by about 26 meV within the SiO₂ Reststrahlen band, resulting from the two coupled modes (symmetric and anti-symmetric). Figure 4 shows the dispersion curves of the surface polaritonic modes sustained in the hybrid system, including Rabi modes between 120 - 180 meV, and several multipolar Al antenna modes which appear above 220 meV. The surface charge configurations of each mode are shown on the schematics. The Rabi mode coupling strength appears comparable to other strong-coupling platforms using novel state-of-art materials, in spite of the modest strength of the vibrational polariton of the silica rod, suggesting that the antenna

morphology plays a key role in strong-coupling systems. Finally, we spatially mapped the EELS distribution for the Rabi modes, identifying a dipolar pattern, parallel to the rod lengths, consistent with the graphic depictions in the figure. We think future work will likely reveal quadrupole symmetry, suggested here for the anti-symmetric mode. This work is currently being written up and will include acknowledgement of DOE support for experimental work at Rutgers.

Comparison of EELS Core Losses with Prior Results – P.E. Batson, H. Yang and Y-W. Yeh

In Fig. 5 we compare Nion high resolution EELS core loss spectra for Si, diamond, and graphite with 0.25 eV resolution results obtained during the 1990s with the VG 120kV STEM equipped with a Wien Filter electron spectrometer [6,7]. These results were controversial at the time, because they disagreed with expectations for the core exciton behavior, showing notably weaker excitonic distortion than observed using synchrotron XANES measurements. We found remarkable agreement, including for expected distortions resulting from the core exciton. Noted differences include the energy resolution, which is better in the Nion case, and, for the graphite, the mismatch of collection conditions, which creates different amounts of π^* and σ^* contributions. In these examples, we shifted the Nion results to match the energy of the Wien filter result. For the time resolved EELS Goal of this project, an accurate energy scale, transferable among several EELS data sets, yet to be obtained, will be crucial for success.

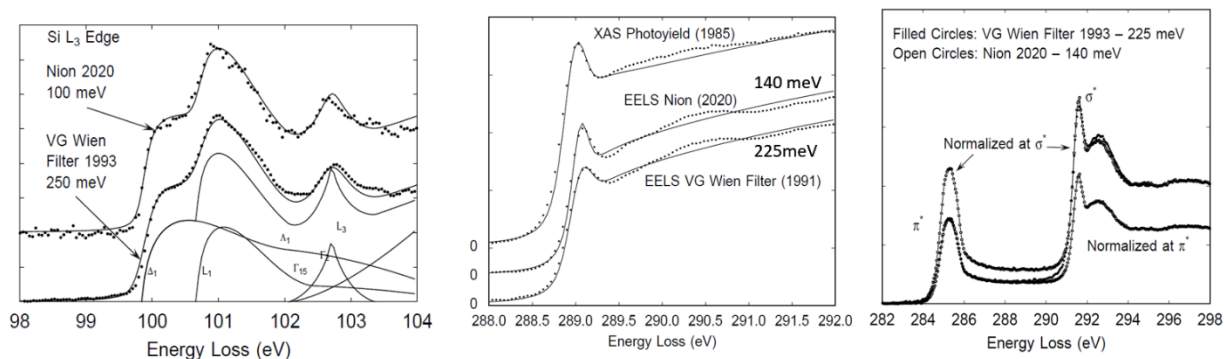


Fig. 5. Comparisons of Nion high resolution data with prior results to verify reproducibility.

Other Activity

We have also collaborated with several other groups including P. Abbamonte (U. Illinois) to compare electron scattering behavior in the “strange” metal Sr_2RuO_4 , F. Celik (Rutgers) on elliptical motion of Ir Pincer molecules tethered to silica (in writing), and R. Stroud on spectroscopy of extraterrestrial compounds using EELS.

References:

- [1] M.J. Lagos, A. Trügler, U. Hohenester and P.E. Batson, *Nature*, **543** 529 – 532 (2017).
- [2] A.Q.R. Baron, arXiv,cond-mat.mtrl-sci, (2015).
- [3] J. Serrano, et al., *Appl. Phys. Lett.*, **80** 4360 (2002).
- [4] J. Soares and H.L. Alves, *Microelectronics Journal*, **36** 1026 - 1028 (2005).
- [5] O. Bitton, et al., *Nature Communications*, **11** 487- (2020).
- [6] P.E. Batson and J. Bruley, *Phys. Rev. Lett.*, **67** 350–353 (1991).
- [7] P.E. Batson, *Phys. Rev. B*, **48** 2608–2610 (1993).

Journal Articles:

- [1] M.J. Lagos, A. Trügler, V. Amarasinghe, L.C. Feldman, C. Leonard, U. Hohenester and P.E. Batson, *Excitation of long-wavelength surface optical vibrational modes in films, cubes and film/cube composite system using an atom-sized electron beam*, *Microscopy*, 67 i3-i13 (2018) doi:10.1093/jmicro/dfx130.
- [2] M.J. Lagos and P.E. Batson, *Nanoscale thermometry with angstrom-resolution in the electron microscope*, *NanoLett*, 18 4556 – 4563 (2018). doi:10.1021/acs.nanolett.8b01791.
- [3] H. Rabie, Y. Zhang, N. Pasquale, M.J. Lagos, P.E. Batson and K.B. Lee, *NIR Biosensing of Neurotransmitters in Stem Cell-Derived Neural Interface Using Advanced Core Shell Upconversion Nanoparticles*, *Advanced Materials*, 31 1806991 (2019) doi:10.1002/adma.201806991.
- [4] T.V. Tsoulos, P.E. Batson and L. Fabris, *Multipolar and Bulk Modes: Exploring Single Particle Plasmonics through the Advances in Electron and Photon Techniques*, *NanoPhotonics*, (in press 2020) doi:10.1515/nanoph-2020-0326.
- [5] A.A. Husain, M. Mitrano, M.S. Rak, S.I. Rubeck, H. Yang, C. Sow, Y. Maeno, P.E. Batson and P. Abbamonte, *Coexisting Fermi Liquid and Strange Metal Phenomena in Sr2RuO4*, (under review 2020).

Extended Abstracts:

- [1] M.J. Lagos and P.E. Batson, *Electron Energy-Gain Processes in Nanostructures in induced by Fast Electrons*, *Microscopy and Microanalysis*, Post Deadline Poster-44 (2017).
- [2] P.E. Batson and M.J. Lagos, *Interpretation of meV Resolution Phonon EELS Data*, *Microscopy and Microanalysis*, (2018).
- [3] M.J. Lagos and P.E. Batson, *Nanoscale Temperature Measurements Using Phonon Scattering*, *Microscopy and Microanalysis*, (2018).

Data-Science Enabled, Robust and Rapid MeV Ultrafast Electron Diffraction Instrument System to Characterize Materials Including for Quantum and Energy Applications

Sandra Biedron, The University of New Mexico (Principal Investigator) and Manel Martínez-Ramón, The University of New Mexico (Co-Investigator)

Keywords: MeV ultrafast electron diffraction (MUED), pump photoexcitation, transfer learning, accelerator controls, machine learning

Research Scope

MeV ultrafast electron diffraction (MUED) is a powerful structural measurement technique recently demonstrated to provide a number of complementary capabilities for novel characterization of matter. MUED takes advantage of the strong interaction between electrons and matter and minimizes space charge problems seen in other low-energy electron diffraction systems. An MUED instrument can resolve much finer structural details enabling us to see how atoms in molecules move and can make molecular movies of ultrafast chemical reactions by utilizing a pump-probe technique.

While a few facilities have been constructed to provide these advanced capabilities to a growing user community, as a relatively young technology, progress is ongoing and much remains to be learned by improving these facilities, especially in maximizing throughput and ease of operation (e.g. rapid initialization and high stability). One class of advancement that can be immediately investigated at MUED facilities is the demonstration of realtime or near-realtime data processing enabled by data science/machine learning/artificial intelligence mechanisms in conjunctions with high-performance computing (HPC) to bring automated operation, data acquisition and processing to the facility control and experiment analysis, thereby enabling faster measurement throughout. For example, applying deep learning to MUED diffraction patterns generated through instrument probing of materials systems is an innovative step to turn-key, high throughput and high research output instruments. Such an approach has been demonstrated with success when applied to X-ray diffraction and many other experiments, and there is high confidence that significant gains are possible for MUED facilities. By fully automating the facility from machine operation through to material property characterization, the user base will be expanded, as experimenters from a wide range of disciplines would no longer need to learn complex machine optimization procedures or rely on other facility experts to do measurements.

Our goals are to utilize the expertise of our collaboration to identify the most promising machine learning (ML) and artificial intelligence (AI) techniques with which we are familiar, as well as others used in the accelerator and facility user communities, apply and optimize them for improved operation of the Brookhaven National Laboratory Accelerator Test Facility MUED instrument in conjunction with enhanced computer interfacing and diagnostic capability of the machine, conduct online ML-control to provide the users the ideal beam with high stability for specific material types, provide experimenters with greatly improved usability and sample throughput, and

consequently demonstrate increased scientific productivity of MUED facilities. We will do this in seamless conjunction with a second user facility, the Argonne Leadership Computing Facility (ALCF).

Scientific advancement will be enabled in a wide range of fields including accelerator science, materials science, ML control, and in AI for Science with HPCs. Some of the materials science focuses we are considering during the validation phase are on compounds applied in diverse uses such as superconductors, battery and fuel cell components, high strength magnets, thermoelectrics, and quantum information storage and manipulation. MUED (and its cousin technique MEU Microscopy) is also emerging for interesting biomolecules.

This research proposal is also important in order to open the door to new collaborations between the UNM and LANL team members and an Office of Science User Facility at Brookhaven – the Accelerator Test Facility – that will enable high-throughput research with materials through the use of data science, ML and AI. Such a research infrastructure is not currently available in the State of New Mexico. Additionally, the UNM and LANL team members, as well as the BNL team members will have access to the ALCF. Finally, the Argonne team members will be interfacing their facility with the new genre of user facility (MUED) at BNL for new explorations in AI for Science.

We acknowledge our collaborators at the DOE national laboratories: DOE/National Laboratory Collaborator(s): David Martins, Michael Papka, (Argonne National Laboratory); Marcus Babzien, Mark Palmer, Jing Tao, Kevin Brown (Brookhaven National Laboratory); Alan Hurd, John Sarrao, Christine Sweeney, Rohit Prasankumar, Julian Chen (Los Alamos National Laboratory). Note underlined person is the designated collaborator but in fact, there are multiple collaborators at each national laboratory

Recent Progress and Future Plans

We plan to make the graduate student and post-doctoral researcher hires in September 2020 and begin our research the week of 21 September 2020.

References

1. Renkai Li, Chuanxiang Tang, Yingchao Du, Wenhui Huang, Qiang Du, Jiaru Shi, Lixin Yan, and Xijie Wang, “Experimental demonstration of high quality MeV ultrafast electron diffraction,” *Review of Scientific Instruments* 80, 083303 (2009); <https://doi.org/10.1063/1.3194047>.
2. M.A. Palmer, M. Babzien, M. Fedurin, C.M. Folz, M. Fulkerson, K. Kusche, J. Li, R. Malone, T. Shaftan, J. Skaritka, L. Snyderstrup, C. Swinson, F.J. Willeke, “Installation and Commissioning of an Ultrafast Electron Diffraction Facility as part of the ATF-II Upgrade,” *Proceedings of NAPAC2016*, 742-744.
3. J. Tao (corresponding author), et al., “Probing pathway of an ultrafast structural phase transition to illuminate the transition mechanism in Cu₂S,” *Applied Physics Letters* 113, 041904 (2018).
4. J. Tao (co-corresponding author) et al., “Reversible structure manipulation by tuning carrier concentration in metastable Cu₂S,” *Proceedings of the National Academy of Sciences*, 114, 9832 (2017).

Infrared Nano-Spectroscopy of Plasmonic Materials with High-Resolution STEM-EELS

Jon P. Camden¹ and David J. Masiello²

¹Department of Chemistry and Biochemistry, University of Notre Dame, Notre Dame, IN 46556, ²Department of Chemistry, University of Washington, Seattle, WA 98195

Keywords: IR Nano-Spectroscopy, Nano-Ellipsometry, Photonics, Plasmonics

Research Scope: Understanding and directing the flow of energy at the nanoscale is critically important for the rational design of the next generation of materials endowed with novel electronic, magnetic, thermal, and optical functionalities. These properties are encoded in the local and bulk dielectric response as well as in particle morphology and cluster geometry, which give rise to the collective resonant excitations sustained by plasmonic and phononic materials. Despite recent progress made using optical spectroscopies, the details of how nano-architectures transduce energy, charge, and heat to their local environment is obscured by the diffraction limit making spatially-resolved measurements increasingly difficult for low energy phenomena, such as infrared (IR) plasmons and lattice vibrations. Electron energy loss spectroscopy (EELS) performed in a scanning transmission electron microscope (STEM) combines sub-nanometer resolving power with the capability to interact with a full spectral range of target excitations in a nanoscale environment. The current generation of aberration corrected and monochromated instruments have also significantly improved the energy range and energy resolution (<6 meV), making STEM-EELS an ideal technique for probing low energy material responses at the single particle level.[Reference 1 and Publication 10]

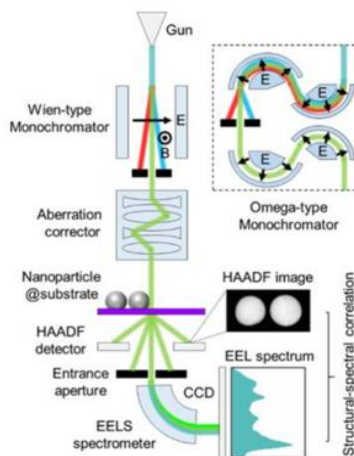


Figure 1. EEL spectrum acquisition in a STEM equipped with a monochromator and an aberration corrector.

Recent Progress:

(1) *Carrier-doped semiconductor nanocrystals and electron beam infrared nano-ellipsometry (Publication 1).* Carrier doped semiconductor nanocrystals (NCs) are a novel class of plasmonic materials endowed with tunable resonance features in the near- to mid-IR spectral range. Importantly, these NCs have resonances that are natively in the IR at nanoscale size that are tunable with dopant concentration, as shown by ensemble measurements. The spectral broadening due to particle heterogeneity, however, obscures the IR responses of individual NCs. By examining a series of Sn⁴⁺ doped indium tin oxide (ITO) NCs with STEM-EELS we show that increasing the dopant concentration is an effective method for tuning the plasmon responses over a broad range of IR energies. We further retrieve the underlying dielectric function representing each individual NC by positioning the STEM electron probe at penetrating and aloof impact parameters to excite both bulk and surface collective responses that are processed through a model-based inversion

procedure. We demonstrate the efficacy of this approach to return the complex-valued, frequency-dependent Drude dielectric function at each dopant concentration at the single-NC level. The power of this technique allows for the determination of the dielectric parameters from arbitrarily rich models in a single measurement, paving the way for broadband measurements of dielectric responses for materials that cannot be prepared in bulk form or as thin films.

(2) *Fundamental Studies in Nano-Spectroscopy (Publications 3-5)*. Motivated by the spectrally narrow photonic mode linewidths of micron-scale

nanowires (NWs), we set out to observe the plasmonic analog of the asymmetric lineshape Fano observed in the EEL autoionization spectrum of He gas. Although Fano interferences have been measured in a variety of optical systems, the observation of an all plasmonic Fano antiresonance in the EELs has been elusive. Generalizing Fano’s original discrete and continuum states as narrow and broad resonances, we designed and measured the spectral response of a plasmonic nanostructure that satisfies two critical requirements (i) the individual plasmonic “configurations” are weakly coupled to each other and (ii) there is at least a factor of 10 or greater between the linewidths of each configuration. These parameters resulted in a long gold NW paired with a gold nanodisk separated by a gap of specific distance. Weak coupling was achieved at the relatively large disk-rod separation distances of ~ 50 nm, resulting in the first observation of an EEL spectra showing multiple plasmonic Fano antiresonance lineshapes (Fig 3A).

While NW plasmons have been the subject of numerous previous studies, the mid-IR Fabry-Perot (FP) resonances remain unexplored due to significant experimental challenges. IR photothermal heterodyne (IR-PHI) imaging offers spectral resolution on the order of a few cm^{-1} and operates in ambient conditions with spatial resolution of a few hundred nanometers. By complement, STEM-EELS is capable of exciting and measuring the complete set of NW FP resonances with sub-nanometer spatial resolution. Using a combination of these techniques we examine the FP resonances of gold NWs with mode energies ranging from ~ 1000 - 8000 cm^{-1} . Changing the length of the NW progressively tunes the FP resonance (Fig. 3B) and, for a given mode, the resonance energy redshifts as rod length increases. Interestingly, the resonance energy linewidth narrows as NW length increases. Approximating the optical response of the NWs using a Drude free-gas model reveals that the full width at half maximum (FWHM) of the dipolar extinction spectrum decreases with increasing aspect ratio, and can even lie below the bulk Drude damping contribution for NWs longer than $2.5\mu\text{m}$. Our combined experimental and theoretical work shows that as the FP resonance moves towards lower energy, the dispersion of the mode approaches the light line and the resonances become less confined within the metal. By deconvolving the FP mode from the width of the elastic scattering peak in EELS the dephasing time can be extracted for individual

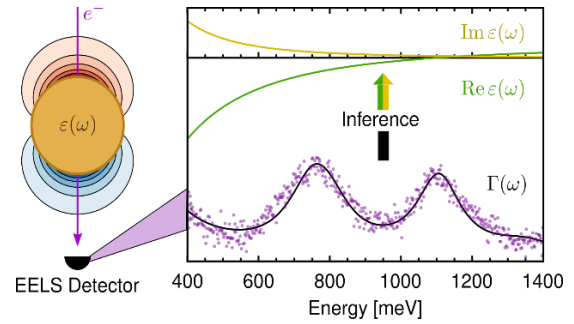


Figure 2. The IR plasmon resonances of individual ITO nanocrystals are resolved by STEM-EELS. By collecting a spectrum that simultaneously measures the bulk and surface plasmon, we implement a dielectric inversion procedure to extract the frequency dependent dielectric function.

NWs. For long NWs the dephasing time can exceed 60 fs when the mode energy approaches the mid-IR, which is ~ 4 times longer than the lifetime of plasmons in the visible range and exceeds the predicted maximum dephasing time for an Au nanoparticle in the quasistatic limit. Considering that a typical C-H stretching mode has a period of ~ 10 fs, the mid-IR NW FP modes can provide a relatively long timescale for energy coupling or plasmon assisted chemical reactions.

(3) *Interactions between plasmonic particles and their environment (Publications 7-9)*. It is well known that localized surface plasmons (LSPs) are highly sensitive to their environment; however, interpreting the myriad interactions of plasmonic systems requires detailed theoretical modeling and experimental observation at the nanoscale. Many studies, for example, have examined nanoparticles on semi-infinite substrates; yet, few explicitly account for the influence of substrate thickness on the LSP modes. The high degree of spatial confinement of the electron beam in STEM-EELS enables a detailed understanding of the influence of substrate dielectric properties and thickness on the individual plasmon modes of a single Ag nanocube. Experiment and theoretical modeling show that the thickness, refractive index, and particle-substrate separation distance can dramatically impact LSP mixing in such a way that significant hybridization may occur even when substrate thickness is well below 100 nm. Another aspect of a particle's environment is the influence of neighboring particles. In most cases simple particle coupling results in so called "plasmon molecules" with hybridized LSP modes, however, in some cases particles with specific circular aggregation orientations may result in plasmonic oligomers with anomalously strong magnetic character. For these structures the quasistatic approximation may not be rigorous enough to justify the magnetic character, resulting in the question of when and how retardation effects matter. Based on theoretical modeling we demonstrate the size dependent evolution of such magnetic plasmon responses and elucidate their radiative properties. Finally, the effects of plasmonic Landau damping in optically active environments are explored by theoretical analysis of individual nanoparticles in the quantum size regime. An accurate analytic theory is used to quantitatively model plasmon decay into electron-hole pairs, and demonstrates the decay depends significantly on the dielectric environment of the nanoparticle, disentangling the effects of competing decay pathways.

(4) *Imaging the photon stimulated excited state of individual nanoparticles with electron energy loss and electron energy gain spectroscopy (Publications 2, 6)*. Understanding plasmon excited states is vital to deciphering the mechanism of electromagnetic energy transfer through radiative, non-radiative, and other energy dissipation pathways. Traditional STEM-EELS is capable of

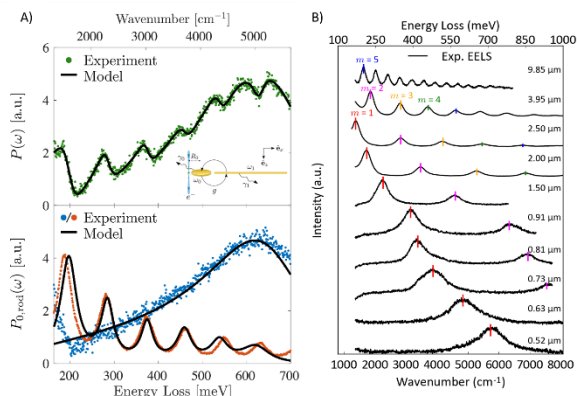


Figure 3. A) STEM-EELS spectra reveal multiple Fano resonances in the all plasmonic disk-rod system. B) Spectra show the energy of individual resonances shifting as a function of Au NW length.

accessing the full set of bright and dark LSP modes, where the STEM electron probe acts as an intense white light source. Recently a novel system coupling a high-frequency pulsed laser to a gated EEL spectrometer has been shown to generate a stimulated electron energy gain and loss (sEEL and sEEG) signal which can interrogate photon-plasmon coupling with nanoscale precision in any electron microscope. By extending that system to include a continuous wave (cw) laser we explore the bright and dark modes of plasmonic nanoparticles due to the ability of sEELS/sEEGS to couple to far-field radiation. As expected by optical selection rules, we find stronger photon-plasmon coupling for optically bright modes compared to dark modes for silver nanorods. Dark modes, however, are accessible by tilting the sample such that s- and p-polarization induce retardation effects and thus increase the extinction coefficient of the mode.

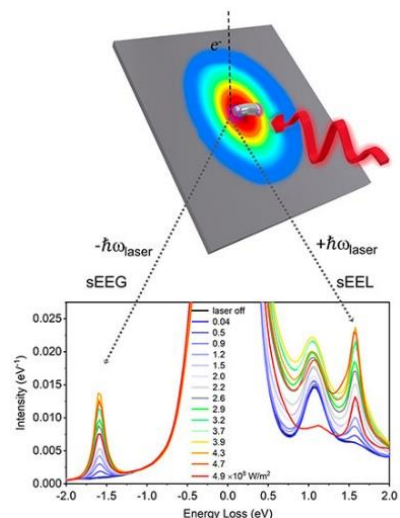


Figure 4. Schematic of an incident photon interacting with a plasmonic nanoparticle, resulting in the laser power dependent sEELS and sEEGs.

Future Plans

Measuring local optical constants by inversion of electron energy loss spectroscopy of plasmonic nanostructures. Expanding the functionality of the STEM-EELS based dielectric inversion is essential for measuring the broadband dielectric properties of a wide range of nanoscale materials, especially the myriad of novel materials that cannot be prepared in bulk form or as thin films. Our goal is to devise extensions of our original model-based inversion method and concurrently establish model free methods based on an analytically determined Green's functions for particles and even simple nanoparticle aggregates on resonant substrates of a finite thickness.

Examining local energy transfer in extended plasmonic arrays. The organization of particles with spacings similar to the LSP resonance wavelength produces a variety of interesting optical properties. Although the ensemble properties of these array have been examined, there have been few studies that examine the response of individual or few particles within the system. A bottom up approach will be employed to study the resonant properties of extended plasmonic arrays by fully characterizing few-particle units and defects using high-energy resolution STEM-EELS and combining these measurements with numerical simulations and analytical modeling. This knowledge will then be used to address large-scale assemblies possessing periodic and aperiodic symmetries and their potential defects

References

- (1) Hachtel, J. A.; Lupini, A. R.; Idrobo, J. C. *Exploring the capabilities of monochromated electron energy loss spectroscopy in the infrared regime.* Scientific Reports, **8**, 5637, (2018).

Publications Resulting from DOE Support (2018-2020)

1. Agust Olafsson, Jacob A. Busche, Jose J. Araujo, Arpan Maiti, Juan Carlos Idrobo, Daniel R. Gamelin, David J. Masiello, and Jon P. Camden. *Electron Beam Infrared Nano-Ellipsometry of Individual Indium Tin Oxide Nanocrystals*. Nano Letters, **Accepted**, (2020)
2. Robyn Collette, David A. Garfinkel, Zhongwei Hu, David J. Masiello, and Philip D. Rack. *Near Field Excited State Imaging via Stimulated Electron Energy Gain Spectroscopy of Localized Surface Plasmon Resonances in Plasmonic Nanorod Antennas*. Scientific Reports **10**, 12537 (2020)
3. Yueying Wu, Zhongwei Hu, Xiang-Tian Kong, Juan Carlos Idrobo, Austin G. Nixon, Philip D. Rack, David J. Masiello, and Jon P. Camden. *Infrared Plasmonics: STEM-EELS Characterization of Fabry-Perot Resonance Damping in Gold Nanowires*. Physical Review B **101**, 085409 (2020)
4. Kyle Aleshire, Iliia M. Pavlovec, Robyn Collette, Xiang-Tian Kong, Philip D. Rack, Shubin Zhang, David J. Masiello, Jon P. Camden, Gregory V. Hartland, and Masaru Kuno. *Far-Field Midinfrared Superresolution Imaging and Spectroscopy of Single High Aspect Ratio Gold Nanowires*. Proceedings of the National Academies of Sciences, **117 (5)**, 2288-2293, (2020)
5. Kevin C. Smith, Agust Olafsson, Xuan Hu, Steven C. Quillin, Juan Carlos Idrobo, Robyn Collette, Philip D. Rack, Jon P. Camden, and David J. Masiello. *Direct Observation of Infrared Plasmonic Fano Antiresonances by a Nanoscale Electron Probe*. Physical Review Letters **123**, 177401 (2019)
6. Chenze Liu, Yueying Wu, Zhongwei Hu, Jacob A. Busche, Elliot K. Beutler, Nicholas P. Montoni, Thomas M. Moore, Gregory A. Magel, Jon P. Camden, David J. Masiello, Gerd Duscher, and Philip D. Rack. *Continuous Wave Resonant Photon Stimulated Electron Energy-Gain and Electron Energy-Loss Spectroscopy of Individual Plasmonic Nanoparticles*. ACS Photonics **6**, 2499-2508 (2019)
7. Nicholas P. Montoni, Steven C. Quillin, Charles Cherqui, and David J. Masiello. *Tunable Spectral Ordering of Magnetic Plasmon Resonances in Noble Metal Nanoclusters*. ACS Photonics **5**, 3272-3281 (2018)
8. Niket Thakkar, Nicholas P. Montoni, Charles Cherqui, and David J. Masiello. *Plasmonic Landau damping in active environments*. Physical Review B - Rapid Communication **97**, 121403(R) (2018)
9. Charles Cherqui, Guoliang Li, Jacob A. Busche, Steven C. Quillin, Jon P. Camden, and David J. Masiello. *Multipolar Nanocube Plasmon Mode-Mixing in Finite Substrates*. Journal of Physical Chemistry Letters **9**, 504-512 (2018)
10. Yueying Wu, Guoliang Li, Jon P. Camden. *Probing Nanoparticle Plasmons with Electron Energy Loss Spectroscopy*. Chemical Reviews **118 (6)**, 2994-3031, (2018)

Non-zero transverse resistance in zero magnetic field in $\text{Al}_2\text{O}_x/\text{SrTiO}_3$ two-dimensional electron gases: Evidence for spatially varying magnetism near the quantum paraelectric transition

Venkat Chandrasekhar, Department of Physics, Northwestern University

Research Scope

The primary current focus of this project is the investigation of correlated electron physics in the two-dimensional carrier gas (2DCG) that forms at interfaces in SrTiO_3 (STO) based heterostructures. Current research focuses on two types of heterostructures: $\text{La}_{0.3}\text{Sr}_{0.7}\text{Al}_{0.65}\text{Ta}_{0.35}/\text{SrTiO}_3$ (LSAT/STO) and $\text{Al}_2\text{O}_x/\text{STO}$ interface devices. In both types of heterostructures, our emphasis is on studying interfaces grown on (111) oriented STO substrates. This crystal orientation is much less studied than the (001) crystal orientation and might potentially show new topological effects due to the hexagonal symmetry of the interface gas.

Recent Progress

2DCGs in STO based interface devices show a variety of complex correlated electron phenomena, including superconductivity, magnetism and strong spin-orbit interactions. Almost all of these phenomena are tunable with an electric field, frequently applied by means of a voltage applied to the STO substrate, a so-called backgate voltage V_g . By varying V_g , one can tune the resistivity, the superconducting transition temperature and the spin-orbit interactions in STO based interfaces. This is similar to the way one can tune the conductance of semiconductors with a gate voltage. In However, in STO interface devices, the voltage is applied through the dielectric STO substrate, so that gating effects are convoluted with the rather rich dielectric properties of STO. STO undergoes a structural transition from a cubic to tetragonal phase at 105 K, forming domain walls between tetragonal domains. It is a quantum paraelectric, a material that would like to go ferroelectric at low temperatures but is prevented from doing so by the zero-point motion of the oxygen atoms [1]. It has a dielectric constant ϵ that is a few hundred at room temperature that rises to a few tens of thousands at low temperatures (<20 K) and depends on the applied electric field [2]. Recently, the quantum paraelectric transition in STO has seen renewed interest [3]. In addition, the role of the domain walls that form between tetragonal domains in determining both the dielectric properties of the STO as well as the conducting properties of 2DCGs in STO based interfaces has attracted attention [4].

Ferromagnetism in STO based interface devices has been widely reported and has been studied through electrical transport, magnetometry and scanning SQUID techniques. In terms of electrical transport, the magnetism manifests itself as a hysteresis in the longitudinal and transverse (Hall) magnetoresistance that is typically seen at very low temperatures (<1 K). At higher temperatures, this hysteresis disappears. However, a small but finite transverse resistance in zero external magnetic field is sometimes seen at higher temperatures, but this effect has mostly been ignored until now. A finite transverse resistance usually arises from time-reversal symmetry breaking, a

sign of intrinsic magnetic ordering in the system. We report here measurements of this zero-field transverse resistance as a function of temperature and V_g , showing that it is much larger in (111) oriented STO interfaces in comparison to (001) oriented interfaces and that it is correlated with changes in ϵ of the STO near the quantum paraelectric transition. We believe this zero-field transverse resistance is associated with an intrinsic magnetism associated with the domain walls. Our results are consistent with recent studies showing that the polar domain walls host magnetism below 40 K, near the quantum paraelectric transition [6].

The devices for this study were fabricated by depositing a thin layer of amorphous oxidized Al on top of Hall bar patterns on (001) and (111) oriented STO substrates. The Al getters oxygen from the STO, creating a conducting surface at the interface. Figure 1 shows the longitudinal (R_L) and

transverse (R_T) resistance of a (001) and a (111) Hall bar at a backgate voltage of 80 V in zero magnetic field. R_L for both samples shows a large decrease in resistance with decreasing temperature, particularly for the (111) device, demonstrating

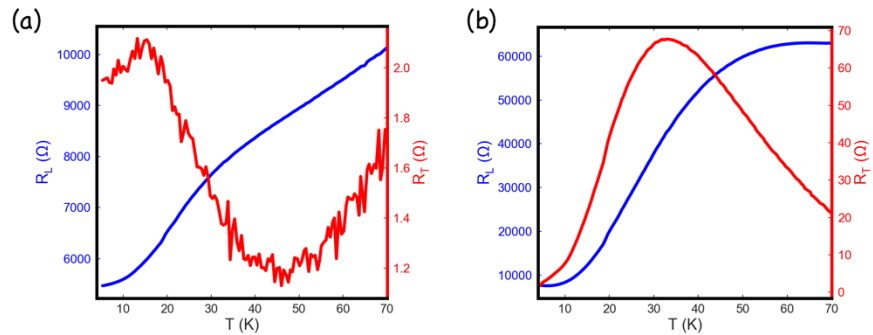


Figure 1. Longitudinal (blue) and transverse resistances as a function of temperature for a (001) oriented device (a) and a (111) oriented device (b). $V_g=80V$.

that these structures have less disorder than LAO/STO devices, likely due to the smaller amount of strain between the Al_2O_x and STO. These plots also demonstrate two important features of the zero-field transverse resistance R_T . First, for both samples, $R_T(T)$ does not scale with $R_L(T)$, showing that the finite zero-field resistance does not arise simply from a misalignment of the transverse voltage probes, the usual explanation given for a finite zero-field transverse resistance. Second, R_T for the (111) sample varies over a range that is more than an order of magnitude larger than the range for the (001) sample. In addition, we find that R_T varies as a function of position: R_T measured on a different set of transverse probes on the same Hall bar shows a different magnitude and temperature dependence.

Figures 2(a) and (b) show the zero-field R_T for (001) and (111) oriented Hall bars as a function of temperature and backgate voltage. As can be seen, the variation in R_T for the (001) device is more than an order of magnitude smaller than that for the (111) device over the entire T - V_g parameter regime. If R_T is associated with magnetic order in the ferroelastic domain walls, it might be expected to correlate with the dielectric constant of the STO. In order to explore this correlation, we have also measured the capacitance C between the backgate and each Hall bar as a function of T and V_g . These data are shown in Fig. 2(c) for the (001) oriented device and Fig. 2(d) for the (111) oriented device. Assuming a simple parallel plate geometry, C is a measure of the dielectric constant of the STO. As expected, C is smaller at higher temperatures and increases with

decreasing temperature, reflecting the well-known increase of the STO dielectric constant with decreasing temperature. For the (001) oriented sample, $C(T)$ is essentially independent of V_g , showing a rapid increase at around 25 K over the entire gate voltage range. For the (111) sample, however, $C(T)$ depends on V_g : the temperature at which C increases rapidly moves from ~ 40 K at $V_g=0$ to 20 K at $V_g=80$ V. This is exactly the temperature regime where one expects the quantum paraelectric transition of STO, and it is also the temperature regime that where R_T in the (111) oriented device shows a significant temperature dependence.

At present, it is not clear why the (111) oriented samples show such a large zero-field transverse resistance. It may be related to the orientation of tetragonal domains, along which a finite magnetic moment is expected to point according to the scanning SQUID studies. In the (001) devices, these

would point in the plane of the sample, or perpendicular to it, while in the (111) oriented devices, the domains would always point out of the sample at specific angles determined by the crystal orientation, and thus may be more likely to contribute to a finite transverse resistance.

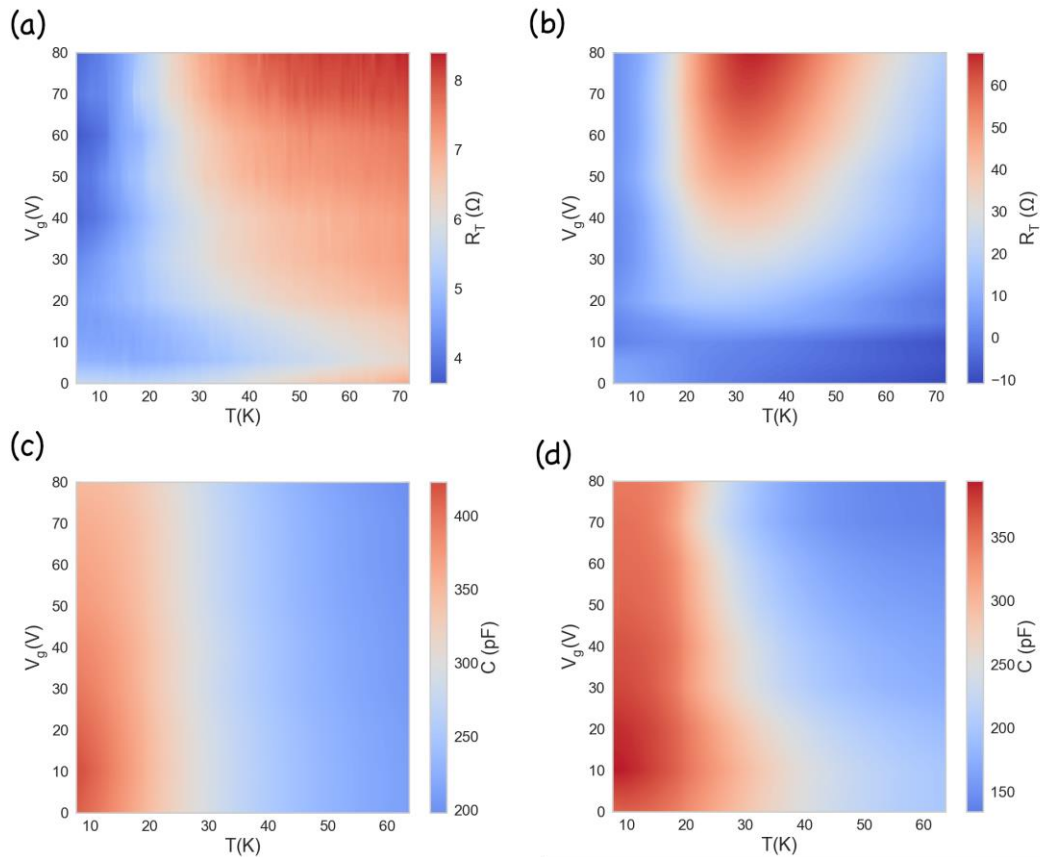


Figure 2. R_T (a) and C (c) for a (001) oriented sample, and R_T (b) and C for a (111) oriented sample as a function of temperature and backgate voltage.

We are continuing our measurements to further explore this phenomenon, as described below.

Future Plans

We have developed a tuning-fork microwave impedance microscope (MIM) based on a Mach-Zehnder interferometer (MZI) that will enable us to image conductivity variations in devices on the scale of tens of nanometers. Since the ferroelastic domain walls in STO discussed above are reported to be more conductive than the rest of the STO crystal, so that current flows preferentially

along the domain walls, we hope to correlate the anomalous finite zero-field transverse resistance with the structure and arrangement of domain walls in (001) and (111) oriented samples as a function of temperature and backgate voltage using the MIM.

One of the potentially interesting properties of (111) oriented STO based heterostructures is the possibility of observing topologically non-trivial superconductivity due to the hexagonal arrangement of atoms at the interface. We have made an interesting observation regarding superconductivity in measuring three different (111) oriented STO based interface systems. In (111) LAO/STO, superconductivity is observed at temperatures comparable to (001) LAO/STO; in (111) LSAT/STO, no superconductivity is observed in our measurement temperature range, but a small downturn in resistance is observed at the lowest temperatures. In (111) Al₂O_x/STO, no hint of a superconducting transition is observed. The difference between these systems is in the amount of strain at the interface. LAO/STO has a 3% strain, LSAT/STO 1% strain, and Al₂O_x/STO presumably has the lowest strain due to the amorphous nature of the Al₂O_x overlayer. Consequently, the Al₂O_x/STO devices are likely closest to pure hexagonal at the interface. We propose to further explore this *absence* of superconductivity in the (111) oriented Al₂O_x/STO devices by measuring the temperature dependence of the resistance as a function of carrier concentration and resistivity, which we can vary over a wide range by annealing the samples in an Ar/H₂ atmosphere to introduce additional oxygen vacancies.

Lastly, we have developed a process for making mesoscopic devices with features size down to 100 nm in Al₂O_x/STO structures. Fabrication of such devices is challenging as the substrate is extremely insulating, and hence it is not easy to fabricate structures by electron-beam lithography due to charging effects. Using a conductive polymer layer, we have been able to overcome this problem, and we plan to explore mesoscopic transport in these structures.

References

1. K. A. Muller and H. Burkard, ‘SrTiO₃: An intrinsic quantum paraelectric below 4 K,’ *Physical Review B* 19, 3593 (1979).
2. R. Viana, P. Lunkenheimer, J. Hemberger, R. Böhmer, and A. Loidl, ‘Dielectric spectroscopy in SrTiO₃,’ *Physical Review B* 50, 601 (1994).
3. P. Chandra, G. G. Lonzarich, S. E. Rowley, and J. F. Scott, ‘Prospects and applications near ferroelectric quantum phase transitions: a key issues review,’ *Reports on Progress in Physics* 80, 112502 (2017).
4. E. K. H. Salje, O. Aktas, M. A. Carpenter, V. V. Laguta, and J. F. Scott, ‘Domains within Domains and Walls within Walls: Evidence for Polar Domains in Cryogenic SrTiO₃,’ *Physical Review Letters* 111, 247603 (2013).
5. D. V. Christensen, Y. Frenkel, Y. Z. Chen, Y. W. Xie, Z. Y. Chen, Y. Hikita, A. Smith, L. Klein, H. Y. Hwang, N. Pryds, and B. Kalisky, ‘Strain-tunable magnetism at oxide domain walls,’ *Nature Physics* 15, 269 (2019).

Publications

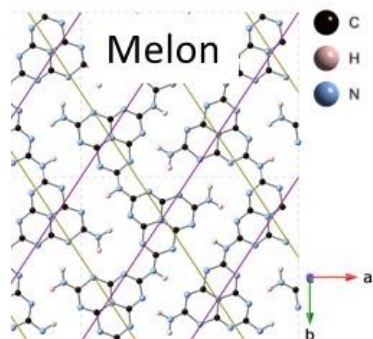
1. S. Davis, Z. Huang, K. Han, Ariando T. Venkatesan and V. Chandrasekhar, “Signatures of electronic nematicity in the (111) LaAlO₃/SrTiO₃ interfaces,” Phys. Rev. B **97**, 041408(R) (2018).
2. S. Davis, Z. Huang, K. Han, Ariando T. Venkatesan and V. Chandrasekhar, “Anisotropic superconductivity and frozen electronic states at the (111) LaAlO₃/SrTiO₃ interface,” Phys. Rev. B **98**, 024504 (2018).
3. V.V. Bal, Z. Huang, K. Han, Ariando, T. Venkatesan and V. Chandrasekhar, “Strong spin-orbit coupling and magnetism in (111) (La_{0.3}Sr_{0.7})(Al_{0.65}Ta_{0.35})/SrTiO₃,” Phys. Rev. B **98**, 085416 (2018).
4. V. V. Bal, Z. Huang, K. Han, Ariando, T. Venkatesan and V. Chandrasekhar, ‘Low temperature magnetoresistance of (111) (La_{0.3}Sr_{0.7})(Al_{0.65}Ta_{0.35})/SrTiO₃,’ Phys. Rev. B **99**, 035408 (2019).
5. P.W. Krantz and V. Chandrasekhar, ‘Etching sharp tips from thin metallic wires for tuning-fork-based scanning probe microscopy,’ J. Vac. Sci Tech. B **38**, 024004 (2020).
6. V. Chandrasekhar, ‘A microchip microcontroller-based transducer controller for non-contact scanning probe microscopy with phase-locked loop, amplitude, and Q control,’ Rev. Sci. Instr. **91**, 023705 (2020).
7. Z. Liu, P.W. Krantz and V. Chandrasekhar, ‘A Mach-Zehnder interferometer based tuning fork microwave impedance microscope,’ submitted to Review of Scientific Instruments, (arXiv:2007.05888 [physics.app-ph]).

Structural Complexity and Photocatalytic Functionality: Carbon Nitride Systems

PI: Peter A. Crozier, Arizona State University, Tempe, AZ 85287-6106

Keywords: Photocatalysis, water splitting, low-dose imaging, Patterson functions, disorder

Research Scope



We are investigating the atomic structure and evolution of photocatalytic materials systems for H_2 generation via photocatalytic water splitting under visible light. Our catalysts are composite materials consisting of light harvesting semiconductors supporting co-catalytic nanoparticles that facilitate the transfer of excited electrons/holes for water reduction/oxidation. We have investigated the role of short-range order on the catalytic functionality of carbon nitride based systems. A fundamental atomic level understanding of the complex relationships between

structural elements controlling light harvesting, charge transfer, and Pt metal dispersions is required to design optimized systems.

Recent Progress

Graphitic carbon nitrides ($g-CN_xH_y$) are an important class of layered materials for driving energy conversion processes such as photocatalysis [1]. The average in-plane structure resembles

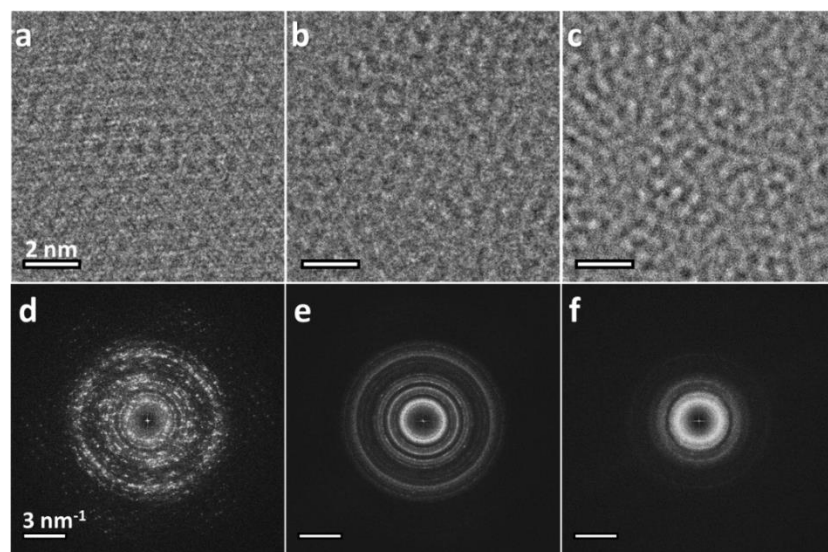


Figure 1: (a)-(c) TEM images of (a) Nicanite (b) U_{240} -gCN, and (c) U_{30} -gCN (d)-(f) Corresponding image diffraction patterns for (d) Nicanite, (e) U_{240} -gCN, and (f) U_{30} -gCN generated from the large FOV images.

polymeric melon (with a limiting composition of C_2N_3H , [2]). However, electron beam damage impedes the ability of transmission electron microscopy (TEM) to determine local structural disorder preventing a clear description of structure-reactivity relationships. Here we employ a direct electron detection system to minimize radiation damage and gain new insights into the role of structural disorder on catalytic functionality. The local structural variations are

explored using a pseudo-Patterson approach. The role of $g\text{-CN}_x\text{H}_y$ structure on Pt co-catalysts dispersion, charge transport and H_2 evolution are revealed.

Three different $g\text{-CN}_x\text{H}_y$ powders with differing degrees of structural disorder were employed (Nicanite, $\text{U}_{240}\text{-gCN}$ and $\text{U}_{30}\text{-gCN}$). The basal plane spacings of each powder was determined from x-ray diffraction to be 3.224 ± 0.006 , 3.235 ± 0.006 , and 3.263 ± 0.006 Å for Nicanite, $\text{U}_{240}\text{-gCN}$ and $\text{U}_{30}\text{-gCN}$, respectively. TEM imaging of the (hk0) basal plane was performed under low electron fluence rates ($<70 \text{ e}/\text{Å}^2/\text{s}$) (see Figure 1) on an aberration-corrected FEI Titan ETEM equipped with a Gatan K2-IS direct electron detector. Nicanite displays a diffractogram showing a pseudo-hexagonal symmetry especially clear at high spatial frequencies and simulations suggest it has an AAA eclipsed stacking. The planar structure of melon is composed of 1D chains of N-H bridged heptazine (C_6N_7) units terminated by N-H_2 groups [2, 3]. To explore local translational and rotational disorder of the in-plane heptazine units, local pseudo Patterson functions (PPF) were extracted by Fourier transforming square regions 6.5 nm in width of the HREM images. Figure 2a-c shows the mean PPF for each $g\text{-CN}_x\text{H}_y$ compounds, generated by averaging over 100 different areas. While Nicanite shows strong structural correlations out to the fourth heptazine-heptazine nearest neighbor shell (HHNN), the other samples exhibit continuous rings showing large degrees

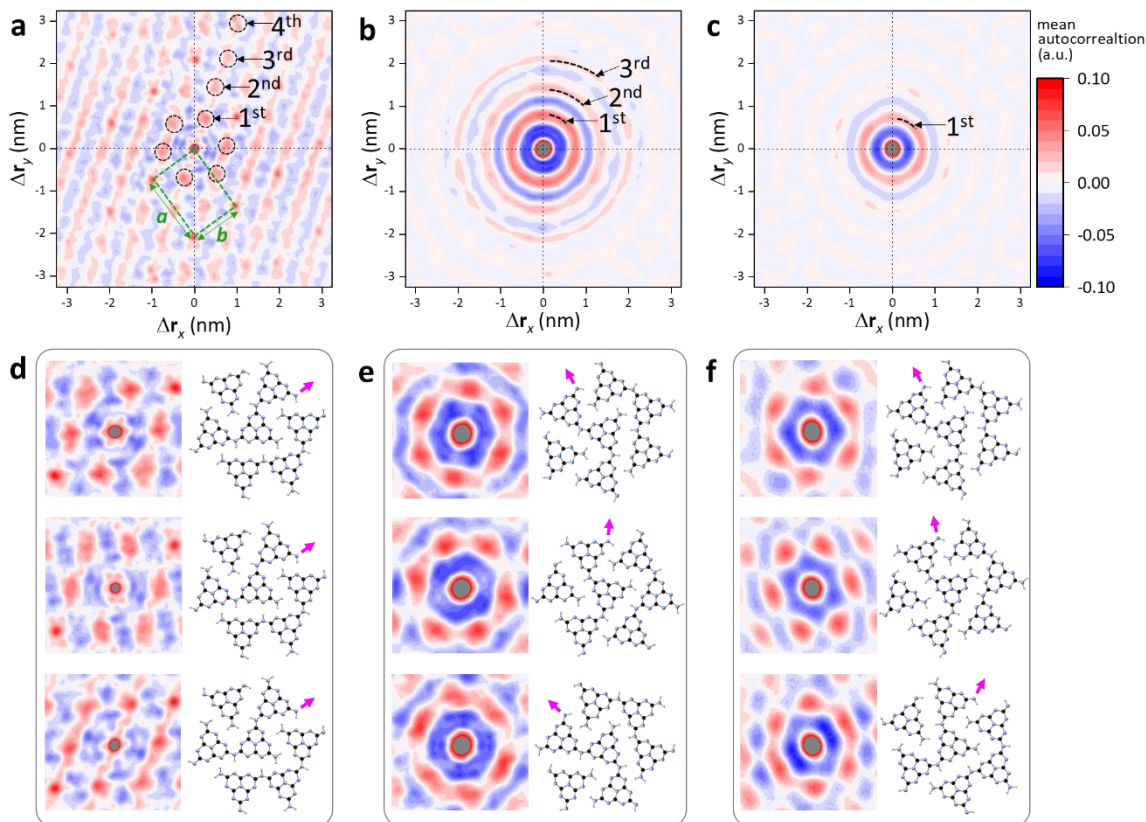


Figure 2: (a)-(c) Mean pseudo Patterson functions (PPFs) for (a) Nicanite, (b) $\text{U}_{240}\text{-gCN}$, and (c) $\text{U}_{30}\text{-gCN}$. The 1st-4th HHNN shells are labelled over each mean PPF and the intensity scale bar next to (c) applies to all mean PPFs. (d)-(f) Examples of three local PPFs from (d) Nicanite, (e) $\text{U}_{240}\text{-gCN}$, and (f) $\text{U}_{30}\text{-gCN}$ demonstrating local structural ordering. To the right of each local PPFs is a structure model containing the first HHNNs depicting the azimuthal orientation in that region is shown.

of rotation between the different domains. On average, U₂₄₀-gCN exhibits relatively strong structural correlations up to the third HHNN shell (Figure 2b) whereas for U₃₀-gCN, the PPF becomes significantly attenuated beyond the first HHNN shell (Figure 2c).

Figure 2d-f compares three local PPFs (displayed over the first HHNN shell) from each material. In each, the azimuthal orientation of the in-plane structural motif can be clearly identified, as shown by the structure models. For Nicanite, the azimuthal orientation is relatively constant compared to the other materials which show large variations and little translational symmetry.

To test the photocatalytic activity, 1.6 wt% Pt nanoparticles was photodeposited over each sample and the activity for H₂ evolution was determined under a Xe lamp with a filter ($\lambda > 400\text{nm}$). The H₂ evolution rate (HER) per mass of catalysts (Figure 3) clearly shows that U₂₄₀gCN produces twice as much H₂ as the other two materials. Two factors that explain the trends observed in Figure 3 are the Pt metal dispersion and the charge transport from the carbon nitride to the Pt surface.

Figure 4a-c shows representative images of each g-CN_xH_y loaded with 1.6 wt% Pt following 5 hours of photoreaction under visible light. Nicanite (Figure 4a) has larger Pt nanoparticles and the higher Pt dispersion on U₂₄₀-gCN and U₃₀-gCN gives a higher number of active sites for H₂ evolution. As pointed out by Lau et al., N-H₂ groups are the preferred adsorption sites for Pt on these materials[4]. Thus, for the more disordered materials, the higher concentration of terminating N-H₂ groups leads to improved Pt dispersion.

A second metric of catalytic activity is the turnover frequency (TOF), in which H₂ production is normalized to the number of surface Pt atoms. The turnover frequency is a measure of the effective efficiency of each Pt site. The Pt particle size distribution can be employed to estimate the TOF which is shown in figure 5a and is highest for the Nicanite. In this case, efficiency is related to the

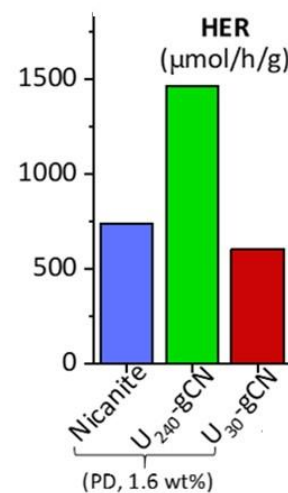


Figure 3: Hydrogen production rate (HER)

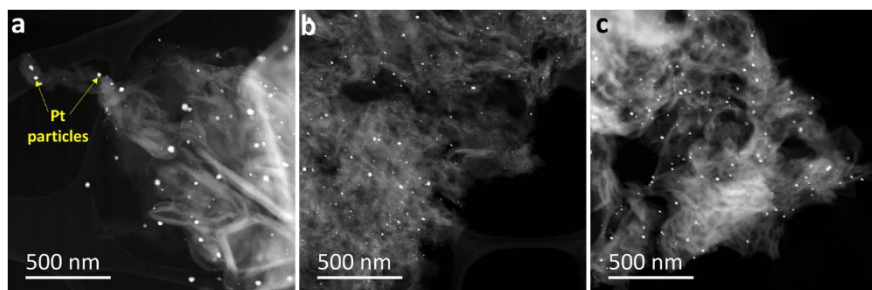


Figure 4: (a)-(c) HAADF-STEM images of the post-photoreaction Pt/g-CN_xH_y photocatalysts, each loaded with 1.6 wt% Pt via photodeposition: (a) Nicanite, (b) U₂₄₀-gCN, and (c) U₃₀-gCN.

electron transfer rate from the carbon nitride to the Pt particle per incident photon. By looking at the correlation of the TOF with bandgap, hydrogen content, and carbon nitride basal stacking distance, which is directly related to carrier mobility [5], the relative importance of these

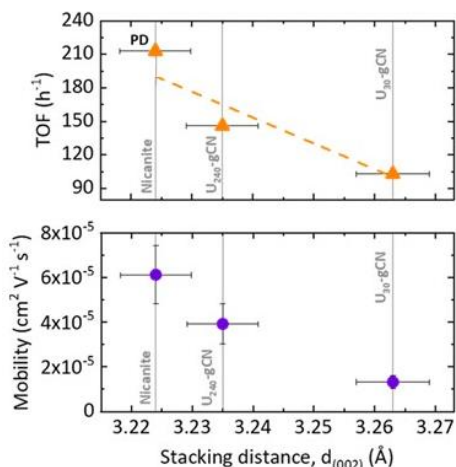


Figure 5: (a) Correlation between the stacking distance in the g-CN_xHy support with the TOF for H₂ production (top) and mobility (bottom).

materials properties to photocatalysis can be determined. Figure 5 shows the TOF and carrier mobility as a function of the layer stacking distance for the three carbon nitrides. The TOF and mobility show the same dependence on layers stacking distance suggesting that the superior TOF of the Nicanite based system is due to the enhanced electron transfer from the carbon nitride to the Pt co-catalysts.

In conclusion, contributions to structure-reactivity relations for carbon nitride based photocatalysts have been elucidated. In-plane short-range order regulates and controls the Pt metal co-catalysts dispersion whereas the basal plane spacing controls charge transfer.

Future Plans

We plan to extend this work to mixed metal oxides systems and oxide systems with cation doping giving photon absorption in the visible. These systems are less sensitive to electron irradiation making them easier to probe at the atomic level with advanced *in situ* imaging and spectroscopy techniques. We are also investigating the role of photonic cavity modes for light harvesting. To drive photochemistry, the photonic resonances must be coupled with plasmons, excitons or phonons to deliver energy to the catalytic surface sites. We will employ electron energy-loss spectroscopy to detect the photonic modes and to understand coupling processes. Fundamental studies will be undertaken to investigate the strength of the coupling for samples of different composition and geometry. *In situ* observations will be performed to understand the role of adsorbates on the coupling process and to identify localized chemical activity on the catalyst surface.

References

1. Cao, S., et al., *Polymeric Photocatalysts Based on Graphitic Carbon Nitride*. *Advanced Materials*, 2015. **27** (13); p. 2150-2176.
2. Lotsch, B.V., et al., *Unmasking Melon by a Complementary Approach Employing Electron Diffraction, Solid-State NMR Spectroscopy, and Theoretical Calculations—Structural Characterization of a Carbon Nitride Polymer*. *Chemistry—A European Journal*, 2007. **13**(17); p. 4969-4980.
3. Miller, T.S., et al., *Carbon Nitrides: Synthesis and Characterization of a New Class of Functional Materials*. *Phys. Chem. Chem. Phys.*, 2017. **19** (24); p. 15613-15638. .
4. Lau, V.W., et al., *Rational design of carbon nitride photocatalysts by identification of cyanamide defects as catalytically relevant sites*. *Nature Communications*, 2016. **7**.
5. Merschjann, C., et al., *Complementing graphenes: 1D interplanar charge transport in polymeric graphitic carbon nitrides*. *Advanced Materials*, 2015. **27**(48); p. 7993-7999.

Publications

- 1) D. Haiber and P.A. Crozier, (2018) “Nanoscale Probing of Local Hydrogen Heterogeneity in Disordered Carbon Nitrides with Vibrational EELS”, ACS Nano 12, 5463–5472, DOI 10.1021/acsnano.8b00884.
- 2) L. Zhang, Q. Liu, T. Aoki, and P.A. Crozier (2019). “Light induced coarsening of metal nanoparticles” (Hot Paper Designation), J. Mater. Chem. A, 7(19): 11756-11763.
- 3) Q. Liu, S C. Quillin, D. J. Masiello, P. A. Crozier, (2019) “Nanoscale Probing of Resonant Photonic Modes in Dielectric Nanoparticles with Focused Electron Beams” (Editor’s Choice), Physical Review B, 99 (16), 165102 DOI 10.1103/PhysRevB.99.165102.
- 4) Barnaby D.A. Levin, Diane Haiber, Qianlang Liu, and Peter A. Crozier (2020). "An Open-Cell Environmental Transmission Electron Microscopy Technique for In-Situ Characterization of Samples in Aqueous Liquid Solutions". Microscopy and Microanalysis, 26 (1), 134-138, doi.org/10.1017/S14319276190153
- 5) K. Venkatraman, B.D.A. Levin, K. March, P. Rez, P.A. Crozier (2019). “Vibrational Spectroscopy at Atomic Resolution with Electron Impact Scattering”, Nature Physics 15 (12), 1237-1241 DOI 10.1038/s41567-019-0675-56) B.D.A. Levin, K. Venkatraman, Katia March and P.A. Crozier (2020). "Parametric Background Modelling for Extracting Peaks from the Vibrational Electron Energy-Loss Spectrum". Microscopy and Microanalysis, (in revision)
- 7) Diane M. Haiber, Barnaby D.A. Levin, Michael M.J. Treacy, and Peter A. Crozier (2020). "In-plane Structural Fluctuations in Differently-Condensed Graphitic Carbon Nitrides". (Submitted to Chemistry of Materials)
- 8) Diane Haiber and Peter A. Crozier (2020). "Competing Structure-Activity Relationships in Photocatalyst Design: Pt-Functionalized Graphitic Carbon Nitrides for Hydrogen Evolution". (Submitted to Journal of Catalysis)
- 9) Qianlang Liu, Barnaby D. A. Levin, Diane M. Haiber, Joshua L. Vincent, and Peter A. Crozier (2020). "An In Situ Light Illumination System for an Aberration-Corrected Environmental Transmission Electron Microscope". (in preparation)

Real-time Measurements of Complex Transition Metal Oxide Nanostructure Growth

Michael A. Filler, School of Chemical & Biomolecular Engineering, Georgia Tech

Frances M. Ross, Department of Materials Science and Engineering, MIT

Keywords: Nanowire growth, metal oxides, vapor-liquid-solid, heterostructures

Research scope

This project, a collaboration between Georgia Tech and MIT, aims to combine *in situ* microscopy and spectroscopy measurements to answer fundamental questions about the physics and chemistry governing the bottom-up vapor-solid-liquid (VLS) growth of one-dimensional (1D) functional oxides. In particular, our overall aim is to develop a framework for using new catalysts and new growth mechanisms to create complex structures that are not available from conventional VLS growth. Current research in this project follows three complementary directions, with each providing a unique perspective on the roles of new catalysts in the growth of 1D nanomaterials: (1) We are using a non-standard catalyst, Ge, to seed the growth of 1D nanostructures of zinc oxide that show unusual morphologies; (2) We are exploring alkaline metal halide catalysts as a route to synthesize NWs of layered materials; (3) We have formed 1D lateral heterostructures of functional oxides by using pulsed laser deposition on 1D, flexible substrates.

Recent progress

(1) 1D twisted and tubular structures of ZnO catalyzed by Ge

Our experiments exploring the use of unconventional catalysts and growth modes to form metal oxide nanostructures have focused on the growth of ZnO nanowires (NWs) using Ge catalysts. ZnO nanowires comprise a well-known materials system that forms a variety of 1D morphologies that include NWs, nanotubes (NTs), and nanoribbons via VLS catalyzed by metals such as Au (1). The phase behavior and chemical bonding of Ge suggested that it might enable alternative growth mechanisms, opening up new opportunities to tune morphology and create heterostructures. Moreover, in optoelectronic applications it is helpful to avoid the deep level traps created by Au and similar elements. To these ends, we replaced Au with Ge in the catalyst.

Figure 1 summarizes the resulting growth morphologies (2), which include twisted and/or hollow NWs in addition to the expected straight solid NWs (Figure 1a-c). Post-growth electron microscopy and spectroscopy allowed us to determine growth conditions that favor each type of structure and determine structural properties such as catalyst geometry, diameter, faceting, and twist rate. Most strikingly, the cores of hollow twisted NTs were much larger than expected from the hollow-pipe mechanism and twist rates were several times larger than that predicted for the Eshelby twist (Figure 1d). Our data indicate a competition between growth and etching processes at the catalyst/nanowire interface (Figure 1e-f), a far more complex behavior than in the conventional VLS mechanism. We

propose that etching is responsible for the large hollow cores and that the NT twisting anomaly stems from a change to the material's mechanical properties following catalyst diffusion during growth. Growth mechanisms that involve a competition between growth and catalyst-induced etching may be useful for creating unusual structures and properties.

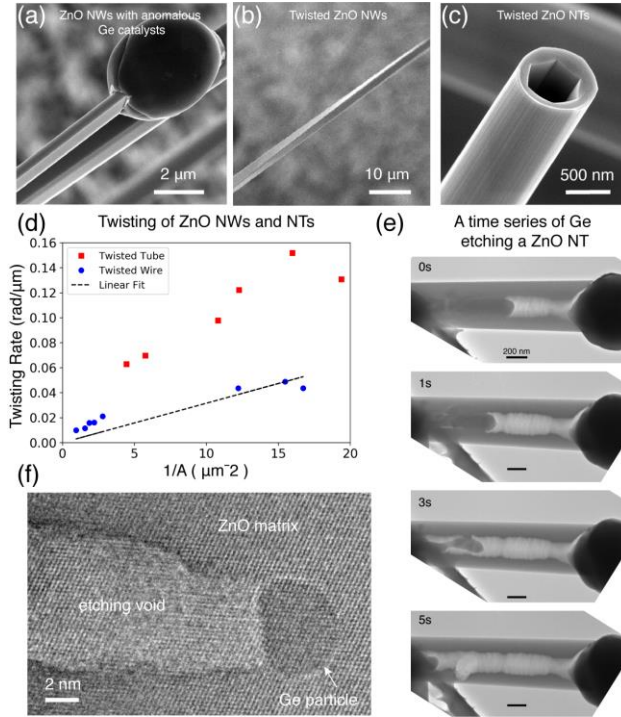


Figure 1. 1D twisted and tubular structures of ZnO catalyzed by Ge. (a-c) SEM images of a straight NW, a twisted NW and a hollow, twisted NT respectively. (d) Twisting rate of NWs (blue) and NTs (red). While the twisting of NWs follow the Eshelby model (dotted line), the NTs show a 3-4 times higher twisting rate than predicted. (e-f) Ge-assisted etching of ZnO imaged using the Titan *in situ* TEM at the Center for Functional Nanomaterials, Brookhaven National Laboratory. (e) A time series showing a Ge-containing solid particle inside the hollow core of a NT at 610°C. A reaction takes place that removes ZnO from the core, enlarging it, while also consuming Ge. (f) HRTEM of a similar etching event where a Ge-containing particle removes ZnO, leaving behind an empty trace with lower contrast.

(b) Salt-assisted growth of layered nanowires

Unconventional catalysts can also enable the growth of NWs in materials that do not otherwise grow in NW form. We have carried out a literature survey to understand common themes and promising opportunities arising from the systems that have been studied (3). Figure 2 shows an experiment that was suggested by catalytic growth of ribbons in a different but related material (4). These NWs are formed of NbS₃, a layered transitional metal trichalcogenide (TMT), catalyzed by a salt (NaCl). TMTs such as NbS₃, NbSe₃, TiS₃ and TaS₃ are quasi-1D van der Waals (vdW) materials built from vdW-bonded trigonal prismatic chains of metal and chalcogens (Figure 2a).

In Figure 2, where the NWs form via NaCl-assisted synthesis, NaCl appears to play a dual role (4): (i) it creates intermediate, more volatile Nb precursors at the growth temperature of 700-750 °C, and (ii) it directs the growth of NbS₃. SEM images and EDS mapping (Figure 2b-c) show the structure and composition of NaCl-catalyzed NbS₃ NWs. While the NWs exhibit well-faceted shapes, the NaCl tips are more varied in their structure. Some are well-rounded, hinting at a VLS mechanism, while the faceting of others hints at a vapor-solid-solid (VSS) mechanism. Observations during growth are required to untangle

the growth mechanism, and we intend to carry out such experiments in the semi-closed high pressure environmental TEM cell under development.

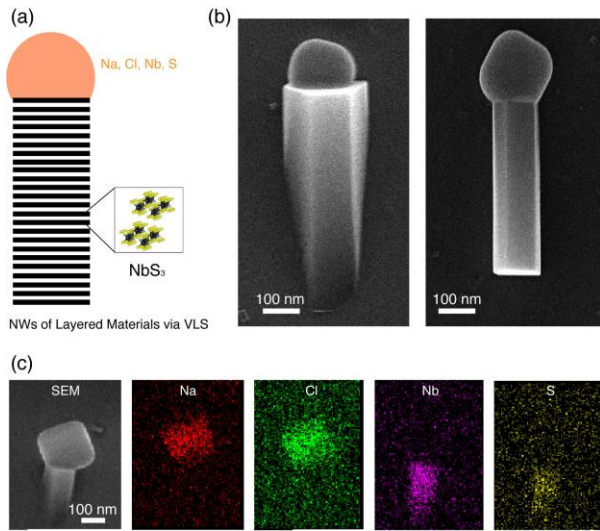


Figure 2. Salt-assisted growth of NbS₃ layered nanowires. (a) Schematic representing the layered structure of NbS₃ and our proposal of using alkaline metal halide (NaCl) as a VLS catalyst for TMTs. (b) Representative SEM images of two NWs. The particles are visible on top of well-faceted short NWs. (c) EDS elemental mapping suggests the particle composition is Na and Cl, while the NWs are Nb and S.

Atomically thin semiconductors have unlocked opportunities to explore a variety of many-body physics, including the fractional quantum Hall effect, exciton condensation and unconventional superconductivity. A majority of the studies of vdW materials have focused on materials such as graphene, boron nitride, transition metal dichalcogenides (TMDs), and their heterostructures. The catalytic formation of 1D nanostructures of 2D materials presents the possibility of diameter and position control as well as the bottom-up integration of dissimilar materials into heterostructures and superlattices. Our initial results suggest that unconventional, non-metallic catalysts can catalyze the growth of such nanostructures, potentially opening a door to explore the synthesis and growth mechanisms of NWs based on layered materials.

(c) *Heterostructures of complex oxides*

An important extension of NW growth is the formation of heterostructures, since integration of dissimilar materials offers opportunities to explore interfacial phenomena. For complex oxides, for example, this includes multiferroic high-temperature ferroelectric and superconducting properties. Recently, strain has been shown to be another knob to further drive the exotic interface physics (5). One of the challenges in strain engineering of oxide thin films is the material's mechanical rigidity. This hinders the maximum strain that can be applied to tune properties without compromising structural integrity. We have started to explore heterostructure formation by lateral (core-shell) heterostructures of a complex oxide onto our as-synthesized ZnO nanomaterials. Figure 3 shows the results of pulsed laser deposition (PLD) of a La_{0.7}Sr_{0.3}MnO₃ (LSMO) shell onto a ZnO core, in collaboration with the C. Ross Group at MIT.

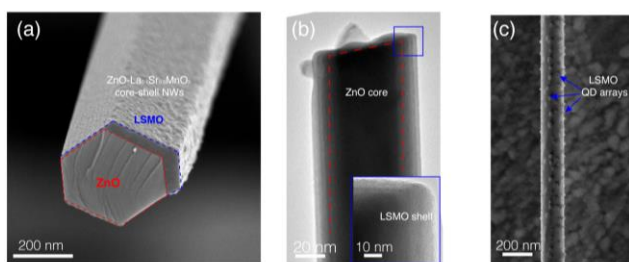


Figure 3. Core-shell heterostructures of complex oxides. (a) SEM image of ZnO-LSMO core-shell heterostructure. (b) TEM image shows a continuous and single crystalline LSMO shell wrapping the ZnO core. (c) Formation of quantum dot arrays of LSMO on 1D ZnO substrate by post-growth annealing at 900 °C.

SEM (Figure 3a) and TEM (Figure 3b) show a single crystalline, smooth and continuous LSMO film conformably deposited on the ZnO NW, creating a faceted shell whose thickness and crystallinity can be controlled via PLD parameters. We find that post-growth annealing can transform the LSMO shell into arrays of LSMO quantum dots (Figure 3c). The integration of complex oxide thin films or arrays of quantum dots on a flexible and 1D ZnO substrate may allow higher applied strain to be transferred to the material interface without introduction of dislocations, and create unique opportunities to study extreme strain-driven emergent properties.

Future Plans

Our results to date have revealed opportunities to use unconventional catalysts and growth modes to create new types of 1D nanostructures. This opens exciting windows to explore other aspects of the physics and chemistry of NW growth and the influence of the catalyst and growth mode on the resulting nanostructures. Looking forward, we have started to grow other metal oxides using Ge catalysts by both physical vapor deposition and chemical vapor deposition techniques, using *ex situ* growth to provide the knowledge needed for *in situ* growth with its opportunities for imaging the catalyst in action. We are particularly interested in investigating the nucleation and growth of Ge-catalyzed Ga₂O₃ and Al₂O₃ NWs using both ultrahigh vacuum TEM and *in situ* FTIR. The complementary synthesis and characterization will create a baseline to understand metal oxide growth kinetics more generally. We also plan to characterize the structural aspects of the salt-assisted NbS₃ NWs and compare with the catalyst-free bulk structure. We will then explore growth conditions for NbS₃ NW synthesis, with particular emphasis on substrates covered with other vdW materials to explore the possibility of epitaxial growth. The understanding from NbS₃ will be used to uncover other vdW NWs in the transition metal chalcogenide material family. We also plan to interface the metal chalcogenide NWs to our oxide NWs via partial oxidation and conversion. The metal chalcogenide/oxide NW heterostructure may further enrich the opportunities for exotic physics at the boundaries of functional materials.

In general, multimodal, *in situ* and *ex situ* approaches interrogate different aspects of catalyst physics and chemistry. We anticipate that the research within this project using both techniques will influence the discovery of new 1D structures and 1D materials with potentially useful applications in quantum electronics and renewable energy.

References

1. Z. L. Wang, Splendid one-dimensional nanostructures of zinc oxide: A new nanomaterial family for nanotechnology. *ACS Nano*. **2**, 1987–1992 (2008).
2. T. Pham, S. Kommandur, H. Lee H, D. Zakharov, M. A. Filler and F. M. Ross, One dimensional twisted and tubular structures of zinc oxide by semiconductor-catalyzed vapor-liquid-solid synthesis. *Nanoscale*, *Under revision* (2020) (available at <http://arxiv.org/abs/2008.10137>).
3. T. Pham, N. Deshmukh, M. A. Filler, F. M. Ross, Vapor-liquid-solid synthesis of nanowires using unconventional catalysts. *To be submitted* (2020).
4. S. Li *et al.*, Vapour-liquid-solid growth of monolayer MoS₂ nanoribbons. *Nat. Mater.* **17**, 535–542 (2018).
5. S. S. Hong *et al.*, Extreme tensile strain states in La_{0.7}Ca_{0.3}MnO₃ membranes. *Science* (80-.). **368**, 71–76 (2020).

Publications

1. T. Pham, S. Kommandur, H. Lee H, D. Zakharov, M. A. Filler and F. M. Ross, One dimensional twisted and tubular structures of zinc oxide by semiconductor-catalyzed vapor-liquid-solid synthesis. *Nanoscale*, *Under revision* (2020) (available at <http://arxiv.org/abs/2008.10137>).
2. T. Pham, N. Deshmukh, M. A. Filler, F. M. Ross, Vapor-liquid-solid synthesis of nanowires using unconventional catalysts. *Prog. Surf. Sci.*, *To be submitted* (2020).

Molecular and Materials Energetics Visualized with Femtosecond TEM

David J. Flannigan

Department of Chemical Engineering and Materials Science, University of Minnesota, Minneapolis, MN

Keywords: phonon dispersion, phase transformations, beam damage, pulsed beams

Research Scope

Our recent work is delineated along three distinct but interrelated thrusts, each of which stems from development and advancement of femtosecond (fs) laser-driven pulsed TEM. The work described here is motivated by a desire to elucidate and understand energy movement and redistribution through molecular and materials systems across a broad range of space and time.

(1) The first thrust is focused on elucidating connections between local phonon dynamics and phase/morphology transformations. Key to this thrust is the direct imaging of real-space, time-varying phonon dispersion behaviors with fs TEM bright-field imaging, particularly as they relate to transition state dynamics. By spatiotemporally mapping behaviors such as phonon softening and morphology-dependent single-mode dispersion, new insights into local evolution of coherent lattice oscillations and phase transformations are being gained.

(2) The second thrust is focused on exploring the potential of using laser-driven pulsed beams in the TEM to study fundamental material-specific damage mechanisms and to mitigate deleterious effects. Here, the precise temporal control over the photoemission process enabled by using a fs pulsed laser rather than conventional thermionic emission is being leveraged and quantitatively explored. In this way, significant reduction in damage – for uniform doses and dose rates – can be realized, and temporal aspects of damage can be explored.

(3) The third thrust focuses on quantification of strains and energies associated with photoexcited coherent acoustic phonons. Evidence of single-mode excitation is emerging, where symmetry is dependent upon excitation conditions, analogous to narrow-band resonant THz spectroscopy. Progress here is being made on developing descriptions of transient scattering and contrast dynamics for quantifying local behaviors directly from fs TEM bright-field images.

(4) Finally, fs TEM technology and method development is driving progress in the project overall. Over the most recent two years, attention has been focused on: (i) Development of a robust and distributable automation package for high-throughput ultrafast electron microscopy experiments. (ii) Design and fabrication of a device for directly measuring the salient properties of the *in situ* photoexcitation laser beam precisely at the specimen location.

Recent Progress

(1) **Imaging phonon dispersion in morphologically-variant semiconductors.** Super-bandgap ultrafast photoexcitation of semiconducting materials induces a cascade of strongly correlated, many-body interactions. Resulting from carrier-carrier and carrier-phonon scattering processes is excitation of propagating coherent acoustic phonons (CAPs), the precise transient behaviors of

which are influenced by intrinsic electronic and structural properties, as well as the specimen boundary conditions and the manner of excitation.^{1,2} Owing to the often-discrete and distributed nature of surface, interfacial, and compositional structure and morphology, combining real-space imaging with ultrafast probes enables determination of local transient responses. While all-optical techniques enable depth-dependent and in-plane imaging with nanometer and micrometer resolutions, respectively, *nanoscale* in-plane dynamics and the associated impact of variable morphology and composition remains challenging to resolve.

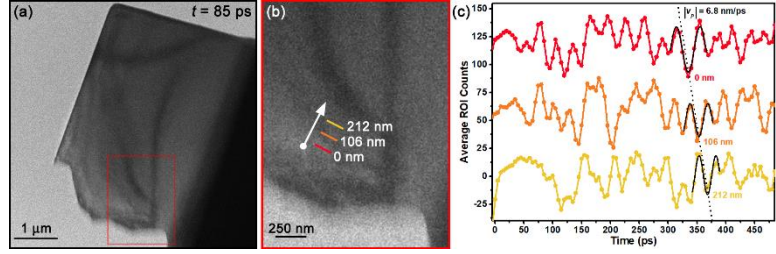


Fig. 1. (a) BF UEM image at $t = 85$ ps following photoexcitation. (b) ROI highlighting the direction of phonon propagation. (c) ROI counts vs. time with a single wavefront noted.

Femtosecond TEM is well-suited for imaging in-plane nanoscale dynamics on picosecond timescales. Our current work has focused on differentiating the impact of amorphous and crystalline morphologies on time-domain CAP dispersion behaviors *via* imaging of nanoscale-picosecond in-plane propagating lattice perturbations. By performing an *in situ* photothermal anneal of an initially amorphized GaAs specimen, distinctly different morphologies and the impact on phonon dispersion behaviors were studied. We observed variations in local phonon dispersion responses (Fig. 1). The high sensitivity of diffraction contrast to slight changes in specimen orientation enabled visualization of individual phonon wavefronts propagating across nanoscale fields of view. For pre- and post-annealed GaAs, phonon dispersion behaviors display hypersonic phase velocities that exponentially decay to the longitudinal speed of sound (Fig. 2). The final asymptotic phase velocity values, however, differ and sensitively depend upon the degree of nanocrystallinity in the specimens.

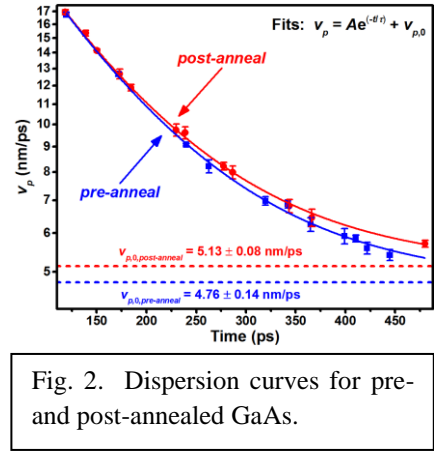


Fig. 2. Dispersion curves for pre- and post-annealed GaAs.

(2) Studying beam damage with pulsed-beam TEM. The effects of pulsed-electron irradiation on damage to tissues, cells, and biomolecules is studied in the field of radiobiology, often by utilizing fs pulsed-laser plasma accelerators. In electron microscopy, the potential benefits of using a pulsed electron beam to mitigate damage have been speculated upon for decades, with glimpses of interesting effects reported under uncontrolled conditions.^{3,4} Further, though not attempting to leverage relaxation or self-healing, proposals for extending the concept of diffract-before-destroy to TEM have also been discussed. Our efforts have focused on first conducting systematic studies to test the hypothesis that pulsed beams cause less damage. Beyond this, we will use pulsed beams to study damage mechanisms in beam sensitive materials.

Ideally, one would have a high level of control over key aspects of the discrete electron packets. Our recent work has leveraged the precise control afforded by using fs pulsed lasers to generate discrete packets of electrons in the fs TEM to precisely control the emission process, confining the probability to a narrow temporal range of 300 fs (fwhm) with extremely regular peak-to-peak emission times (Fig. 3). Using a Bragg-spot fading-curve method and a model beam-sensitive, soft-matter material (*n*-hexatriacontane, $C_{36}H_{74}$), we observed a nearly two-fold reduction in damage when the dose is delivered (statistically) one electron at a time with up to 0.1 ms between the arrival of each at the specimen. We also uncover trends for increased numbers of electrons per packet and decreases in time between packets, both of which increase the observed damage. Finally, we identify crossover points where more damage occurs for the pulsed beams relative to conventional beams upon increasing the electrons per packet.

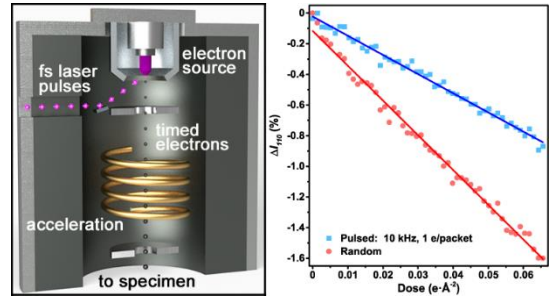


Fig. 3. (Left) Schematic of the pulsed-beam TEM gun region. (Right) Fading curves of $C_{36}H_{74}$ for pulsed and conventional beams.

(3) Quantitative description of phonon-mode behavior *via* models of fs TEM imaging.

Ultrafast imaging with fs TEM provides capabilities that are complementary to ultrafast diffraction measurements.⁵ Accordingly, disparate dynamics influenced by individual lattice discontinuities, as well as spatiotemporally varying phonon dispersion and relaxation behaviors, can be directly surveyed relatively efficiently. As previously noted, fs TEM bright-field imaging has been successfully used to observe coherent contrast-wave dynamics in semiconducting and metallic materials. Quantifying phonon phase-velocity dispersion behaviors enabled indirect identification of mode symmetries, indicating a single mode was

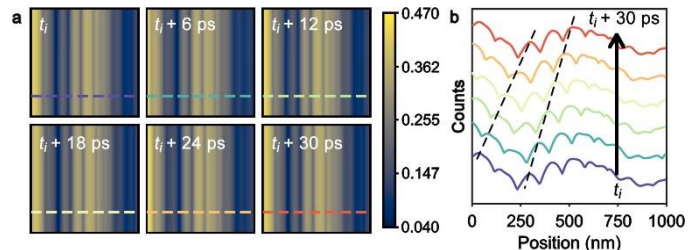


Fig. 4. (a) Simulated UEM images of phonon dynamics. (b) ROI counts as a function of time.

responsible for the observed contrast dynamics. Qualitative interpretations of the observed contrast dynamics typically invoke physical pictures of transient bend-contour dynamics in TEM imaging and modulation of the excitation error. Dynamical theory extends this to inclusion of multiple scattering, which is often necessary for achieving accurate descriptions.

Our recent work has made use of dynamical scattering models in order to make progress toward developing a quantitative approach to fs TEM imaging of acoustic-phonon dynamics. We have applied descriptions of dynamical scattering in real space to simulations of wedge-shaped specimens experiencing transient, propagating elastic deformations due to excitation of Lamb-type guided wave modes (Fig. 4). We take the approach of first explicitly testing and demonstrating how the kinematic approximation for the chosen conditions falls short of

accurately describing the quantitative strain profiles before illustrating how inclusion of dynamical effects *via* multi-slice techniques is necessary for accurately capturing the scattering response. Our methods largely follow the general approaches to simulating electron micrographs developed by Howie and Whelan and extended by others to the development of descriptions of contrast formation by discrete defects. We thus extended these approaches to fs TEM bright-field image series on relevant spatiotemporal scales on which acoustic phonons are active, largely following the formulations of kinematic and dynamical models by De Graef.

Future Plans

Work is currently underway to directly image, with fs TEM, the transient phonon-softening behaviors and associated phase-transition dynamics in SrTiO₃ at cryogenic temperatures. This particular study will serve as a paradigm test for conducting studies of transient phase transition dynamics with fs TEM. For thrust two, much work still needs to be done to test the basic hypothesis that using pulsed electron beams leads to a reduction in specimen damage. Owing to the multiple sources of error and artifacts, key to this will be conducting and documenting control experiments and methods of data acquisition. We will extend the work to two specific areas: **(1)** Exploring specific damage mechanisms. **(2)** Testing whether reduced damage with pulsed beams leads to demonstrable improvements in resolution and data quality. Key to the second point will be conducting the experiments with the pulsed beam, perhaps supplementing with additional capabilities (*e.g.*, use of a LN₂ holder). The model developed as part of the third thrust will continue to be improved and increased in sophistication, and we are currently in the process of applying it to real fs TEM images in order to extract phonon properties, including energies and strains, directly from the transient contrast features. Underlying all of this future work will be continued development of automation and analysis methods for increasing throughput and fabrication of an *in situ* laser beam profiler for quantification of the pump excitation beam at the specimen location.

References

1. Cremons, D. R.; Plemmons, D. A.; Flannigan, D. J. Fs Electron Imaging of Defect-Modulated Phonon Dynamics. *Nat. Commun.* **2016**, *7*, 11230.
2. Zhang, Y.; Flannigan, D. J. Observation of Anisotropic Strain-Wave Dynamics and Few-Layer Dephasing in MoS₂ with Ultrafast Electron Microscopy. *Nano Lett.* **2019**, *19*, 8216-8224.
3. Bonham, R. A.; Kennerly, R. E. Pulsed Electron Beams to Reduce Radiation Damage? *Ann. N. Y. Acad. Sci.* **1978**, *306*, 85-94.
4. Flannigan, D. J.; Lobastov, V. A.; Zewail, A. H. Controlled Nanoscale Mechanical Phenomena Discovered with Ultrafast Electron Microscopy. *Angew. Chem. Int. Ed.* **2007**, *46*, 9206-9210.
5. Flannigan, D. J.; Lindenberg, A. M. Atomic-Scale Imaging of Ultrafast Materials Dynamics. *MRS Bull.* **2018**, *43*, 485-490.

Publications

1. Du, D. X.; Reisbick, S. A.; Flannigan, D. J. UEMtamaton: A System for Automating Ultrafast Laser-Pump, Electron-Probe Transmission Electron Microscopy Experiments. (*submitted*)
2. VandenBussche, E. J.; Clark, C. P.; Holmes, R. J.; Flannigan, D. J. Mitigating Damage to Hybrid Perovskites Using Pulsed-Beam TEM. *ChemRxiv* **2020**, <https://doi.org/10.26434/chemrxiv.12756461.v1>
3. VandenBussche, E. J.; Flannigan, D. J. High-Resolution Analogue of Time-Domain Phonon Spectroscopy in the Transmission Electron Microscope. *Philos. Trans. R. Soc. A* **2020**, *378*, 20190598. (Invited contribution to themed issue *Dynamic In-Situ Microscopy Relating Structure and Function*)
4. Du, D. X.; Flannigan, D. J. Imaging Phonon Dynamics with Ultrafast Electron Microscopy: Kinematical and Dynamical Simulations. *Struct. Dyn.* **2020**, *7*, 024103. (*Featured article*) (*AIP Scilight article*)
5. VandenBussche, E. J.; Clark, C. P.; Holmes, R. J.; Flannigan, D. J. Pulsed Electron Beams for Mitigating Damage in Next-Generation Electronic Materials. *Microsc. Microanal.* **2020**, <https://doi.org/10.1017/S1431927620023041>
6. Du, D. X.; Flannigan, D. J. Quantifying Transient Strain and Energy of Coherent Acoustic Phonons with UEM Imaging. *Microsc. Microanal.* **2020**, <https://doi.org/10.1017/S1431927620013823>
7. Flannigan, D. J.; VandenBussche, E. J. Pulsed-Laser-Driven TEM for Studying Temporal Aspects of Beam Damage. *Microsc. Microanal.* **2020**, <https://doi.org/10.1017/S1431927620020322> (*Invited*)
8. VandenBussche, E. J.; Flannigan, D. J. Reducing Radiation Damage in Soft Matter with Fs-Timed Single-Electron Packets. *Nano Lett.* **2019**, *19*, 6687-6694.
9. VandenBussche, E. J.; Flannigan, D. J. Reducing Radiation Damage Using Pulsed Beams in the TEM. *Microsc. Microanal.* **2019**, *25* (Suppl. 2), 1646-1647.
10. Du, D. X.; Flannigan, D. J. Exploring the Connection between Coherent Acoustic Phonons and Bright-Field Contrast in Ultrafast Electron Microscopy. *Microsc. Microanal.* **2019**, *25* (Suppl. 2), 2006-2007.

Magneto-thermal microscopy of complex topological spin textures

Gregory D. Fuchs, Cornell University Applied and Engineering Physics, Ithaca, NY

Research Scope

This research project aims to develop magneto-thermal microscopy for the study of unconventional magnetic materials and heterostructures with picosecond time resolution and nanometer spatial resolution. Our table-top approach is based time-resolve anomalous Nernst effect microscopy [1,2] and time-resolved spin Seebeck effect microscopy [3] that has ~ 10 ps temporal resolution for magnetic order and applied currents, [2] but to date is limited by the spatial resolution of optical focusing. Magneto-thermal microscopy has proven to be a flexible probe of magnetism in both metal and insulator samples, and for both ferromagnetic [1–3] and antiferromagnetic [4,5] samples.

We have three principle aims in this project. First, we seek to extend and develop magneto-thermal microscopy as a table-top probe of magnetism and current that combines picosecond temporal with nanosecond spatial resolution, limited only by the sharpness of a scanning metal tip. [6] Second, we seek to apply this capability to the study of magnetization dynamics in topological magnetic materials including magnetic skyrmions. Third, we seek to further develop our understanding of magneto-thermal microscopy to probe antiferromagnetic order and use that capability to study antiferromagnetic skyrmions and their dynamics.

Recent Progress

First we discuss our recent progress in implementing scanning probe magneto-thermal microscopy combining temporal resolution with near-field spatial resolution. Figure 1 shows the geometry of scanning probe magneto-thermal microscopy. We focus a picosecond pulsed laser on the apex of a gold-coated scanning tip. Via a near-field interaction, an intense optical field is confined between the metal material under the tip with an area that is comparable to the tip radius. [6] The localized heating under the tip induces a local temperature gradient that, through the anomalous Nernst effect (ANE), produces a voltage that is proportional to the in-plane component of the magnetization within the localized region of the sample under the tip. If a current density is passing through the sample under the tip, it will also contribute a voltage due to the local heating, which changes the material's local resistance. Since we excite with picosecond laser pulses and re-thermalization times are picosecond scale in thin-film samples with thermally conductive substrates, these signals are stroboscopically time resolved.

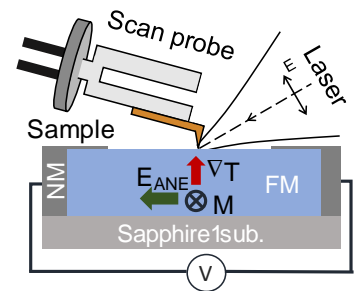


Figure 1. Geometry of near-field magneto-thermal microscopy.

We demonstrate that this set-up is sensitive to both magnetic order and current density using a simple $5 \times 12 \mu\text{m}^2$ bar of CoFeB patterned with high bandwidth electrical contacts. To verify we study a near field signal we perform tip-sample distance dependent measurements while we lock-in to harmonics of the probe oscillation (not shown). As expected, the near-field signal

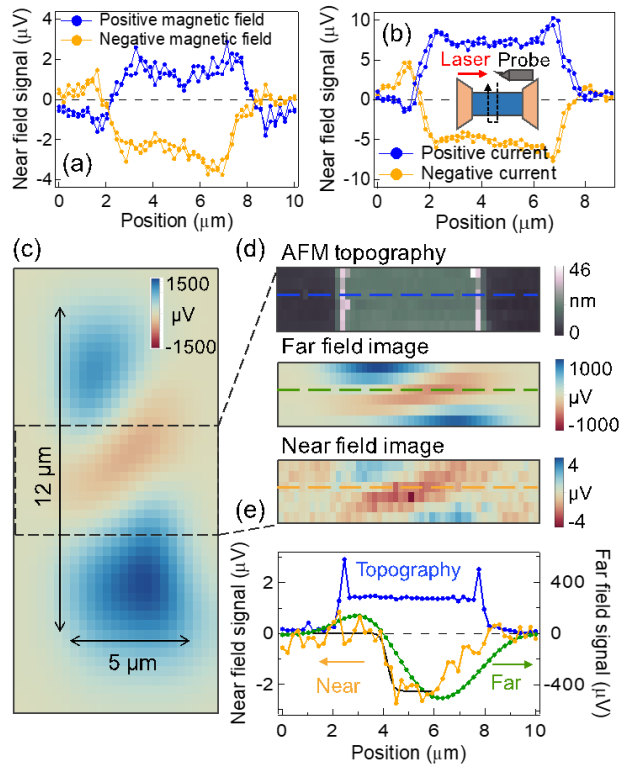


Figure 2. The near field signal varies with direction of (a) magnetization and (b) current. (c) – (d) show far-field, topography, and nearfield magnetization near a domain wall. (e) Line cuts through the domain wall.

distribution and the magnetism with resolution exceeding the optical diffraction limit.

While CoFeB has an excellent ANE coefficient, it does not have sharp enough magnetic features to test the spatial resolution of our microscopy. To do this, we focus on current imaging, because currents are very predictable within a sample, thus providing a good benchmark. We pattern a sample with nanoscale constrictions for current. Figure 3 shows topography and current imaging of a constriction, again showing spatial resolution that far exceeds the optical diffraction limit. To understand the precise spatial resolution of our technique, these data must be compared with numerical calculations of the current density in such a structure, which is underway.

We can also use this structure to assess temporal resolution of scanning probe magnetothermal microscopy. We use time domain homodyne techniques [1] to stroboscopically probe microwave current as it passes through the constriction region using our near-field

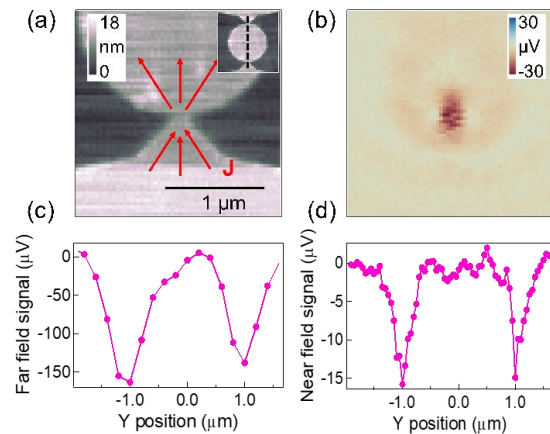


Figure 3. (a) topographic and (b) current images of a sample with a constriction. (c) and (d) show linecuts through the constriction for current density using far-field and near-field imaging, respectively.

is zero until the tip apex-sample distance is comparable to the probe radius (~ 50 nm). Figure 2 shows static near-field measurements comparing the signal size of far-field and near-field signals for both a uniform magnetic state, and magnetization in the vicinity of a domain wall. We find that the near-field signal captures both the current

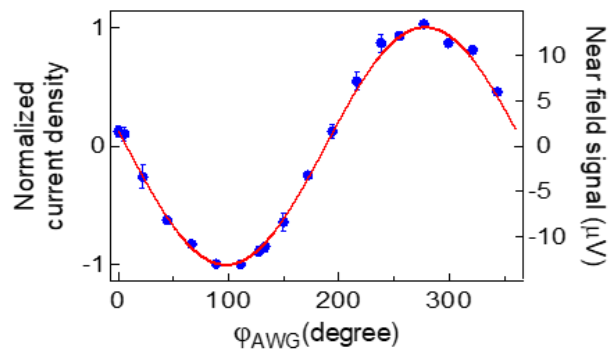


Figure 4. 3 GHz RF current measured in the near field at the constriction as we vary the microwave phase.

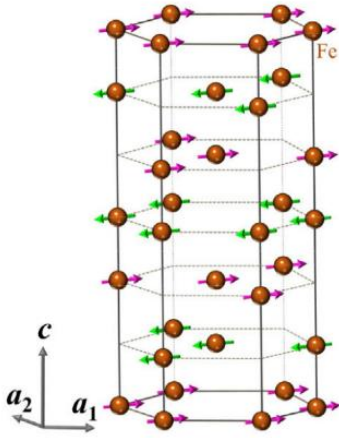


Figure 5. Crystalline and spin order of α - Fe_2O_3 from Ref. [7].

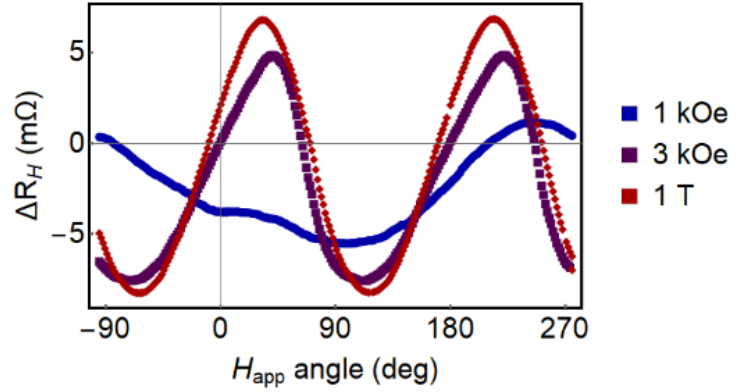


Figure 6. Anomalous Hall effect measurements of α - $\text{Fe}_2\text{O}_3/\text{Pt}$ similar to those in Ref. 8.

probe. The thermal pulse repetition rate is phase-locked to the microwave current source, thus enabling phase sensitive measurements of the current. As we rotate the phase of the current, the near-field signal also rotates. This not only demonstrates a resource for microwave current imaging, but also serves to demonstrate that our near-field microscope retains its time resolution.

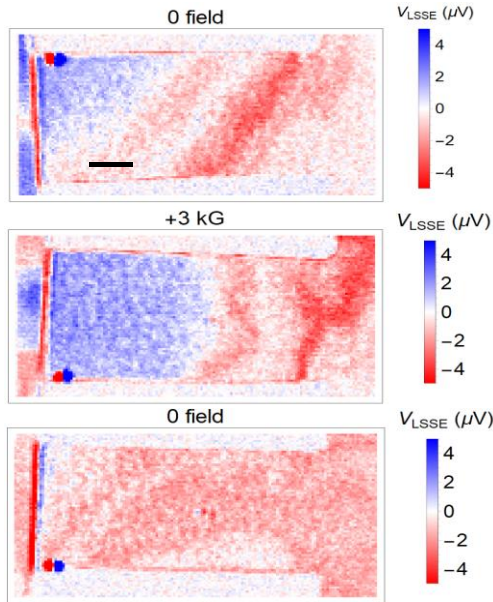


Figure 7. Magneto-thermal microscopy of α - $\text{Fe}_2\text{O}_3/\text{Pt}$ heterostructure.

Next we discuss our progress using far-field magneto-thermal microscopy to probe antiferromagnetic order. Previously, we demonstrated the interfacial spin Seebeck effect in antiferromagnetic NiO [111]/Pt heterostructures as the contrast mechanism for imaging Néel order. [5] Here we consider α - $\text{Fe}_2\text{O}_3/\text{Pt}$ heterostructures. [7,8] Like NiO [111], this material has antiferromagnetic order with planes of spins aligned in the sample plane (Figure 5). Unlike NiO, α - Fe_2O_3 has a very small magnetic moment that originates from spin canting, induced by the Dzyaloshinskii-Moriya interaction. As a result we can apply magnetic fields to see changes in the spin order (Figure 6).

When we measure the samples in magneto-thermal microscopy, we do see signal contrast that reproducibly changes with magnetic field (Figure 7). However, the results are puzzling. Contrary to the anomalous Hall effect (AHE) data, we do not see saturation. These images are reproducible on repeated measurements, but field cycling creates neither saturated states as one would expect from AHE measurements, nor do we find the same states on different field preparations. To make things more puzzling, we see long-time creep relaxation effects. Although such effects are plausible in antiferromagnets where strong magneto-electric effects induced by the strain from sample

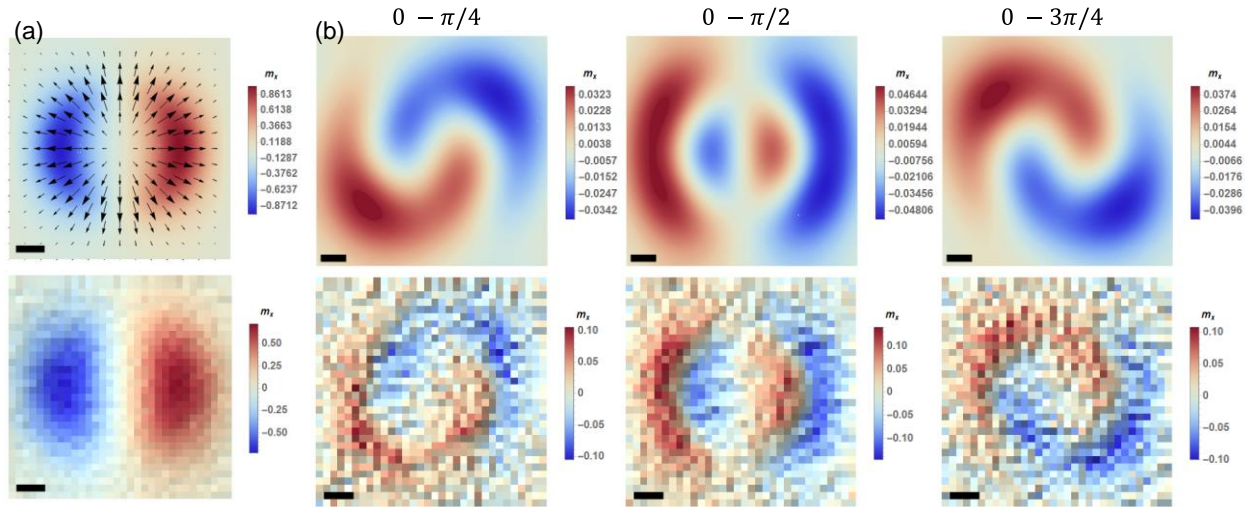


Figure 8. Top row shows micromagnetic simulations while the bottom row shows calculated magneto-thermal signals of 100 nm skyrmions. (a) is a static skyrmion whereas (b) shows gyrotropic motion at different phases as a difference with the zero phase.

heating, [8] there is clearly a mechanism in this material system – either spin Seebeck contrast or the effect of laser fluence – that we do not yet understand.

Future Plans

We plan to continue to develop techniques of scanning probe magneto-thermal microscopy, including making the first measurement of time-resolved dynamics. We plan to study the dynamics of ~ 100 nm skyrmions such as their breathing and gyrotropic modes. We have previously developed a material heterostructure with ~ 100 nm skyrmions, verified via Lorentz TEM in collaboration with David Muller. We have numerically simulated that this is feasible given the signal-to-noise ratio demonstrated above, including realistic noise (Figure 8).

References

- [1] J. M. Bartell, D. H. Ngai, Z. Leng, and G. D. Fuchs, “Towards a table-top microscope for nanoscale magnetic imaging using picosecond thermal gradients” *Nat. Commun.* **6**, 8460 (2015).
- [2] F. Guo, J. M. Bartell, D. H. Ngai, and G. D. Fuchs, “Phase-sensitive imaging of ferromagnetic resonance using ultrafast heat pulses” *Phys. Rev. Appl.* **4**, 044004 (2015).
- [3] J. M. Bartell, C. L. Jermain, S. V. Aradhya, J. T. Brangham, F. Yang, D. C. Ralph, and G. D. Fuchs, “Imaging Magnetization Structure and Dynamics in Ultrathin $\text{Y}_3\text{Fe}_5\text{O}_{12}$ / Pt Bilayers with High Sensitivity Using the Time-Resolved Longitudinal Spin Seebeck Effect” *Phys. Rev. Appl.* **7**, 044004 (2017).
- [4] I. Gray, G. M. Stiehl, J. T. Heron, A. B. Mei, D. G. Schlom, R. Ramesh, D. C. Ralph, and G. D. Fuchs, “Imaging uncompensated moments and exchange-biased emergent ferromagnetism in FeRh thin films” *Phys. Rev. Mater.* **3**, 124407 (2019).
- [5] I. Gray, T. Moriyama, N. Sivadas, G. M. Stiehl, J. T. Heron, R. Need, B. J. Kirby, D. H. Low, K. C. Nowack, D. G. Schlom, D. C. Ralph, T. Ono, and G. D. Fuchs, “Spin Seebeck imaging of spin-torque switching in antiferromagnetic Pt/NiO heterostructures” *Phys. Rev. X* **9**, 041016 (2019).
- [6] J. C. Karsch, J. M. Bartell, and G. D. Fuchs, “Near-field coupling of gold plasmonic antennas for sub-100 nm magneto-thermal microscopy” *APL Photonics* **2**, 086103 (2017).
- [7] Y. Cheng, S. Yu, M. Zhu, J. Hwang, and F. Yang, “Electrical Switching of Tristate Antiferromagnetic Néel Order in $\alpha\text{-Fe}_2\text{O}_3$ Epitaxial Films” *Phys. Rev. Lett.* **124**, 027202 (2020).
- [8] P. Zhang, J. Finley, T. Safi, and L. Liu, “Quantitative Study on Current-Induced Effect in an Antiferromagnet Insulator/Pt Bilayer Film” *Phys. Rev. Lett.* **123**, 247206 (2019).

Development of a Coherent Spin-Magnon Interface Between Quantum Spins and a High-Q Organic Based Magnet

Gregory D. Fuchs, Cornell University Applied and Engineering Physics, Ithaca, NY

Daniel C. Ralph, Cornell University Department of Physics, Ithaca, NY

Ezekiel Johnston-Halperin, The Ohio State University Department of Physics, Columbus, OH

Michael E. Flatté, University of Iowa Department of Physics, Iowa City, IA

Keywords: quantum transduction, hybrid quantum systems, nitrogen-vacancy centers

Research Scope

This project examines the coupling between single quantum spins and the magnons of ultra-low damping magnetic resonators. Our goal is to experimentally and theoretically understand how to enable coherent quantum transduction through magnons at very low temperature, both from single-spin to single-spin and from single-spin to other quantum elements such as a microwave resonator. We focus on nitrogen-vacancy (NV) centers in diamond as a quantum spin platform and $V[TCNE]_x$ as an organic-based ferrimagnet with a high material quality factor. Key steps for achieving our goal include theoretical modeling of spin-magnon coupling to better assess experimentally realizable geometries, understanding the material properties of $V[TCNE]_x$, development of $V[TCNE]_x$ magnetic resonator fabrication that evades degradation due to air exposure, and integration with high-quality NV centers.

Recent Progress

To advance our understanding of the hybrid quantum system described above, we derive an analytical expression for the spin-magnon cooperativity as a function of NV position under a micron-scale perpendicularly magnetized disk. Surprisingly, we predict a higher cooperativity than in magnetic materials with larger magnetic moments, due to in part to

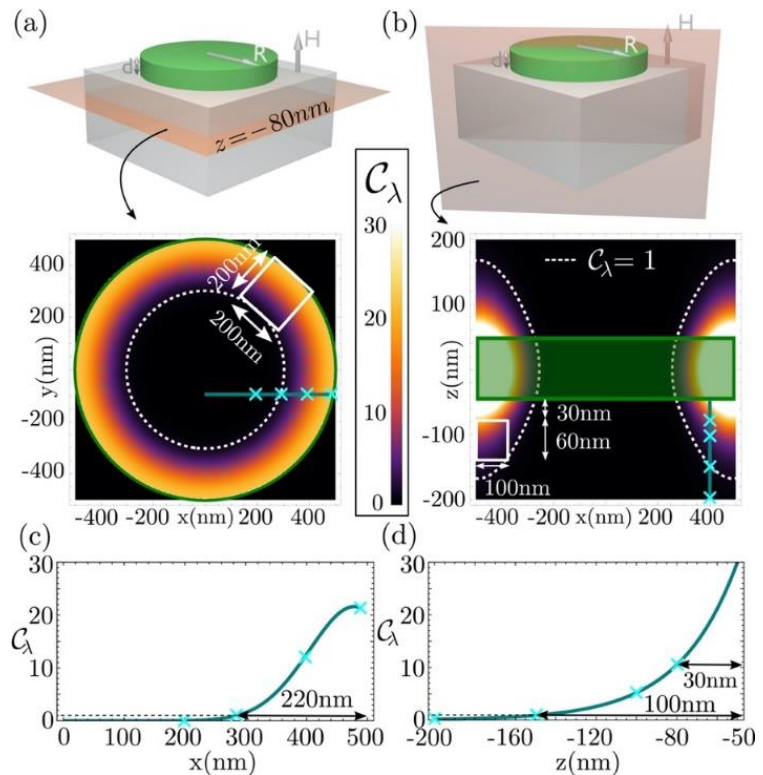


Figure 1. Spatial plot of the cooperativity of the $\lambda=(6,1,1)$ magnon mode for NV centers located (a) at 30 nm below the 100 nm thick disk ($z=-80$ nm), (b) within cross-section plane, (c) along the teal line within panel (a), (d) along the teal line within panel (b). The dashed white border shows the strong-coupling regime stability region where $C \geq 1$, where the white rectangle indicates a tolerance for spatial implantation imprecision for the NV centers while still achieving high cooperativity. The green lines delimit the disk dimension (100 nm thick and radius of 500 nm). From Ref. [1].

the reduced demagnetization field. For reasonable experimental parameters, we calculate the spin-magnon-mode coupling strength is $g \sim (2\pi)10$ kHz. For isotopically pure ^{12}C diamond we predict strong coupling of an NV spin to the unoccupied magnon mode, with cooperativity $C=15$ for a wide range of NV spin locations within the diamond, well within the spatial precision of NV center implantation. This analysis validates our proposed pathway for single-spin-state-to-single-magnon-occupancy transduction and for entangling NV centers over micron length scales. In general, for disks with diameter smaller than $4 \mu\text{m}$ we find $C>1$ for the magnon mode with mode index 6,1,1 (shown in Figure 1) [1].

We have measured for the first time the low temperature magnetic resonance properties of $\text{V}[\text{TCNE}]_x$ films [2]. We identify two regimes. In the high temperature regime, extending from 300 K down to 10 K, we observe a monotonic shift in the resonance frequency consistent with a temperature dependent strain (Figure 2, upper panel). This strain results in a crystal-field anisotropy that increases with decreasing temperature with a magnitude of at least 140 Oe and the same symmetry, but opposite sign, to the shape anisotropy of the thin film. In addition, we observe an increase in linewidth consistent with magnon scattering from paramagnetic impurities similar to what has been observed in YIG (Figure 2, lower panel), but with an amplitude 3 times smaller (*i.e.* an increase in linewidth by 9 times in $\text{V}[\text{TCNE}]_x$ as compared to 28 times in YIG). In the low temperature regime, starting at 10 K and extending to 5 K, we observe a discontinuous change in both anisotropy and linewidth: the anisotropy abruptly reverts to the room temperature symmetry (in-plane easy axis) and the linewidth drops close to room temperature values (2.58 G). This behavior can be explained using a model for scattering between magnons and paramagnetic impurities that considers the finite spin-lifetime of excitations of the impurity spins. At high temperatures (above 100 K) the spin lifetime is sufficiently short that changes in temperature do not lead to significant changes in scattering rate, and at low temperatures (below 10 K) the spin lifetime is sufficiently long that the ensemble completely polarizes and precesses in phase with the magnons. At intermediate temperatures (from 10 K to 100 K) this spin-magnon scattering dominates relaxation and results in a local maximum in the linewidth that is 9 times larger than the room temperature value. These results are extremely promising for low

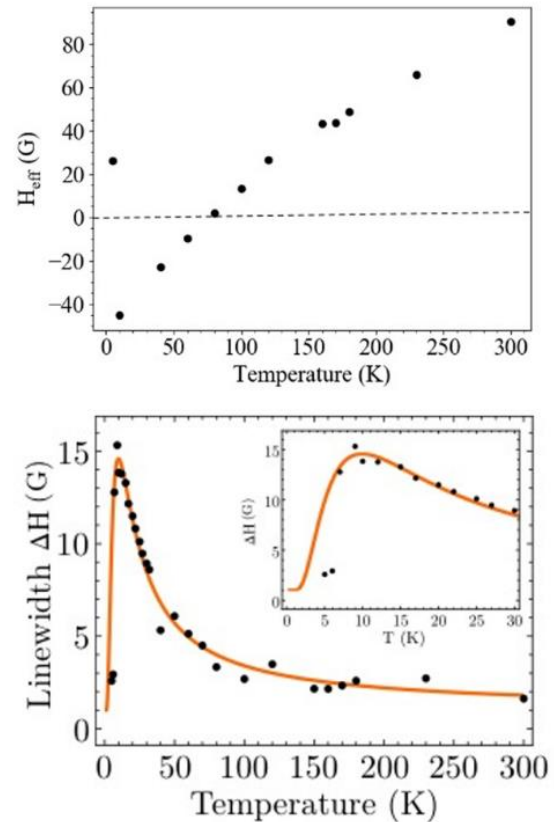


Figure 2. Upper Panel: Temperature dependent magnetic anisotropy of a thin film of $\text{V}[\text{TCNE}]_x$ showing switch of easy axis from in plane (300 K) to out of plane (100 K – 10 K) back to in plane (5 K). Lower Panel: Temperature dependence of magnetic resonance linewidth of the same film showing recovery of room temperature linewidth below 10 K. Orange line is a fit to a model describing temperature dependent spin-magnon scattering.

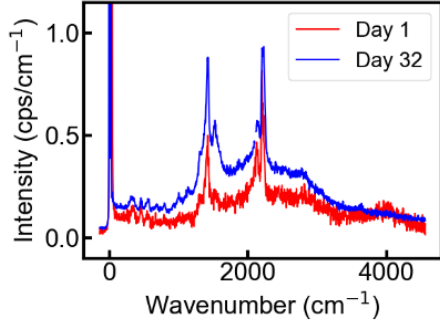


Figure 3. Raman spectra of pristine and aged V[TCNE]_x.

temperature applications of V[TCNE]_x magnonics, promising low temperature magnon resonators with unprecedented low loss that can be integrated on-chip into microwave electronic circuits and devices.

Considering that V[TCNE]_x is an air-sensitive material, requiring encapsulation to prevent oxygen or water vapor exposure, it is a practical concern to understand how an encapsulated sample degrades over time under ambient conditions (e.g. at room temperature in moist air), and to develop simple to implement spectroscopies to assess the quality of a sample prior to extensive study. To that end we

apply Raman spectroscopy to probe V[TCNE]_x, focusing on the vibronic changes that occur as the material degrades with intentional ambient exposure. We simultaneously study the sample using ferromagnetic resonance (FMR) to correlate changes in the Raman features with the magnetic properties of the material.

Figure 3 shows the Raman spectrum of pristine V[TCNE]₂ and a spectrum after 32 days of exposure to ambient conditions. In both spectra, we observe features associated with the cyanide bond stretch as well as C-C/C=C bond stretch modes (Table 1). As the aging proceeds, all features remain present, with a relative increase in the 1308 cm⁻¹ and the 1530 cm⁻¹ peaks. Additionally, a broad increase in the signal levels increases, which we interpret as a photoluminescence (PL) rate associated with broken and/or unsatisfied bonds being formed as the material chemically degrades. The PL rate increases exponentially in time, with a characteristic time constant τ that depends sensitively on the details of the encapsulation. In this sample $\tau = 6.4$ days. Similar changes to the Raman spectrum and PL are observed for laser power densities greater than $\approx 10^5$ W/cm², which appears to be a laser-induced damage threshold.

Bonds	Wavenumber (cm ⁻¹)
	336.2 ± 4.9
	458.6 ± 3.2
	543.0 ± 3.5
C=C	1308.4 ± 4.4
C-C	1410.6 ± 0.9
	1529.9 ± 3.7
C≡N	2120.8 ± 1.6
	2202.2 ± 0.5
	2224.5 ± 1.2

Table 1. Chemical stretch features associated with the Raman spectra

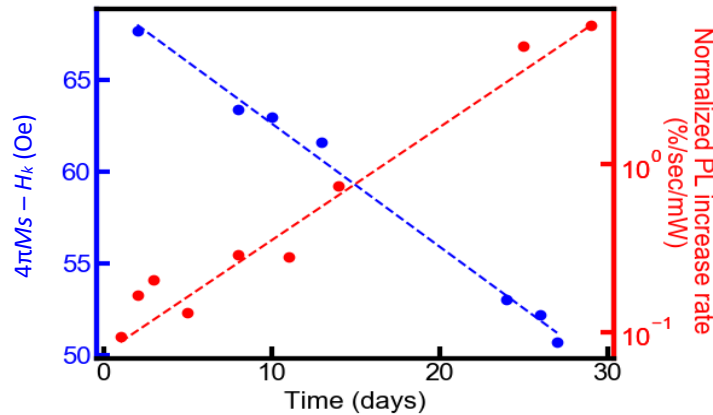


Figure 4. Changes in V[TCNE]_x PL and $4\pi M_s$ as a function of time over 30 days under ambient conditions.

To establish the magnetic properties, we perform angle dependent FMR. The shift of the FMR resonance establishes the quantity $4\pi M_s - H_k \approx 4\pi M_s$, where M_s is the saturation magnetization and H_k is the uniaxial anisotropy field. Correlating these results with spectroscopy, we find an inverse relationship between $\log(\text{PL rate})$ and $4\pi M_s$, suggesting that as the V[TCNE]_x degrades, the

Raman-active bonds remain intact, however, the increase in dangling/unsatisfied bonds reduces spin order in the material.

Understanding how the optical linewidth depends on environmental noise is important for coherent read-out. Our newly developed theory [3] for the suppression of the optical linewidth of a quantum spin center due to charge fluctuation noise quantitatively describes the optical transition shift and linewidth for a spin center in a tunable

electric field, in agreement with recent experiment. Remarkably, we show that an accurate description of the decoherence of such spin centers requires a complete spin-1 formalism that yields a bi-exponential decoherence process.

Future Plans

We are integrating patterned $V[TCNE]_x$ microdisk resonators on diamond with high-quality implanted NV centers. Figure 5 shows an SEM image of $V[TCNE]_x$ patterned using an ebeam lift-off process that does not disturb the $V[TCNE]_x$ chemistry. We have been building the experimental infrastructure and protocols to study the quantum dynamics in this hybrid quantum system, both at room temperature and in the quantum limit at $T < 0.1$ K in a custom confocal dilution refrigerator set-up. We are collaborating with Argonne National Lab to create “delta doped” NV centers created in ^{12}C diamond membranes – combining ultra-long spin coherence lifetimes with shallow placement to enhance cooperativity. From a theory perspective, we seek non-trivial coupling geometries that are not analytically accessible. We have verified the analytic calculations above using numerical calculations of the spin-wave dynamics (Mumax3 numerical code) and are now considering more complex situations including irregularities in the disk shape, tapering near the edge which may help concentrate the field lines. We are also deriving the expressions for NV’s oriented along an axis different from the disk’s symmetry axis.

References

- [1] D. R. Candido, G. D. Fuchs, E. Johnston-Halperin, and M. Flatté, “Predicted strong coupling of solid-state spins via a single magnon mode” *Mater. Quantum Technol.* (2020) DOI: 10.1088/2633-4356/ab9a55.
- [2] H. Yusuf, M. Chilcote, D. R. Candido, D. S. Cormode, Y. Lu, M. E. Flatté, and E. Johnston-Halperin, “Temperature dependent anisotropy and linewidth in the high-Q ferrimagnet $V(TCNE)_x$ ” *ArXiv: 2008.13061* (2020).
- [3] D. R. Candido and M. E. Flatté, “Suppression of the optical linewidth and spin decoherence of a quantum spin center in a p-n diode” *ArXiv: 2008.13289* (2020).

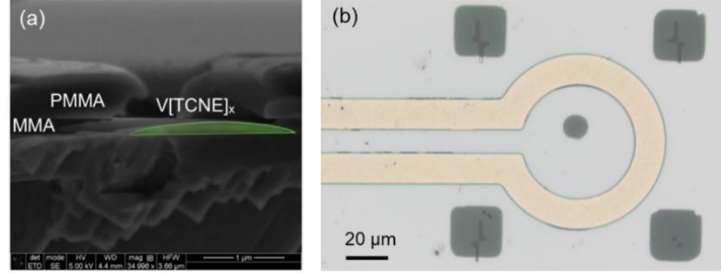


Figure 5. (a) Cross-sectional SEM micrograph of $V[TCNE]_x$ grown on e-beam patterned PMMA. Patterned $V[TCNE]_x$ is shown with green shading. (b) Optical micrograph of a full device on NV diamond patterned with a $10 \mu\text{m}$ microdisk of $V[TCNE]_x$. The image was taken through the coverslip and encapsulation epoxy in air. The four squares of $V[TCNE]_x$ in (b) result from the alignment procedure used during the e-beam pattern exposure

Publications

1. D. R. Candido, G. D. Fuchs, E. Johnston-Halperin, and M. Flatté, “Predicted strong coupling of solid-state spins via a single magnon mode” *Mater. Quantum Technol.* (2020) DOI: 10.1088/2633-4356/ab9a55.
2. H. Yusuf, M. Chilcote, D. R. Candido, D. S. Cormode, Y. Lu, M. E. Flatté, and E. Johnston-Halperin, “Temperature dependent anisotropy and linewidth in the high-Q ferrimagnet V(TCNE)_x” ArXiv: 2008.13061 (2020).
3. D. R. Candido and M. E. Flatté, “Suppression of the optical linewidth and spin decoherence of a quantum spin center in a p-n diode” ArXiv: 2008.13289 (2020).

Multimodal Hyperspectral Scanning Probe Microscopy for Understanding Low Dimensional Perovskite Semiconductors

PI: David S. Ginger, University of Washington, Department of Chemistry

Keywords: scanning probe microscopy, halide perovskites, ion migration

Research Scope

This project aims to develop new microscopy tools for analyzing semiconductor materials, with a particular emphasis on improving our understanding of hybrid organic-inorganic halide perovskite semiconductors for photovoltaics applications. We seek to develop new methods combining advances in scanning probe microscopy with insight into the structure-function relationships. In this project we focus on coupling advances in “big data” analytics and machine learning with development of microscopy methods to acquire large, multimodal datasets. As a materials system of interest, we focus on layered 2D Ruddlesden-Popper phases that have emerged as promising materials for optoelectronics applications such as photovoltaics or LEDs. Specifically, we (1) use time-resolved scanning probe methods combined with data science-based methods to understand the relationship between optoelectronic dynamic response and grain sizes in perovskite materials and; (2) develop a better understanding of ion motion as it relates to the dimensionality in Ruddlesden-Popper materials; final we, (3) correlate photoinduced force microscopy (PiFM) with multimodal AFM microscopy data, using principal component regression and non-negative matrix factorization as a tool for hyperspectral unmixing of component spectra, with preliminary results on mixed-cation layered perovskites. These methods are highly useful for understanding perovskites specifically but are also generalizable—indeed, much of our time-resolved microscopy code is publicly available online and we are active in integrating the larger Python-based “Pycroscopy” ecosystem into our work.

Recent Progress

We have made significant progress advancing our goal of developing new tools and methods for extracting structure-function relationships in 2D semiconducting halide perovskite materials. Key accomplishments include furthering our progress on time-resolved microscopy for analyzing perovskite materials,¹ development of analytical tools for correlating scanning electron microscopy and confocal photoluminescence information,² and expanding our lateral junction work to study the effects of perovskite dimensionality on ion motion (in preparation). We also have begun to apply hyperspectral unmixing methods to PiFM IR data on perovskite systems.

Mapping Microsecond-Scale Dynamics in Layered Perovskites

Our group combined two dynamic scanning probe methods, fast free time-resolved electrostatic force microscopy (FF-trEFM) and “general mode” Kelvin probe force microscopy (G-KPFM) to provide high time-resolution analysis of 2D Ruddlesden-Popper perovskites.¹ We studied the photoresponse of layered 2D perovskite $(\text{C}_4\text{H}_9\text{NH}_3)_2\text{PbI}_4$ (BAPI), and we have found that the photovoltage dynamics are dominated by surface-mediated effects either by ionic motion, in contrast to other reports, or trap-mediated dynamics. In particular, we found that these effects are spatially-correlated with proximity to grain boundaries in the film.

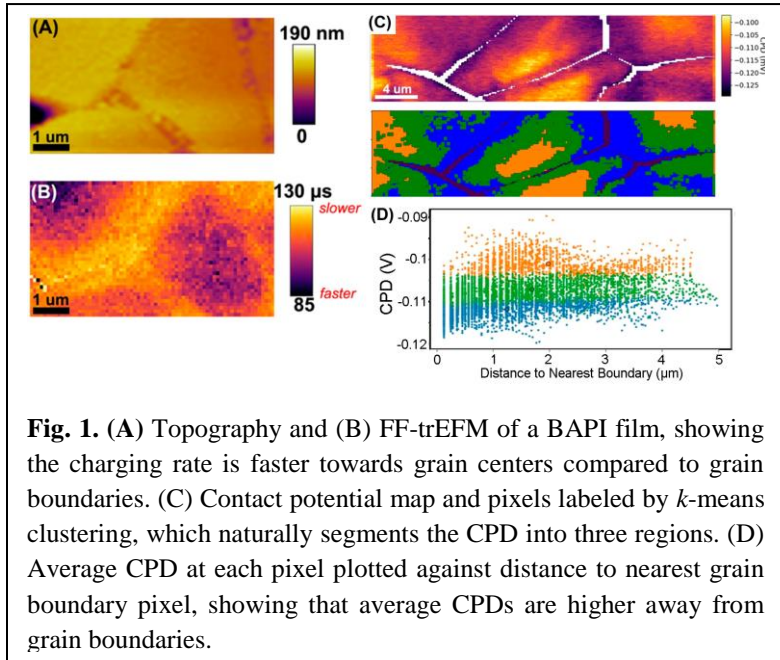


Fig. 1. (A) Topography and (B) FF-trEFM of a BAPI film, showing the charging rate is faster towards grain centers compared to grain boundaries. (C) Contact potential map and pixels labeled by *k*-means clustering, which naturally segments the CPD into three regions. (D) Average CPD at each pixel plotted against distance to nearest grain boundary pixel, showing that average CPDs are higher away from grain boundaries.

Since our initial report, we have significantly improved the signal-to-noise analysis of FF-trEFM by exploiting principal component analysis-based filtering and enabled correlation on other BAPI samples in our lab. In **Fig. 1**, we illuminate the samples while measuring the time-dependent response of the atomic force microscopy (AFM) cantilever. By post-processing the AFM data to extract the cantilever’s instantaneous frequency, it is possible to map out the efficiency on a pixel-by-pixel basis. **Fig. 1** shows that the charging time is significantly shorter at grain centers as compared to grain boundaries, indicating that grain boundaries are either centers for ion motion or significant population of non-radiative traps. We employed *k*-means clustering on the G-KPFM data to categorize the data as a function of distance to nearest grain boundary as an unsupervised method of categorizing the potential variations relative to nearest grain boundary.

Dimensionality-Dependence of Ion Motion in Layered Perovskites using Lateral Junctions

We have made significant improvements in our experiments and modeling of lateral ionic motion in Ruddlesden-Popper perovskites. In these experiments, we use frequency modulated scanning Kelvin probe microscopy (FM-SKPM) to study the lateral potential profile in a $\sim 10 \mu\text{m}$ junction using insulating layers to block charge injection into the junction. In previous work on 3D perovskites, we showed the insulating contacts are important for separating charge injection from the ion migration process.^{4,5} Here, we extend these experiments to 2D perovskites and compare the ion migration both in the dark, and under in situ photoexcitation, as a function of dimensionality. In layered Ruddlesden-Popper systems with the general form $\text{BA}_2\text{MA}_{n-1}\text{Pb}_n\text{I}_{3n+1}$, the

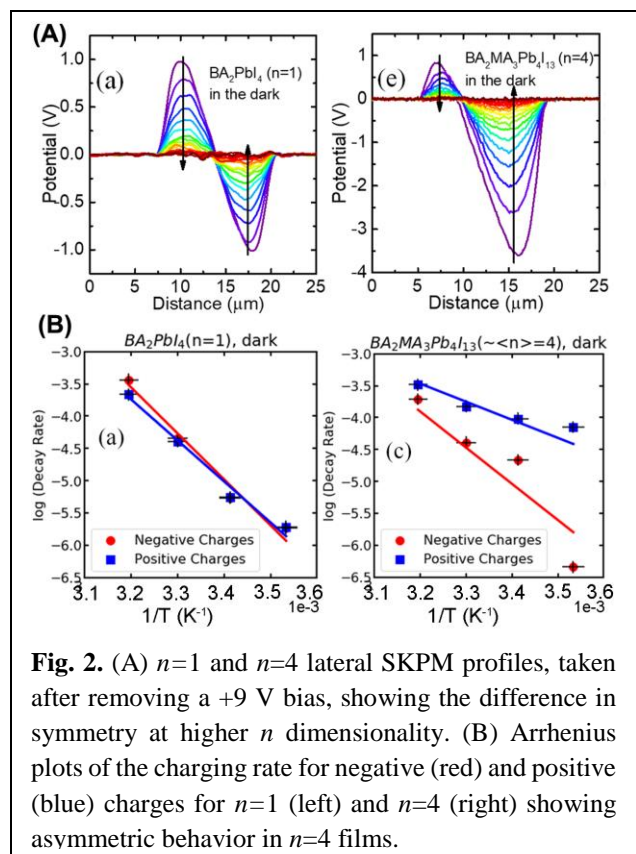


Fig. 2. (A) $n=1$ and $n=4$ lateral SKPM profiles, taken after removing a +9 V bias, showing the difference in symmetry at higher n dimensionality. (B) Arrhenius plots of the charging rate for negative (red) and positive (blue) charges for $n=1$ (left) and $n=4$ (right) showing asymmetric behavior in $n=4$ films.

dimensionality factor n controls the perovskite layer thickness between insulating organic cation spacer molecules (butylammonium, BA). As the dimensionality increases, the films become more quasi-2D with thicker perovskite layers between spacer molecules.

In **Fig. 2**, we show that upon applying a bias, we observe little screening in $n=1$ and a highly symmetric response, whereas in $n=4$ we see an asymmetric potential; in both cases the potential recovers slowly, on the order of tens of minutes. For $n=4$, the potential becomes increasingly symmetric under illumination. These data are in striking contrast to the 3D perovskite lateral junctions. We repeat these measurements at different temperatures and extract activation energies. Comparing the activation energies for ion migration in $n=1$ and $n=4$ films, we observe that there is a striking contrast between the two. For $n=1$, the

activation energies for positive and negative charges are similar (0.55 and 0.61 eV for positive and negative charges), where for $n=4$ they differ significantly (0.24 and 0.64 eV for positive and negative charges). We propose these observations indicate that ion migration in $n=4$ is a complex interplay between paired halide-vacancies and methylammonium vacancies.

Hyperspectral Unmixing of Perovskite Composition Using Photoinduced Force Microscopy

We have used PiFM to analyze the component spectra in quasi-2D perovskite materials, in an effort to determine if conventional hyperspectral unmixing methods can be extended to work with scanning probe microscopy data. PiFM uses a tunable infrared laser from 800 – 1800 cm^{-1} to probe vibrational spectra in the material at ~ 10 nm length scales. Our initial results are highly promising. Focusing on a mixed $PEA_2MA_{n-1}Pb_3Br_{10}$ system,⁵ we observe a contrast inversion across different wavenumbers. We use nonnegative matrix factorization (**Fig. 3**) to show that the spectra can be unmixed into component spectra, with a prominent feature at 1265 cm^{-1} possibly corresponding to MA^+ and a broad feature from 1400 to ~ 1580 cm^{-1} possibly corresponding to aromatic C=C (PEA). We use these component spectra to generate composition maps. Experiments to correlate these data with confocal PL to compare the optical spectra with PiFM composition are ongoing, with a preliminary example in **Fig. 3** showing heterogeneity in PL peak position.

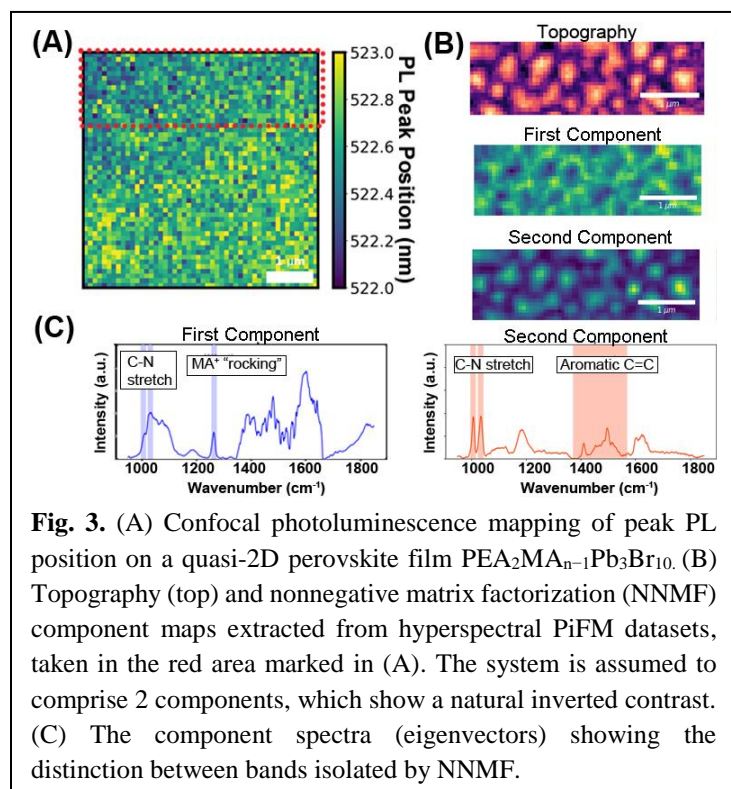


Fig. 3. (A) Confocal photoluminescence mapping of peak PL position on a quasi-2D perovskite film $\text{PEA}_2\text{MA}_{n-1}\text{Pb}_3\text{Br}_{10}$. (B) Topography (top) and nonnegative matrix factorization (NNMF) component maps extracted from hyperspectral PiFM datasets, taken in the red area marked in (A). The system is assumed to comprise 2 components, which show a natural inverted contrast. (C) The component spectra (eigenvectors) showing the distinction between bands isolated by NNMF.

Future Plans

Our current projects will continue our efforts on multimodal analysis of layered perovskites. We will expand our work on blind unmixing of hyperspectral datasets on two- and three-component perovskite materials. We will correlate these results with PL spectra, as shown in our preliminary results, as well as comparing PL lifetime. Additionally, we will further our trEFM studies by focusing on non-single exponential behavior in perovskites. Conventional trEFM has focused on single exponential type responses, whereas in systems that conduct both electronic and ionic charge (like halide perovskites), the behavior is expected to exhibit non-

single exponential behavior. Lastly, we will continue our work in lateral diffusion measurements using conducting AFM. In these experiments we control the laser excitation in the system independent of the tip position and record the current as a function of laser position. We have initial experiments validating this technique and have improved the experimental code in the past two years, enabling more reliable probes of diffusion in layered perovskite films.

References

- (1) Giridharagopal, R.; Precht, J. T.; Jariwala, S.; Collins, L.; Jesse, S.; Kalinin, S. V.; Ginger, D. S. Time-Resolved Electrical Scanning Probe Microscopy of Layered Perovskites Reveals Spatial Variations in Photoinduced Ionic and Electronic Carrier Motion. *ACS Nano* **2019**, *13* (3), 2812–2821.
- (2) Jariwala, S.; Sun, H.; Adhyaksa, G. W. P.; Lof, A.; Muscarella, L. A.; Ehrler, B.; Garnett, E. C.; Ginger, D. S. Local Crystal Misorientation Influences Non-Radiative Recombination in Halide Perovskites. *Joule* **2019**. <https://doi.org/10.1016/j.joule.2019.09.001>.
- (3) Birkhold, S. T.; Precht, J. T.; Liu, H.; Giridharagopal, R.; Eperon, G. E.; Schmidt-Mende, L.; Li, X.; Ginger, D. S. Interplay of Mobile Ions and Injected Carriers Creates Recombination Centers in Metal Halide Perovskites under Bias. *ACS Energy Lett.* **2018**, *3* (6), 1279–1286.
- (4) Birkhold, S. T.; Precht, J. T.; Giridharagopal, R.; Eperon, G. E.; Schmidt-Mende, L.; Ginger, D. S. Direct Observation and Quantitative Analysis of Mobile Frenkel Defects in Metal Halide Perovskites Using Scanning Kelvin Probe Microscopy. *J. Phys. Chem. C* **2018**, *122* (24), 12633–12639.
- (5) Han, Y.; Park, S.; Wang, J.; Jariwala, S.; Lee, K.; Bischak, C. G.; Kim, S.; Hong, J.; Kim, S.; Lee, M. J.; et al. Controlling Spatial Crystallization Uniformity and Phase Orientation of Quasi - 2D Perovskite - Based Light - Emitting Diodes Using Lewis Bases. *Adv. Mater. Interfaces* **2020**, *7* (3), 1901860.

Publications citing BES

1. R. Giridharagopal, J. T. Pecht, J. T., S. Jariwala, S., L. Collins, L., S. Jesse, S. V. Kalinin, D. S. Ginger. “Time-Resolved Electrical Scanning Probe Microscopy of Layered Perovskites Reveals Spatial Variations in Photoinduced Ionic and Electronic Carrier Motion.” *ACS Nano* 13, 2812–2821 (2019).
2. D. W. deQuilettes, K. Frohna, D. Emin, T. Kirchartz, V. Bulovic, D. S. Ginger, S. D. Stranks. “Charge-Carrier Recombination in Halide Perovskites.” *Chemical Reviews* 119, 11007–11019 (2019).
3. S. Jariwala, H. Sun, G. W. P. Adhyaksa, A. Lof, L. A. Muscarella, B. Ehrler, E. C. Garnett, D. S. Ginger. “Local Crystal Misorientation Influences Non-Radiative Recombination in Halide Perovskites.” *Joule* 3, 3048–3060 (2019).
4. Z. Yang, X. Zhang, W. Yang, G. E. Eperon, D. S. Ginger. “Tin-Lead Alloying for Efficient and Stable All-Inorganic Perovskite Solar Cells.” *Chemistry of Materials* 32, 2782–2794 (2020).
5. A. M. Tirmzi, R. P. Dwyer, F. Jiang, J. A. Marohn. “Light-dependent Impedance Spectra and Transient Photoconductivity in a Ruddlesden-Popper 2D Lead-Halide Perovskite Revealed by Electrical Scanned Probe Microscopy and Accompanying Theory.” *Journal of Physical Chemistry C* 124, 13639–13648 (2020).
6. M. Hermes, A. Best, L. Winkelmann, J. Mars, S. M. Vorpahl, M. Mezger, L. Collins, H.-J. Butt, D. S. Ginger, K. Koynov, S. A. L. Weber. “Anisotropic carrier diffusion in single MAPbI₃ grains correlates to their twin domains.” *Energy and Environmental Science*. In press. DOI: 10.1039/D0EE01016B

Tuning exchange interactions at the atomic scale in 2D magnet / semiconductor heterostructures

Jay A. Gupta¹, Roland Kawakami¹ and Michael E. Flatté²

¹Department of Physics, Ohio State University, Columbus OH 43210, USA

²Department of Physics and Astronomy, University of Iowa, Iowa City, IA 52242, USA

Keywords: 2D magnets, spin polarized STM, spin transport theory, magnetic semiconductors, magnetic topological insulators

Research Scope

The atomically thin nature of 2D materials leads to highly tunable properties that are of considerable interest for spintronics. For example, the effects of electrostatic gating, surface adsorption, and proximity- or interfacial-induced phenomena can be much stronger than in 3D materials. This program is focused on the growth, atomic-scale characterization, and theoretical modeling of 2D magnet (2DM) / III-V semiconductor heterostructures with the following objectives:

(A) **Explore interfacial tuning of 2D magnetism by molecular beam epitaxial growth on III-Vs.** The III-V family of substrates offers high quality surfaces for 2DM growth, with varying polarity, band offsets, spin orbit coupling, and electrical doping, any or all of which are likely to influence the 2D magnetism. For example, growth on high spin orbit InSb may stabilize magnetic Skyrmions in the 2D magnets, and variation of electrical doping may tune the ferromagnetic TC. On the theory side, we are developing a mixed approach combining ab initio and tight binding methods to simulate the electronic states in these 2D-3D systems.

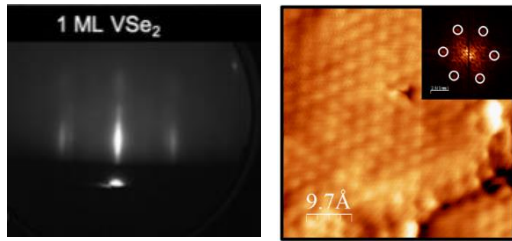
(B) **Quantify and control FM/AFM order in 2D magnets at the atomic scale with spin polarized scanning tunneling microscopy.** SPSTM imaging and spectroscopy are used to explore the dependence of 2D magnetism on layer thickness, where even/odd FM/AFM order may be expected, and interfacial spin orbit coupling, which can produce non-collinear magnetic textures via the Dzyaloshinskii-Moriya interaction. We *tune* magnetism on an atomic level by STM manipulation of the position and charge state of individual adatoms and dopants (e.g., Fe, Co, Mn) and elements with high atomic number (e.g., Bi, Sn, Sb) help test the hypothesis that adatoms can tune the local exchange and spin orbit character of the 2DMs. We are also extending the theoretical descriptions of model dopants in traditional 3D dilute magnetic semiconductors to 2DMs for the first time.

(C) **Develop new microscopy tools for magnetic dynamics at the atomic scale.** While SPSTM has traditionally been used to study the static properties of surface magnetism, we are developing new SPSTM methods based on pulsed inelastic tunneling techniques for studying magnetic excitations and dynamics in the 2DM heterostructures. This effort is guided by our theoretical discovery of current-detected resonance in coupled spin/FM tunnel junctions, where we established that spin-dependent tunneling through single defect levels can be used to measure coherent dynamics at the atomic scale.

Recent Progress

Growth of III-V / 2D magnet heterostructures: VSe₂ / GaAs(111)

We report epitaxial growth of vanadium diselenide (VSe₂) thin films in the octahedrally-coordinated (1T) structure on GaAs(111)B substrates by molecular beam epitaxy (1). Film thickness from a single monolayer (ML) up to 30 ML is demonstrated. Structural and chemical studies using by x-ray diffraction, transmission electron microscopy, scanning tunneling

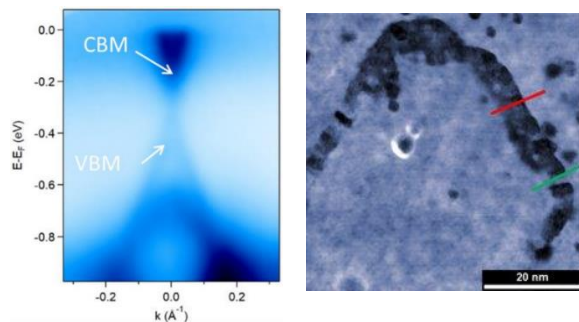


(left) RHEED pattern of 1ML VSe₂ on GaAs(111)B showing uniform film growth (right) Corresponding atomic-resolution STM image showing the VSe₂ lattice

microscopy and x-ray photoelectron spectroscopy indicate high quality thin films. Further studies show that monolayer VSe₂ films on GaAs are not air-stable and are susceptible to oxidation within a matter of hours, which indicates that a protective capping layer should be employed for device applications. This work demonstrates that VSe₂, a candidate van der Waals material for possible spintronic and electronic applications, can be integrated with III-V semiconductors via epitaxial growth for 2D/3D hybrid devices.

Growth and characterization of layered AFM w/ topological surface states

The intrinsic magnetic topological insulators MnBi₂X₄ (X = Se, Te) are promising candidates in realizing various novel topological states related to symmetry breaking by magnetic order. Although much progress had been made in MnBi₂Te₄, the study of MnBi₂Se₄ has been lacking due to the difficulty of material synthesis of the desired trigonal phase. Here, we report the synthesis of multilayer trigonal MnBi₂Se₄ with alternating-layer molecular beam epitaxy (2). Systematic thickness-dependent magnetometry studies illustrate the layered antiferromagnetic ordering as predicted by theory. Angle-resolved photoemission spectroscopy (ARPES) reveals the gapless Dirac-like surface state of MnBi₂Se₄, which demonstrates that MnBi₂Se₄ is a topological insulator above the magnetic ordering temperature. Atomic-resolution STM images identify a well-ordered



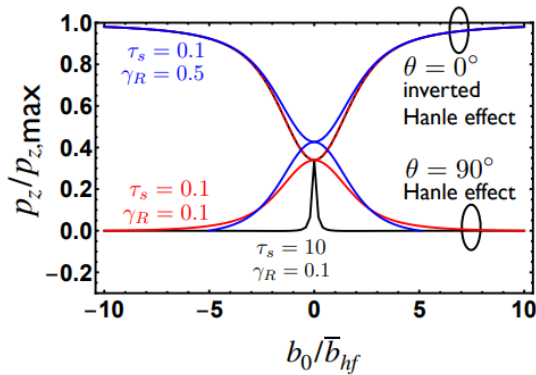
(left) ARPES of MnBi₂Se₄ showing linear Dirac dispersion at the Fermi level. (right) Spatial map of the local density of states on a MnBi₂Se₄ island. Dark contrast at the boundary of the island reflects in-gap states measured in tunneling spectroscopy.

multilayer van der Waals crystal with septuple-layer (SL) base units in agreement with the trigonal structure. Two distinct terminations of the layered structure are identified on the surface by their distinct atomic contrast and adsorbate decoration. We attribute these to Se- and Bi-terminations based on their separation by fractional SL step heights and their distinct electronic density of states in tunneling spectroscopy. Spatially-resolved spectroscopy across SL step edges reveals gapped behavior on either side, while a variety of sharp, in-gap

states are observed within a $\sim 5\text{nm}$ strip localized to the edge. These studies show that MnBi_2Se_4 is a promising candidate for exploring the rich topological phases of layered antiferromagnetic topological insulators.

Theory of spin-polarized STM into small collections of spin-interacting dopants.

We predict strong, dynamical effects in the dc magnetoresistance of current flowing from a spin-polarized electrical contact through a magnetic dopant in a nonmagnetic host (3, 4). Using the stochastic Liouville formalism we calculate clearly-defined resonances in the dc magnetoresistance when the applied magnetic field matches the exchange interaction with a nearby



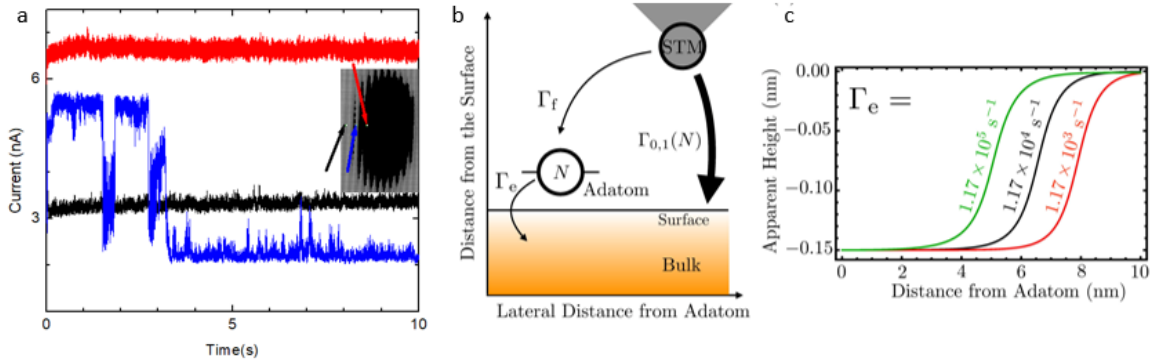
Calculations of Hanle effects in magnetotransport with varying intrinsic (γ_R) and interface defect ($1/\tau_s$) spin relaxation rates. A new regime is discovered (black curve) that provides insight into the relevant spin transport mechanisms.

Calculations of the spin injection efficiency as a function of oblique field. We find that using an oblique field it is possible to efficiently distinguish between spin injection and spin bottleneck effects when identifying the source of a Hanle curve for spin injection (4). This theoretical advance should be very useful to clarify when spin injection has been achieved and when not in a three-terminal Hanle spin injection experiment.

At these resonances spin precession in the applied magnetic field is canceled by spin evolution in the exchange field, preserving a dynamic bottleneck for spin transport through the dopant. Similar features emerge when the dopant spin is coupled to nearby nuclei through the hyperfine interaction. These features provide a precise means of measuring exchange or hyperfine couplings between localized spins near a surface using spin-polarized scanning tunneling microscopy, without any ac electric or magnetic fields, even when the exchange or hyperfine energy is orders of magnitude smaller than the thermal energy. Shown in the Figure are

Tunable surface conductance via control of adatom charge states:

We report scanning tunneling microscopy studies of individual In adatoms on an $\text{InSb}(110)$ surface (5). The adatoms can be reproducibly dropped off from the tip by voltage pulses, and can suppress the surface conductance by 10-100X over a relatively large area ($100 \times 100 \text{nm}^2$). The effect can be broadly tuned by varying imaging conditions such as bias voltage, STM set current and photoillumination and is attributed to tunneling occupation of a (+/0) charge transition level. Theoretical modeling considering competing filling/emptying rates reproduces the observed topography and provides estimates of these rates even when they exceed the experimentally-accessible measurement bandwidth. These studies demonstrate how individual atoms can be used to sensitively control current flow in future nanoscale devices.



a) Switching noise associated with tunneling into and out of an adatom charge transition level. The inset shows an STM image of a ‘crater’ due to the suppression of surface conductance when the level is occupied. b) model indicating competing tunneling channels to/from the adatom and bulk. c) calculated change in apparent height as a function of emptying tunnel rates.

Future Plans

Our overarching plan for this next year is to continue applying experimental tools such as SPSTM and theoretical tools such as spin-dependent two-level transport modeling to the 2DM materials that are now being grown in high quality thin films. Our initial efforts will focus on extending our prior work on individual magnetic impurities to dimers and heterodimers in GaAs and InSb with SPSTM characterization. The goal of these studies is to demonstrate avenues for atomic-scale control of magnetic properties building on prior work by Gupta, and provide a test bed for extending and applying the prior theoretical work by Flatté. For example, the Mn dopant in GaAs is a spin-1 dopant but has strong orbital interactions; we will consider the regime relevant for III-V’s where the spin decoherence rates are comparable to hopping rates to/from spin bottleneck defects. These methods will then be applied to probe magnetism in the existing set of mono/few layer 2DMs (e.g., MnSe_2 , VSe_2 , MnBi_2Se_4) grown on III-V substrates by Kawakami. The next major step in the materials development is to start synthesizing telluride-based 2D magnets including Fe_3GeTe_2 , CrGeTe_3 , and MnBi_2Te_4 , a compatible family with metallic (FGT), semiconducting (CGT) and topological (MBT) states.

References

1. T. Zhu, D. J. O’Hara, B. A. Noesges, M. Zhu, J. J. Repicky, M. R. Brenner, L. J. Brillson, J. Hwang, J. A. Gupta, R. K. Kawakami, Coherent growth and characterization of van der Waals 1T-VSe₂ layers on GaAs(111)B using molecular beam epitaxy. *Phys. Rev. Materials*. **4**, 084002 (2020).
2. T. Zhu, A. J. Bishop, T. Zhou, M. Zhu, D. J. O’Hara, A. A. Baker, S. Cheng, R. C. Walko, J. J. Repicky, J. A. Gupta, C. M. Jozwiak, E. Rotenberg, J. Hwang, I. Žutić, R. K. Kawakami, Magnetic Properties and Electronic Structure of Magnetic Topological Insulator MnBi_2Se_4 *arXiv:2003.07938 [cond-mat]* (2020) (available at <http://arxiv.org/abs/2003.07938>).
3. S. R. McMillan, N. J. Harmon, M. E. Flatté, Image of dynamic local exchange interactions in the dc magnetoresistance of spin-polarized current through a dopant. *arXiv:1907.05509 [cond-mat, physics:quant-ph]* (2019) (available at <http://arxiv.org/abs/1907.05509>).
4. N. J. Harmon, M. E. Flatté, Theory of oblique-field magnetoresistance from spin centers in three-terminal spintronic devices. *arXiv:2008.05623 [cond-mat]* (2020) (available at <http://arxiv.org/abs/2008.05623>).
5. S. M. Mueller, D. Kim, S. R. McMillan, S. J. Tjung, J. J. Repicky, S. Gant, E. Lang, F. Bergmann, K. Werner, E. Chowdhury, A. Asthagiri, M. E. Flatte, J. A. Gupta, Tunable control over InSb(110) surface conductance utilizing charged adatoms. *arXiv:1909.04156 [cond-mat]* (2020) (available at <http://arxiv.org/abs/1909.04156>).

Publications

1. Zhu, Tiancong, Dante J. O'Hara, Brenton A. Noesges, Menglin Zhu, Jacob J. Repicky, Mark R. Brenner, Leonard J. Brillson, Jinwoo Hwang, Jay A. Gupta, and Roland K. Kawakami. "Coherent Growth and Characterization of van Der Waals 1T-VSe₂ Layers on GaAs(111)B Using Molecular Beam Epitaxy." *Physical Review Materials* 4, no. 8 (August 17, 2020): 084002. <https://doi.org/10.1103/PhysRevMaterials.4.084002>.
2. Noesges, Brenton A., Tiancong Zhu, Jacob J. Repicky, Sisheng Yu, Fengyuan Yang, Jay A. Gupta, Roland K. Kawakami, and Leonard J. Brillson. "Chemical Migration and Dipole Formation at van Der Waals Interfaces between Magnetic Transition Metal Chalcogenides and Topological Insulators." *Physical Review Materials* 4, no. 5 (May 8, 2020): 054001. <https://doi.org/10.1103/PhysRevMaterials.4.054001>.
3. Corbett, Joseph P., Tiancong Zhu, Adam S. Ahmed, Steven J. Tjung, Jacob J. Repicky, Takahiro Takeuchi, Jonathan Guerrero-Sanchez, Noboru Takeuchi, Roland K. Kawakami, and Jay A. Gupta. "Determining Surface Terminations and Chirality of Noncentrosymmetric FeGe Thin Films via Scanning Tunneling Microscopy." *ACS Applied Materials & Interfaces* 12, no. 8 (February 26, 2020): 9896–9901. <https://doi.org/10.1021/acsami.9b19724>.
4. Lee, Donghun, and Jay A. Gupta. "Perspectives on Deterministic Control of Quantum Point Defects by Scanned Probes." *Nanophotonics* 8, no. 11 (November 2019): 2033–40. <https://doi.org/10.1515/nanoph-2019-0212>.
5. O'Hara, Dante J., Tiancong Zhu, Amanda H. Trout, Adam S. Ahmed, Yunqiu Kelly Luo, Choong Hee Lee, Mark R. Brenner, et al. "Room Temperature Intrinsic Ferromagnetism in Epitaxial Manganese Selenide Films in the Monolayer Limit." *Nano Letters* 18, no. 5 (May 2018): 3125–31. <https://doi.org/10.1021/acs.nanolett.8b00683>.
6. Zhu, Tiancong, Simranjeet Singh, Jyoti Katoch, Hua Wen, Kirill Belashchenko, Igor Zutic, and Roland K. Kawakami. "Probing Tunneling Spin Injection into Graphene via Bias Dependence." *Physical Review B* 98, no. 5 (August 13, 2018): 054412. <https://doi.org/10.1103/PhysRevB.98.054412>.
7. Katoch, Jyoti, Tiancong Zhu, Denis Kochan, Simranjeet Singh, Jaroslav Fabian, and Roland K. Kawakami. "Transport Spectroscopy of Sublattice-Resolved Resonant Scattering in Hydrogen-Doped Bilayer Graphene." *Physical Review Letters* 121, no. 13 (September 24, 2018): 136801. <https://doi.org/10.1103/PhysRevLett.121.136801>.

Emergent Phenomena in Ferroelectric/van der Waals Heterostructures

Xia Hong, Department of Physics and Astronomy, University of Nebraska-Lincoln

Keywords: ferroelectric domain, 2D van der Waals material, ferroelectric field effect, second harmonic generation, superlattice

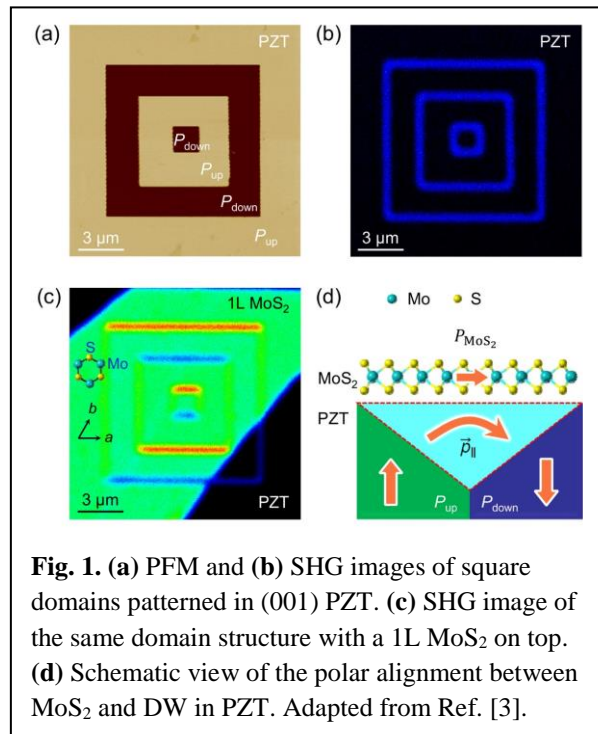
Research Scope

This research explores a range of novel electronic and optical phenomena emerged at the hetero-interfaces between ferroelectrics and two-dimensional (2D) van der Waals (vdW) materials, leveraging the synergy between the constituents facilitated by the ferroelectric polarization and underlying symmetry. The current research projects include: 1) exploring the interfacial polar coupling between ferroelectric domain wall (DW) and monolayer (1L) MoS₂ via nonlinear optics; 2) probing the anisotropic band structure of ReS₂ via ferroelectric domain defined nanoscale conduction path, and 3) realizing one-dimensional (1D) graphene superlattice via periodic domain gating. Our studies can enhance the fundamental understanding of the interfacial coupling mechanisms between ferroelectrics and vdW materials, showcasing ferroelectric domain writing as a powerful tool for designing the functionalities of 2D materials.

Recent Progress

1. Nonlinear Optical Signature of Polar Coupling at Ferroelectric/MoS₂ Heterointerface

Monolayer MoS₂ is non-centrosymmetric and possesses in-plane polar axes. The direct coupling of the polar axes of 1L MoS₂ and ferroelectric PbZr_{0.2}Ti_{0.8}O₃ (PZT) can modify the symmetry of the heterointerface, which can be sensitively detected by the second harmonic generation (SHG) technique [1-3]. Figure 1a shows the piezo-response force microscopy (PFM) image of a series of concentric square domains with alternating polarization up (P_{up}) and down (P_{down}) states written on a 50 nm epitaxial (001) PZT thin film. As it possesses out-of-plane polarization, SHG signal is only detected at the DWs (Fig. 1b) [2,3]. We then transfer a mechanically exfoliated 1L MoS₂ flake on top of the domain structure, with one of the polar axes aligned with the horizontal DWs. As shown in Fig. 1c, the heterostructure exhibits either



strongly enhanced or substantially quenched SHG response at the horizontal DWs, while no appreciable SHG contrast has been observed at the vertical DW. The SHG signal is polarized along the vertical DW direction, even without the presence of an analyzer. Theoretical modeling via density functional theory (DFT) calculations shows that the chiral rotation of the surface dipole at a 180° DW in PZT can produce an in-plane polarization (\vec{p}_{\parallel}) that is comparable with that of MoS₂. The unconventional light filtering effect can thus be attributed to the polar alignment between \vec{p}_{\parallel} at the PZT DW and the polar axis of MoS₂ (Fig. 1d) [3]. For the transmitted SHG signal, in contrast, the SHG tailoring effect is enabled by the out-of-plane polar domain rather than the DW. Our study points to a new strategy for designing nanoscale smart optical applications that can be programmed electrically.

2. Probing the Anisotropic Band of ReS₂ via Nanoscale Ferroelectric Domain Gating

The ferroelectric field effect, when combined with nanoscale domain patterning, is a powerful tool to design local potential profile in a neighboring 2D channel. Exploiting polarization doping through ferroelectric copolymer P(VDF-TrFE), we have examined the anisotropic band structure of layered 2D direct band gap semiconductor ReS₂. The 1T'-ReS₂ exhibits highly anisotropic properties between the lattices orientations of *a*- and *b*- (along the Re-chain) orientations [4]. We have fabricated ReS₂ field effect transistor (FET) devices sandwiched between P(VDF-TrFE) top-gates and SiO₂-backgates. Switching polarization of P(VDF-TrFE) between the uniform P_{up} (depletion) and P_{down} (accumulation) states has led to over five orders of magnitude change in the channel conductivity in 1L ReS₂. We then polarize the entire top-gate to the P_{up} domain, setting the channel to the highly insulating state. By writing nanowires of P_{down} domain

along different crystalline orientations (Fig. 2a), we have created well-defined directional conducting current path, which allows us to map out the transport anisotropy. As shown in Fig. 2b, the sample is more than one order of magnitude more conductive along the Re chain (*b*-axis) than perpendicular to the *b*-axis. The transport anisotropy is clearly shown in the polar plot of normalized channel conductivity taken on four 1L ReS₂ devices (Fig. 2c). Qualitatively similar angular dependence has been observed in the theoretical mobility values of ReS₂ (Fig. 2d), which is calculated based on DFT modeling of the effective mass m^* . Next, we will examine the effect of the ReS₂ layer thickness on the anisotropic transport, and correlate the results with theoretical band structure calculations.

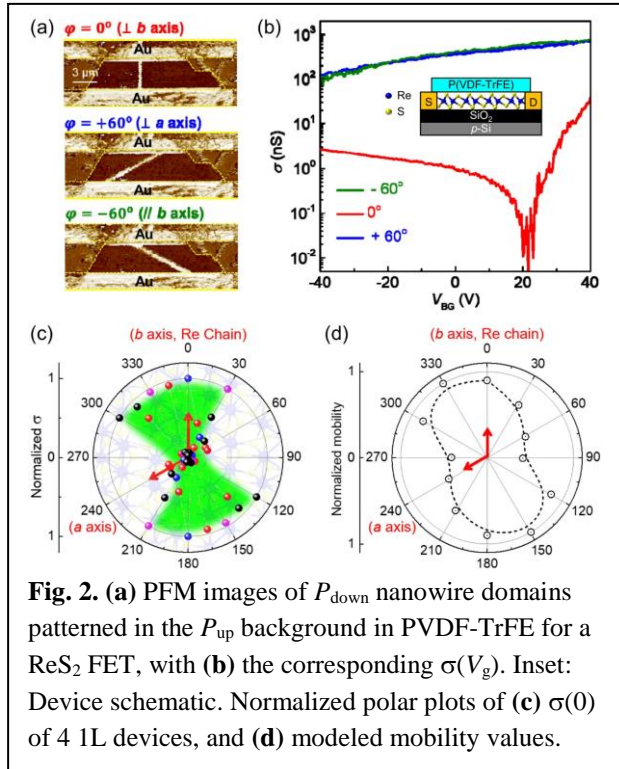


Fig. 2. (a) PFM images of P_{down} nanowire domains patterned in the P_{up} background in PVDF-TrFE for a ReS₂ FET, with (b) the corresponding $\sigma(V_{\text{g}})$. Inset: Device schematic. Normalized polar plots of (c) $\sigma(0)$ of 4 1L devices, and (d) modeled mobility values.

3. Exploring Ferroelectric Domain Imposed 1D Graphene Superlattice

Nanoscale ferroelectric domain g to impose periodic potential modulation in graphene, which can induce additional Dirac points and result in renormalization of electron velocity [5]. As shown in Fig. 3a, we have created an array of 1D stripe domains with 200 nm period (100 nm P_{up} /100 nm P_{down}) on a 50 nm epitaxial (001) PZT film deposited on 10 nm $\text{La}_{0.33}\text{Sr}_{0.67}\text{MnO}_3$ buffered SrTiO_3 substrate between two pre-patterned Au electrodes. A graphene/hBN stack is transferred on top of the domain structure, and fabricated into a top-gated transistor device (Fig. 3b). Upon cooling, the polarization difference between the P_{up} and P_{down} domains can lead a Kronig-Penny-type 1D periodic potential due to the pyroelectric effect, which corresponds a carrier density variation on the order of $3 \times 10^{13} \text{ cm}^{-2}$ in graphene. The 1D superlattice leads to the formation of two additional Dirac bands quasi-symmetrically positioned around the original Dirac point (Fig. 3c). The separation between the extra Dirac points can be further modulated by magnetic field (Fig. 3d). We also observe strong electron-hole asymmetry of the induced Dirac bands. Next we will investigate the effects of period and width ratio of the P_{up}/P_{down} domain on the superlattice band design, and complement the results with theoretical modeling.

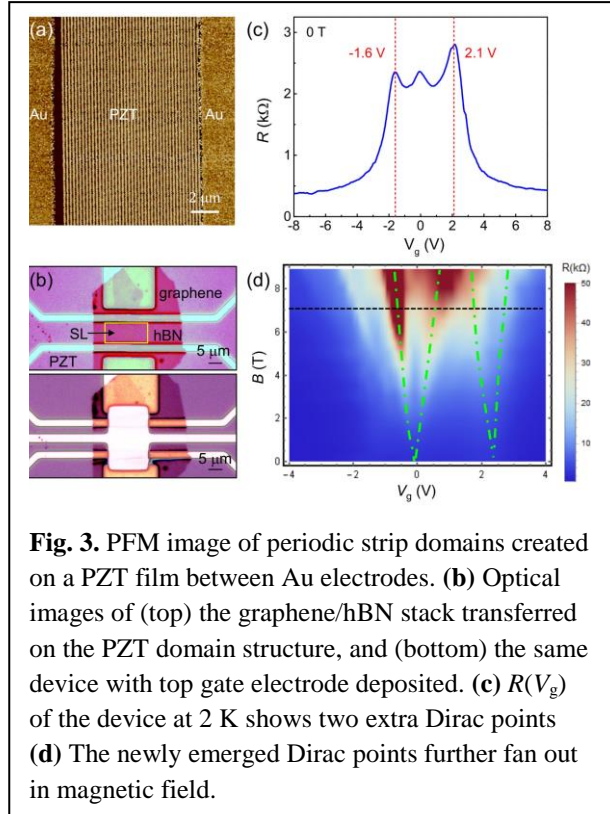


Fig. 3. PFM image of periodic strip domains created on a PZT film between Au electrodes. (b) Optical images of (top) the graphene/hBN stack transferred on the PZT domain structure, and (bottom) the same device with top gate electrode deposited. (c) $R(V_g)$ of the device at 2 K shows two extra Dirac points (d) The newly emerged Dirac points further fan out in magnetic field.

Future Plans

Based on the current progress, we plan to carry out research in the following directions.

1) Carry out systematic studies of the nonlinear optical filtering effect in the transmission mode in PZT/MoS₂ heterostructures, examining the coupling mechanism between the out-of-plane polarization and the SHG signal.

2) Leverage the ferroelectric domain-gating induced nano-constrictions in various vdW materials to explore their band structure and magnetotransport anomalies, and correlate the experimental results with theoretical modeling.

3) Carry out systematic studies of graphene 1D superlattices, examining the effects of superlattice period and P_{up}/P_{down} domain width ratio on the band structure, as well as gaining theoretical insights into the effect of magnetic field.

References

1. D. Li, C. Wei, J. Song, X. Huang, F. Wang, K. Liu, W. Xiong, X. Hong, B. Cui, A. Feng, L. Jiang, and Y. Lu, *Anisotropic Enhancement of Second-Harmonic Generation in Monolayer and Bilayer MoS₂ by Integrating with TiO₂ Nanowires*, Nano Letters **19**, 4195 (2019).
2. S. Cherifi-Hertel, H. Bulou, R. Hertel, G. Taupier, K. D. Dorkenoo, C. Andreas, J. Guyonnet, I. Gaponenko, K. Gallo, and P. Paruch, *Non-Ising and chiral ferroelectric domain walls revealed by nonlinear optical microscopy*, Nature Communications **8**, 15768 (2017).
3. D. Li, X. Huang, Z. Xiao, H. Chen, L. Zhang, Y. Hao, J. Song, D.-F. Shao, E. Y. Tsymbal, Y. Lu, and X. Hong, *Polar Coupling Enabled Nonlinear Optical Filtering at MoS₂/Ferroelectric Heterointerfaces*, Nature Communications **11**, 1422 (2020).
4. L. Hart, S. Dale, S. Hoyer, J. L. Webb, and D. Wolverson, *Rhenium Dichalcogenides: Layered Semiconductors with Two Vertical Orientations*, Nano Letters **16**, 1381 (2016).
5. M. Barbier, P. Vasilopoulos, and F. M. Peeters, *Extra Dirac points in the energy spectrum for superlattices on single-layer graphene*, Physical Review B **81**, 075438 (2010).

Publications

1. H. Ryu, K. Xu, D. Li, X. Hong, and W. Zhu, *Empowering 2D Nanoelectronics via Ferroelectricity*, Applied Physics Letters **117**, 080503 (2020).
2. D. Li, X. Huang, Z. Xiao, H. Chen, L. Zhang, Y. Hao, J. Song, D.-F. Shao, E. Y. Tsymbal, Y. Lu, and X. Hong, *Polar Coupling Enabled Nonlinear Optical Filtering at MoS₂/Ferroelectric Heterointerfaces*, Nature Communications **11**, 1422 (2020).
3. D. Li, C. Wei, J. Song, X. Huang, F. Wang, K. Liu, W. Xiong, X. Hong, B. Cui, A. Feng, L. Jiang, and Y. Lu, *Anisotropic Enhancement of Second-Harmonic Generation in Monolayer and Bilayer MoS₂ by Integrating with TiO₂ Nanowires*, Nano Letters **19**, 4195 (2019).
4. A. Rajapitamahuni, L. L. Tao, Y. Hao, J. Song, X. Xu, E. Y. Tsymbal, and X. Hong, *Ferroelectric Polarization Control of Magnetic Anisotropy in PbZr_{0.2}Ti_{0.8}O₃/La_{0.8}Sr_{0.2}MnO₃ Heterostructures*, Physical Review Materials **3**, 021401(R) (2019).
5. J. Song, Y. Qi, Z. Xiao, K. Wang, D. Li, S.-H. Kim, A. I. Kingon, A. M. Rappe, and X. Hong, *Domain Wall Enabled Hysteresis-Free Steep Slope Switching in MoS₂ Transistors*, arXiv: 1909.00113 (2019).

Sub-picometer precision imaging of 2D materials enabled by deep learning

Pinshane Y. Huang and Bryan K. Clark

University of Illinois at Urbana-Champaign

Keywords: scanning transmission electron microscopy, machine learning, 2D materials

Research Scope

The main goal of this project is to develop and apply a machine learning platform to identify and determine the 3D atomic coordinates of every atom in a 2D material using massive, atomic-resolution electron microscopy datasets. This approach will create new characterization methods to understand the atomic-scale point defects that lead to room temperature quantum emission in 2D materials and the relationships between growth parameters, point defects, and the optical and electronic properties of 2D transition metal dichalcogenides.

Recent Progress

A key challenge in characterizing 2D materials is determining the structure of defects with picometer precision. Defect and strain engineering of 2D materials are emerging tools to tune the optical and electronic properties of atomically thin layers^{1,2}. Yet, while techniques such as aberration-corrected scanning transmission electron microscopy (STEM) have the spatial resolution to image each atom in 2D materials, the precision of atom-by-atom electron microscopy has so far been limited to the scale of 8-20 picometers, or strains on the order of 3% or more. This precision is fundamentally limited by the signal-to-noise ratio (SNR): high radiation doses are required to precisely measure the position of single atoms, yet ionization and knock-on damage alter the structure of defects at high electron dose for 2D materials, severely limiting the achievable SNR.

We applied machine learning to locate and classify each point defect in large datasets of atomic-resolution images acquired via aberration-corrected annular dark-field (ADF) STEM images (Figure 1a-e), then used the resulting data to generate class-averaged images of single-atom defects in 2D materials. (Figure 1f-i) This method enables sub-picometer precision measurements of beam-sensitive structures because it combines information measured from large numbers of nominally identical defects while limiting the dose to any individual atom.

To analyze the data, we trained a deep learning model based on fully convolutional networks (FCNs) with ResUNet architecture to locate and classify the point defects in $WSe_{2-2x}Te_{2x}$, producing 2D maps of the defect positions. Neural networks have recently been applied to identify atomic defects in atomic-resolution (S)TEM images because they make it possible to efficiently locate large numbers of defects while minimizing human intervention^{3,4}. We trained FCNs using

simulated data generated via incoherent image simulations. In order to make our simulations more realistic, we apply a set of post-processing steps to the images, including the addition of Gaussian noise, probe jittering, image shear, and varying spatial sampling, to create

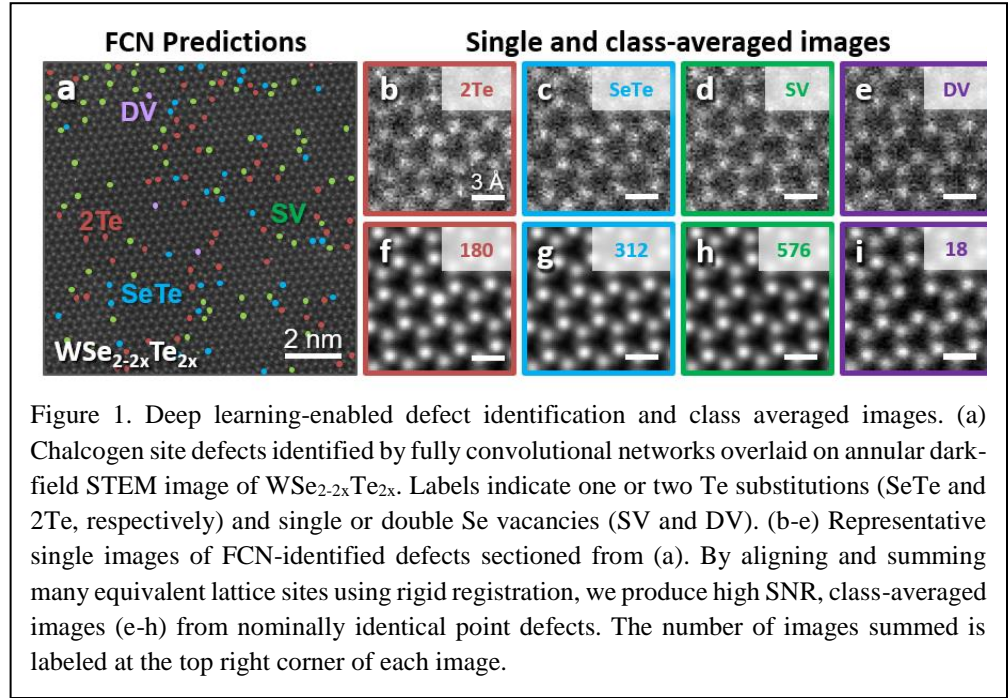


Figure 1. Deep learning-enabled defect identification and class averaged images. (a) Chalcogen site defects identified by fully convolutional networks overlaid on annular dark-field STEM image of $WSe_{2-2x}Te_{2x}$. Labels indicate one or two Te substitutions (SeTe and 2Te, respectively) and single or double Se vacancies (SV and DV). (b-e) Representative single images of FCN-identified defects sectioned from (a). By aligning and summing many equivalent lattice sites using rigid registration, we produce high SNR, class-averaged images (e-h) from nominally identical point defects. The number of images summed is labeled at the top right corner of each image.

our final training data. While similar methods are well-established in the literature, this was not sufficient for training; the FCN could distinguish between the simulated and real images leading to a lack of transferability in the training. To overcome this, we found by introducing low-frequency contrast variations in the simulated data to emulate surface contamination, we achieved the highest classification precision of the neural networks on experimental data.

We focused on the four primary types of chalcogen-site defects present in our samples, which we refer to as 2Te, SeTe, SV, and DV. Our naming convention describes the composition and filling of the chalcogen sites in $WSe_{2-2x}Te_{2x}$. In projection, the chalcogen columns can contain either two Se atoms (no defects, 2Se), one or two Te substitutions (SeTe and 2Te), or one or two Se vacancies (SV and DV). The accuracy (i.e. average of the true and false positivity rates) in identification of defects was higher than 99.7% for all four types of defects. Out of the thousands of defects identified via the FCN, we selected only isolated defects separated by 6.6 angstroms or more from any other defects. This step allowed us to study the structure of the defects with minimal external perturbations. These high SNR images allow us to measure 2D atomic coordinates of a single-atom defect with up to 0.3 pm precision, a 20-fold improvement when compared with the 6 pm precision of the original images

Finally, we measure the displacement and strain fields for each defect type (strain fields for a single Se vacancy are shown in Figure 2). To visualize the local distortions, we calculate the 2D strain components ϵ_{xx} , ϵ_{yy} , and the dilation ($\epsilon_{xx} + \epsilon_{yy}$) as shown in Figure 2a-c. We next compare these experimental strain fields to those calculated by elastic continuum theory using the 2D version of Eshelby's inclusion model (Figure 2d-f). We obtained excellent agreement with the strain fields extracted from relaxed defect structures calculated by first-principle simulations using density

functional theory (DFT). The key finding is that radially oscillating strain fields are observed in experiment and density functional theory predictions (Figure 2g-i) but were absent in the elastic model. We attribute the presence of these radially oscillating strain fields to a combination of defect-induced charge redistribution and Coulomb interactions between charge perturbations at the defect site.

In conclusion, we have developed techniques based on machine learning and aberration-corrected STEM to visualize the strain fields induced by single-atom defects in 2D materials. We used these methods to directly observe the strain fields of vacancies and substitutions in $WSe_{2-2x}Te_{2x}$, where the sub-pm precision enabled by class averaging revealed oscillations in the strain field around chalcogen vacancies that deviate from isotropic elastic continuum theory but agree well with DFT simulations. We show that deep learning enables the first direct imaging of radial strain field oscillations around vacancies, a phenomenon originally predicted in the mid-1950s⁵ but never experimentally imaged. A key advantage of these methods is that they enable high precision measurements of beam-sensitive materials by leveraging computer vision to mine atomic-resolution datasets without requiring any changes in instrumentation. These methods should be particularly useful for studying 2D materials and other radiation-sensitive crystals and elucidating the complex strain phenomena that arise from structural rearrangements and defect-defect interactions.

Future Plans

Future Plans

In the next phase of our work, we will extend our machine learning methods on two main fronts. First, we will extend the flexibility and speed of our neural network training procedures and apply our machine-learning enabled class averaging methods to other dose-sensitive materials systems, including a broader range of 2D materials and molecules on graphene. Second, we will utilize our methods to interpret large atomic resolution datasets with the goal of identifying the

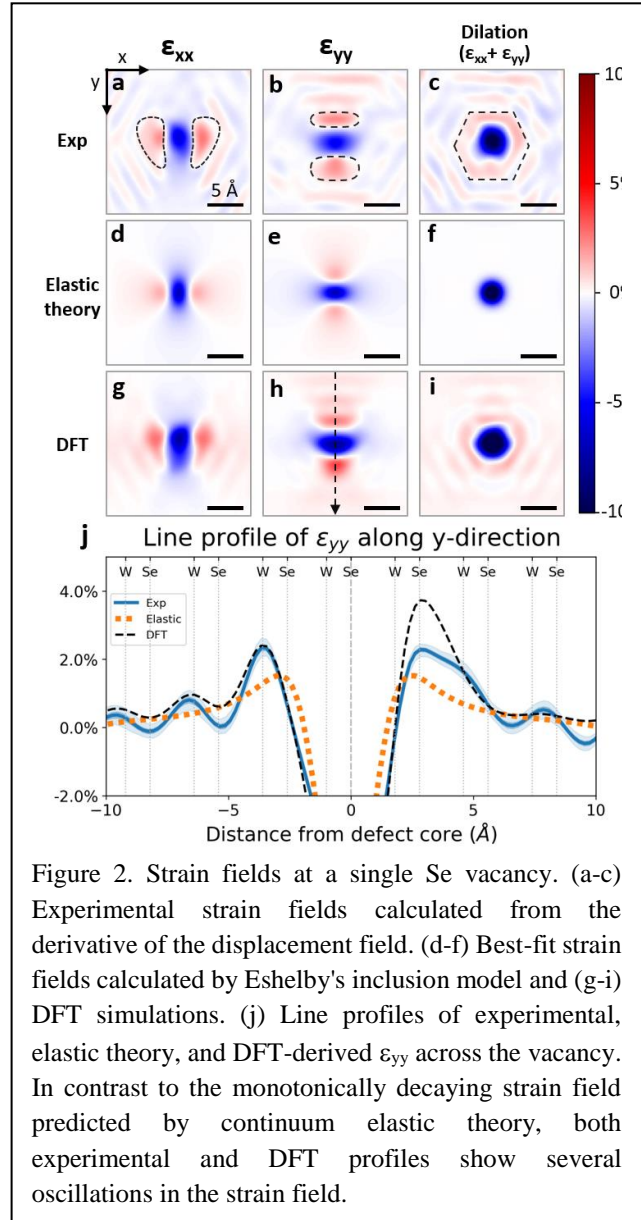


Figure 2. Strain fields at a single Se vacancy. (a-c) Experimental strain fields calculated from the derivative of the displacement field. (d-f) Best-fit strain fields calculated by Eshelby's inclusion model and (g-i) DFT simulations. (j) Line profiles of experimental, elastic theory, and DFT-derived ϵ_{yy} across the vacancy. In contrast to the monotonically decaying strain field predicted by continuum elastic theory, both experimental and DFT profiles show several oscillations in the strain field.

defects that produce quantum emission in 2D materials. These defects are a promising platform for quantum computing but are too rare and diverse to conclusively identify using current methods.

References

1. Z. Lin, McCreary A., Briggs N., Carvalho B. R., Kahn E., Lv R., Rao R., Terrones H., Pimenta M. A. & Terrones M. *Defect engineering of two-dimensional transition metal dichalcogenides*. 2D Materials **3**, 022002-022002 (2016).
2. J. Feng, Qian X., Huang C. W. & Li J. *Strain-engineered artificial atom as a broad-spectrum solar energy funnel*. Nature Photonics **6**, 866-872 (2012).
3. M. Ziatdinov, Dyck O., Maksov A., Li X., Sang X., Xiao K., Unocic R. R., Vasudevan R., Jesse S. & Kalinin S. V. *Deep Learning of Atomically Resolved Scanning Transmission Electron Microscopy Images: Chemical Identification and Tracking Local Transformations*. ACS Nano **11**, 12742-12752 (2017).
4. J. Madsen, Liu P., Kling J., Wagner J. B., Hansen T. W., Winther O. & Schiøtz J. *A deep learning approach to identify local structures in atomic-resolution transmission electron microscopy images*. Advanced Theory and Simulation **1**, 1800037-1800037 (2018).
5. H. Kanzaki. *Point Defects in Face-Centred Distortion Cubic Lattice-Distortion around Defects*. Journal of Physics and Chemistry of Solids **2**, 24-36 (1957).

Publications

1. C.-H. Lee, A. Khan, D. Luo, T. P. Santos, C. Shi, B. E. Janicek, S. Kang, W. Zhu, N. A. Sobh, A. Schleife, B. K. Clark, and P. Y. Huang, *Deep Learning Enabled Strain Mapping of Single-Atom Defects in 2D Transition Metal Dichalcogenides with Sub-picometer Precision* Nano Letters **20** 3369-3377 (2020).

Mesoscopic Imaging of Electronic Landscape in Complex Materials

PI: Keji Lai (kejilai@physics.utexas.edu)

Department of Physics, University of Texas at Austin, Austin, TX 78712

Keywords: Electron correlation, microwave microscopy, phase coexistence, 2D semiconductors, Moiré superlattice

Research Scope

The goal of this DOE program is to probe the mesoscopic electronic inhomogeneity in complex materials under cryogenic temperatures, high magnetic fields, and various electrical gating methods. Specifically, we utilize the microwave impedance microscope (MIM)¹, a novel technique capable of resolving nanoscale dielectric and conductivity information, to study bulk crystals and thin films of strongly correlated oxides and 2D semiconductor heterostructures. The work is significant in that it directly addresses the nanoscale electrical homogeneity in metal-insulator transitions (MITs) and other exotic phenomena. The research will ultimately facilitate the applications of advanced quantum materials in energy-related science and technology.

Recent Progress

In the past two years, our team has obtained exciting results in strongly correlated $\text{Ca}_3\text{Ru}_2\text{O}_7$, WS_2/WSe_2 moiré superlattices, solid-electrolyte gated MoS_2 transistors, and atomically thin Bi_2SeO_5 dielectrics. Details of the accomplishments are as follows.

Visualization of Competing Stripe Phase in Ti-doped $\text{Ca}_3\text{Ru}_2\text{O}_7$

As a prototypical strongly correlated electron system, the bilayer $\text{Ca}_3\text{Ru}_2\text{O}_7$ with Ti doping can exhibit G-type antiferromagnetic (AFM) Mott insulator, A-type AFM metal, and paramagnetic metal (PM-M) phases², making it an ideal testbed to explore the correlation physics in complex oxides. A major effort of this DOE program is to investigate the nature of mesoscopic phase separation, which is widely observed in $3d$ correlated materials such as manganites but less studied in $4d$ electrons such as ruthenates.

In this work, we studied $\text{Ca}_3(\text{Ru}_{0.9}\text{Ti}_{0.1})_2\text{O}_7$ single crystals by both macroscopic transport and mesoscopic MIM experiments. In the cryogenic chamber with high magnetic field (Fig. 1a), the 1 GHz signal is delivered to a tungsten tip glued to a quartz tuning fork (TF). The demodulated MIM signals provide a measure of the local conductivity with ~ 100 nm spatial resolution. As seen in Fig. 1b, when $T < T_{\text{MIT}} \sim 114$ K, the sample was mostly in the insulating state (phase I or G-AFM-I), with some ribbon-like conductive areas along the high-symmetry $[110]$ and $[1-10]$ directions (phase II, lower Ti-doping). Starting from 114.04 K, metallic stripes (phase III, A-AFM) oriented along the a -axis of the crystal were observed, whose length and areal density grew rapidly

with increasing T at 0.1 K steps. At 114.72 K, another metallic phase (phase IV, PM-M) set in, which quickly swept through the scanned area with an additional ~ 0.3 K. The observation of an additional phase distinct from the two terminal phases of a Mott transition in strongly correlated materials highlights the complexity in $4d$ -ruthenates. The mesoscopic MIM imaging also allows us to divide the magnetotransport curves (e.g. at 112.6 K, Fig. 1c) into four sections due to the coexisting phases. Together with the magnetization and transport data, we can now construct a new phase diagram for $\text{Ca}_3(\text{Ru}_{0.9}\text{Ti}_{0.1})_2\text{O}_7$ that includes the nanoscale phase separation. Our work provides a model approach to correlate the macroscopic properties and mesoscopic phase separation in complex oxide materials.

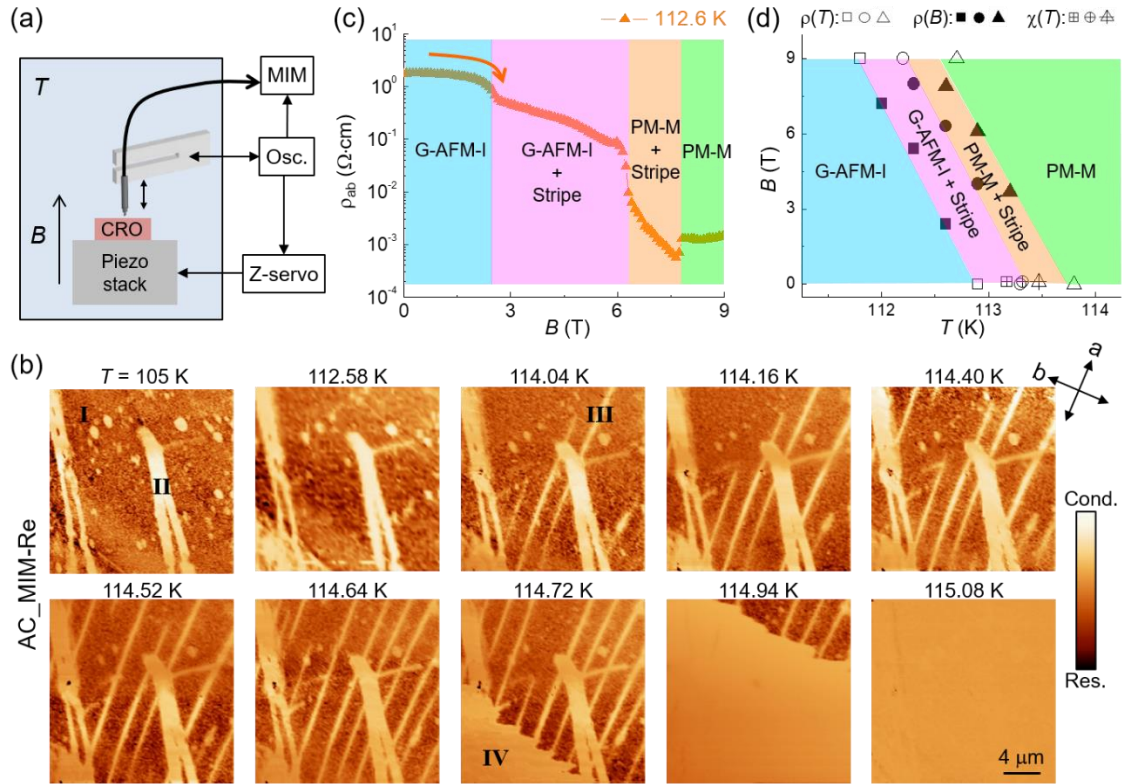


Figure 1. (a) Schematic of the tuning-fork-based cryogenic MIM setup. (b) AC_MIM-Re images at various temperatures across the transition. Phases I to IV are labeled in the images. The crystalline axes (a and b) are indicated in the top right corner. All images are $20 \mu\text{m} \times 20 \mu\text{m}$. (c) Magnetotransport curve at $T = 112.6$ K divided into four sections based on sudden changes of the signals. (d) Phase diagram including the phase separation.

Imaging Correlated Electronic States in WSe_2/WS_2 Moiré Superlattices

The vertical stacking of 2D transition metal dichalcogenide (TMD) materials with similar lattice constants at small twist angles produces long-wavelength moiré superlattices, giving rise to an ideal playground to simulate the Mott-Hubbard physics in 2D triangular lattices³. Despite the rapid progress in the research of TMD-based correlated states, a critically missing element is the real-space visualization of a highly resistive electronic phase in the heterostructure and the study of its spatial homogeneity, which is the main subject of our investigation here.

The samples in our study are WSe₂/WS₂ hetero bilayers encapsulated by top and bottom hexagonal boron nitride (hBN) dielectrics. Fig. 2a displays the sample topography at 24 K, where some surface impurities or air bubbles are clearly visible. The simultaneously acquired MIM-Im image at $V_{bg} = 0$ V (Fig. 2b) shows that only the contact and top-gate few-layer graphene regions are conductive. Strikingly, while the individual TMD layers and the heterostructure (HS) region are highly insulating at zero V_{bg} , they exhibit very different gate dependences. As seen in the inset of Fig. 2b, monolayer WSe₂ is conductive at $V_{bg} = -2$ V due to the hole doping, whereas the HS region is strongly insulating. Fig. 2c shows the MIM-Im response on three points in Fig. 2a when V_{bg} is swept from -2.7 to 2.7 V. The ambipolar FET behavior is observed in both monolayers. In the HS region, on the other hand, two prominent drops of MIM-Im signals appear at around $V_{bg} \sim -2.1$ V and $+1.8$ V, corresponding to a filling factor $n/n_0 = -1$ and $+1$, i.e. one hole/electron per moiré unit cell, respectively. The Mott states persist up to ~ 150 K and eventually vanish at 295 K. A rough estimate of the thermal activation gap of the Mott state is thus $10 \sim 20$ meV. In all, the ability to probe local conductivity in buried structures allows us to observe the Mott insulating phases with both hole and electron doping at temperatures up to 150 K, providing a guideline for improving the material quality towards novel electronic states in 2D moiré systems.

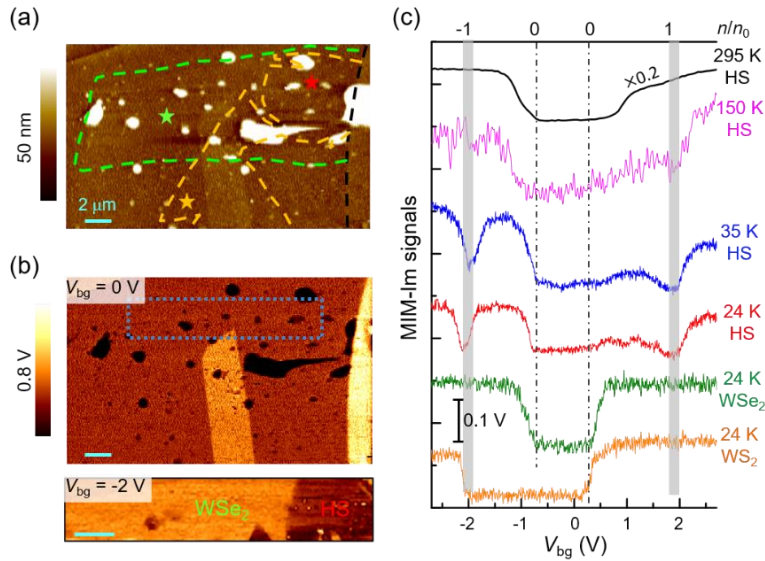


Figure 2. (a) Topographic image of the WSe₂/WS₂ device. The WSe₂, WS₂, and top few-layer graphene regions are labeled by green, orange, and black dashed lines, respectively. (b) MIM image at $T = 24$ K and $V_{bg} = 0$ V. Inset: MIM-Im images in the blue dashed box in (b) taken at $V_{bg} = -2$ V. Scale bars are $2 \mu\text{m}$. (c) MIM-Im signals at various locations and temperature. The dash-dotted lines denote the charge-neutral points. The shaded areas correspond to the Mott insulating states at $n/n_0 = \pm 1$.

Solid Electrolyte Gating and Ultrathin 2D Dielectrics

Electrostatic gating of 2D materials with electrolytes leads to the accumulation of very high surface charge carrier densities. In our work, a lithium-ion solid electrolyte substrate⁴ is used for n-type MoS₂ transistors (Fig. 3a). Fig. 3b shows the MIM images as a function of the gate voltage V_{BG} . Below the threshold voltage, there is little contrast between MoS₂ and the substrate, indicating that the channel is highly resistive. As V_{BG} gradually increases, charge carriers start to appear near the two electrodes and continue to extend towards the center. Interestingly, during the whole process when the transistor turns on, the MoS₂ channel is uniformly conductive. Our results indicate a smooth interface between the 2D material and underlying electrolytic substrate.

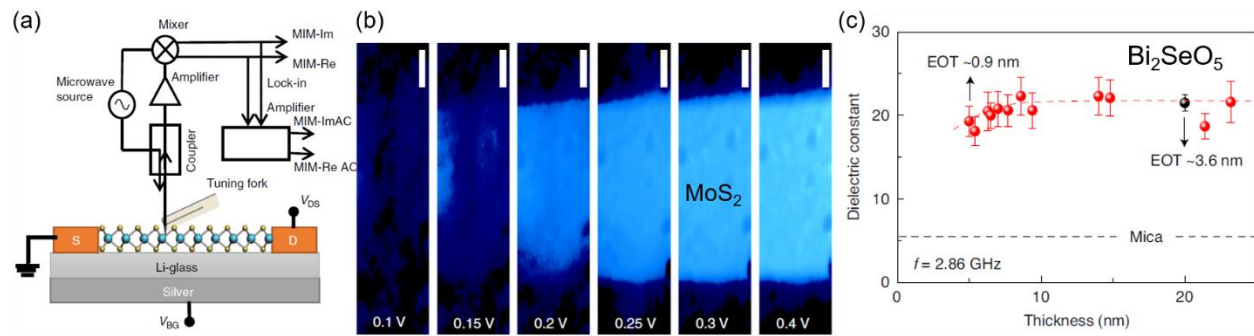


Figure 3. (a) Schematic diagram of the Li-glass-gated MoS₂ device and the tuning-fork-based MIM setup. (b) MIM conductance map in a section of the MoS₂ channel at different gate voltages. All scale bars are 500 nm. (c) Thickness-dependent dielectric constant of Bi₂SeO₅ at 2.86 GHz measured by MIM.

Using the TF-based MIM, we have also studied atomically thin Bi₂SeO₅ dielectrics formed by oxidizing the underlying 2D semiconducting Bi₂O₂Se⁵. As shown in Fig. 3c, we quantitatively measured the high dielectric constant ($\epsilon_r \sim 21$) of Bi₂SeO₅, which allows the reduction of equivalent oxide thickness (EOT) to as small as 0.9 nm while maintaining low gate leakage. The combination of a high-mobility 2D semiconductor and its high- κ oxide makes Bi₂O₂Se/Bi₂SeO₅ a very competitive candidate for next-generation electronics beyond Si/SiO₂.

Future Plans

We will continue to work on the ruthenate single-crystal samples. For instance, multiple A-type AFM phases are expected in 3% and 5% Ti-doped Ca₃Ru₂O₇ crystals, while the phase separation has not been studied. In addition to Ti doping, we will also look at the magnetically doped (Mn or Fe) samples, where the B -field dependence of the stripe phases may be different from the non-magnetic counterparts. We will also study the moiré superlattice of WS₂/WSe₂ heterostructures at lower temperatures and high B -fields. Secondly, it is clear that the study of Mott transition in 2D materials has greatly extended the realm of strongly correlated systems. We aim to investigate the local inhomogeneity in these materials and compare the microscopic evolution when controlling temperature, magnetic field, and electric field. We expect to continue with exciting discoveries through the unique MIM measurements.

References

1. Z. Chu, L. Zheng, and K. Lai, "Microwave Microscopy and Its Applications", *Annu. Rev. Mater. Res.* **50**, 105 (2020).
2. X. Ke, J. Peng, D. J. Singh, Tao Hong, Wei Tian, C. R. Dela Cruz, and Z. Q. Mao, "Emergent electronic and magnetic state in Ca₃Ru₂O₇ induced by Ti doping", *Phys. Rev. B* **84**, 201102(R) (2011).
3. F. Wu, T. Lovorn, E. Tutuc, A. H. MacDonald, "Hubbard Model Physics in Transition Metal Dichalcogenide Moiré Bands", *Phys. Rev. Lett.* **121**, 026402 (2018).
4. M. Philippi, I. Gutiérrez-Lezama, N. Ubrig, A.F. Morpurgo, "Lithium-ion conducting glass ceramics for electrostatic gating", *Appl. Phys. Lett.* **113**, 033502 (2018).
5. J.X. Wu *et al.* "High electron mobility and quantum oscillations in non-encapsulated ultrathin semiconducting Bi₂O₂Se", *Nature Nanotechnol.* **12**, 530 (2017).

Publications

1. D. Wu, W. Li, A. Rai, X. Wu, H. C.P. Movva, M. N. Yogeesh, Z. Chu, S. K. Banerjee, D. Akinwande, and K. Lai, “Visualization of Local Conductance in MoS₂-WSe₂ Heterostructure Transistors”, *Nano Lett.* **19**, 1976 (2019).
2. A. Gangshettiwar, Y. Zhu, Z. Jiang, J. Peng, Y. Wang, J. He, J. Zhou, Z. Mao, and K. Lai, “Emergence of a competing stripe phase near the Mott transition in Ti-doped bilayer calcium ruthenates”, *Phys. Rev. B* **101**, 201106(R) (2020).
3. Md H. Alam, Z. Xu, S. Chowdhury, Z. Jiang, D. Taneja, S. K. Banerjee, K. Lai, M. H. Braga, and D. Akinwande, “Lithium-ion electrolytic substrates for sub-1V high-performance transition metal dichalcogenide transistors and amplifiers”, *Nature Commun.* **11**, 3203 (2020).
4. Z. Chu, L. Zheng, and K. Lai, “Microwave Microscopy and Its Applications”, *Annu. Rev. Mater. Res.* **50**, 105 (2020).
5. T. Li, T. Tu, Y. Sun, H. Fu, J. Yu, L. Xing, Z. Wang, H. Wang, R. Jia, J. Wu, C. Tan, Y. Liang, Y. Zhang, C. Zhang, Y. Dai, C. Qiu, M. Li, R. Huang, L. Jiao, K. Lai, B. Yan, P. Gao, and H. Peng, “A native oxide high-k gate dielectric for two-dimensional electronics”, *Nature Electron.* **3**, 473 (2020).
6. T. Tu, Y. Zhang, T. Li, J. Yu, L. Liu, J. Wu, C. Tan, J. Tang, Y. Liang, C. Zhang, Y. Dai, Y. Han, K. Lai, and H. Peng, “Uniform high-k amorphous native oxide synthesized by oxygen plasma for top-gated transistors”, *Nano Lett.* (2020) ASAP <https://pubs.acs.org/doi/10.1021/acs.nanolett.0c02951>
7. Z. Chu, E. C. Regan, X. Ma, D. Wang, Z. Xu, M. I. B. Utama, K. Yumigeta, M. Blei, K. Watanabe, T. Taniguchi, S. Tongay, F. Wang, and K. Lai, “Nanoscale Conductivity Imaging of Correlated Electronic States in WSe₂/WS₂ Moiré Superlattices”, <https://arxiv.org/abs/2007.06469>, under review with *Phys. Rev. Lett.*

Nematic transitions in iron pnictide superconductors imaged with a quantum gas

Benjamin Lev, Stanford University

Keywords: magnetometer, BEC, nematic, pnictide superconductor

Research Scope

With DOE funding, the Lev group has recently developed the SQCRAMscope (Scanning Quantum Cryogenic Atom Microscope), a novel quantum sensor that uses an ultracold quantum gas as a micron-resolution magnetometer. It is capable of imaging DC transport in both room-temperature and cryogenically cooled quantum materials with unprecedented sensitivity. Lev's group is working to improve the capabilities of the SQCRAMscope, especially the temperature range and AC sensitivity.

We have already improved the temperature range of the SQCRAMscope. This is the result of a major upgrade we performed this reporting period. We replaced the existing helium flow cryostat, which was a LHe hog, with a cryogen-free, closed-cycle pulse tube cryostat we designed with ColdEdge. The new cryostat is vibration isolated from the atom chip and sample, and we have measured vibrations to be < 100 -nm RMS, smaller than our resolution. The new system is augmented with a heat shield and improved sample mounting for more robust installation. We have established that our new system allows us to cool the sample from 300 K to 5.7 K. This is an improvement from the minimum temperature of 35 K achieved with the previous system. Additionally, we have procured and tested a lens system that will improve our imaging resolution by at least a factor of 2, from 2 μm to 1 μm and below.

We have also achieved the dispersive imaging of the BEC near the sample surface using a novel technique. Usually dispersive (i.e., nondestructive imaging) requires that a central portion of the imaging light pass through a π phase plate to ensure that the phase of the light is what is recorded by the CCD. We were able to eliminate this optical element by using the fact that the surface of the sample reflects part of the imaging light onto the atoms, which sets up an interference pattern due to the phase shift between this field and the direct field impinging upon the atoms. By placing the atoms at optimal parts of this interference pattern, we can perform phase contrast (i.e., dispersive) imaging without a phase plate. This constitutes an important step toward realizing the goal of AC scanning probe magnetometry by rapidly imaging the gas many times non-destructively.

Recent Progress

Our most recent achievement is the scientific use of the SQCRAMscope for imaging the nematic transition in an iron pnictide superconductor; see Fig. 1. The paper, published this year in Nature Physics [2], details the first direct use of a quantum gas as an experimental probe of quantum materials.

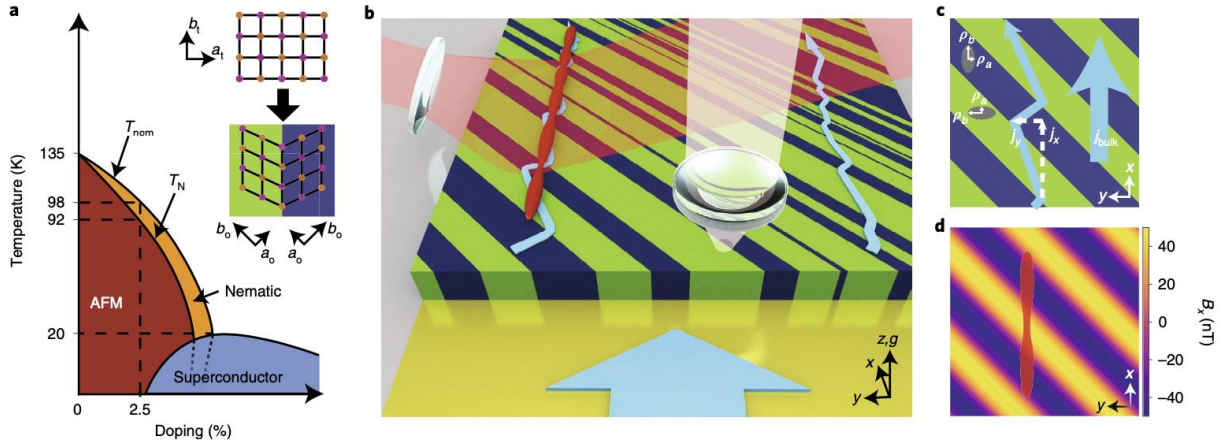


Fig 1. Multimodal SQCRAMscope. **a**, Schematic phase diagram of the iron superconductor we studied, $\text{Ba}(\text{Fe}_{1-x}\text{Co}_x)_2\text{As}_2$. In the high-temperature phase (white), the material is a metal with a tetragonal crystal structure. At the phase boundary, T_{nem} , the material undergoes a transition to a nematic state (orange) that breaks four-fold rotational symmetry while preserving lattice translational symmetry. At the lower-temperature phase boundary, T_N (Néel temperature), the material becomes a stripe-like antiferromagnet (AFM, crimson). A dome of superconductivity (blue) intersects the nematic transition line near its maximum critical temperature. Inset: schematic of the crystal structure of BaFe_2As_2 above and below the structural transition. Shown is the a - b plane of iron (brown) and arsenic (pink), with the tetragonal (subscript ‘t’) and orthorhombic (subscript ‘o’) crystal axes labelled. Blue and green show the formed domains. **b**, A quasi-one-dimensional BEC (red) is magnetically confined $2\ \mu\text{m}$ from the surface of the pnictide sample using an atom-chip trap (not shown). The crystal forms domains with anisotropic resistivity on cooling (blue and green stripes). Consequently, a homogeneous injection of electric current (cyan arrows) into these domains flows in a zigzag fashion from one gold contact (bottom) to the other (not shown). The density of the BEC is imaged with a high-numerical-aperture lens (left) by absorption imaging of a resonant laser (transparent red). The density modulation is proportional to the local magnetic field along x , generated by the inhomogeneous current in the sample. Vertical optical imaging through a second lens (right of centre) using polarized light (transparent white) measures the near-surface birefringence of the crystal. The penetration depth of the imaging light is of the order of $30\ \text{nm}$, much shorter than the $\sim 20\ \mu\text{m}$ -thick sample. The g label on the z axis indicates the direction of gravity. **c**, In the orthorhombic phase, domains form with one of two crystal axis orientations (blue and green). These domains have $\rho_a < \rho_b$ (grey ellipses). When crossing a domain wall, the principal axes of the resistivity tensor interchange. As a result, an average j_{bulk} (large cyan arrow), sent through the crystal in x , bends towards $\pm y$ at each domain boundary, forming a zigzag pattern (thin cyan arrow). **d**, Simulation of the x component of the magnetic field produced by the current shown in **c**. The BEC density (red) changes according to the sign and magnitude of j_y . From [2].

Not only is this a significant advance in the experimental state-of-the-art, but the resultant observations reveal important insights into nematicity in iron-based superconductors. The SQCRAMscope is a quantum-noise-limited scanning-probe magnetometer that leverages the techniques of ultracold atomic physics to image magnetism and electronic transport in solid-state materials. By employing a magnetically levitated atomic Bose-Einstein condensate (BEC) that can be scanned within microns of the surface of a material, the microscope makes 2D spatially resolved measurements of magnetic fields and electronic transport currents with unprecedented sensitivity. While the SQCRAMscope's operation has previously been demonstrated using gold test samples [1], it had not yet been used to study complex quantum materials.

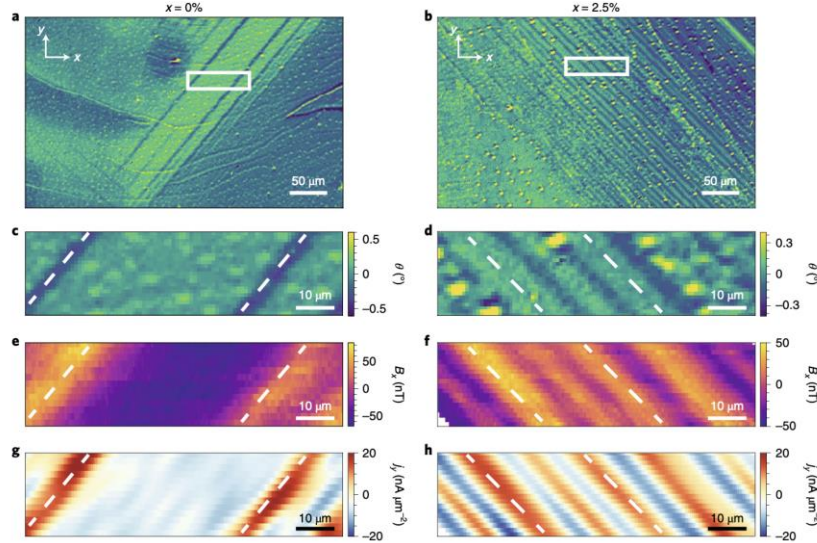


Fig. 2: Optical birefringence, magnetometry and transport images. **a,b**, Typical optical birefringence images of the parent compound BaFe_2As_2 at 92.5 K **(a)** and 2.5% cobalt-doped $\text{Ba}(\text{Fe}_{1-x}\text{Co}_x)_2\text{As}_2$ at 81 K **(b)**. The x and y axes are aligned with the orthorhombic crystal axes. Alternating stripes in birefringence mark the location of nematic domains. A large spatial variation of domain visibility, size and orientation is observed in both samples. The spatial distribution of domains does not change appreciably with thermal cycling, suggesting that they are weakly pinned by local strain introduced during the crystal growth or sample preparation and mounting. **c,d**, Optical birefringence maps of typical SQCRAMscope scans taken in the regions marked by white boxes in **a,b** for the $x = 0\%$ **(c)** and $x = 2.5\%$ **(d)** sample. **e,f**, Magnetometry scans for the $x = 0\%$ **(e)** and $x = 2.5\%$ **(f)** sample. **g,h**, Reconstructed current densities for the $x = 0\%$ **(g)** and $x = 2.5\%$ **(h)** sample. Dashed lines in **c,d** mark the center of two negative θ domains in **c** and two positive domains in **d**; the lines are overlaid at the same positions in the magnetometry and transport images as guides to the eye. From [2].

In this work, we used the SQCRAMscope to study nematicity in iron pnictides. Nematicity, or the breaking of crystal rotational symmetry, has been intensely studied in these materials due to its proximity to high-temperature superconductivity and putative quantum criticality. Several factors confound the experimental study of these materials. The first is a classic chicken and egg problem: if both the lattice and electrons break rotational symmetry at the same temperature, which are driving and which come along for the ride? To address this question in iron pnictides, and other nematic materials, we augmented the SQCRAMscope with an in situ microscope that measures optical birefringence at the surface. Combined with the SQCRAMscope's innate sensitivity to electronic nematicity through imaging transport currents, this enables simultaneous and spatially resolved detection of both bulk and surface manifestations of nematicity via transport and structural deformation channels, respectively.

Another confounding factor is that nematic materials can break rotational symmetry in one of two energetically degenerate ways. Consequently, any probe that averages over a sample volume larger than the characteristic domain size will not accurately measure the behavior of a single domain. Previous bulk measurements investigations of nematicity have required the application of a large strain to coerce the crystal into a single domain, limiting the inferences that

can be drawn about the strain-free material. We overcome this by imaging bulk transport locally within domains of a nominally unstrained sample using our new SQCRAMscope technique; see Fig. 2.

In addition to the significant technical advances noted above, our work also sheds light on an open question of intense current debate. While bulk scattering and thermodynamic probes detect a single nematic transition at a temperature T_{Nem} , a number of probes are reported as detecting nematicity several tens of kelvin higher in temperature. Using the SQCRAMscope's multimodal imaging capability, we performed local measurements of emergent resistivity anisotropy in iron pnictides and observed sharp, nearly concurrent transport and structural transitions. More broadly, these measurements demonstrated the SQCRAMscope's ability to reveal important insights into the physics of complex quantum materials.

Future Plans

We will implement AC magnetometry imaging capabilities up to a few hundred Hz bandwidth with $\text{nT/Hz}^{1/2}$ sensitivity. We have already performed extensive numerical calculations that predict this bandwidth and sensitivity are achievable with spatially resolved AC Ramsey magnetometry using our Rb quasi-1D BEC. We are currently setting up the apparatus to test this scheme; this was delayed by the COVID shutdowns. Also, we are developing the capability to image circular photogalvanic effects in various materials.

References

1. F. Yang, A. Kollár, S. Taylor, R. Turner, & B. Lev, *Scanning Quantum Cryogenic Atom Microscope*, Phys. Rev. Appl. **7**, 034026 (2017).
2. F. Yang, S. Taylor, S. Edkins, J. Palmstrom, I. Fisher, and B. Lev, *Nematic Transitions in Iron-Pnictide Superconductors Imaged with a Quantum Gas*, Nature Physics **16**, 514 (2020).

Publications

1. F. Yang, S. Taylor, S. Edkins, J. Palmstrom, I. Fisher, and B. L. Lev, *Nematic Transitions in Iron-Pnictide Superconductors Imaged with a Quantum Gas*, Nature Physics **16**, 514 (2020).
News coverage:
 - Nature Physics **16**, 506 (2020): News & Views: Cooking with quantum gas, by James Analytis
 - Phys.org article: "Imaging nematic transitions in iron pnictide superconductors"

Interfacial superconductivity in epitaxial single layer FeTeSe/SrTiO₃

Lian Li

Department of Physics and Astronomy, West Virginia University, Morgantown, WV

Keywords: FeSe, SrTiO₃, MBE, interfacial superconductivity, persistent superconductivity

Research Scope

By designing and synthesizing epitaxial ultrathin quantum materials on the order of one to a few unit cells, we aim to modulate their properties through quantum confinement and proximity effects. The focus is on the superconducting and topological properties of single and multilayer FeTeSe epitaxially grown on perovskite oxide substrates. Of particular interests are 1) controlling high temperature superconductivity in single layer by engineering interface with oxide substrates, 2) probing pairing symmetry in single layer via quasiparticle scattering off impurities and 1D edges, and 3) exploring the interplay of topology and superconductivity in both single and multilayers by detecting topological edge states.

Recent Progress

1. Sign-change pairing symmetry in single layer FeSe/SrTiO₃ by quasiparticle scattering

The discovery of high-temperature superconductivity in single layer FeSe epitaxially grown on SrTiO₃ (STO) has instigated extensive debate over its pairing symmetry. In this work, we have grown single layer FeSe films on STO substrates, which exhibit a two-gap structure (**Fig. 1a-b**).

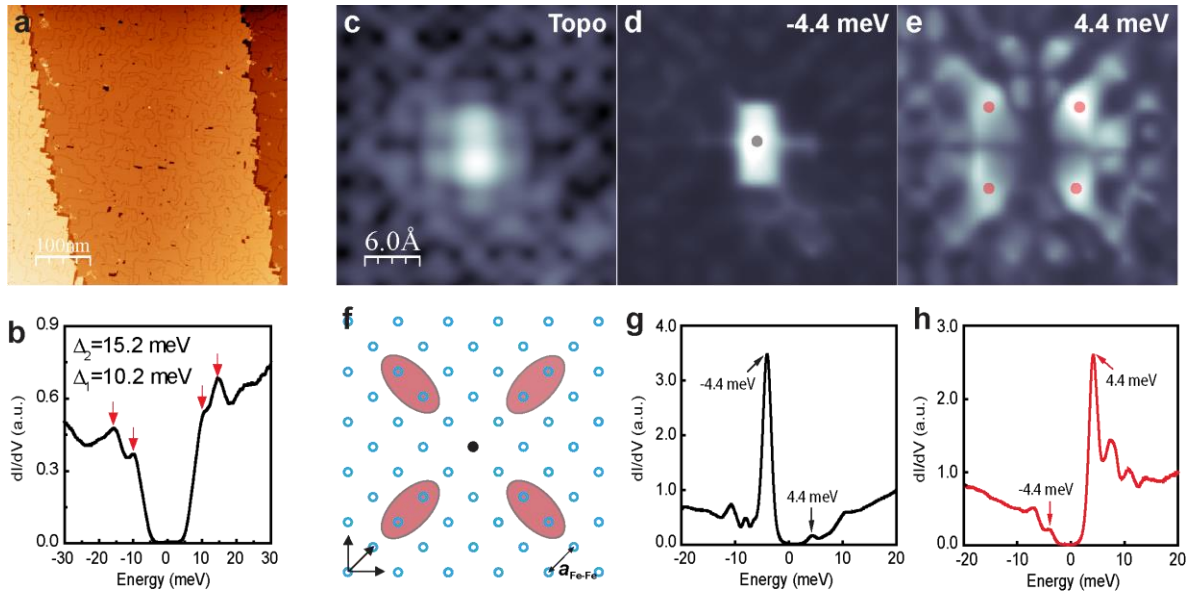


Fig. 1 Spatial distribution of bound states for Fe vacancy defect in single layer FeSe/STO. **a**, Topographic image of the epitaxial single layer FeSe/STO film. ($V_s=1.0$ V, $I=10$ pA). **b**, dI/dV spectrum showing the superconducting gap structure. **c**, Topographic image of the defect ($V_s=-30$ mV, $I=1000$ pA). **d&e**, Differential conductance maps at -4.4 meV and 4.4 meV, respectively, over the same region in (c) (Setpoint: $V=12$ mV, $I=500$ pA). **f**, Schematic representation of the bound state at positive energy. **e,f** dI/dV spectrum measured at the defect center (at the gray dot in d), and at one of the four bright lobes as marked by red dots in (e).

We observe robust in-gap bound states induced by non-magnetic Fe-vacancy defects, which exhibit strong spatial electron-hole asymmetry (**Fig. 1c-h**) and no energy shift or splitting under an applied magnetic field, all hallmarks of a sign-changing order parameter. We further confirm this by defect bound-state quasiparticle interference (QPI), which also shows a pair of corresponding peaks at the positive and negative energies of the bound states, another signature of sign-changing behavior. These findings provide strong evidence for a sign-changing pairing symmetry for single layer FeSe/STO, contrary to the currently presumed sign-preserving s-wave symmetry. These results have been published in *Commun. Phys.* **3**, 75 (2020).

We further measure the de Gennes extrapolation length, which is expected to be infinite and isotropic for plain *s*-wave pairing, and finite and anisotropic for *d*-wave. We find a 40% reduction of the superconducting gap near specular $[110]_{\text{Fe}}$ edges, yielding an extrapolation length of 8.0 nm., while near specular $[010]_{\text{Fe}}$ edges it is nearly infinite, indicating phase change pairing with 2-fold symmetry, consistent with *d*-wave pairing. This is further supported by the observation of in-gap states near the specular $[110]_{\text{Fe}}$, but not the $[010]_{\text{Fe}}$ edges. These findings provide strong experimental evidence for *d*-wave superconductivity in single layer FeSe/STO, and demonstrates that quasiparticle scattering off 1D boundaries can be a viable phase sensitive probe of pairing symmetry in Fe-based superconductors. These results have been published in *Nano Lett.* **19**, 2497 (2019).

2. Light-induced persistent superconducting state in single layer FeSe/SrTiO₃ heterostructures

Superconductors rarely exhibit strong photo-responses, and optically sensitive materials are often not superconducting, thus efficient coupling between these two characteristics is very challenging in a single material. In this part of the research, we explore a different strategy to optically manipulate superconductivity in epitaxial heterostructures where the photoactive and superconducting layers are strongly coupled through the interface. In single layer FeSe/STO heterostructures, we find that the T_C can be effectively raised by 20% with interband

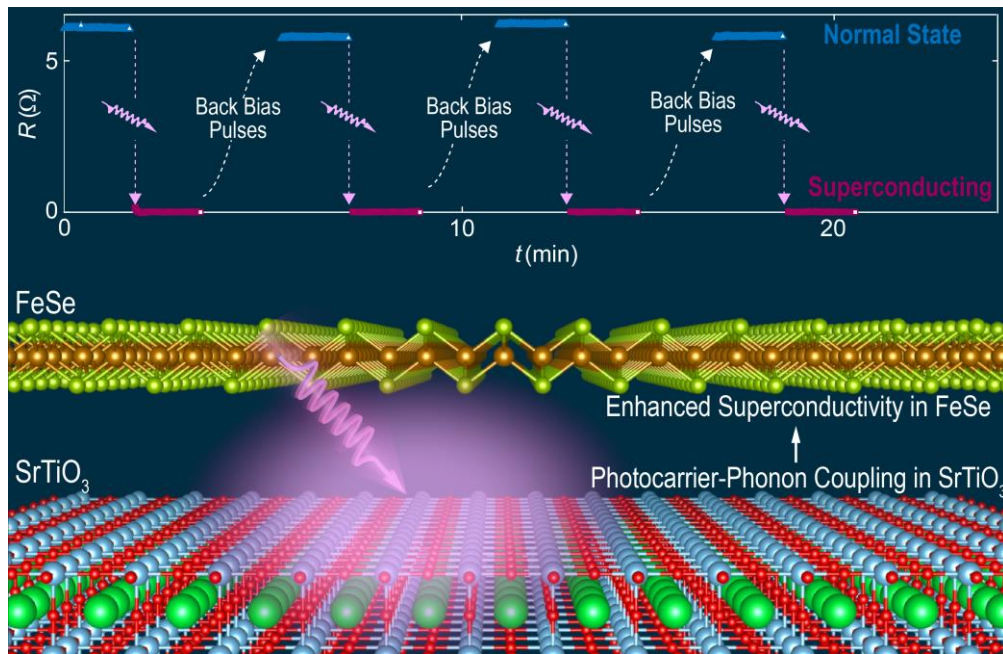


Fig. 2 UV light induced persistent superconductivity in single layer FeSe/STO.

photoexcitations in the STO substrate. Attributed to a light induced metastable polar distortion uniquely enabled by the FeSe/STO interface, this effect only requires a less than $50 \mu\text{Wcm}^{-2}$ continuous-wave light field. More importantly, the enhancement in superconductivity is also nonvolatile, persisting even when the light is removed. Furthermore, this optically generated superconducting zero resistance state can also be rapidly reversed by voltage pulses to the STO substrate (**Fig. 2**). This capability of switching FeSe repeatedly and reliably between normal and superconducting states demonstrates a path towards high-speed superconducting switches with infinite on/off ratio. These results have been published in *Nat. Commun.* **10**, 85 (2019), and were also featured in the DOE Office of Science Highlights in August 2019.

3. One-dimensional superconducting channel at the edges of $\text{FeTe}_{1-x}\text{Se}_x/\text{SrTiO}_3(001)$ nanoribbons

Bulk crystal of FeTe exhibits a distinct long-range BCL antiferromagnetic order, which can be suppressed by alloying with Se, and superconductivity emerges with T_C of 10 K at a critical Se concentration of $x = 0.3$. This phase transition can be further manipulated by reducing the thickness

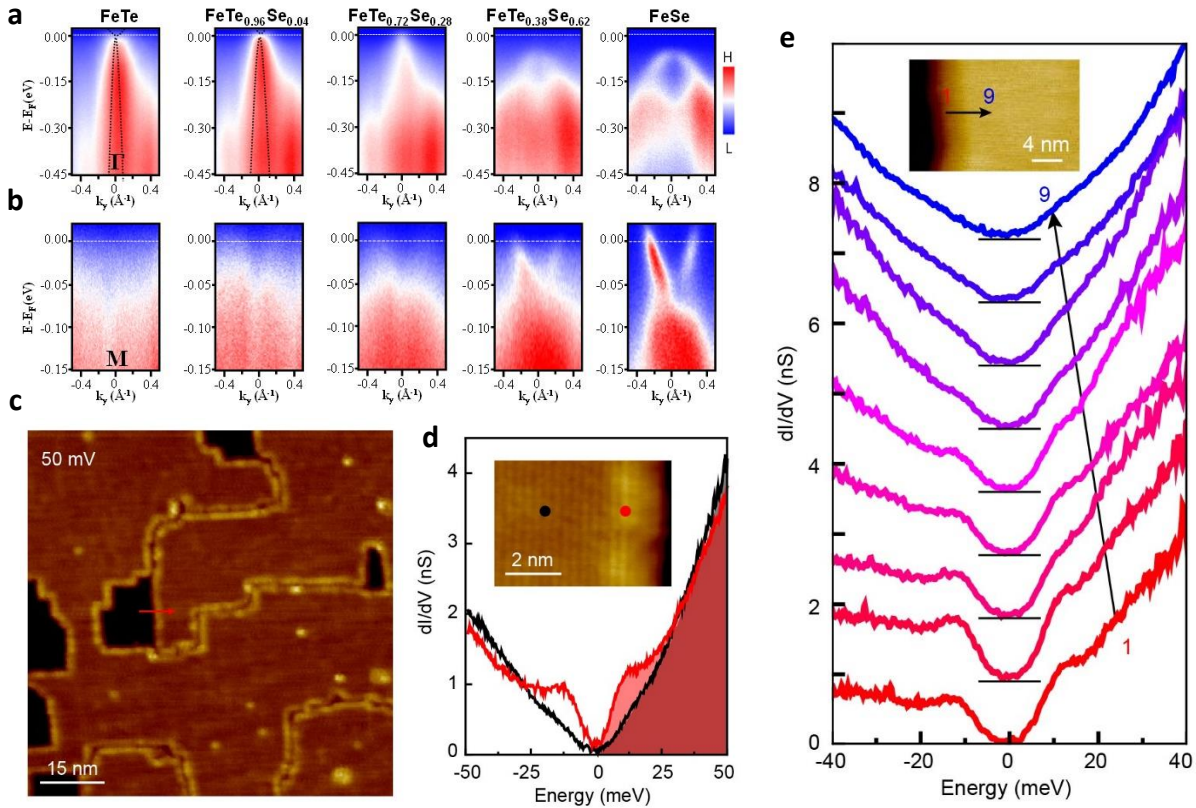


Fig. 3 1D superconductivity at the edges of single layer FeTeSe nanoribbons. **a,b**, ARPES measurements of the valence band structure at (a) Γ and (b) M points for $\text{FeTe}_{1-x}\text{Se}_x$ films with different Se concentrations. The dotted lines in (a) highlight hole and electron-like bands at Γ . **c**, STM image showing the 1D edge mode (Set-point: 50 mV, 0.1 nA). **d**, dI/dV spectra taken in the interior (black) and on the edge (red) of a ribbon at 6 K (Set-point: 50 mV, 0.1 nA). The inset is an STM image with colored dots showing the locations where spectra are taken. **e**, Spatially resolved dI/dV taken along a line marked as a black arrow in the inset. The starting point 1 (red) is on the edge, and the end point 9 (blue) is in the interior. Each spectrum is vertically shifted by 1 nS for clarity, and the black horizontal lines mark the zero conductance. The inset is an STM image of a $\text{FeTe}_{1-x}\text{Se}_x$ ($x < 0.1$) ribbon edge (Set point: 600 mV, 70 pA).

of $\text{FeTe}_{1-x}\text{Se}_x$ to a single atomic layer. In this work, we have explored the effect of dimensionality on the interplay between antiferromagnetic ordering and superconductivity by investigating nanoribbons of single layer $\text{FeTe}_{1-x}\text{Se}_x$ films grown on STO substrates by MBE (**Fig. 3**). Using STM/S, we find a one-dimensional (1D) superconducting channel 2 nm wide with a T_C of 42 K on the edge of $\text{FeTe}_{1-x}\text{Se}_x$ ($x < 0.1$) ribbons, coexisting with a non-superconducting ribbon bulk that remains BCL antiferromagnetically ordered. Density functional theory calculations indicate that both Se and the presence of the edge destabilize the BCL magnetic order, resulting in a paramagnetic region near the edge with strong local CB quantum fluctuations that are conducive to superconductivity. Our findings demonstrate an effective route towards stabilizing superconductivity in Fe-based superconductors at reduced dimensions, and have been published in *ACS Nano*, **14**, 6539 (2020).

4. Interplay of paramagnetism and topology in Fe-chalcogenide high- T_c superconductors

The question of whether high- T_c FeSe-based superconductors are topological remains controversial. The paramagnetism in these materials complicates the situation in that the simple rules appropriate for time-reversal invariant systems are not applicable, and the lack of long-range magnetic order similarly prevents the straightforward use of magnetic symmetries. In non-magnetic calculations, a gap that can host a topologically non-trivial surface state is found, but is located significantly above the chemical potential. Calculations explicitly including magnetic contributions modify the band topology, yielding band structures in good agreement with angle resolved photoemission spectroscopy (ARPES) experiments, including bringing the calculated

chemical potential naturally into alignment with the experimental observations. As a result of magnetic ordering and static compositional fluctuations, the calculated bands for both in-plane and perpendicular moments show behavior indicative of the type of inverted gaps capable of supporting a topological state (**Fig. 4**). Because of the mixing of spatial and magnetic degrees of freedom in the symmetry operations, the inversion of the gaps involves both orbital and spin character. These findings have been published in *Phys. Rev. B* **99**, 205117 (2019).

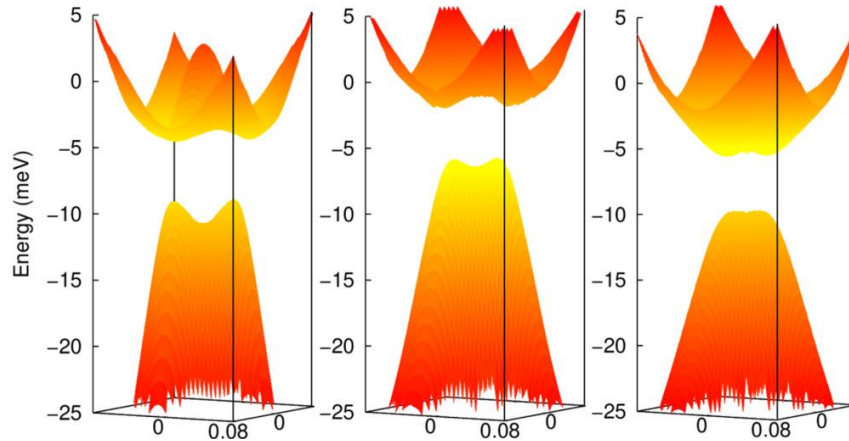


Fig. 4 Calculated saddle-shaped topology characteristic of band inversion. Bands for perpendicular moments over a $0.08 \times 0.08 \text{ \AA}^{-1}$ region for k_z at $\sim 0.4Z$, at Z , and at $\sim 0.6Z$. Note the two maxima in the lower band, and that the gap remains for each k_z .

Future Plans

We will continue the systematic studies already underway to investigate the superconducting and topological transitions in multilayer FeTeSe/STO .

Publications supported by the DOE grant over the previous two years (2019 - 2020)

1. H. Zhang, Z. Ge, M. Weinert, and L. Li, “Sign changing pairing in single layer FeSe/SrTiO₃ revealed by nonmagnetic impurity bound states”, *Commun. Phys.* **3**, 75 (2020).
2. Z. Ge, Q. Zou, H. Zhang, C. Yan, D. Agterberg, M. Weinert, and L. Li, “Superconductivity on edge: Evidence of a one-dimensional superconducting channel at the edges of single-layer FeTeSe antiferromagnetic nanoribbons”, *ACS Nano* **14**, 6539 (2020).
3. Z. Ge, C. Yan, H. Zhang, D. Agterberg, M. Weinert, L. Li, “Evidence for d-wave superconductivity in single layer FeSe/SrTiO₃ probed by quasiparticle scattering off step edges”, *Nano Lett.* **19**, 2497 (2019).
4. M. Yang, C. Yan, Y. Ma, L. Li, and C. Cen, “Light induced nonvolatile switching of superconductivity in single layer FeSe on SrTiO₃ substrate”, *Nat. Commun.* **10**, 85 (2019).
5. J. D. Rameau, N. Zaki, G. D. Gu, P. D. Johnson, and M. Weinert, “Interplay of paramagnetism and topology in the Fe-chalcogenide high-T_c superconductors”, *Phys. Rev. B* **99**, 205117 (2019).
6. Y. Y. Li, M. X. Chen, M. Weinert, and L. Li, “1D metallic edge states of oxygen-terminated zigzag graphene edges”, *2D Mater.* **6**, 025038 (2019).
7. C.H. Li, O.M.J. van’t Erve, S. Rajput, L. Li, and B.T. Jonker, “Reply to: “On the understanding of current-induced spin polarization of three-dimensional topological insulators”, *Nat. Commun.* **10**, 2523 (2019).
8. C. H. Li, O. M. J. van ‘t Erve, C. Yan, L. Li and B. T. Jonker, “Electrical detection of current generated spin in topological insulator surface states: Role of interface resistance”, *Sci. Rep.* **9**, 6906 (2019).
9. T. Shishidou, H. G. Suh, P. M. R. Brydon, M. Weinert, and D. F. Agterberg, “Topological band and superconductivity in UTe₂”, *Phys. Rev. Lett.* (submitted).

Probing dynamic phase changes and interfaces with cryogenic and *in situ* analytical electron microscopy

PI: Dr. Y. Shirley Meng University of California San Diego

Keywords: Cryogenic temperature, *in situ* observation, electron microscopy, electrochemical devices, dynamic phase changes

Research Scope

The goal of this project is to develop unique *in situ* and cryogenic analytic electron microscopy techniques to probe dynamic phase changes and interfaces of susceptible materials for electrochemical devices. Intrinsic chemical reactivity and beam sensitivity of Li metal and solid electrolyte interphase (SEI) impede mechanistic studies by electron microscopy. Solar cells with hybrid perovskite materials are also beam sensitive and their degradation issues need to be studied upon operation under the electrical bias. To study these materials, prerequisite techniques are required including cryogenic focused ion beam (cryo-FIB) and cryogenic transmission electron microscopy (cryo-TEM). These efforts are based on the advances of the chip-based *in situ* methods of characterizing solid-state interfaces. Our recent work on Li/LiPON interphase through cryo-FIB and cryo-TEM elucidates the coexistence of several nanostructured species that embedded in an amorphous matrix, which can stabilize Li metal anode during the electrochemical reaction. Another work on perovskite materials under the electrical biasing via chip-based *in situ* holder has revealed for the first time the degradation mechanisms of perovskite solar cells through facet dependent amorphization.

Recent Progress

1. Characterization of beam sensitive materials *via* Cryo-FIB: Our previous work demonstrated that the chemical and morphological information of Li metal can be largely preserved during cross-sectional TEM specimen preparation *via* cryo-FIB by mitigating the local heating damage and ion implantation, which has enabled the quantitative analysis of the impact of electrolyte on the nucleation and morphology of Li metal (Figure 2A, B).¹ Cryo-FIB has also shown potential to elucidate the structure and chemistry of Li metal/electrolyte interfaces when coupled with cryo-TEM. Following up on this study, the combination of cryo-FIB and cryo-TEM was then exploited to preserve and identify extremely beam- and air-sensitive solid electrolyte interphase (SEI) between lithium phosphorus oxynitride (LiPON) and Li metal electrodes. Successful analysis of LiPON/Li SEI will not only provide the validity of cryo-FIB and cryo-TEM, but also lead to a more comprehensive understanding of the electrochemical stability of this SEI. However, conventional organometallic Pt or alternative amorphous ice deposition as a connection material to bond the lamella with the TEM grid can react with Li inducing potential damage and artifacts to the LiPON/Li interphase. By introducing a novel re-deposition mounting methodology in the cryo-FIB that utilizes the redeposition of etched Li metal material at the gap between lamella

and TEM grid as a connection material, beam-sensitive Li/LiPON interphase can be analyzed via cryo-TEM.

2. Characterization of beam-sensitive solid electrolyte interphase via Cryo-TEM: LiPON solid-state electrolyte has been reported to achieve capacity

retention of 90 % for 10,000 cycles with a Li metal anode and high-voltage $\text{LiNi}_{0.5}\text{Mn}_{1.5}\text{O}_4$ (LNMO) cathode,² indicating the extremely stable interfaces between LiPON and electrodes. Our novel fabrication method for LiPON and LNMO thin film solid-state battery using pulsed laser deposition (PLD) and sputtering can also achieve Coulombic efficiency over 99.85% after 400 cycles (Figure 1). In this work, we primarily focused on the interface between LiPON and Li metal

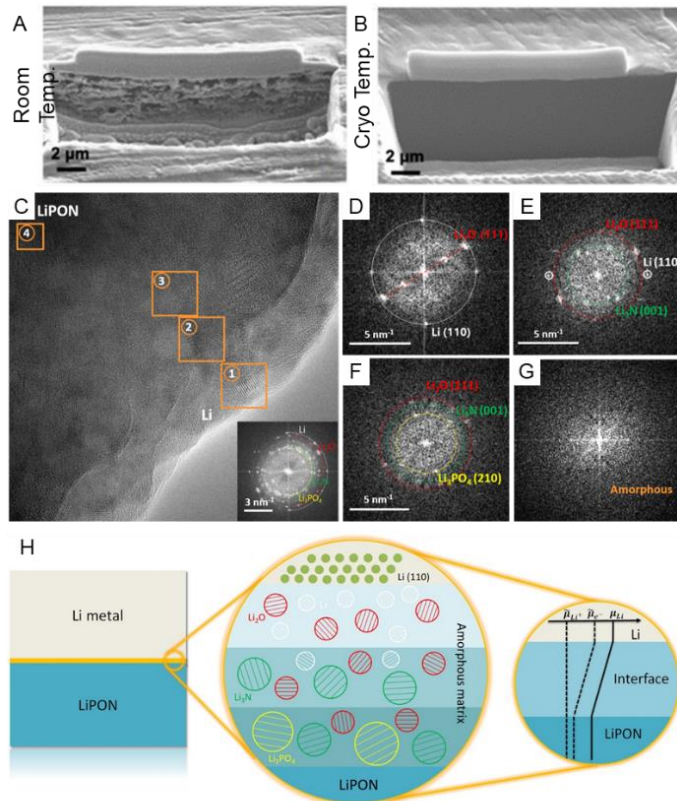


Figure 2. FIB cross-section SEM images for Li metal foil prepared at (A) room temperature (25 °C) and (B) cryogenic temperature (-170 °C). (C) High-resolution TEM (HRTEM) image for LiPON/Li SEI attained via cryo-TEM and (B-E) SAED patterns correspond to 1-4 areas in (A). (F) Schematic for the LiPON/Li SEI consist of Li, Li_2O , Li_3N and Li_3PO_4 .

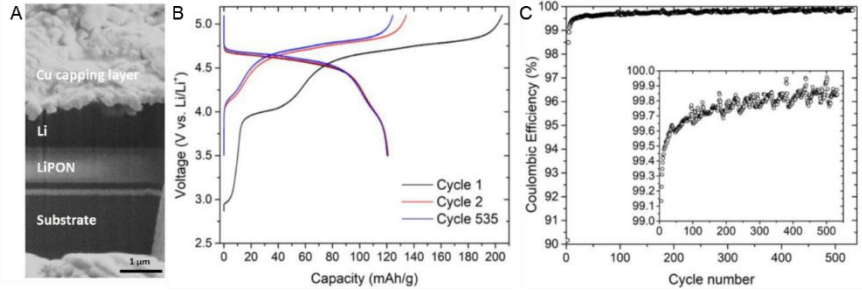


Figure 1. (A) Cryo-STEM dark field image of Li/LiPON interface. (B) A representative voltage profile for the LNMO/LiPON/Li thin film solid-state battery for 1st, 2nd and 535th cycle. (C) Coulombic efficiency trend of thin film solid-state battery over 500 cycles. (from Publication 4)

by combining cryo-FIB and cryo-TEM. Our results revealed that this SEI is a complex, nanostructured interphase with the coexistence of Li_2O , Li_3N and Li_3PO_4 species that are embedded in an amorphous matrix (Figure 2C-G). The unique multilayer mosaic SEI structure can electronically insulate Li metal anode and shield the solid electrolyte from further decomposition as demonstrated in Figure 2H. The successful preservation and observation of LiPON/Li interface has provided a mechanistic understanding of the formation of such an interface that can stabilize Li metal anode, but also give rise to the possibility of apply the similar methodology on other beam-sensitive materials such as Li titanate based electrode and solid-state electrolyte (LTO and LLTO) or hybrid perovskite materials.

3. In situ bias for Perovskite materials: Past solid-state nano-device fabrications and their *in situ* imaging

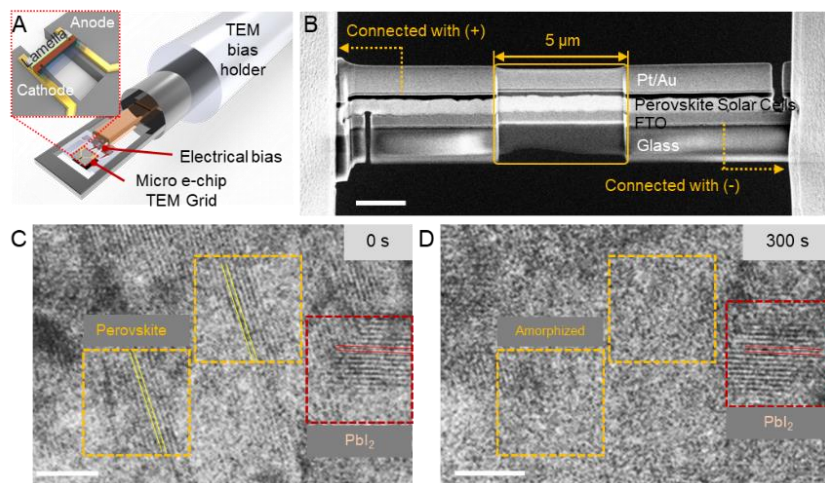


Figure 3. (A) Schematic for fabricating chip-based electrochemically activated nano-devices. (B) SEM image for the perovskite nano-solar-cell fabricated on chip. *In situ* TEM images for perovskite materials under electrical bias taken at (C) 0 s and after (D) 300 s. (submitted in 2020)

in situ TEM setup with a micro-chip was optimized for perovskite nano solar cell, and to apply the electrical bias without any shorting, perovskite lamella was disconnected at both ends to separate cathode/anode as described in Figure 3B.

Prior to *in situ* TEM observation under electrical bias, stable electrical connection between FIB lamella and low-current potentiostat was verified by voltage-current response measured in TEM column. Our *in situ* biasing TEM observation for perovskite materials under electrical bias reveals that the perovskite materials can experience partial amorphization under the 1 V of electrical bias, equivalent to the operating photovoltage of perovskite solar cells (Figure 3C, D). A facet-dependent amorphization along the [001] groups of perovskite materials (such as Formamidinium lead triiodide (FAPbI₃)) was the indicative of iodide ion migration-induced amorphization since (001) planes of perovskite crystals are mainly comprising of iodide ions. This result suggests the degradation mechanisms of perovskite solar cells in nanoscale regime during the operation under electrical bias, and further proposes the possible solution for the electrical bias-related degradation. The partial amorphization effect in the device regime was confirmed that only the device with the application of electrical bias degraded under the light-illumination and the performance recovery at the dark-state from the recrystallization. Employing the thermal energy on the degraded device, interestingly, can speed up the recovery process by driving the recrystallization of amorphous phase.

Future Plans

As robust *in situ* biasing has been verified with the perovskite materials and buried information of Li/LiPON SEI has been revealed *via* novel cryo-FIB and cryo-TEM methodologies, we commit to expanding the range of materials systems and interfaces, and further capture the memristive switching behavior of beam-sensitive materials in TEM through the combination of

relied on a probe-based methodology^{3, 4} which has relatively unstable electrical biasing property and possible probe drift at cryogenic temperature. Therefore, chip-based architectures should be adopted for cryogenic holder usage. To fabricate the chip-based electrochemical nano-devices, scooped up lamella *via* FIB carefully mounted on micro-chip and connected with the low-current potentiostat using dedicated biasing holder (Figure 3A). *In*

cryo-FIB and cryo-TEM techniques. Memristive phase changes of crystalline LTO and amorphous LLTO will be characterized with currently being developed *in situ* cryo-biasing holder. The cryogenic temperature will slow down the memristive phase change kinetics which occurs with the order of micro/nano-seconds while mitigating beam damage simultaneously. With the development of *in situ* cryo-biasing holder, through newly developed advanced acquisition techniques such as 4D STEM and windowless EDS, the evolution of electronic structure and its lithium concentration can be explored in detail for the future.

References

1. Lee, J. Z., Wynn, T. A., Schroeder, M. A., Alvarado, J., Wang, X., Xu, K. and Meng, Y. S., *Cryogenic Focused Ion Beam Characterization of Lithium Metal Anodes*. ACS Energy Letters **4**, (2), 489-493.(2019)
2. Li, J., Ma, C., Chi, M., Liang, C. and Dudney, N. J., *Solid Electrolyte: the Key for High-Voltage Lithium Batteries*. Advanced Energy Materials **5**, (4), 1401408.(2015)
3. Lee, J. Z., Wynn, T. A., Meng, Y. S. and Santhanagopalan, D., *Focused Ion Beam Fabrication of LiPON-based Solid-state Lithium-ion Nanobatteries for In Situ Testing*. J. Vis. Exp. (133), e56259.(2018)
4. Wang, Z., Santhanagopalan, D., Zhang, W., Wang, F., Xin, H. L., He, K., Li, J., Dudney, N. and Meng, Y. S., *In Situ STEM-EELS Observation of Nanoscale Interfacial Phenomena in All-Solid-State Batteries*. Nano Lett. **16**, (6), 3760-3767.(2016)

Publications

1. M.-c. Kim, S.-Y. Ham, D. Cheng, T. A. Wynn, H. S. Jung, Y. S. Meng, *Advanced Characterization Techniques for Overcoming Challenges of Perovskite Solar Cell Materials*, Advanced Energy Materials, <https://doi.org/10.1002/aenm.202001753>, online published, 2020.
2. M.-c. Kim, N. Ahn, D. Cheng, M. Xu, X. Pan, Y. Luo, D. P. Fenning, S. J. Kim, S.-Y. Ham, K. Jeong, M. Choi, Y. S. Meng, *In-situ TEM observation of Perovskite Materials Amorphization under electrical bias*, Nature Nanotechnology, *under review*
3. T. A. Wynn, M. A.T. Marple, D. Cheng, R. Shimizu, H. Mason, and Y. S. Meng, *Structure of LiPON Glassy Electrolyte: Implications Toward Stable Cycling with Lithium Metal*, Angewandte Chemie, *Accepted*.
4. D. Cheng, T. A. Wynn, S. Wang, M. Zhang, S. Bai, H. Nguyen, R. Shimizu, C. Fang, B. Lu, X. Wang, Y. S. Meng, *Unveiling the Li/LiPON Interface via Cryogenic Electron Microscopy*, Joule, *Accepted*.
5. S. N. Raja, J. Z. Lee, T. A. Wynn, F. P. McGrogan, T. Swamy, Y.-M. Chiang, Y. S. Meng, and K. J. Van Vliet, *LIPON Solid Electrolyte Stiffens Upon Exposure to Ambient Humidity*, Advanced Energy Materials, *under review*.
6. J. Z. Lee, T. A. Wynn, M. A. Schroeder, J. Alvarado, X. Wang, K. Xu, and Y. S. Meng, *Cryogenic Focused Ion Beam Characterization of Lithium Metal Anodes*, ACS Energy Letters, **4**, 489, 2019.
7. C. Wang, Y. S. Meng, and Kang Xu, *Fluorinating Interphases*, Journal of The Electrochemical Society, **166** (3), A5184, 2019
8. T. A. Wynn, J. Z. Lee, A. Banerjee, and Y. S. Meng, *In Situ and Operando Probing of Solid-Solid Interfaces in Electrochemical Devices*, MRS Bulletin, **43** (10), 768, 2018.
9. J. Z. Lee, T. A. Wynn, Y. S. Meng, and D. Santhanogopalan, *Focused Ion Beam Fabrication of LiPON-based Solid-state Lithium-ion Nanobatteries for In Situ Testing*, Journal of Visualized Experiments, e56259, 2018.

Atomic electron tomography: Determining the 3D structure of crystal defects and amorphous materials at the single-atom level

Jianwei (John) Miao Department of Physics & Astronomy and California NanoSystems Institute, University of California, Los Angeles, CA 90095-1547

Keywords: atomic electron tomography, 2D materials, amorphous materials, crystal nucleation, 4D atomic resolution

Research Scope

Visualizing the 3D arrangement of atoms has played an important role in the evolution of modern science and technology. Over the last century, crystallography has been the primary method for determining the 3D structure of crystals at atomic resolution. However, crystallography is blind to crystal defects and disorders, which strongly affect material properties and functionality. Although cryo-electron microscopy has revolutionized the 3D structural determination of macromolecules with identical or similar conformations at near atomic resolution, this method cannot be readily applied to physical science samples because most materials do not have identical copies and cannot be averaged to achieve atomic resolution. Such difficulties have made the objective of solving the 3D atomic structure of individual defects and non-crystalline systems a major challenge of structural characterization in the physical sciences.

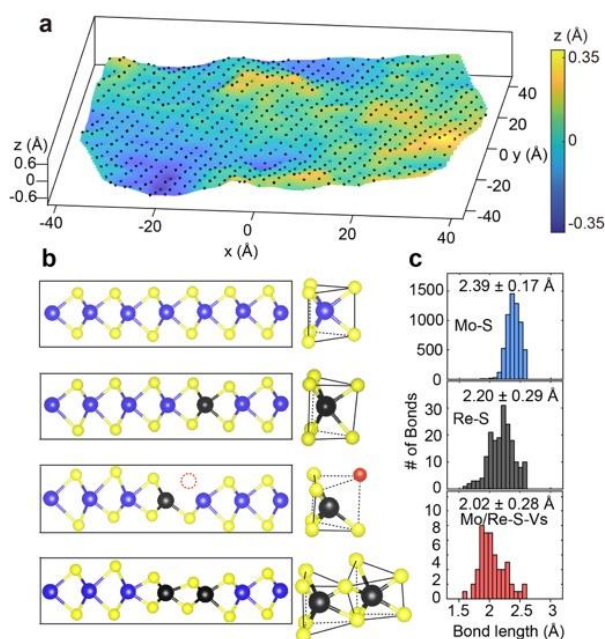


Fig. 1. 3D imaging of Re-doped MoS₂ by sAET with picometer precision², showing atomic ripples (a) and local bond distortion (b, c).

To address this challenge, Miao and collaborators have pioneered atomic electron tomography (AET) to determine the 3D structure of crystal defects and non-crystalline materials at atomic resolution with assuming crystallinity¹. Recently, we used a Re-doped MoS₂ monolayer as a model and developed scanning AET (sAET) to determine the 3D coordinates of individual atoms and crystal defects such as dopants, vacancies and ripples with picometer precision². By providing the experimental 3D atomic coordinates as direct input to density functional theory (DFT), we revealed more truthful electronic band structures than those obtained from conventional DFT calculations relying on relaxed atomic coordinates, which was further confirmed by photoluminescence spectra measurements. Moreover, we advanced AET to study early stage

nucleation in FePt nanoparticles at 4D atomic resolution³. We made three experimental observations that are inconsistent with classical nucleation theory (CNT). i) Each nucleus has a core of one to a few atoms with the maximum order parameter and the order parameter gradient points from the core to the boundary of the nucleus. ii) Nuclei undergo growth, fluctuation, dissolution, merging and/or division, which are regulated by the order parameter and its gradient. iii) Early stage nuclei are anisotropic. Our experimental results indicate that a theory beyond CNT is needed to describe early-stage nucleation at the atomic scale. More recently, we have applied AET to determine for the first time the 3D atomic structure of monatomic amorphous materials, including a Ta thin film and two Pd nanoparticles⁴. Despite the different synthesis methods, we observed that pentagonal bipyramids are the most abundant atomic motifs in these amorphous materials. Instead of forming icosahedral order, the pentagonal bipyramids are closely connected with each other to form networks that extend to medium-range scale. Looking forward, we anticipate that the series of experiments opens the door to studying the structure and dynamics of crystal defects and amorphous materials at 4D atomic resolution.

Recent Progress

Correlating the 3D atomic defects and electronic properties of 2D materials. 2D materials and heterostructures exhibit exceptional electronic, optical and chemical properties, promising to find applications ranging from electronics and photovoltaics to quantum information science. However, the exceptional properties of these materials strongly depend on their 3D atomic structure especially crystal defects. Using Re-doped MoS₂ as a model, we developed sAET to determine the atomic positions and crystal defects such as dopants, vacancies and ripples with a 3D precision down to 4 picometers² (Fig. 1). We measured the full 3D strain tensor and quantified local strains induced by single dopants. By directly providing experimental 3D atomic coordinates to DFT, we obtained more truthful electronic band structures than those derived from conventional DFT calculations relying on relaxed 3D atomic models, which was verified by photoluminescence spectra measurements. Furthermore, we observed that the local strain induced by atomic defects along the z-axis is larger than that along the x- and y-axis and thus more strongly affects the electronic property of the 2D material. We anticipate that sAET is not only generally applicable to the determination of the 3D atomic coordinates of 2D materials, heterostructures and thin films, but also could transform *ab initio* calculations by using experimental atomic coordinates as direct input to reveal more realistic physical, material, chemical and electronic properties.

Direct observation of crystal nucleation at 4D atomic resolution. Nucleation plays a critical role in many physical and biological phenomena ranging from crystallization, melting and evaporation to the formation of clouds and the initiation of neurodegenerative diseases. However, nucleation is a challenging process to study especially in the early stage when several atoms/molecules start to form a new phase from its parent phase. Here, we trapped the same nuclei at different annealing times and applied AET to capture the structure and dynamics of the nuclei at 4D atomic resolution³. We revealed that early stage nuclei are irregularly shaped, each has a core of a maximum order parameter, and an order parameter gradient points from the core to the boundary of the nucleus.

We captured the structure and dynamics of the same nuclei undergoing growth, fluctuation, dissolution, merging and/or division, which are regulated by the distribution of the order parameter and its gradient. These experimental observations were corroborated by molecular dynamics simulations of heterogeneous and homogeneous nucleation in liquid–solid phase transitions of Pt. Both our experimental and molecular dynamics simulation results are inconsistent with CNT, indicating a new theory is needed to explain early stage nucleation at the atomic scale.

Direct observation of 3D atomic packing in monatomic amorphous materials. Liquids and solids are two fundamental states of matter in nature. Although the structure of crystalline solids has long been solved by crystallography, the 3D atomic structure of liquids and amorphous solids could not be determined by any experimental method. We have recently advanced AET to resolve the 3D atomic arrangement of an amorphous Ta thin film and two amorphous Pd nanoparticles⁴. We observed that pentagonal bipyramids are the most abundant atomic motifs in these amorphous materials. Contrary to the traditional understanding, these pentagonal bipyramids do not assemble full icosahedra, but instead connect with each other to form networks that extend to medium-range scale⁸. Molecular dynamic simulations further confirmed that pentagonal bipyramid networks are prevalent in monatomic liquids and rapidly grow in size during the quench from a liquid to a metallic glass state, providing a possible new picture of structural evolution through the glass transition.

Future Plans

Probing emerging 3D topologies of ferroelectric order at the single-atom level. In recent years, the research frontier of ferroelectricity has been the spatial downscaling of ferroelectric materials to the nano-architecture regime, aiming for a significant enhancement of device efficiency. However, since ferroelectric properties are strongly related to the size and dimensionality as well as their polar nature, it is challenging to fully utilize them in nanoscale devices without a comprehensive understanding of the low-dimensional behavior of ferroelectrics. We will apply AET to reveal the polar topologies in PbTiO_3 and BiFeO_3 nanoparticles and thin films in three dimensions. Solid state synthesize/pulsed laser deposition will be used to fabricate PbTiO_3 and BiFeO_3 nanoparticles/thin films from several to tens of nanometers in size, which is ideally suitable for AET studies. High-quality tomographic tilt series will be acquired using the TEAM microscopes at NCEM at LBNL's Molecular Foundry. After post-processing on the measured tilt series, 3D atomic coordinates and chemical species will be reconstructed and traced with high precision. The large Z contrast among the cations in PbTiO_3 (Pb: 82, Ti: 22) and BiFeO_3 (Bi: 83, Fe: 26) will greatly benefit the determination of the atom species with high precision. From the experimental 3D atomic coordinates, ferroelectric polarizations will be directly calculated using relative displacements between cations and their Born effective charges within each perovskite unit cell. The cation displacements are expected to be larger than 30 pm for both PbTiO_3 and BiFeO_3 , which is larger than our current 3D AET precision of 4-20 pm. The precision can be further improved through convoluting with a Gaussian kernel at a sacrifice of resolution.

Ptychographic AET as the frontier of 3D atomic metrology for low-Z and dose-sensitive materials.

Through numerical simulations, we have demonstrated the combination of ptychography and AET (termed pAET) as an effective method for low dose imaging of individual low-Z atoms in three-dimensions⁵. After generating noisy diffraction patterns with multislice simulation of an aberration-corrected scanning transmission electron microscope through a 5 nm zinc oxide nanoparticle, we achieved 3D imaging of individual zinc and oxygen atoms and their defects by performing tomography on ptychographic projections. We have also numerically applied pAET to 2D materials, resolving individual sulfur atoms in vertical WS₂/WSe₂ van der Waals heterostructure with a low total electron dose where annular-dark-field images fail to resolve⁵. Building upon these numerical simulation results, we will apply pAET to study complex oxide SrTiO₃, one of the prototypical perovskites that possesses extraordinary dielectric properties and is widely used in transducers, capacitors. The oxygens in SrTiO₃ form corner connected octahedra, which can distort and rotate, strongly mediating the properties of SrTiO₃, even inducing paraelectric to ferroelectric phase transition. Resolving the oxygen octahedra distortion in SrTiO₃ is critically important for understanding its phase competition and can provide a guideline for engineering high performance dielectric devices. SrTiO₃ nanoparticles and thin films will be fabricated using solid states synthesize and modern thin film deposition techniques. Ptychographic tilt series will be performed using the TEAM microscope at LBNL's Molecular Foundry under different temperatures and strain conditions with the specially designed sample holder. By combining the ptychographic projections with tomographic reconstruction, high-quality 3D atomic information of each individual atoms, including oxygen, will be resolved. A multidisciplinary approach will be employed to correlate the 3D atomic structure of SrTiO₃ with its electronic and dielectric properties, including metrologies of energy dispersion spectrum and first-principle calculation at atomic level. This exemplary demonstration of the performance and power of the pAET is anticipated to inspire its broad application in dose-sensitive inorganic and organic materials.

References

1. J. Miao, P. Ercius & S. J. L. Billinge. Atomic electron tomography: 3D structures without crystals. *Science* **353**, aaf2157 (2016).
2. X. Tian, D. S. Kim, S. Yang, C. J. Ciccarino, Y. Gong, Yo. Yang, Ya. Yang, B. Duschatko, Y. Yuan, P. M. Ajayan, J. C. Idrobo, P. Narang and J. Miao. Correlating the three-dimensional atomic defects and electronic properties of two-dimensional transition metal dichalcogenides. *Nature Mater.* **19**, 867-873 (2020).
3. J. Zhou, Y. Yang, Y. Yang, D. S. Kim, A. Yuan, X. Tian, C. Ophus, F. Sun, A. K. Schmid, M. Nathanson, H. Heinz, Q. An, H. Zeng, P. Ercius and J. Miao. Observing crystal nucleation in four dimensions using atomic electron tomography. *Nature* **570**, 500-503 (2019).
4. Y. Yuan, D.S. Kim, J. Zhou, D.J. Chang, F. Zhu, Y. Nagaoka, Y. Yang, M. Pham, S. J. Osher, O. Chen, P. Ercius, A. K. Schmid and J. Miao. Direct observation of 3D atomic packing in monatomic amorphous materials. Submitted, arXiv:2007.03881 (2020).
5. D. J. Chang, D. S. Kim, X. Tian, J. Zhou, P. Ercius and J. Miao. Ptychographic Atomic Electron Tomography: Towards 3D Imaging of Individual Light Atoms in Materials. *Phys. Rev. B*, in revision.

Publications

1. Y. Yuan, D.S. Kim, J. Zhou, D.J. Chang, F. Zhu, Y. Nagaoka, Y. Yang, M. Pham, S. J. Osher, O. Chen, P. Ercius, A. K. Schmid and J. Miao. Direct observation of 3D atomic packing in monatomic amorphous materials. Submitted, arXiv:2007.03881 (2020).
2. Y. Yang, J. Zhou, F. Zhu, D. Chang, D. S. Kim, Y. Yuan, M. Pham, A. Rana, X. Tian, Y. Yao, S. Osher, L. Hu, P. Ercius and J. Miao. Determining the three-dimensional atomic structure of a metallic glass. Submitted, arXiv:2004.02266.
3. X. Tian, D. S. Kim, S. Yang, C. J. Ciccarino, Y. Gong, Yo. Yang, Ya. Yang, B. Duschatko, Y. Yuan, P. M. Ajayan, J. C. Idrobo, P. Narang and J. Miao. Correlating the three-dimensional atomic defects and electronic properties of two-dimensional transition metal dichalcogenides. *Nature Mater.* **19**, 867-873 (2020).
4. Y. Yao, Z. Liu, P. Xie, Z. Huang, T. Li, D. Morris, Z. Finfrock, J. Zhou, M. Jiao, J. Gao, Y. Mao, J. Miao, P. Zhang, R. Shahbazian-Yassar, C. Wang, G. Wang and L. Hu. Computationally aided, entropy-driven synthesis of highly efficient and durable multi-elemental alloy catalysts. *Sci. Adv.* **6**, eaaz0510 (2020).
5. A. Rana, J. Zhang, M. Pham, A. Yuan, Y. H. Lo, H. Jiang, S. Osher and J. Miao. Potential of attosecond coherent diffractive imaging. *Phys. Rev. Lett.* **125**, 086101 (2020).
6. J. Zhou, Y. Yang, P. Ercius and J. Miao. Atomic electron tomography in three and four dimensions. *MRS Bulletin* **45**, 290 (2020).
7. J. Zhou, Y. Yang, Y. Yang, D. S. Kim, A. Yuan, X. Tian, C. Ophus, F. Sun, A. K. Schmid, M. Nathanson, H. Heinz, Q. An, H. Zeng, P. Ercius and J. Miao. Observing crystal nucleation in four dimensions using atomic electron tomography. *Nature* **570**, 500-503 (2019).
8. Y. H. Lo, C. Liao, J. Zhou, A. Rana, C. S. Bevis, G. Gui, B. Enders, K. M. Cannon, Y. Yu, R. Celestre, K. Nowrouzi, D. Shapiro, H. Kapteyn, R. Falcone, C. Bennett, M. Murnane and J. Miao. Multimodal x-ray and electron microscopy of the Allende meteorite. *Sci. Adv.* **5**, eaax3009 (2019).
9. J. Deng, Y. H. Lo, M. Gallagher-Jones, S. Chen, A. Pryor Jr, Q. Jin, Y. P. Hong, Y. S. G. Nashed, S. Vogt, J. Miao, and C. Jacobsen. Correlative 3D x-ray fluorescence and ptychographic tomography of frozen-hydrated green algae. *Sci. Adv.* **4**, eaau4548 (2018).
10. Y. H. Lo, L. Zhao, M. Gallagher-Jones, A. Rana, J. Lodico, W. Xiao, B. C. Regan and J. Miao. *In situ* coherent diffractive imaging. *Nat. Commun.* **9**, 1826 (2018).

Magnetic imaging of topological phases of matter

Katja C. Nowack, Laboratory of Atomic and Solid State Physics, Cornell University

Research Scope

The overarching goal of this project is to advance our understanding and control of topologically nontrivial materials. A variety of electronic phenomena can occur in these materials including topological insulating phases, the quantum anomalous Hall effect and topological superconductivity.

Our experimental approach consists of magnetic imaging using scanning superconducting quantum interference devices (SQUID) combined with electronic transport. Local magnetic probes enable several ways to probe topological phases of matter ranging from basic material characterization to advanced measurements on mesoscopic structures. The goals of this project include exploring, characterizing and controlling new materials predicted to realize topological phases of matter and to gain a deeper understanding of topological phenomena such as the quantum anomalous Hall effect in established material systems.

Recent Progress

Spatial control of electronic order through strain fields in microstructures

To date, only a fraction of materials predicted to have a topologically non-trivial electronic structure have been experimentally explored in detail. A challenge is that often novel compounds are first available as bulk crystals; limiting options for their characterization and device fabrication. Micromachining using a focused ion beam (FIB) is a versatile approach to fabricate devices on the micron scale from bulk crystals.

Using scanning SQUID microscopy, we studied FIB defined microstructures fabricated from single crystals of heavy fermion superconductor CeIrIn₅. This work revealed a new opportunity for spatially modulating superconductivity: Differential thermal contraction between CeIrIn₅ and the substrate results in strain in the microstructure. The strain field can be controlled in a predictable way by changing the geometry of the microstructure. The strain field induces a complex pattern of superconductivity due to the dependence of the superconducting transition temperature, T_c , on the strength and direction of strain. Strain can have significant effects on the electronic properties of materials beyond superconductivity. These results therefore showcase a generic approach to manipulating electronic order on micrometer length scales without compromising the cleanliness, stoichiometry, or mean free path.

In the following, we provide more details about this work. The microstructures were prepared from lamellas of typical dimensions $100\mu\text{m} \times 50\mu\text{m} \times 2\text{-}3\mu\text{m}$ carved from a single crystal which are joined to a sapphire substrate by a thin layer of epoxy and further patterned with a FIB. Fig.1 (a) and Fig.3 (a) show scanning electron microscope images of two devices. We use scanning SQUID

microscopy to image the local diamagnetic susceptibility, which is enabled by a field coil integrated in the SQUID that is used to apply a local magnetic field. Superconducting regions exhibit a strong diamagnetic response, allowing us to distinguish them from metallic and insulating regions.

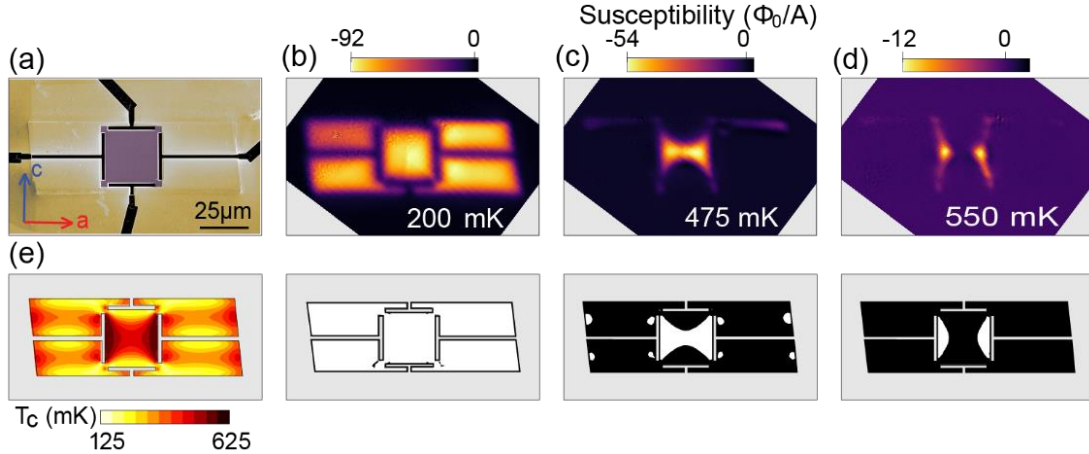


Fig. 1: (a) SEM-image of the device. Au contacts are yellow. Center square is $25 \times 25 \times 3 \mu\text{m}^3$. Crystallographic axes as indicated. (b-d) Magnetic susceptibility images at three temperatures illustrate spatially modulated superconductivity. Lower panels show superconducting patterns extracted from simulated T_c map in (e).

Susceptibility images as a function of temperature (Fig. 1b-d) show that superconductivity develops in a non-uniform pattern. The first superconducting regions form along the edges aligned with the c -direction of the crystal (Fig. 1d). These regions extend towards the center of the structure

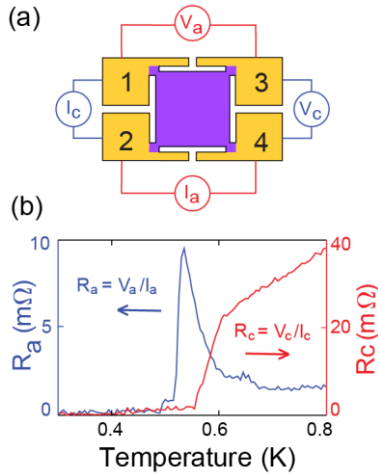


Fig. 2: (a) Schematic for transport measurement. (b) Transport of device shown in Fig. 1.

at lower temperature, eventually connecting in the middle of the device. The observed patterns lead to three distinct regimes in transport through the imaged device (Fig. 2): a) all contacts are separated by metallic regions, b) only the contact pairs along the c -direction are connected by superconducting regions, c) all contacts are connected by a single superconducting region leading to the striking differences including different temperatures at which zero resistance is reached when measuring in the two different configurations shown in Fig. 2a.

The observed pattern arises due to a combination of a strain field in the structure and the strain sensitivity of T_c in CeIrIn_5 . The latter can be extracted from uniaxial pressure measurements performed on single crystals¹: T_c (400mK) increases (decreases) by 56mK/kbar (-66mK/kbar) for compression along the crystallographic a - (c -) direction. Using finite element methods,

we simulate the strain field originating from differential thermal contraction of the substrate and the structure. Combined this allows us to compute a local T_c map (Fig. 1e). We find remarkable

agreement between the simulation and the observed spatial modulation. We fabricated and imaged a second device in which the contacts connect in the middle of the sides of the central square, which displayed a qualitative different spatial pattern compared to the first device. This contrast shows that the spatial structure can be tailored through the geometry of the microstructure. This approach offers opportunities to manipulating electronic order through strain on micron length scales in quantum materials including topologically non-trivial materials.

Penetration depth measurements of thin film Sr_2RuO_4

For the past two decades, Sr_2RuO_4 has been a leading candidate to realize an intrinsic topological superconductor, yet the nature of its superconductivity remains controversial. Until recently, only high-quality bulk single crystals of Sr_2RuO_4 showed superconductivity due to its sensitivity to disorder and impurities. Using scanning SQUID microscopy, we characterize superconducting Sr_2RuO_4 thin films that have recently been synthesized by collaborator Darrell Schlom. Thin films open the door to more advanced measurements on mesoscopic devices in the future. We extract the penetration depth from measurements of the diamagnetic susceptibility of the superconducting state; our preliminary results show that the penetration depth follows a linear dependence on temperature suggestive of line nodes in the order parameter. The power law we observe is different from what has been observed on bulk single crystals – an aspect that we are analyzing further.

Imaging of current distributions in quantum anomalous Hall effect (QAHE) devices

The key signatures of the QAHE are a quantized Hall and vanishing longitudinal resistance without requiring an applied magnetic field. The QAHE was first realized in magnetically doped topological insulators such as Cr-doped $(\text{Bi}_x\text{Sb}_{1-x})_2\text{Te}_3$ ². Similar to the quantum Hall effect, the QAHE is typically understood to result from the presence of dissipationless, chiral edge states and an insulating two-dimensional bulk. However, from the quantum Hall effect it is known that the current can also be present in the bulk of the device despite the values of the resistance. Furthermore, in the QAHE an interplay between magnetism and the current distribution is expected.

Here, we image QAHE devices from collaborator Nitin Samarth defined by optical lithography from Cr-doped $(\text{Bi}_x\text{Sb}_{1-x})_2\text{Te}_3$ thin films. Scanning SQUID microscopy allows us to image the magnetic field produced by both the magnetization and the current flowing in the devices. We modulate a transport current at low frequency to separate its contribution from the static magnetic fields and reconstruct the corresponding current distribution. In our initial images, we observe that the transport current is concentrated at the edges of the devices. Opposite edges carry current only in opposing directions and the directionality switches, when the magnetization of the device is inverted. These observations are consistent with the expected presence of chiral edge states. However, the simplest picture is not sufficient to explain the observed behavior: we see indications of current also in the bulk of the device and application of a transport current causes circulating currents within the device that are larger than the applied current.

Future Plans

The possibility of tailoring strain fields in FIB defined microstructures opens up a number of interesting opportunities. Strain can have a significant effect on the electronic structure of e.g. half-Heusler compounds, which include candidate topological insulating phases combined with intrinsic magnetism and superconductivity^{3,4}. We are currently exploring which compounds are suitable and interesting for strain engineering using microstructures.

We plan to continue studying the QAHE both in well-established magnetically doped topological insulators and to extend our imaging to stoichiometric materials with intrinsic magnetic order that exhibit or may exhibit the QAHE such as MnBi_2Te_4 ⁵ and CoSn_2S_2 ⁶.

Acknowledgments

Work on the CeIrIn_5 microstructures is done in close collaboration with Philip Moll (Max Planck Institute for Chemical Physics of Solids in Dresden, Germany; EPFL, Switzerland).

References

1. Dix, O. M. *et al.* Anisotropic Dependence of Superconductivity on Uniaxial Pressure in CeIrIn_5 . *Phys. Rev. Lett.* **102**, 197001 (2009).
2. Chang, C. Z. *et al.* Experimental Observation of the Quantum Anomalous Hall Effect in a Magnetic Topological Insulator. *Science*. **340**, 167–170 (2013).
3. Chadov, S. *et al.* Tunable multifunctional topological insulators in ternary Heusler compounds. *Nat. Mater.* **9**, 541–545 (2010).
4. Lin, H. *et al.* Half-Heusler ternary compounds as new multifunctional experimental platforms for topological quantum phenomena. *Nat. Mater.* **9**, 546–549 (2010).
5. Deng, Y. *et al.* Quantum anomalous Hall effect in intrinsic magnetic topological insulator MnBi_2Te_4 . *Science*. **367**, 895–900 (2020).
6. Liu, E. *et al.* Giant anomalous Hall effect in a ferromagnetic kagome-lattice semimetal. *Nat. Phys.* **14**, 1125–1131 (2018).

Publications

M. D. Bachmann*, G. M. Ferguson*, F. Theuss, T. Meng, C. Putzke, T. Helm, K.R. Shirer, Y.-S. Li, K.A. Modic, M. Nicklas, M. Koenig, D. Low, S. Ghosh, A. P. Mackenzie, F. Arnold, E. Hassinger, R. D. McDonald, L. E. Winter, E. D. Bauer, F. Ronning, B.J. Ramshaw, K. C. Nowack†, P.J.W. Moll†, “Spatial control of heavy-fermion superconductivity in CeIrIn_5 ”, *Science* 366, 221 (2019). *These authors contributed equally. †Corresponding authors/These authors contributed equally.

Probing the Atomic Scale Structure and Electronic Properties of Ferroelectric Interfaces

Xiaoqing Pan

**Department of Materials Science & Engineering and Department of Physics & Astronomy,
University of California, Irvine, CA 92697**

Research Scope

Oxide heterostructures with unusual physical properties have attracted intense interdisciplinary research with a focus on controlling different degrees of freedom at the interface to tailor the functionality of heterostructures. One of the most prominent examples is the discovery of two-dimensional electron gas (2DEG) and ferromagnetism at the interface of $\text{LaAlO}_3/\text{SrTiO}_3$ (LAO/STO) with an interfacial polar discontinuity. On the other hand, ferroelectric materials can provide an intrinsic spontaneous polarization and cause polar discontinuity at the ferroelectric/insulator interface that can also lead to a 2DEG or a spin-polarized 2DEG for certain ferroelectrics. An immediate advantage of the 2DEG at a ferroelectric/insulator interface is that it allows modulation of the interfacial properties such as electronic conductivity and magnetic ordering via polarization switching, enabling unprecedented control of multiple degrees of freedom. Thus, multiple orderings can emerge at the same interface, offering opportunities for the advancement of ferroelectric memories, tunnel functions and magnetoelectric devices, in addition to the design of novel functionalities.

A major challenge of this research was a direct measurement of multiple properties, including the local electric dipole moment, electric field, charge, and conductivity at the same interfaces or domain walls as those imaged by atomic resolution transmission electron microscopy, which is critical to unravel the fundamental mechanisms for the formation of 2DEG at interfaces in oxide heterostructures. To address this challenge, we have developed a unique multimodal approach based on probing the cross-sectional specimens of the same sample by a combination of atomic resolution scanning transmission electron microscopy (STEM), electron energy loss spectroscopy (EELS), piezoresponse force microscopy (PFM) and conductive atomic force microscopy (cAFM). With this method, the macroscopic functional properties of oxide interfaces can be directly correlated with atomic scale observations of both structure and electronic properties. In addition, we have developed several methods for analyzing the atomic scale electric field, charge distribution and dipole moment at ferroelectric interfaces based on sub-Å resolution four-dimensional STEM (4D STEM). We showed that direct analysis of the local electric field and charge density images can reveal the formation mechanism of the polarization in ferroelectrics and the evolution of polarization across interfaces in ferroelectric/multiferroic heterostructures. By comparing the positive/negative charge separation calculated from the charge density map with the atomic structure obtained from the same 4D STEM data set, we demonstrated that the evolution of the atomic lattice and the charge distribution across the interface can be separated. Finally, we also showed that integrating the charge of individual atomic columns can reveal their charge state. These new methods for studying interfacial properties based on the charge density map allow us to measure the polarization state with greater detail and accuracy than is possible from the atomic structure alone.

Recent Progress

Anisotropic polarization-induced conductance at a ferroelectric-insulator interface

To investigate the electrical properties of a BiFeO₃/TbScO₃ (BFO/TSO) interface, we developed a multimodal approach based on probing the cross-sectional specimens with a combination of STEM, PFM, and cAFM [1]. We studied the interface in the 400 nm thick (001)_p BFO thin films grown on insulating (110)_o TSO single-crystalline substrates (where the p and o subscripts represent pseudocubic and orthorhombic indices, respectively). To observe the domain structures, the specimens were prepared by cutting perpendicular and parallel to the 109° domain stripes in the BFO film, respectively. As shown in Fig. 1, cAFM of the specimen cutting perpendicular to the 109° stripe domains revealed that the interface exhibits regions of alternating low and high conductivity parallel to the domain stripes. By correlating with PFM images, the alternating conductivity was found to correspond with the alternating polarization in the domain stripes. cAFM of the specimen cutting parallel to the 109° stripe domains showed that there is no conductivity at the interface perpendicular to the domain stripes [1].

Combined atomic resolution STEM and EELS measurements from the interface reveal that the regions with upward polarization are hole doped, while the regions with downward polarization are electron doped (Fig. 1d and e). These results were further confirmed by first principles calculations [1]. Since holes and electrons have different conductivities in BFO, this alternating doping pattern leads to the high and low conductivity states observed at the interface parallel to the domain stripes. The alternating doping also leads to the formation of a series of pn-junctions along the interface that block conduction perpendicular to the domain stripes while allowing it along the stripes.

Using similar methods, we also studied the conductivity of the 71° and 109° domain walls in (001)_p BFO thin films grown on (110)_o TSO substrates [2]. 71° domain walls are insulating when measured in plan-view, but conducting in cross-section, indicating high conductivity along the film surface/interface. This was

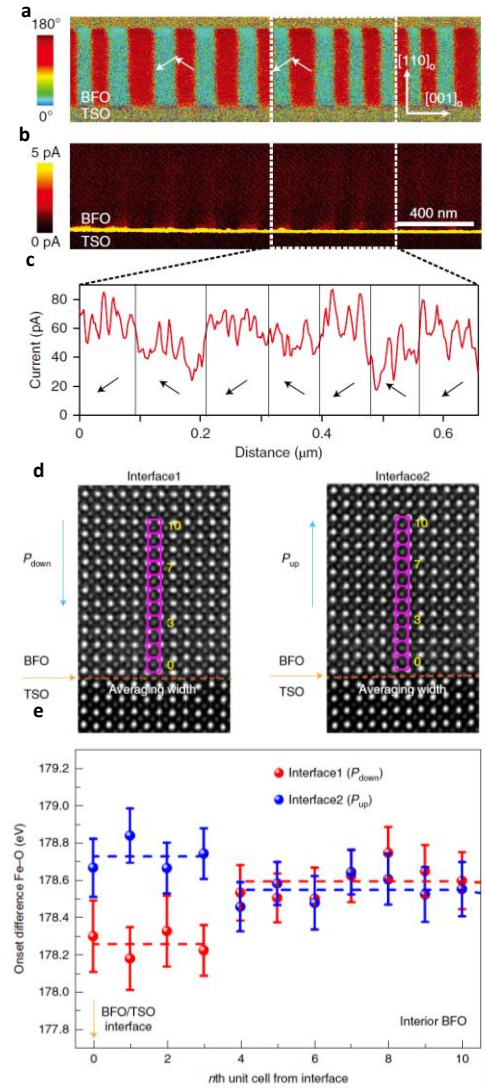


Fig. 1 | Characterization of the BFO interface. (a) PFM image of the cross-section of a BFO film, cut perpendicular to the stripe domain. (b) CAFM image of the same region as in (a). (c) An averaged current profile along the interface taken from the outlined region showing how conductivity varies with the polarization of the ferroelectric domains. (d), HAADF-STEM images at the BFO/TSO interface with down and up polarizations. An EELS linescan averaged within a larger area was carried out at the BFO/TSO interface. (e), The energy onset difference between the O K and Fe L₃ edges obtained from the interface to interior BFO via EELS linescans.

further supported by EELS measurements across domain wall which showed a charge build-up at 71° domain walls. Based on phase-field simulations, the anisotropic conductivity of 71° domain walls results from a pn-junction forming in the middle of the domain wall. This finding of intrinsic anisotropy in conductivity of 71° domain walls indicates that the domain wall conductance measured in the direction normal to the film surface—experimental geometry used in most of the previous works—does not reveal the true conductance of the 71° domain walls in BFO.

Electronic properties of ferroelectric interfaces studied by 4D STEM

The redistribution of electrons to form chemical bonds is a fundamental process which determines the characteristics of materials. Thus, the measurement of electron charge density is critical for understanding structure-property relationships in solids. 4D STEM provides one avenue for directly imaging the local electric field, from which the charge density can be derived [3, 4]. By studying the behavior of the electric field as a function of the electron probe focus and sample thickness, we have found that optimal placement of the probe focus can improve the accuracy of the electric field measurement in thicker samples and local charge density can be determined with sub-Å resolution [3].

We have used this 4D STEM technique to study the electric field and charge density at a BFO/STO interface (Fig. 2) and, in the process, we have developed new methods for analyzing the polarization and charge state based on the electric field and charge density [4].

We found that changes in the atomic structure and charge distribution are not synchronized across the interface. By measuring the displacement of the Bi and Sr columns, we can see that the polarization in the BFO is decreased at the interface and also persists a few unit cells into the STO (schematically shown in Fig. 2b, quantified in Fig. 5e). The electric dipoles are visible in the electric field map (Fig. 2c) in BFO, particularly near the Bi columns. On approaching the

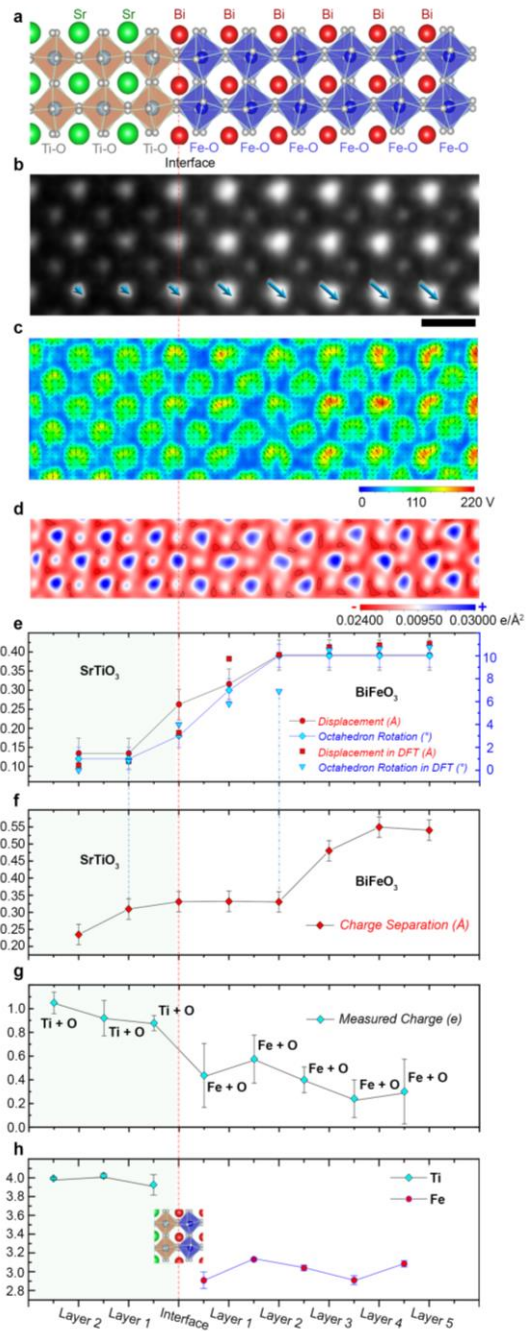


Fig. 2 | BFO-STO interface. (a) Atomic structure, (b) HAADF image, (c) electric field, (d) charge density image derived from 4D STEM data acquired at the interface between BFO and STO. (e) displacement of A-site atoms and oxygen octahedral rotation from experiment and DFT calculation. (f) separation of positive and negative charge centers. (g) valence state based on integration of charge density image. (h) B-site valence state measured by EELS. Scale bar: 4 Å.

interface, the electric dipoles become weaker in the bottom BFO layers and some induced dipoles appear around the Sr columns of top STO layers in the substrate.

Using the charge density map (Fig. 2d), we found that the onset of the atomic structure changes in both cation displacement and oxygen octahedral rotation occur 1-2 u.c. from the interface. However, based on the separation of positive and negative charge centers in each unit cell, changes in the charge distribution occur 3-4 u.c. from the interface, resulting in a charge build-up at the interface. This was further confirmed by integrating the charge of each B-site atomic column, a measure of the charge state of the atom. EELS was also used to measure the charge distribution by identifying the change in valence state of B-site cations; changes in both Ti and Fe valence near the interface also confirm a charge accumulation. This asynchronous response shows that the electrons are more responsive to the electric field of the polarized BiFeO₃, while the atomic displacement is more rigidly affected by the atomic strain. This leads to the phenomenon of interface charging which is the key for understanding and engineering the 2D electron or hole gas emergent at the interface.

Future Plans

The recent development of 4D STEM and vibrational EELS have further expanded the avenues for characterizing the structure and properties such as local charge, field, electric and magnetic ordering and their coupling to the lattice vibration (phonon) of the material. In addition, the successful synthesis of freestanding 2D ferroelectric oxide films has unlocked a new frontier in the study of ferroelectrics and their applications. The future plan of our research will focus on the further development 4D STEM and vibrational EELS towards studying the novel polarization states and properties of freestanding ferroelectric oxide films which are under different boundary conditions in comparison with bulk crystals. For examples, freestanding films have been shown to host exceptionally large strain, it is necessary to measure the cation and anion positions, as well as the change in electric field and electronic charge distribution to accurately describe the polarization. In addition, changes to the vibrational spectra may elucidate aspects of the polarization that are hidden in the projection direction as they are sensitive to the vibrational modes of the 3D structure. The combination of 4D STEM with vibrational EELS may reveal the novel polarization states and emergent functional properties of freestanding ferroelectric films.

References

- [1] Y. Zhang, H. D. Lu, L. Xie, X. X. Yan, T. R. Paudel, J. Kim, X. X. Cheng, H. Wang, C. Heikes, L. Z. Li, M. J. Xu, D. G. Schlom, L. Q. Chen, R. Q. Wu, E. Y. Tsymlal, A. Gruverman, and X. P. Pan. *Anisotropic polarization-induced conductance at a ferroelectric-insulator interface*. Nature Nanotechnology **13**, 1132-1136 (2018).
- [2] Y. Zhang, H. D. Lu, X. X. Yong, X. X. Cheng, L. Xie, T. Aoki, L. Z. Li, C. Heikes, S. P. Lau, D. C. Schlom, L. Q. Chen, A. Gruverman, and X. Q. Pan. *Intrinsic Conductance of Domain Walls in BiFeO₃*. Advanced Materials **31**, 7 (2019).
- [3] C. Addiego, W. P. Gao, and X. Q. Pan. *Thickness and defocus dependence of inter-atomic electric fields measured by scanning diffraction*. Ultramicroscopy **208**, 7 (2020).
- [4] W. P. Gao, C. Addiego, H. Wang, X. X. Yan, Y. S. Hou, D. X. Ji, C. Heikes, Y. Zhang, L. Z. Li, H. X. Huyan, T. Blum, T. Aoki, Y. F. Nie, D. G. Schlom, R. Q. Wu, and X. Q. Pan. *Real-space charge-density imaging with sub-angstrom resolution by four-dimensional electron microscopy*. Nature **575**, 480-484 (2019).

Publications

1. J. Li, X. Yang, Y. Liu, B. Huang, R. Wu, Z. Zhang, B. Zhao, H. Ma, W. Dang, Z. Wei, K. Wang, Z. Lin, X. Yan, M. Sun, B. Li, X. Pan, J. Luo, G. Zhang, Y. Liu, Y. Huang, X. Duan, and X. Duan. *General synthesis of two-dimensional van der Waals heterostructure arrays*. *Nature* **579**, 368-374 (2020).
2. X. X. Yan, F. Xue, C. A. Gadre, Z. Wang, J. Y. Zheng, L. Xie, Y. Zhang, M. J. Xu, M. Zhang, L. Y. Jiao, R. Q. Wu, P. Wang, and X. Q. Pan. *Anomalous Linear Layer-Dependent Blue Shift of Ultraviolet-Range Interband Transition in Two-Dimensional MoS₂*. *Journal of Physical Chemistry C* **124**, 1609-1616 (2020).
3. C. Addiego, W. P. Gao, and X. Q. Pan. *Thickness and defocus dependence of inter-atomic electric fields measured by scanning diffraction*. *Ultramicroscopy* **208**, 7 (2020).
4. L. Z. Li, L. Xie, and X. Q. Pan. *Real-time studies of ferroelectric domain switching: a review*. *Reports on Progress in Physics* **82**, 39 (2019).
5. W. P. Gao, C. Addiego, H. Wang, X. X. Yan, Y. S. Hou, D. X. Ji, C. Heikes, Y. Zhang, L. Z. Li, H. X. Huyan, T. Blum, T. Aoki, Y. F. Nie, D. G. Schlom, R. Q. Wu, and X. Q. Pan. *Real-space charge-density imaging with sub-angstrom resolution by four-dimensional electron microscopy*. *Nature* **575**, 480-484 (2019).
6. L. Z. Li, X. X. Cheng, T. Blum, H. X. Huyan, Y. Zhang, C. Heikes, X. X. Yan, C. Gadre, T. Aoki, M. J. Xu, L. Xie, Z. J. Hong, C. Adamo, D. G. Schlom, L. Q. Chen, and X. Q. Pan. *Observation of Strong Polarization Enhancement in Ferroelectric Tunnel Junctions*. *Nano Letters* **19**, 6812-6818 (2019).
7. X. X. Yan, C. Y. Liu, C. A. Gadre, S. Dai, L. Gu, K. H. Yu, T. Aoki, R. Q. Wu, and X. Q. Pan. *Unexpected Strong Thermally Induced Phonon Energy Shift for Mapping Local Temperature*. *Nano Letters* **19**, 7494-7502 (2019).
8. Y. Zhang, H. D. Lu, X. X. Yong, X. X. Cheng, L. Xie, T. Aoki, L. Z. Li, C. Heikes, S. P. Lau, D. C. Schlom, L. Q. Chen, A. Gruverman, and X. Q. Pan. *Intrinsic Conductance of Domain Walls in BiFeO₃*. *Advanced Materials* **31**, 7 (2019).
9. H. X. Huyan, L. Z. Li, C. Addiego, W. P. Gao, and X. Q. Pan. *Structures and electronic properties of domain walls in BiFeO₃ thin films*. *National Science Review* **6**, 669-683 (2019).
10. S. H. Lee, V. Stanev, X. H. Zhang, D. Stasak, J. Flowers, J. S. Higgins, S. Dai, T. Blum, X. Q. Pan, V. M. Yakovenko, J. Paglione, R. L. Greene, V. Galitski, and I. Takeuchi. *Perfect Andreev reflection due to the Klein paradox in a topological superconducting state*. *Nature* **570**, 344-348 (2019).
11. D. X. Ji, S. H. Cai, T. R. Paudel, H. Y. Sun, C. C. Zhang, L. Han, Y. F. Wei, Y. P. Zang, M. Gu, Y. Zhang, W. P. Gao, H. X. Huyan, W. Guo, D. Wu, Z. B. Gu, E. Y. Tsymbal, P. Wang, Y. F. Nie, and X. Q. Pan. *Freestanding crystalline oxide perovskites down to the monolayer limit*. *Nature* **570**, 87-90 (2019).
12. J. Y. Wang, L. Z. Li, H. X. Huyan, X. Q. Pan, and S. S. Nonnenmann. *Highly Uniform Resistive Switching in HfO₂ Films Embedded with Ordered Metal Nanoisland Arrays*. *Advanced Functional Materials* **29**, 11 (2019).
13. Y. Zhang, H. D. Lu, L. Xie, X. X. Yan, T. R. Paudel, J. Kim, X. X. Cheng, H. Wang, C. Heikes, L. Z. Li, M. J. Xu, D. G. Schlom, L. Q. Chen, R. Q. Wu, E. Y. Tsymbal, A. Gruverman, and X. P. Pan. *Anisotropic polarization-induced conductance at a ferroelectric-insulator interface*. *Nature Nanotechnology* **13**, 1132-1136 (2018).

Combining microscopy and quantum calculations to unveil nanostructure properties

Sokrates T. Pantelides

Department of Physics and Astronomy, Vanderbilt University, Nashville, TN 37235

Keywords: STEM, STM, proximal probes, DFT calculations, nanostructures

Research Scope

Research under this project focuses on highlighting the power of combining microscopy or proximal probes with quantum calculations based on density functional theory (DFT) to unveil the structural, electronic, magnetic, electromechanical, and optical properties of complex materials and nanostructures. Theoretical research is conducted collaboratively with experimentalists in the U.S. and abroad. Focus areas in the last two years include ferroelectrics [studied experimentally primarily via piezoresponse force microscopy (PFM)], complex-oxide heterostructures, and two-dimensional (2D) materials [studied by scanning transmission electron microscopy (STEM)].

Recent Progress

Novel and unique properties of the ferrielectric layered material CuInP₂S₆ (CIPS)

A series of three papers¹⁻³ on the ferrielectric van-der-Waals (vdW) layered material CuInP₂S₆ (CIPS), published jointly with Nina Balke et al. (ORNL) are anchored on an initial theoretical

prediction that was validated by PFM measurements: Unlike conventional ferroelectrics that feature a double-well total-energy profile (Fig. 1a,b,c): Sheets of Cu atoms spontaneously displace from the central planes of layers to stable sites near the layer surfaces [low-polarization states (LP)] or further out just outside the layers [high-polarization states (HP)]. Calculations of the quadruple-well evolution with longitudinal strain (Fig. 1d) yield values of the longitudinal piezoelectric constant $d = d_{333}$ (Fig. 1e,f). PFM d -maps (Fig. 1g) led to the histogram of Fig. 1h, which confirms both the existence of the predicted four polarizations phases (stabilized by local strains as per Fig. 1d) and the calculated values. The theoretical d - P connection served to convert measured d values to polarization values to explore polarization loops in subsequent work.

Extensive experimental data and DFT calculations subsequently built synergistically on the foundation laid out by the above results. Measurements of polarization switching by an external electric field (polarization loops) confirmed normal

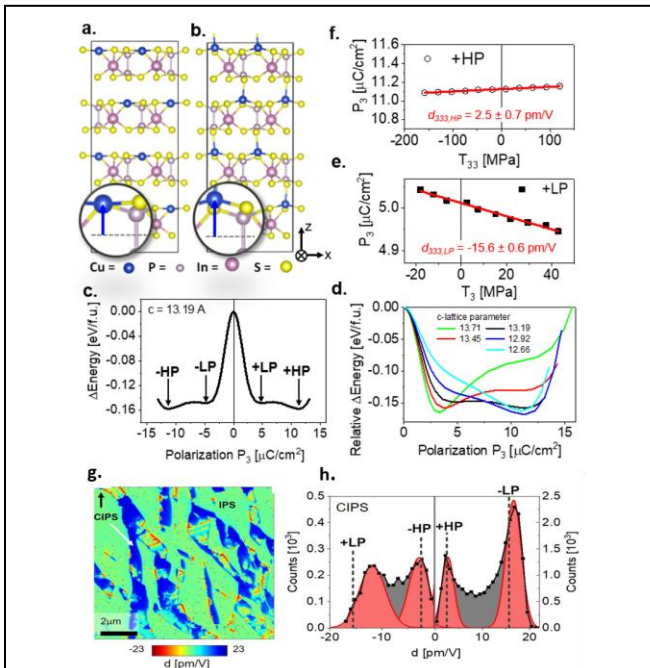


Figure 1. **a,b.** The relaxed structure of CIPS in the +LP and +HP states. **c;** The quadruple well of CIPS as a function of the polarization extracted from the Cu displacements. **d.** The quadruple well for different values of uniaxial strain, which are used to predict the longitudinal piezoelectric constant d for the LP and HP phases. **g.** Quantified piezoelectric-constant map measured by PFM at room temperature. **h.** Histogram of the measured d values with Gaussian fits of the four peaks. Dotted lines are the four theoretically predicted d values.

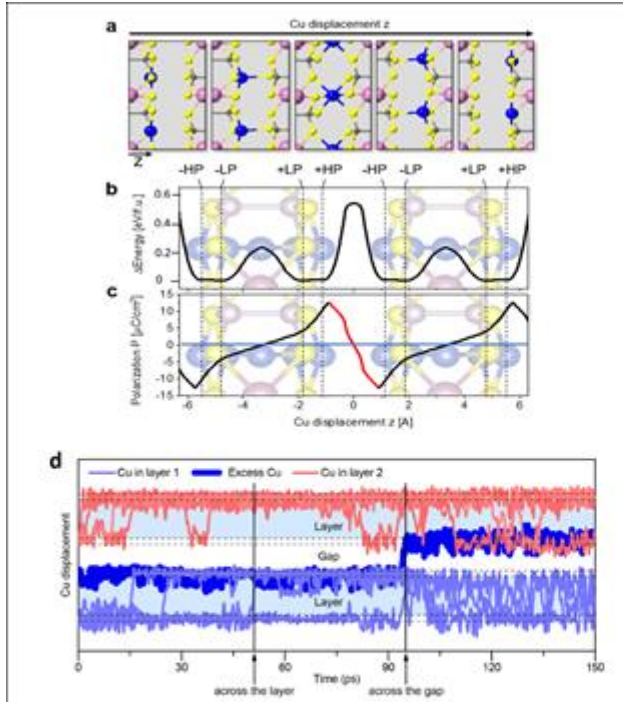


Fig. 2. **a.** Structural images of Cu sheets crossing the vdW gaps. **b.** Total energy and **c.** polarization as functions of Cu-sheet displacement across layers and vdW gaps. The red line in **c** indicates a regime of negative capacitance ($dP/dE \propto dP/dz < 0$). **d.** Quantum MD simulation of Cu-ion trajectories with an excess Cu ion (dark blue) and an external electric field.

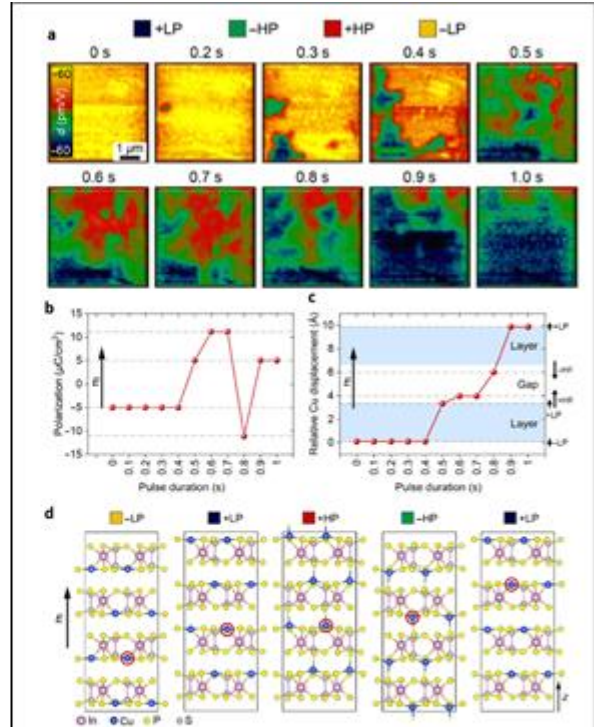


Fig. 3. **a.** PFM d -maps of d values for different voltage pulse durations. **b.** A particular polarization sequence extracted from **a**, converted to a sequence of Cu-sheet positions in **c** and **d**, demonstrating polarization alignment against the electric field when the Cu sheets cross the vdW gaps.

transitions between positive and negative polarizations, but also unveiled novel, complex behavior that is predicated on the total energy curve for Cu-sheet displacements through the layers and then across the vdW gaps as depicted in Fig. 2**a,b**, the way a constant external electric field would drive the Cu sheets. The energy barrier for Cu sheets crossing the vdW gaps is double the size of the barrier for displacements across the layers, but it is small enough to be easily overcome at room temperature, which is consistent with the fact that CIPS is an ionic conductor, with Cu ions again generating the ionic currents. Figure 2**c** shows the evolution of the polarization P for the same sequence of Cu-sheet displacements as in Fig. 2**b**. In Fig. 2**d**, we show the trajectories of Cu ions obtained by quantum molecular dynamics, demonstrating the feasibility of crossing the vdW gap under an applied electric field, here facilitated by an excess Cu atom.

In Fig. 2**c**, we note the drop of the polarization from its maximum value just past the HP configuration, its passing through zero when the Cu sheets cross the mid-planes of the vdW gaps, where the system is again centrosymmetric as when the Cu sheets occupy the mid-planes of the layers, and the negative polarization when the Cu sheets finally arrive at the next layers in their stable -HP and -LP configurations. Negative polarization means *that the polarization aligns opposite the electric field* that continuously drives the Cu sheets in the forward direction. This highly unusual feature is clearly enabled by the layered structure of CIPS and has been demonstrated experimentally by the PFM data shown in Fig. 3.

Figure 3**a** shows a series of PFM d -maps obtained by applying a sequence of -6 V voltage pulses of increasing duration, in each case preconditioning the system using a 2-second voltage pulse of +6 V, which sets the system at the -LP polarization state. The d maps show the remnant

domain structure after each negative pulse. A comparison of the theoretical and experimental d values at the HP and LP states allowed the assignment of ranges of d values in Fig. 3a to -HP, -LP, +LP, and +HP states as indicated above the PFM maps. It is straightforward to recognize regions that transition from red (+HP) to green (-HP), which, as illustrated in Fig. 2, correspond to transitions that result in the polarization aligning against the external field. In Fig. 3b, we show the polarization evolution of a particular small region in the maps through the ten pulse durations and in Fig. 3c we show the corresponding sequence of Cu-sheet positions.

The final novel and unique property of CIPS is unveiled by Fig. 2c. The part of the polarization curve that is colored red signifies the presence of negative capacitance ($C \sim \frac{dP}{dE} \sim \frac{dP}{dz} < 0$). By applying suitable continuous electric fields, PFM-obtained “ d loops” were converted to polarization loops, which then demonstrated the existence of a transient negative-capacitance regime. The mechanism that underlies this manifestation of negative capacitance is distinct from previously identified mechanisms in other ferroelectrics, but the possibility of fabricating negative-capacitance devices still remains to be explored.

Interface-induced magnetic polar metal phase in complex oxides

In this project, we combined theory with growth and magnetic measurements by Ward Plummer’s group and STEM/ EELS by Yimei Zhu’s group to unveil novel magnetic behavior in $\text{La}_{2/3}\text{Sr}_{1/3}\text{MnO}_3$ films on a SrTiO_3 (001) substrate (LSMO/STO), *governed by the interface*.⁴

Atomic-resolution STEM imaging revealed a structurally perfect heterostructure (Fig. 4a,b), tracked octahedral tilt angles and the out-of-plane lattice constant (not shown), which revealed small departures from bulk values at the two interfacial LSMO unit cells. Atomic-resolution EELS

found that LSMO is stoichiometric except for the two interfacial unit cells where it is Sr-rich (Fig. 4d). In those same two interfacial unit cells, the nominal Mn oxidation state, as extracted from the $L_{2,3}$ ratio, dips from the bulk value of 3.2 to 3.0 (Fig. 4c).

Magnetic measurements found the following unusual behavior. A sample is first cooled to 2 K in the presence of an in-plane magnetic field, which aligns all magnetic moments in the direction of the magnetic field. Under zero-field warming, the remanent magnetization $M(T)$ is found to first decrease slowly, then rapidly at 60 K, exhibiting a sharp spontaneous magnetic reversal (SMR) at ~ 75 K (Fig. 4e). SMR is a common phenomenon in *multimaterial* magnetic heterostructures, but here it is observed in a monolithic film. Phenomenological concepts provided a possible explanation (inset in Fig. 4e), but DFT

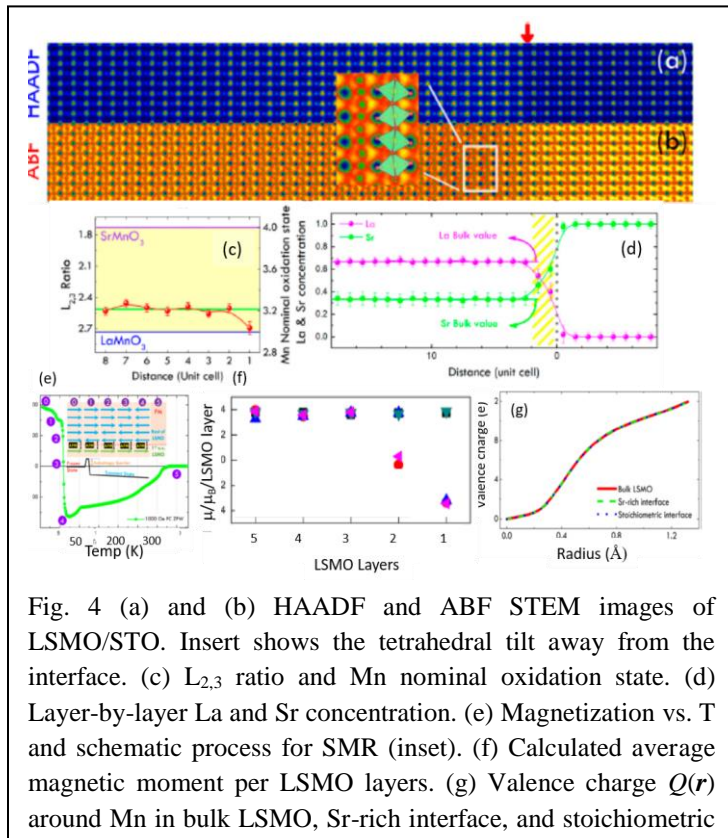


Fig. 4 (a) and (b) HAADF and ABF STEM images of LSMO/STO. Insert shows the tetrahedral tilt away from the interface. (c) $L_{2,3}$ ratio and Mn nominal oxidation state. (d) Layer-by-layer La and Sr concentration. (e) Magnetization vs. T and schematic process for SMR (inset). (f) Calculated average magnetic moment per LSMO layers. (g) Valence charge $Q(r)$ around Mn in bulk LSMO, Sr-rich interface, and stoichiometric

calculations offered an atomic-scale explanation. A key result is that a Sr-rich interface (Fig. 4d) and suppression of octahedral tilts at the interface are essential to obtain the Mn magnetic moments that yield an account of the observed SMR (Fig. 4f). In the LSMO film, the Mn magnetic moments align ferromagnetically except for the first interfacial layer where they align antiparallel. The surface termination of the LSMO film has no influence on this magnetic ordering. The interfacial spin alignment causes SMR in a domino-like fashion during zero-field warming from 2 K.⁴ The final theoretical result is that, despite the Mn oxidation-state drop at the interface, no charge is transferred to the interface: Figure 4g shows that the spherically averaged charge distribution is identical around Mn atoms at the interface, in the film's middle layers, and in bulk LSMO. SMR and other magnetic properties of the LSMO/STO heterostructure⁴ may have uses in applications.

Monolayer amorphous carbon (MAC)

A collaboration with Barbaros Özyilmaz's growth-and-characterization group (Singapore) and STEM microscopy by the PI's former student Junhao Lin in Kazuo Suenaga's group in Tokyo produced the first truly amorphous monolayer carbon sheet (Fig. 5).⁵ Theory provided understanding of the structure and properties of the amorphous monolayer and cast the results as a resolution of the long-standing issue of the structure of amorphous solids, at least for 2D materials: the MAC is not a continuous random network (CRN) – it contains graphene-like nanocrystallites, embedded in a CRN network.

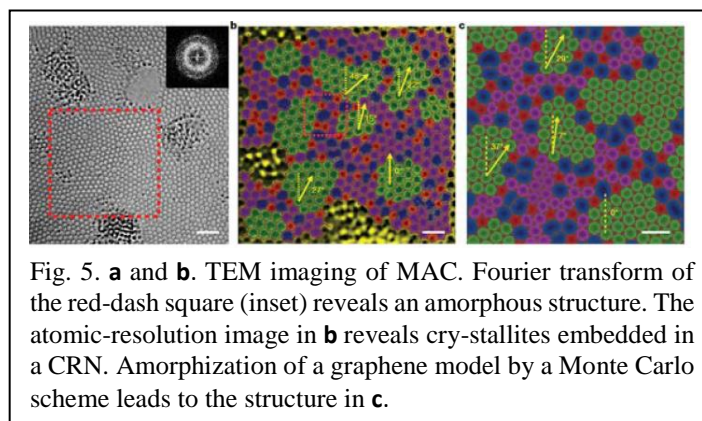


Fig. 5. **a** and **b**. TEM imaging of MAC. Fourier transform of the red-dash square (inset) reveals an amorphous structure. The atomic-resolution image in **b** reveals cry-stallites embedded in a CRN. Amorphization of a graphene model by a Monte Carlo scheme leads to the structure in **c**.

Future plans

Current and future work focuses on combining DFT calculations with PFM data to explore the coupling of ferroelectric switching and ionic current in CIPS and the role of the electrodes in the polarization switching process; explore the existence of CIPS-like materials that are multiferroic or polar metals, explore the role of defects, etc. On complex oxides, we are exploring magnetism in ultrathin ruthenate layers and will explore unusual properties of SmNiO_3 and superlattices where STEM low-loss EELS can detect localized phonons.

References

1. J. A. Brehm, S. Neumayer, L. Tei, A. O'Hara, M. Chyasnavichus, M. A. Susner, M. A. McGuire, S. V. Kalinin, S. Jesse, P. Ganesh, S. T. Pantelides, P. Maksymovych, N. Balke, "Tunable quadruple-well ferroelectricity in a van-der-Waals crystal", *Nature Materials* **19**, 43 (2020).
2. S. M. Neumayer, L. Tao, A. O'Hara, J. Brehm, M. Si, P.-Y. Liao, T. Feng, S. V. Kalinin, P. D. Ye, S. T. Pantelides, P. Maksymovych, N. M. Balke, "Alignment of polarization against an electric field in van der Waals ferroelectrics", *Physical Review Applied* **13**, 064063 (2020).
3. S. M. Neumayer, L. Tao, A. O'Hara, M. A. Susner, M. A. McGuire, P. Maksymovych, S. T. Pantelides, N. Balke, "The concept of negative capacitance in ionically conductive van-der-Waals ferroelectrics", *Advanced Energy Materials*, in press.
4. M. Saghayezhian, S. Kouser, Z. Wang, H. Guo, R. Jin, J. Zhang, Y. Zhu, S. T. Pantelides, and E. W. Plummer, "Atomic-scale determination of spontaneous magnetic reversal in oxide heterostructures", *Proceedings of the National Academy of Sciences* **116**, 10309 (2019).
5. C.-T. Toh, H. Zhang, J. Lin, A. S. Mayorov, Y.-P. Wang, C. Orofeo, D. B. Ferry, H. Anderson, N. Kakenov, H. Sims, K. Suenaga, S. T. Pantelides, B. Özyilmaz, "Synthesis and properties of free-standing monolayer amorphous carbon", *Nature* **577**, 199 (2020).

Other relevant publications

1. O. S. Ovchinnikov, A. O'Hara, R. Nicholl, K. Bolotin, J. Hachtel, A. Lupine, S. Jesse, A. Y. Borisevich, S. T. Pantelides, and S. V. Kalinin, "Theory-assisted determination of nano-rippling in atomic resolution images of angle-mismatched bilayer graphene", *2D Materials* **5**, 041008 (2018).
2. S.-Z. Yang, W.-W. Sun, Y.-Y. Zhang, Y. Gong, M. Oxley, A. R. Lupini, P. Ajayan, M. F. Chisholm, S. T. Pantelides, and W. Zhou, "Direct cation exchange in monolayer MoS₂ via 'explosive' recombination-enhanced migration", *Physical Review Letters* **122**, 106101 (2019).
3. J. A. Hachtel, S. Y. Cho, R. B. Davidson II, M. F. Chisholm, R. F. Haglund, J. C. Idrobo, S. T. Pantelides, and B. J. Lawrie, "Spatially and spectrally resolved orbital angular momentum interactions in plasmonic vortex generators", *Light: Science & Applications* **8**, 33 (2019).
4. A. D. Oyedele, S. Yang, T. Feng, Y. Gu, A. Haglund, A. A. Puretzky, D. Briggs, C. Rouleau, M. F. Chisholm, R. R. Unocic, D. Mandrus, D. B. Geohegan, S. T. Pantelides, and K. Xiao, "Defect-mediated phase transformation in anisotropic 2D PdSe₂ crystals for seamless electrical contacts", *Journal of the American Chemical Society* **141**, 8928, (2019).
5. J. Bonacum, A. O'Hara, J.-C. Idrobo, O. S. Ovchinnikov, R. F. Haglund, S. T. Pantelides, and K. Bolotin, "Atomic-resolution visualization and doping effects of complex structures in intercalated bilayer Graphene", *Physical Review Materials* **3**, 064004 (2019).
6. M. Meng, Z. Wang, A. Fathima, S. Ghosh, M. Saghayezhian, R. Jin, Y. Zhu, S. T. Pantelides, J. Zhang, W. Plummer, H. Guo, "Interface-induced magnetic polar metal phase in complex oxides", *Nature Communications* **10**, 5248 (2019).
7. O. S. Ovchinnikov, A. O'Hara, S. Jesse, B. M. Hudak, S.-Z. Yang, A. R. Lupini, M. F. Chisholm, W. Zhu, S. V. Kalinin, A. Y. Borisevich, S. T. Pantelides, "Detection of defects in atomic-resolution images of materials using cycle analysis", *Advanced Structural and Chemical Imaging* **6**, (2020).
8. Y. Zhou, S. Kouser, A. Y. Borisevich, S. T. Pantelides, S. J. May, "Evidence for interfacial octahedral coupling as a route to enhance magnetoresistance in perovskite oxide superlattices", *Advanced Materials Interfaces* **7**, 1901576 (2020).
9. A. Dziaugys, K. Kelley, J. A. Brehm, Lei Tao, A. Puretzky, T. Feng, A. O'Hara, S. Neumayer, M. Chyasnavichyus, E. A. Eliseev, J. Banys, Y. Vysochanskii, F. Ye, B. Chakoumakos, M. A. Susner, M. A. McGuire, S. V. Kalinin, G. Panchapakesan, N. Balke, S. T. Pantelides, A. N. Morozovska, P. Maksymovych, "Piezoelectric domain walls in van der Waals antiferroelectric CuInP₂Se₆", *Nature Communications* **11**, 3623 (2020).
10. S. M. Neumayer, J. Brehm, L. Tao, A. O'Hara, P. Ganesh, S. Jesse, M. Susner, M. McGuire, S. T. Pantelides, P. Maksymovych, N. Balke, "Local strain and polarization mapping in ferroelectric materials", *ACS Applied Materials Interfaces* **12**, 38546 (2020).

Nano-optical imaging, spectroscopy, and control of quantum materials

Markus B. Raschke, Department of Physics, and JILA, University of Colorado, Boulder

Research Scope: Optical tip-based scanning probe microscopy has emerged as a frontier in optical imaging, proving *intrinsic few-nanometer spatial optical resolution* through near-field enhancement, localization, and coupling between the tip and sample. Unique to our approach in this project is the *extension into a wider range of optical spectroscopic modalities* including linear (vis to far-IR/THz), inelastic (Raman), nonlinear (second-harmonic generation SHG, and four-wave mixing FWM), and ultrafast spectroscopy with as high as few-femtosecond temporal resolution to *probe and control structure, coupling, and dynamics of elementary excitations in different quantum materials on the nanoscale* (see. **Fig. 1**).

With the combinations of different linear, nonlinear, broadband, and ultrafast spectroscopies which couple with high specificity to, e.g., excitons, phonons, lattice strain, Drude metallicity, and crystal symmetry, we gain *simultaneous* insight into *structure, coupling, and dynamics* of elementary excitations on the nanoscale in our applications to 2D, polaritonic, and correlated materials. Even in nominally homogeneous single component systems, intrinsic and extrinsic nanoscale phenomena in the form of *defects or domain/grain boundaries* control the macroscopic material property. While conventional far-field spectroscopy and imaging often obscures the origin of the macroscopic material response by spatial and ensemble averaging, *local optical probing and nano-imaging* can resolve the origin of the underlying heterogeneity.

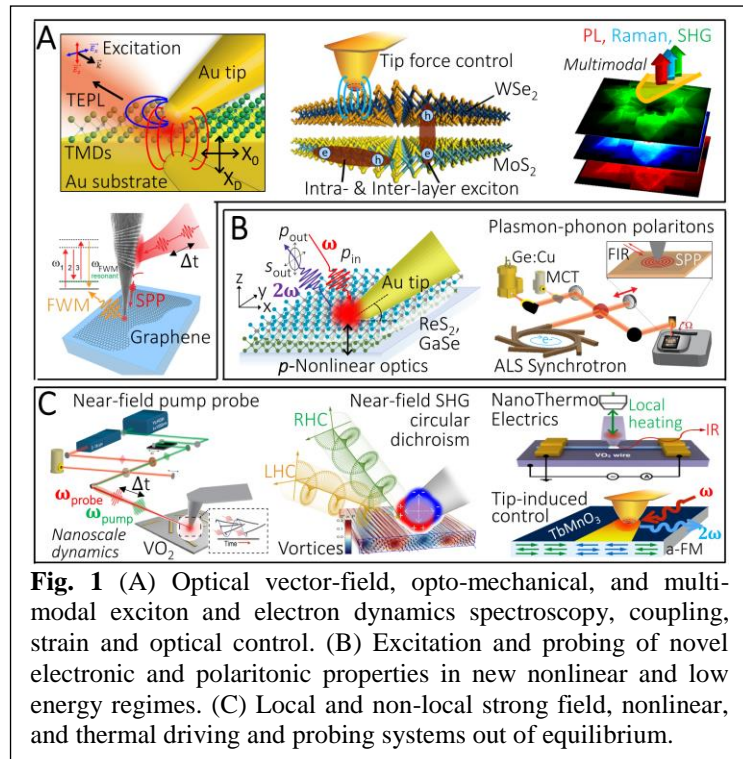


Fig. 1 (A) Optical vector-field, opto-mechanical, and multimodal exciton and electron dynamics spectroscopy, coupling, strain and optical control. (B) Excitation and probing of novel electronic and polaritonic properties in new nonlinear and low energy regimes. (C) Local and non-local strong field, nonlinear, and thermal driving and probing systems out of equilibrium.

Recent Progress: We have used the optical antenna tip properties, also in combination with broadband spectroscopy [1,2,7], nano-mechanical tip-sample force interaction [3-5], and ultrafast coherent spectroscopy [6], for nano-scale *excitation, imaging, and control of polaritonic and excitonic properties in graphene, transition metal dichalcogenides (TMDs), and their heterostructures*, with the following exemplary highlights:

A) Anisotropic flow control and gate modulation of hybrid phonon polaritons [1,2]

Light-matter interaction in two-dimensional photonic or phononic materials allows for the confinement and manipulation of free-space radiation at sub-wavelength scales. Following our work on the nano-confinement of surface plasmons in graphene (G) [Phys. Rev. Lett. 113, 055502 (2014)] and surface phonon polaritons in hexagonal boron nitride (hBN) [ACS Photonics,

2, 790 (2015)], we aimed to combine their unique attributes. In G-hBN heterostructures the hybrid hyperbolic plasmon phonon polariton (HP3) of reduced damping have been predicted theoretically to exhibit gate-tunable directional and rectified flow of polariton waves. Using ultra-broadband *s*-SNOM we demonstrated the anisotropic flow control and gate-voltage modulation of HP3 modes in GhBN on an air-Au micro-structured substrate [1,2]. The HP3 hybridization is modulated by varying the gate voltage between graphene and Au. This modifies the coupling of continuum graphene plasmons with the discrete hBN hyperbolic phonon polaritons, which is described by an extended Fano model. This work represents the first demonstration of the control of polariton propagation and augments the degree of control of polaritons in G-hBN and related hyperbolic metamaterial nanostructures.

B) Nano-optical cavity imaging and control of interlayer exciton emission [3]

Building on our earlier work on the nano-imaging of both bright [Park et al. Nano Lett. 16, 2621 (2016)] and dark excitons [Park et al. Nature Nanotechnol. 13, 59 (2018)] we have pioneered the use of plasmonic scanning probe tips as *optical nano-cavities* to enhance and control the spontaneous emission of interlayer excitons in a TMD hetero-bilayers. TMD hetero-bilayers have attracted significant attention for their ability to support *intralayer* excitons, *interlayer* excitons in which the electron and hole are trapped in separate material layers, and ultra-fast interlayer charge transfer. To realize the potential of heterobilayers for, e.g., optoelectronic applications, the ability to tune and control their properties is highly desirable. Tuning the relative decay rates of both intra- and interlayer excitons in a WSe₂/MoSe₂ heterobilayer over six orders of magnitude in tip-enhanced photoluminescence spectroscopy (TEPL) (**Fig. 2**) reveals cavity-induced crossover from nonradiative quenching to Purcell-enhanced radiation. Rate equation modeling with the interlayer charge transfer time as a reference clock allows determination from the long interlayer exciton radiative lifetime (94 ± 27) ns to the five orders of magnitude faster competing nonradiative lifetime (0.6 ± 0.2) ps. This technique of *nanocavity clock spectroscopy* (NCS) thus provides a new approach to quantify complex and competing dynamics of multi-excitonic systems complementing conventional ultrafast time-domain spectroscopy.

Building on our earlier work on the nano-imaging of both bright [Park et al. Nano Lett. 16, 2621 (2016)] and dark excitons [Park et al. Nature Nanotechnol. 13, 59 (2018)] we have pioneered the use of plasmonic scanning probe tips as *optical nano-cavities* to enhance and control the spontaneous emission of interlayer excitons in a TMD hetero-bilayers. TMD hetero-bilayers have attracted significant attention for their ability to support *intralayer* excitons, *interlayer* excitons in which the electron and hole are trapped in separate material layers, and ultra-fast interlayer charge transfer. To realize the potential of heterobilayers for, e.g., optoelectronic applications, the ability to tune and control their properties is highly desirable. Tuning the relative decay rates of both intra- and interlayer excitons in a WSe₂/MoSe₂ heterobilayer over six orders of magnitude in tip-enhanced photoluminescence spectroscopy (TEPL) (**Fig. 2**) reveals cavity-induced crossover from nonradiative quenching to Purcell-enhanced radiation. Rate equation modeling with the interlayer charge transfer time as a reference clock allows determination from the long interlayer exciton radiative lifetime (94 ± 27) ns to the five orders of magnitude faster competing nonradiative lifetime (0.6 ± 0.2) ps. This technique of *nanocavity clock spectroscopy* (NCS) thus provides a new approach to quantify complex and competing dynamics of multi-excitonic systems complementing conventional ultrafast time-domain spectroscopy.

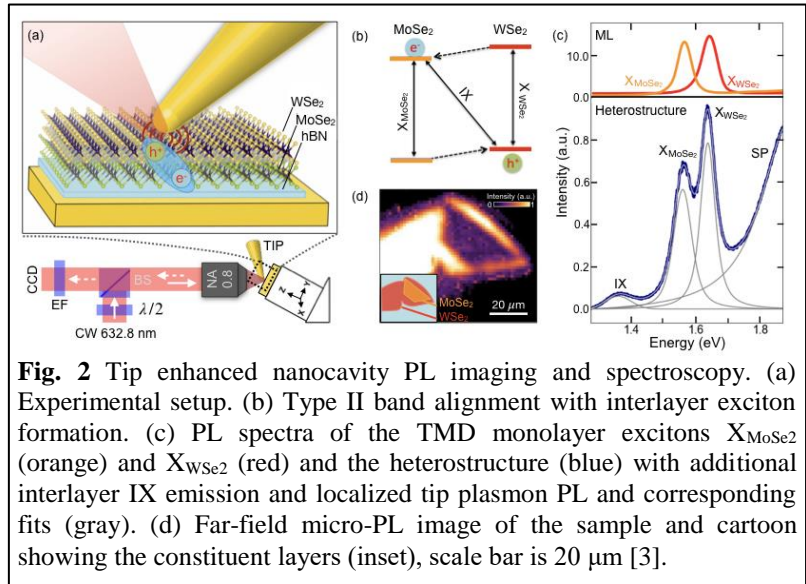


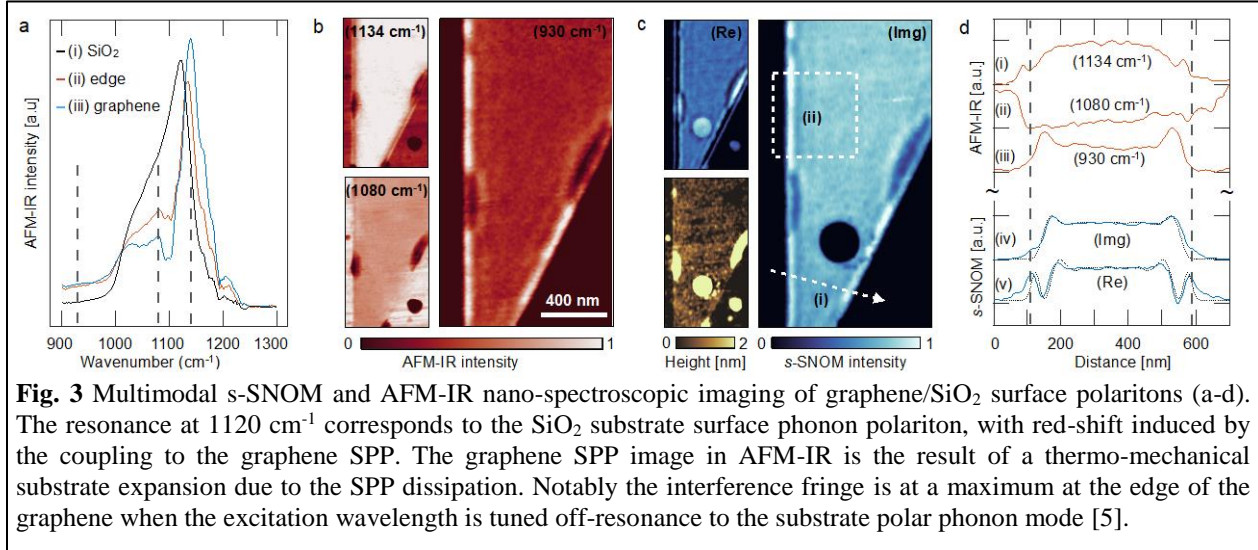
Fig. 2 Tip enhanced nanocavity PL imaging and spectroscopy. (a) Experimental setup. (b) Type II band alignment with interlayer exciton formation. (c) PL spectra of the TMD monolayer excitons X_{MoSe_2} (orange) and X_{WSe_2} (red) and the heterostructure (blue) with additional interlayer IX emission and localized tip plasmon PL and corresponding fits (gray). (d) Far-field micro-PL image of the sample and cartoon showing the constituent layers (inset), scale bar is 20 μm [3].

Building on our earlier work on the nano-imaging of both bright [Park et al. Nano Lett. 16, 2621 (2016)] and dark excitons [Park et al. Nature Nanotechnol. 13, 59 (2018)] we have pioneered the use of plasmonic scanning probe tips as *optical nano-cavities* to enhance and control the spontaneous emission of interlayer excitons in a TMD hetero-bilayers. TMD hetero-bilayers have attracted significant attention for their ability to support *intralayer* excitons, *interlayer* excitons in which the electron and hole are trapped in separate material layers, and ultra-fast interlayer charge transfer. To realize the potential of heterobilayers for, e.g., optoelectronic applications, the ability to tune and control their properties is highly desirable. Tuning the relative decay rates of both intra- and interlayer excitons in a WSe₂/MoSe₂ heterobilayer over six orders of magnitude in tip-enhanced photoluminescence spectroscopy (TEPL) (**Fig. 2**) reveals cavity-induced crossover from nonradiative quenching to Purcell-enhanced radiation. Rate equation modeling with the interlayer charge transfer time as a reference clock allows determination from the long interlayer exciton radiative lifetime (94 ± 27) ns to the five orders of magnitude faster competing nonradiative lifetime (0.6 ± 0.2) ps. This technique of *nanocavity clock spectroscopy* (NCS) thus provides a new approach to quantify complex and competing dynamics of multi-excitonic systems complementing conventional ultrafast time-domain spectroscopy.

C) Photothermal nano-imaging of dissipative surface polaritons [4,5]

We have extended our initial work on heterodyne tapping AFM-IR from nanoimaging of chemical heterogeneities [4] to the real-space characterize of photo-induced thermo-physical processes in graphene/SiO₂/silicon structures [5]. The key question we addressed is how to image the *non-radiative* thermal energy decay that inevitably accompanies the excitation of surface polariton modes? Most current experimental approaches to visualize hybridized states of

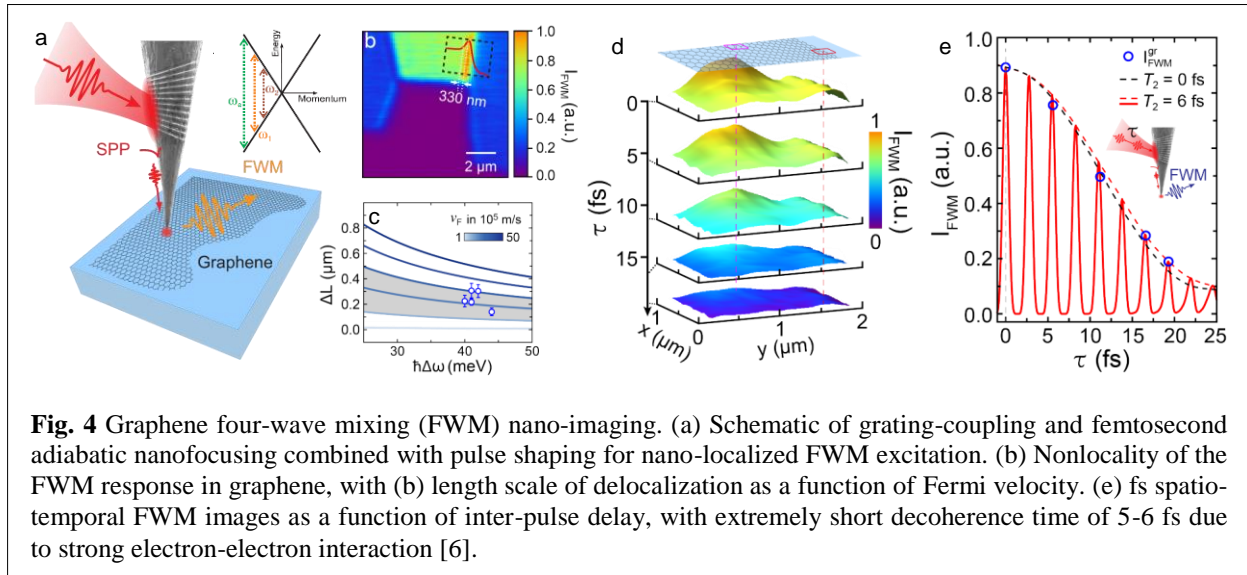
strongly confined light fields and dipolar matter excitations (e.g. plasmons, excitons, phonons) are essentially ‘blind’ to the local decay of excited SPs. To address the dissipation into the thermal bath, we have developed a multi-modal imaging approach to locally excite and visualize dissipative surface plasmon-phonon polaritons in graphene exfoliated on SiO₂. Based on correlative AFM-IR and IR-*s*SNOM measurements, we could illustrate (**Fig. 3**) that photo-thermal expansion forces uniquely facilitate the direct mechanical detection of SP modes with



down to single-atom layer sensitivity. By revealing the reflection of SPs at graphene edges in both imaging modalities, we found distinct differences between the location and the intensity of radiative and non-radiative processes, in good agreement with a phenomenological cavity model. Our observations indicated that the heat source density of the locally excited SPs could be controlled via free-carrier mobilities and geometrical interference effects of the traveling modes. Beyond the fundamental relevance to understand the details of SP decay in 2D material systems, this opens a promising route towards the dynamical shaping of nanoscale temperature fields.

D) Ultrafast coherent nonlinear nano-optics and nano-imaging of graphene [6]

Graphene exhibits unique coherent and nonlinear optical properties due to its linear energy dispersion and large dipole matrix element of the optical transitions, leading to promising optoelectronic applications. However, many details regarding the mechanism underlying the strong nonlinear response, its ultrafast coherent dynamics, and the effect of heterogeneities have remained elusive. Here, using our unique approach of femtosecond adiabatic nanofocusing and -imaging, we explore the nonlinear response of graphene in the nanometer and femtosecond regime in broadband four-wave mixing (FWM) (**Fig. 4**). We detect distinct edge enhancement and layer dependence with a strong nonlinear response from nanoscopic areas of less than 10⁴ carbon atoms. Femtosecond spatio-temporal FWM nano-imaging and concomitant frequency domain measurements reveal dephasing on $T_2 = 5-6$ fs timescales which we attribute to strong electron-electron interaction. We further identify an unusual non-local FWM response on length scales as large as 100-300 nm, which we attribute to a Doppler effect controlling the nonlinear interaction between tip plasmons with large near-field momenta and the graphene electrons with high Fermi velocity. These results highlight the distinct nonlinear nano-optical properties of graphene, expected also in related classes of 2D materials, which may pave the way for new nonlinear and ultrafast nano-photonics devices.



Future Plans: *Interlayer excitons:* We will extend the work above (B) and investigate the effects of plasmonic nanostructure proximity and layer separation on charge transfer and interlayer coupling in a variety of other TMD heterobilayers. *Localized states:* We will extend TEPL to the study of localized excitons and their quantized emitting state. These experiment will provide insight into the single photon emitting quantum devices at room temperature with active control on the nanoscale. *Coherent nano-imaging:* Continuing to address competing relaxation pathways in TMDs we are extending the few-fs coherent nonlinear nano-imaging of graphene (D) to the study of the nanometer-spatio and femtosecond-temporal of incoherent-2PPL and coherent-FWM characteristics in monolayer WSe₂. *Ultrafast pump-probe nano-imaging:* To extend spatio-temporal imaging with far-from equilibrium excitation to also probe the full transient optical response function which encodes electronic and phonon dynamics and their coupling, we recently developed ultrafast heterodyne pump-probe nano-imaging through this program. With access to space, time, and frequency of the elementary interactions, we will probe from the distinct strain vs. doping controlled heterogeneity in the photoinduced insulator-to-metal transition in VO₂ to intrinsic and extrinsic exciton relaxation pathways in WSe₂.

Publications (supported by BES, past 2 years)

- [1] F.C.B. Maia, et al. “Anisotropic flow control and gate modulation of hybrid phonon-polaritons”, *Nano Lett.* **19**, 708 (2019).
- [2] H.A. Bechtel, S.C. Johnson, O. Khatib, E.A. Muller, and M.B. Raschke, “Synchrotron infrared nano-spectroscopy and -imaging”, *Surface Science Reports* (in press).
- [3] M.A. May, T. Jiang, C. Du, K.-D. Park, X. Xu, A. Belyanin, and M.B. Raschke. “Nanocavity clock spectroscopy: resolving competing exciton dynamics in WSe₂/MoSe₂ heterobilayers”. (submitted).
- [4] B.T. O’Callahan, J. Yan, F. Menges, E.A. Muller, and M.B. Raschke, “Photoinduced tip-sample forces for chemical nano-imaging and -spectroscopy”, *Nano Lett.* **18**, 5499 (2018).
- [5] F. Menges, H. Yang, S. Berweger, T. Jiang, and M.B. Raschke, “Photothermal nano-imaging of surface polaritons”, (submitted).
- [6] T. Jiang, V. Kravstov, M. Tokman, A. Belyanin, and M. B. Raschke, “Ultrafast coherent nonlinear nano-optics and nano-imaging of graphene”, *Nature Nanotechnology* **14**, 838 (2019).
- [7] K.A. Smith, et al., “Infrared nano-spectroscopy of ferroelastic domain walls in hybrid improper ferroelectric Ca₃Ti₂O₇”, *Nature Commun.* **10**, 1 (2019).

Exploring Energy Conversion and Non-Equilibrium Carrier Distributions at the Nanoscale via Novel Scanning Probe Approaches

Pramod Reddy, Departments of Mechanical Engineering and Materials Science and Engineering, University of Michigan, Ann Arbor, MI, USA, 48109

Edgar Meyhofer, Department of Mechanical Engineering, University of Michigan, Ann Arbor, MI, USA, 48109

Keywords: Scanning Thermal Microscopy, Hot Carriers, Thermoelectrics, Single Molecule Junctions,

Research Scope

In this project we are seeking to both develop and employ novel scanning probe approaches to answer key questions regarding energy transport, conversion and dissipation at the nanoscale. Specifically, we propose to elucidate (a) the limits to energy conversion at the molecular scale by tuning the electronic structure of molecular junctions (MJs) via quantum interference and electrostatic effects and (b) probe non-equilibrium distributions of hot carriers in nanostructured plasmonic systems by leveraging MJs' unique transport characteristics. Molecular junctions, created by trapping organic molecules between inorganic electrodes, are of great current interest due to the novel quantum phenomena that arise in them. In fact, a number of recent computational studies have suggested that quantum interference effects that arise in MJs make them ideal candidates for performing energy conversion at thermodynamic limits—i.e. the Carnot limit, which describes the maximum possible efficiency achievable via reversible operation, and the Curzon-Ahlborn (CA) limit, which describes the thermodynamically maximum efficiency under conditions where the power output is maximized. However, all these predictions remain experimentally unresolved due to serious experimental challenges. A second problem of great current interest is the highly non-equilibrium distributions of charge carriers that are created when surface plasmon polaritons (SPPs) or when localized surface plasmon resonances (LSPRs) decay non-radiatively. While radiative decay pathways have been extensively explored, non-radiative decay has largely remained unexplored, because currently no experimental approach is available for quantitatively probing the carrier distributions with nanometer spatial resolution.

Recent Progress

Probing Hot Carriers in Plasmonic Thin Films (*H. Reddy et al., Science (2020)*) Plasmonic nanostructures are of great current interest due to their potential for controlling and tailoring light-matter interactions at unprecedented length scales. More recently they have drawn significant attention due to their potential for generating hot carriers that can be exploited for use in a number of important applications, including novel energy conversion approaches, catalysis, photo-detection and photo-thermal therapy. However, experimental elucidation of steady-state hot carrier energy distributions, which is key for systematically advancing and evaluating competing theoretical frameworks as well as for rationally engineering the aforementioned technologies, has not been possible to date. In recent work, we developed a novel scanning probe-based method that

overcame this outstanding challenge and showed first direct measurements of hot carrier distributions under steady-state conditions.

In our approach, we combined single molecule charge transport measurements with nanoplasmonics making possible quantitative measurement of hot carrier distributions generated from the excited surface plasmon polaritons. The central idea of this technique is to create single molecular junctions (SMJs) by trapping single molecules between the gold surfaces of the tip of a scanning probe and an excited plasmonic nanostructure. With appropriately selected molecules, the SMJs feature sharp resonances in their transmission characteristics and serve as tunable voltage-controlled energy-dependent filters—which in turn are used to directly quantify the hot carrier distributions from charge transport measurements through the junctions. From our measurements we provide the first direct experimental evidence that hot carrier generation is significantly enhanced in nanostructures due to “Landau damping” that arises from surface scattering in tightly confined nanostructures.

Probing Thermal Transport in Atomic and Molecular Junctions (*L. Cui et al., Science (2017); L. Cui et al., Nature (2019)*): One of the central goals in the last two decades in nanoscale energy transport was to extend thermal transport measurements all the way to the atomic scale and to elucidate the ultimate limits of energy and heat flow. However, while it has been possible to study charge transport and thermoelectric effects in junctions formed by single atoms and molecules, quantum thermal transport measurements in such systems involve formidable challenges that had been insurmountable previously. In 2017, we achieved (*L. Cui et al., Science (2017)*) direct measurements of the thermal conductance of metallic atomic contacts at the single-atom limit and reported the first observation of quantized thermal transport at room temperature. More recently, we further enhanced the resolution of our approach and achieved the first direct measurements of the thermal conductance in single-molecule junctions (*L. Cui et al., Nature (2019)*). Specifically, we reported the first observation of length-independent thermal transport in molecular junctions.

Probing Energy Transport via Photons in Nanoscale Gaps and Nanodevices (*B. Song et al., Nature Nanotechnology (2016); L. Cui et al., Nature Communications (2017); A. Fiorino et al., Nano Letters (2018); A. Fiorino et al., ACS Nano (2018); D. Thompson et al., Nature (2018)*): We recently achieved important breakthroughs in exploring nanoscale radiation. Specifically, we overcame several technical challenges to demonstrate that it is possible to achieve almost three orders of magnitude enhancements in the heat flux above the blackbody limit when the gap size between objects is reduced to the nanoscale. (*B. Song et al. Nature Nanotechnology (2016)*, *A. Fiorino et al., Nano Letters (2018)*, *A. Fiorino et al., ACS Nano (2018)*). In addition, by employing nanofabricated calorimeters we achieved detailed experimental evidence to demonstrate that heat transfer rates between sub-wavelength nanodevices located in the far-field of each other can surpass the blackbody limit by 100 times (*D. Thompson et al., Nature (2018)*). In addition to the results described above we also explored nanoscale thermal radiation in single-digit nanometer gaps and demonstrated that current theories are capable of describing nanoscale thermal radiation down to 1 nm gap sizes (*L. Cui et al., Nature Communications (2017)*).

Probing Energy Conversion in Nanoscale Gaps (*A. Fiorino et al., Nature Nanotechnology (2018); L. Zhu et al., Nature (2019)*): We also made key contributions to elucidate the potential of nanoscale thermal radiation for energy conversion. We showed for the first time, by employing microfabricated scanning probes and a novel nanopositioning platform, that the power output for thermophotovoltaic energy conversion at the nanoscale can exceed that at macroscopic gaps by ~40 times due to strong contributions from evanescent modes (*A. Fiorino, et al., Nature*

Nanotechnology (2018)). Next we accomplished an important breakthrough when we experimentally showed for the first time that photonic cooling can be accomplished using incoherent radiation from a semiconductor diode. This demonstration of active cooling (refrigeration) is based on controlling the chemical potential of photons in a photodiode and by taking advantage of enhanced photon transfer rates (due to photon tunnelling) that are possible in the near-field. Given the importance and novelty of these results they were published recently in *Nature* (L. Zhu *et al.*, *Nature* (2019)).

First Observation of Quantum Interference Effects on Thermoelectric Properties (*R. Miao et al.*, *Nano Letters* 2018): Recently, we reported first experimental evidence that quantum interferences can be used to enhance the thermoelectric properties of molecular junctions. Specifically, we performed both single-molecule and ensemble measurements of the electrical conductance and thermopower on molecular junctions using novel scanning probe tools. Our experiments showed that *meta*-OPE3 junctions, which are expected to exhibit destructive interference effects, yield a higher thermopower (a factor of two larger) compared to *para*-OPE3 junctions which do not feature quantum interferences. These results show that quantum interference effects can indeed be employed to enhance the thermoelectric properties of molecular junctions at room temperature.

Future Plans

In the next two years we plan to leverage the advances described above to address open questions critical in energy conversion and non-equilibrium distributions at the nanoscale. Specifically, we seek to answer the following key questions: 1) Can the electronic structure of MJs be controlled to achieve thermoelectric energy conversion efficiencies at or near the Carnot limit? 2) Can quantum interference effects be employed to achieve operation at the CA limit by creating MJs with transmission characteristics that feature both a sharp gradient and a finite width as proposed theoretically? 3) What are the thermal conductances of molecular junctions? Can phonon quantum interference effects strongly influence the heat transport properties of MJs? 4) What are the non-equilibrium distributions of hot carriers in plasmonic nanostructures when plasmons decay non-radiatively by generating electron-hole pairs? 5) What is the role of geometry of plasmonic nanostructures and plasmonic hotspots on hot carrier generation? 6) Can confinement-induced Landau damping lead to the generation of highly energetic and long lived hot carriers?

Publications

1. H. Reddy, K. Wang, Z. Kudyshev, L. Zhu, S. Yan, A. Vezzoli, S. J Higgins, V. Gavini, A. Boltasseva, P. Reddy, V. M. Shalaev, E. Meyhofer, *Determining plasmonic hot-carrier energy distributions via single-molecule transport measurements*, Science **369**, 423-426 (2020)
2. D. Thompson, L. Zhu, E. Meyhofer and P. Reddy, *Nanoscale radiative thermal switching via multi-body effects*, Nature Nanotechnology **15** (2), 99-104 (2020)
3. L. Cui, S. Hur, Z-A Akbar, J. Klockner, W. Jeong, F. Pauly, S-Y. Jang, P. Reddy and E. Meyhofer, *Thermal conductance of single-molecule junctions*, Nature **572**, 628-633 (2019)
4. L. Zhu, A. Fiorino, D. Thompson, R. Mittapally, E. Meyhofer and P. Reddy, *Near-field photonic cooling through control of the chemical potential of photons*, Nature **566**, 239-244 (2019)
5. D. Thompson, L. Zhu, R. Mittapally, S. Sadat, Z. Xing, P. McArdle, M. M. Qazilbash, P. Reddy and E. Meyhofer, *Hundred-fold enhancement in far-field radiative heat transfer over the blackbody limit*, Nature **561**, 216–221 (2018)
6. R. Miao, H. Xu, M. Skripnik, L. Cui, K. Wang, K. G. L. Pedersen, M. Leijnse, F. Pauly, K. Wärnmark, E. Meyhofer and P. Reddy, and H. Linke, *Influence of quantum interference on the thermoelectric properties of molecular junctions*, Nano Letters **18**, 5666–5672 (2018)
7. A. Fiorino, L. Zhu, D. Thompson, R. Mittapally, P. Reddy and E. Meyhofer, *Nanogap near-field thermophotovoltaics*, Nature Nanotechnology **13**, 806–811 (2018)
8. A. Fiorino, D. Thompson, L. Zhu, R. Mittapally, S-A. Biehs, O. Bezenenet, N. El-Bondry, S. Bansropun, P. Ben-Abdallah, E. Meyhofer and P. Reddy, *A thermal diode based on nanoscale thermal radiation* ACS Nano **12**, 5774–5779 (2018)
9. L. Cui, R. Miao, K. Wang, D. Thompson, L. A. Zotti, J. C. Cuevas, E. Meyhofer and P. Reddy, *Peltier Cooling in Molecular Junctions*, Nature Nanotechnology **13**, 122-127 (2018)
10. A. Fiorino, D. Thompson, L. Zhu, B. Song, P. Reddy and E. Meyhofer, *Giant enhancement in radiative heat transfer in sub-30 nm gaps of plane parallel surfaces*, Nano Letters **18**, 3711–3715 (2018)

Symmetry-breaking mechanism and metastable states in charge-ordered systems probed using femtosecond electron diffraction and spectroscopy

Chong-Yu Ruan

Michigan State University, East Lansing, MI 48824. E-mail: ruanc@msu.edu

Research Scope

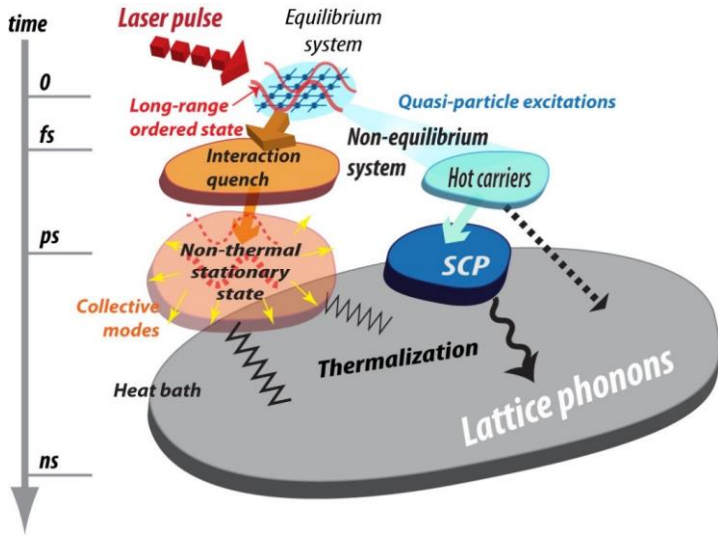
The scope of this project encompasses fundamental sciences centered on strongly correlated electrons confined in one or two-dimensional potential leading to novel phases, as well as technical development necessary to address underlying scientific questions. Our research methods are time, spatial and momentum resolved ultrafast electron probes designed to resolve light-induced transient states and associated processes. Our project will leverage on the high-brightness electron beam technology for high-throughput to critically address key aspects of photo-induced phase transition (PIPT). Our research project consists of two main thrusts centered on the different aspects of PIPT. The first thrust is to continue on the research initiative for elucidating the hitherto unresolved processes of spontaneous symmetry breaking (SSB) leading to long-range states in the charge-density waves (CDW) and strongly correlated electron systems. In this research, we will detail the subtle phonon modes tied to CDW, and the fluctuating short-range orders and emergent states through momentum and time-resolved diffuse scattering and diffraction with high-brightness electron pulses. The second thrust will address the universal nature of the nonequilibrium steady states, which exhibit scaling behaviors far from equilibrium. We seek to classify their dynamics near the nonthermal critical point.

Recent Progress

We have applied the newly developed next-generation instrumentation of femtosecond electron diffraction and microscopy systems to study PIPT phenomena in the density-wave systems and the transient state of plasma matters. The high resolutions and sensitivity of our experiments make it possible to address hitherto-unresolved dynamical features that lead to new ways of understanding and controlling non-equilibrium phases in these systems.

(i) On the study of quantum material phase transitions: universal behavior out of equilibrium. Identifying universal behavior far from equilibrium is a central goal in diverse areas ranging from quantum gases, to condensed matters(*I*). Here, we report the universal self-organization dynamics of charge-density waves (CDW) using coherent electron pulses(A1). The material is 1T-type tantalum disulfide, which harbors a variety of CDW states. We probe the evolution upon applying ultrafast laser pulses from the near-commensurate (NC) to the incommensurate (IC) state. We show that the CDW, after an ultrafast relaxation, is trapped in a nonthermal state over a long period of time, orders of magnitude longer than microscopic timescales. We can identify the remarkable universality of these non-thermal states across different laser fluences and characterize their robust dynamical criticality. Additionally, we demonstrate a sharp onset of thermalization and its

distinct universal behavior. A key phenomenon is the emergence of ‘slow’ modes of the CDW dynamics that are responsible for the long prethermalization timescales and the universal kinetics of the phase transition upon thermalization. A remarkable feature is the emergence of a hidden chiral state where a diffusion constant, characteristic of coarsening, increases by an order of magnitude. Our observation of the universal dynamics ensuing an interaction quench provides new insight beyond relevant quantum gas experiments(2); the high resolution of our experiment makes it possible to see several stages of the evolution at timescales spanning several orders of magnitude.



This figure considers the case of laser interaction quench scenario for introducing PIPT. Here, the majority of the excitation energy is stored in the photo-excited hot carriers, which effectively couple to the lattice modes through electron phonon coupling. Yet, ultrafast thermal shock of the electronic system also effectively impacts the order parameter of the long-range collective state in a nonthermal fashion -- for TaS₂, it is the suppression of the polaronic coupling between the CDW and the lattice; for CeTe₃, the driving force is changing the nesting condition. Both scenarios effectively change “the system parameters” relevant for introducing new formations of the CDW in the system before the system thermalizes with the quasiparticle bath.

(ii) **On the study of quantum material phase transitions: light-induced spontaneous symmetry breaking.** The remarkable feature associated with spontaneous symmetry breaking (SSB) is emergent scale-invariant critical dynamics in approaching a thermal critical point(1). There have been strong incentives to understand how this self-organization may proceed out of equilibrium upon approaching a nonthermal critical point(2). Here, we demonstrate a non-equilibrium SSB process where the system breaks an additional symmetry to evolve from a uniaxial order into a hidden bi-directional state. The system is cerium tritelluride in which the naturally occurring SSB ground state is the stripe-phase *c*-CDW order near room temperature(3). The ability to disentangle subtle changes in the scattering functions with a fs coherent electron probe lead to the rare opportunities to investigate the non-equilibrium physics during SSB. To this end, we resolve the non-equilibrium dynamics involving the early stage of structural formation of the new incommensurate density wave state: the spontaneous emergence of soft-mode instabilities of the new CDW order, followed by a slow onset of the coarse-graining stage to develop the long-range correlations(4). Finally, after the system relaxation back to the thermal ground state the remnants of transient orders survive as longer lived topological defects for more than 1 ns.

(iii) On the technological development: Incorporating femtosecond electron pulses into electron microscopes has enabled ultrafast electron microscopy (UEM) of solids and macromolecules with unprecedented temporal resolutions. With their ingrained field sensitivity to the local electrodynamics, ultrafast electron imaging of plasma matters or the metamaterials represents yet another frontier. In particular, retrofitting high-brightness electron sources into an UEM system may boost the sensitivity for resolving dynamics on the fs-nm scale. We have achieved both time and energy compressions in a generation II ultrafast electron microscope (UEM-II) implementing the radio-frequency cavities to establish a longitudinal optical system. This addition allows the electron microscope to utilize a large number of electrons while achieving high temporal and energy resolutions. A femtosecond field imaging modality based on this new development is introduced. Here, we employ a fine mesh close to field objects to sort out the imaging-forming electron rays, which facilitates a direct mapping between the local field perturbations and dynamical images regardless of the optical settings.

Using such a new approach, we have conducted studies of plasma waves and non-linear dynamics of the free electrons emitted from micro-structured copper surfaces upon applying intense fs laser pulses under a range of applied magnetic fields (A3). This experimental system represents a prototype for demonstrating the robustness of a field-imaging protocol for extracting the dynamical field profile from micro-structured plasma objects. The dynamics of non-equilibrium states are resolved with details of mode structures, field strengths, damping, and effective temperatures. A key finding is the cyclotron echo phenomenon underpinned by microscopically reversible cyclotron dynamics in warm plasma systems. The relatively long decay time of echoes features the weakly collisional nature and the ability of the laser-generated plasma to support new wave modes out of equilibrium. Ultimately, the image resolution is limited by the probe beam transverse emittance, which is estimated to be $\sim 0.02 \text{ mm}\cdot\text{mrad}$ (5). This gives a resolution at least on the 10 nm scale, as demonstrated by characterizing the step-edge of the supporting mesh. Time-compression of the pulses to 100 fs however leads to increase energy spread degrading the resolution to $\sim 100 \text{ nm}$. Reducing particle numbers in the electron pulses will decrease both the transverse and longitudinal emittances, leading to better performance at the cost of beam flux. We thus envision the highly flexible beam parameters and robust field-imaging protocol as demonstrated here to be very useful in efforts of directly resolving the fs/nm scale phenomena essential for studying microscopic field-active systems, from plasmonics, electrodynamics of microwave-resonators, to high-speed micro-electronics.

Future Plans

We will pursue the leads on the establishment of non-thermal critical points to understand the nature of emerging orders, which would have been destroyed had the system maintained its thermal equilibrium. The robustness of this transient ordering phenomena is closely linked to the emergent slow mode dynamics near the nonthermal critical point(1), and their protection from rapid thermalization. The theoretical understanding of the prethermalization phenomenon has been limited to relatively small systems and at low dimensionalities based on the cold atom simulator experiments(2). The non-equilibrium

universal responses from the macroscopic quantum material systems to sudden quench of the system parameters by light may serve as effective platforms to explore the non-equilibrium physics in the large condensed matter settings (A4), which will have important ramifications. Here, in the nonperturbatively driven regime, the electron and lattice distributions are strongly displaced from those at nonequilibrium. In such an environment, we expect new nesting conditions and different types of electron-lattice couplings could play a part in introducing the hidden states. To further the understanding, one would also like to know the electronic properties pertaining to the new states and understand how they would co-evolve along with the changing structural orders of the system. To this end, we will also pursue the ultrafast electron energy loss spectroscopy experiments on these systems. Providing both spectroscopic and spatial fingerprints of the hidden or transient meta-stable phases will be critical for their understanding.

References

1. U. C. Tauber, *Critical dynamics: A field theory approach to equilibrium and non-equilibrium scaling behavior*. Critical Dynamics: A Field Theory Approach to Equilibrium and Non-Equilibrium Scaling Behavior (Cambridge University Press, Cambridge, 2014), pp. 1-511.
2. T. Langen, T. Gasenzer, J. Schmiedmayer, Prethermalization and universal dynamics in near-integrable quantum systems. *Journal of Statistical Mechanics: Theory and Experiment* **2016**, 064009 (2016).
3. C. D. Malliakas, M. G. Kanatzidis, Divergence in the behavior of the charge density wave in RETe₃ (RE = rare-earth element) with temperature and RE element. *Journal of the American Chemical Society* **128**, 12612-12613 (2006).
4. L. W. Clark, L. Feng, C. Chin, Universal space-time scaling symmetry in the dynamics of bosons across a quantum phase transition. *Science* **354**, 606-610 (2016).
5. J. Williams *et al.*, Active control of bright electron beams with RF optics for femtosecond microscopy. *Structure Dynamics* **4**, 044035 (2017).

Publications

- A1. J. Williams *et al.*, Direct observation of universal dynamics of charge-density wave far from equilibrium, under review.
- A2. F. Zhou *et al.*, Nonequilibrium dynamics of spontaneous symmetry breaking into a hidden state of charge-density wave, under review.
- A3. S. Sun, X. Sun, D. Bartles, E. Wozniak, J. Williams, and C.-Y. Ruan, Direct observation of echoes and wave instabilities in laser-induced plasmas by ultrafast electron microscope, under review.
- A4. C.-Y. Ruan, (Mini-review) Non-equilibrium many-body physics with light-excited quantum materials: Viewpoints through femtosecond scattering by coherent electron pulses, submitted.

Electronic Properties of Organic Photovoltaic Systems under Mechanical Stress

Santiago D. Solares, Department of Mechanical and Aerospace Engineering, The George Washington University, Washington, DC 20052

Hanning Chen, Department of Chemistry, American University, Washington, DC 20016

Keywords: Organic Photovoltaics, Mechanical Stress, Thermal Stress, Electronic Structure

Research Scope

The overarching goal of this project is to acquire new fundamental understanding into the evolution of the electronic structure, electrical transport and nanomechanical properties of single polymer chains and bulk organic photovoltaic (OPV) devices, which operate under practical working conditions, where uncontrollable static and dynamic stresses exist due to thermal or mechanical perturbations. This work is complementary to studies focusing on highly controlled laboratory conditions. Specifically, we seek (i) to explore the degradation of OPV device performance under the application of static and dynamic mechanical and thermal stresses, studied through scanning probe microscopies, explaining such phenomena in terms of the electron physics in bulk disordered systems, and (ii) to develop a simulation platform that combines virtual scanning probe microscopy with electronic structure and transport methods, with specific application to disordered polymeric systems, such as those found in OPV devices. The project also includes SPM methodology developments for enabling intermittent-contact electrical measurements.

Recent Progress

We have recently focused on studying computationally and experimentally the transport mechanisms occurring through an organic bulk heterojunction (BHJ) consisting of the semiconducting conjugated polymer PCDTBT and the fullerene derivative PCBM, which are commonly used in organic solar cells (OSCs)

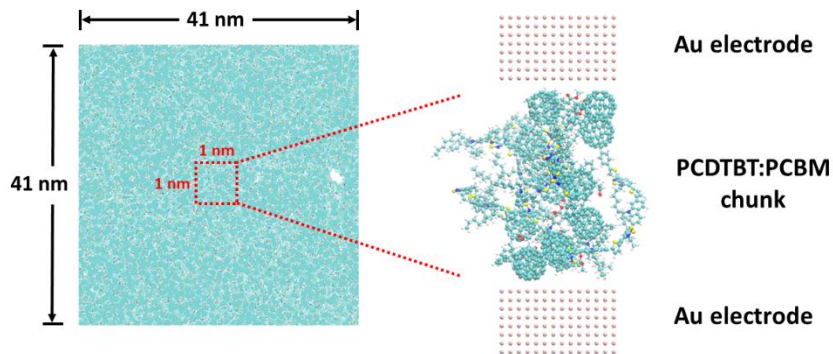


Figure 1. (411.3 x 411.2 x 200.0) Å³ structure of the PC₆₁BM/PCDTBT mixture (left), containing 500 PCDTBT trimers and 5,000 PCBM molecules, annealed by molecular dynamics simulation. Sub-domains (right) were extracted from the simulation box and placed between two gold electrodes in order to perform quantum mechanics electrical transport calculations.

[1,2]. For the computational approach (Figure 1), we have employed a numerically efficient wave function calculation approach, which is mathematically equivalent to the non-equilibrium Green's function (NEGF) formalism, to study the electrical structure and charge transport in the BHJ. We have calculated the I-V characteristics for various model structures, investigating the physical pathways of electron transport and have also visualized the local electronic density and delocalization effects. For the experimental work, we have employed a combination of macro- and microscale setups to acquire the corresponding I-V characteristics of the BHJ (Figure 2). For the macroscopic experiment, BHJ active layers were sandwiched between two centimeter-sized gold electrodes of roughly the same size. For the microscopic experiment, a gold coated microscale AFM probe bead was used as the top electrode in order to focus on a small area of interest.

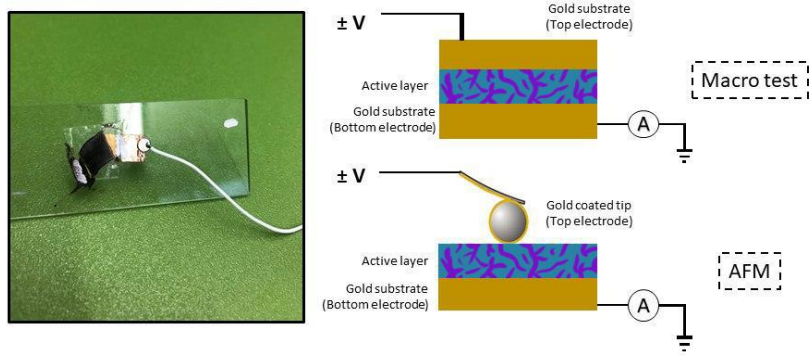


Figure 2. Schematic of the experimental setups. An active layer containing PCDTBT and PCBM (1:4) was drop cast on a gold substrate (left). Two types of experiments were performed to record the I-V curves. In the first (macro test) case, the active layer was sandwiched between two gold electrodes of roughly the same size (the active-layer coated bottom electrode with electrical contact is shown on the left). For the second case, a gold coated AFM probe was used as the top electrode in order to focus on a small area of interest.

For the experimental work, we have employed a combination of macro- and microscale setups to acquire the corresponding I-V characteristics of the BHJ

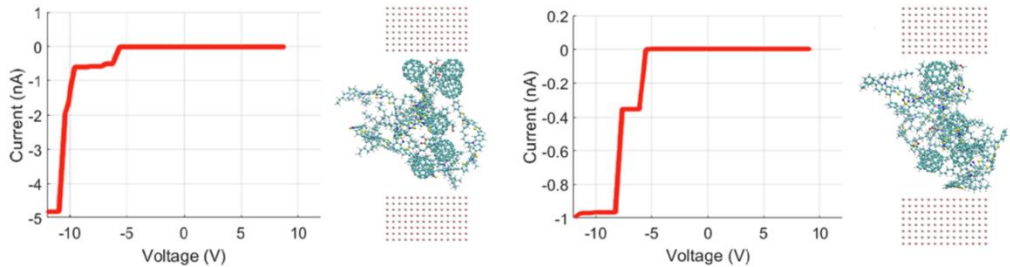


Figure 3. Examples of calculated I-V response curves for different BHJ structures. In all cases, the traces appear as step-like functions due to highly unpopulated conductance.

For the macroscopic experiment, BHJ active layers were sandwiched between two centimeter-sized gold electrodes of roughly the same size. For the microscopic experiment, a gold coated microscale AFM probe bead was used as the top electrode in order to focus on a small area of interest.

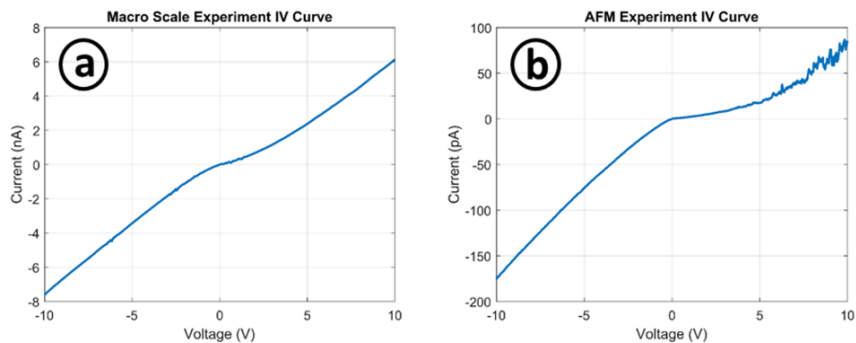


Figure 4. Examples of experimental I-V curves obtained for macroscopic (a) and microscopic experiments (see Figure 2).

The calculated I-V behavior (Figure 3) exhibited sharp, step-like curves, in contrast to the very smooth behaviors observed in the macro- and microscopic experiments (Figure 4). To explain the

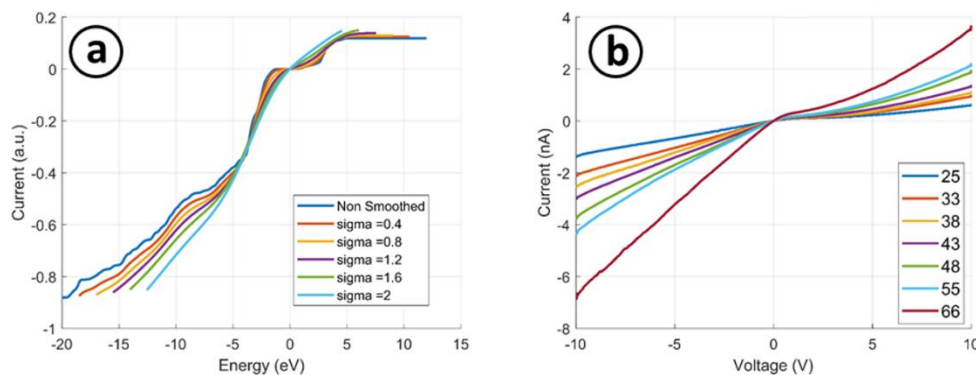


Figure 5. (a) I-V curves constructed from smoothed conductance data for the multi-molecule BHJ model. The standard deviation introduced to the conductance in broadening the calculated peaks (in eV) is provided in the figure legend. (b) Experimental macroscale I-V curves at different temperatures.

discrepancies, we applied simple models of few-molecule conductance, based on the quantum mechanics results of molecular structures similar to those of Figure 3, but including only one molecule (either PCDTBT or PCBM). Bulk behaviors were estimated assuming a large set of permutations of PCDTBT and PCBM molecules in a hypothetical conductive path containing many molecules, whereby the conductance at a specific voltage was calculated through a probabilistic combination of the conductance of the individual molecules involved in the current path. In doing this, we paid particular attention to effects such as spatial experimental length scale, spatial molecular arrangement, and localized electronic states. We also considered inelastic charge transport, allowing carrier thermalization and decay to lower-energy transport paths, as well as electron-phonon coupling, which was modeled as a low-order approximation through broadening of the conductance peaks of the molecules. Incorporation of these effects into the models led to smoother calculated I-V curves, which exhibited closer (although not perfect) resemblance to the experimental results. Figure 5 illustrates results for varying temperatures. A particularly important conclusion of this work is that no elastic conduction is expected in the positive-bias region of the I-V curve for the polymer blend (see Figure 3), and that conduction at positive bias requires the electrons to cascade down different energy levels in order to find a current path that connects the required orbitals of the polymer blend to the electrodes.

Regarding SPM methodology developments, an intermittent-contact, conductive AFM imaging mode has been developed computationally using Fourier methods, an analysis of which has been recently published [3].

Future Plans

On the experimental side, future plans will focus on the completion of the experimental matrices considering different levels of mechanical stresses (bending, uniaxial stress, etc.), considering also different solvents for the spin casting sample preparation steps, which in the past have led to different behaviors. On the computational side, larger systems will be explored through

million-atom systems using massively parallel linear-scaling density functional theory (DFT), considering explicitly electron-phonon coupling, which was only approximated statistically in the above results. These calculations will reveal the gradual perturbation of the BHJ electronic properties, which will be referenced to specific molecular deformations, rearrangements and/or segregation within the films. On the experimental methodology development front, efforts will focus on the *experimental* implementation of the intermittent-contact conductivity measurement scheme using AFM, whereby mechanical and electrical properties will be characterized simultaneously during a single 2D raster scan.

References

1. G. Li, R. Zhu, and Y. Yang, *Polymer solar cells*, Nature Photonics, **6**, 153–161 (2012).
2. S. Beaupré and M. Leclerc, *PCDTBT: en route for low cost plastic solar cells*, Journal of Materials Chemistry A, **1**, 11097 (2013).
3. B. Uluutku and S.D. Solares, *Current measurements in the intermittent contact mode of atomic force microscopy using the Fourier method: a feasibility analysis*, Beilstein Journal of Nanotechnology **11**, 453-465 (2020).

Publications

1. S. Sadewasser, N. Nicoara, and S.D. Solares, *Artefacts in time-resolved Kelvin probe force microscopy*, Beilstein Journal of Nanotechnology **9**, 1272-1281 (2018).
2. B. Uluutku and S.D. Solares, *Current measurements in the intermittent contact mode of atomic force microscopy using the Fourier method: a feasibility analysis*, Beilstein Journal of Nanotechnology **11**, 453-465 (2020).
3. R. Maiti, C. Patil, M.A.S.R. Saadi, T. Xie, J.G. Azadani, B. Uluutku, R. Amin, R. A.F. Briggs, M. Miscuglio, D. van Thourhout, S.D. Solares, T. Low, R. Agarwal, S.R. Bank and V.J. Sorger, *Strain-engineered high-responsivity MoTe₂ photodetector for silicon photonic integrated circuits*, Nature Photonics 2020 (early print, DOI: <https://doi.org/10.1038/s41566-020-0647-4>).
4. M.A.S.R. Saadi, B. Uluutku, C.H. Parvini and S.D. Solares, *Soft sample deformation, damage and induced electromechanical property changes in contact- and tapping-mode atomic force microscopy*, Surface Topography Metrology & Properties, in press.

Probing Quantum Materials with Quantitative STEM

Susanne Stemmer, Materials Department, University of California, Santa Barbara

Keywords: Scanning transmission electron microscopy, SrTiO₃, ferroelectricity, superconductivity

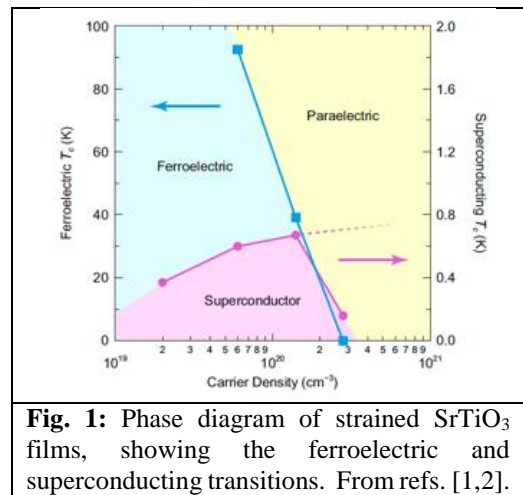
Research Scope

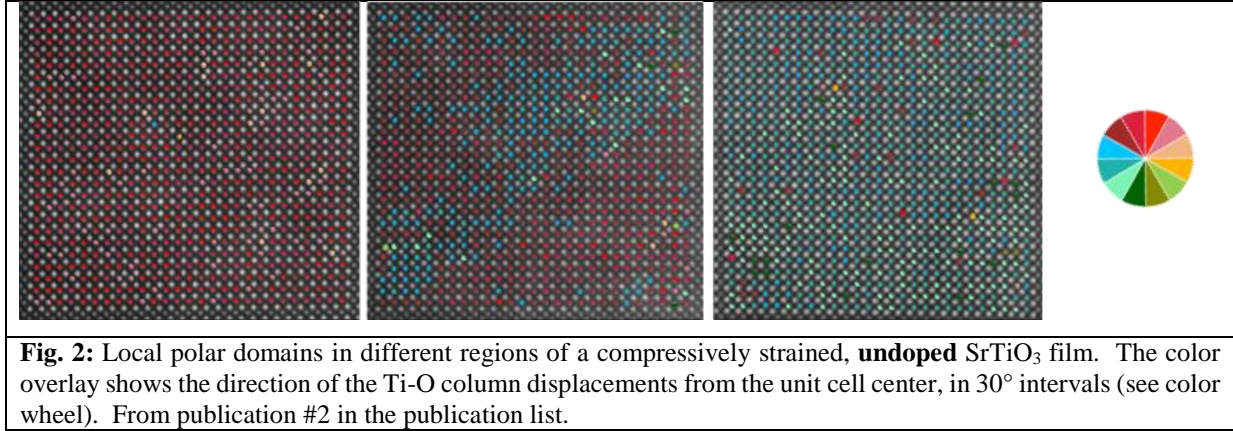
The goal of the project is to use quantitative scanning transmission electron microscopy techniques to advance our understanding of correlated quantum materials. A second important goal is to further develop quantitative STEM techniques, with a particular focus on point defects. We aim at establishing quantitative correlations between defects, local lattice distortions, global changes in crystal structure and macroscopic properties that arise from strong electron correlations. The overarching premise is a quantitative understanding of the pathways between different quantum states and the predictive description of their properties.

Recent Progress

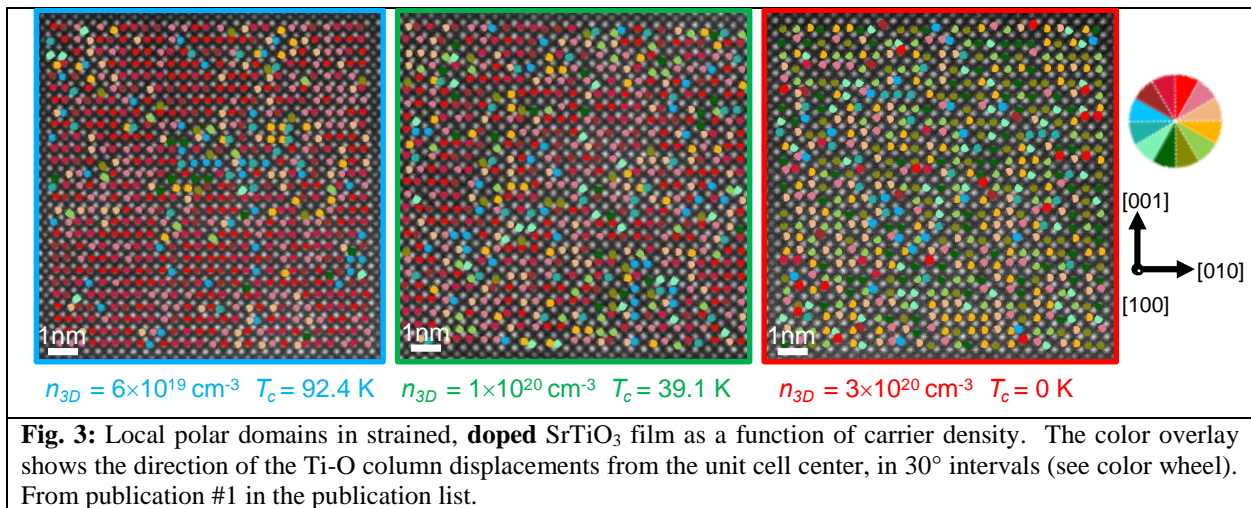
The competition between itinerant carriers and polar crystal distortions is a problem of longstanding interest and relevance to the development of a quantum theory of ferroelectricity. Elucidating the nature of this competition is also of great interest for polar superconductors, which have attracted significant interest for their potential to host unconventional superconducting states. One such candidate is doped strontium titanate (SrTiO₃), which can undergo successive ferroelectric and superconducting transitions (Fig. 1). Recent experimental observations of a factor of two enhancement of the superconducting transition temperature in ferroelectric samples [1,2] and the fact that both ferroelectricity and superconductivity vanish around the same carrier density, hint at common physical interactions that are relevant for both phenomena.

Although the ferroelectric transition of strained, undoped SrTiO₃ is usually described as a classic displacive transition, we showed that it has pronounced order-disorder characteristics. A hallmark of an order-disorder transition is the presence of a correlated symmetry-breaking distortions that are present already above the Curie temperature. In this project period, we showed that static, polar crystal distortions already exist in the *paraelectric* phase of epitaxially strained, undoped SrTiO₃ films, consistent with an order-disorder transition (Fig. 2). Doping such films with trivalent rare-earth ions, such as La and Sm, causes superconductivity to emerge from the ferroelectric state at low temperatures (Fig. 1).



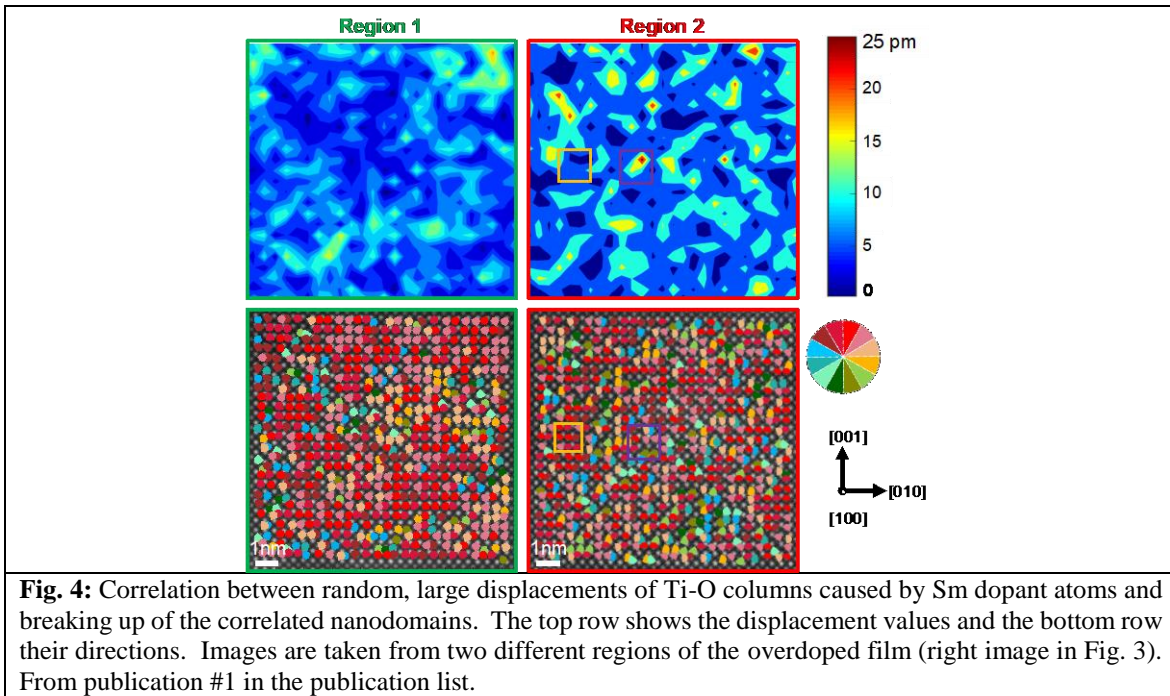


Next, we studied the evolution of polar distortions and nanodomains in the paraelectric phase of epitaxially strained SrTiO₃ films *as a function of doping density*, e.g., across the phase diagram in Fig. 1. We investigated films with carrier densities in a regime where both ferroelectric and superconducting transitions are observed (Fig. 3). We showed that the Curie temperature is inversely proportional to the *size of the nanodomains* in the paraelectric phase. Increasing the carrier concentration (Fig. 3), causes the polar nanodomains to break up into smaller clusters. The polar domains are separated by regions of randomly displaced Ti-O columns. The Ti-O column displacements become completely random in the film with the highest carrier density. No ferroelectric transition is observed in the highest doped film with only random distortions and no nanodomains. The first important conclusion, which is consistent with results from undoped films, is that polar domains in the paraelectric phase are a *necessary condition* for ferroelectricity to emerge at low temperature. The nanodomain size scales with how close the film is to the phase transition temperature. The results show that a high configurational entropy makes the ferroelectric phase transition energetically unfavorable.



Moreover, we found a second, distinct type of Ti-column displacements, which are uncorrelated and are directly associated with the Sm dopant atoms (Fig. 4). Figure 4 shows that region 1, which contains fewer dopants, has fewer large displacements. As a result, region 1 contains a large region (nanodomain) of correlated Ti-O column displacements. In contrast, region 2 only contains small polar regions that are disrupted by the random local distortions. The locations of the large displacements due to the dopants coincide with the disordered regions that break up the nanodomains.

Our results elucidate the microscopic mechanisms by which doping suppresses the ferroelectric transition. The decrease in size of the nanodomains with increasing carrier concentration is indicative of screening of long-range Coulomb interactions, which give rise to the correlated displacements, by the free carriers. While the nanodomains and displacements gradually shrink with increasing carrier density, reflecting the electronic screening, there is a second factor, namely the disorder caused by the dopant atoms themselves. Evidence of the importance of disorder is clearly seen in the overdoped sample, as discussed above. It is this second factor that contributes to the complete destruction of the nanodomains at high doping, e.g., by frustrating the dipole interactions leading to the polar displacements, thereby completely suppressing the ferroelectric transition.



Additional research in this project: We also carried out advanced STEM characterization of thin films a topological semimetal, cadmium arsenide. For example, in publication #3, we elucidated the role of dislocations in the transport properties of bulk and topological surface states,

respectively. In publication #5, we used CBED to determine the point group symmetry, which had been controversial.

Future Plans

Our immediate future work concerns the role of different types dopant atoms in the superconductivity of the SrTiO₃ films discussed above. We also continue to investigate the role of point and extended defects in topological materials.

References

1. R. Russell, N. Ratcliff, K. Ahadi, L. Dong, S. Stemmer, and J. W. Harter, *Ferroelectric enhancement of superconductivity in compressively strained SrTiO₃ films*, Phys. Rev. Mater. **3**, 091401(R) (2019).
2. K. Ahadi, L. Galletti, Y. Li, S. Salmani-Rezaie, W. Wu, and S. Stemmer, *Enhancing Superconductivity in SrTiO₃ Films with Strain*, Sci. Adv. **5**, eaaw0120 (2019).

Publications (2019-2020)

1. S. Salmani-Rezaie, K. Ahadi, and S. Stemmer, *Polar nanodomains in a ferroelectric superconductor*, Nano Lett. **20**, 6542–6547 (2020).
2. S. Salmani-Rezaie, K. Ahadi, W. M. Strickland and S. Stemmer, *Order-Disorder Ferroelectric Transition of Strained SrTiO₃*, Phys. Rev. Lett. **125**, 087601 (2020).
3. M. Goyal, S. Salmani-Rezaie, T. N. Pardue, B. Guo, D. A. Kealhofer, and S. Stemmer, *Carrier mobilities of (001) cadmium arsenide films*, APL Mater. **8**, 051106 (2020).
4. S. Salmani-Rezaie, H. Kim, K. Ahadi and S. Stemmer, *Lattice relaxations around individual dopant atoms in SrTiO₃*, Phys. Rev. Mater. **3**, 114404 (2019).
5. H. Kim, M. Goyal, S. Salmani-Rezaie, T. Schumann, T. N. Pardue, J.-M. Zuo and S. Stemmer, *Point group symmetry of cadmium arsenide thin films determined by convergent beam electron diffraction*, Phys. Rev. Mater. **3**, 084202 (2019).
6. M. Goyal, H. Kim, T. Schumann, L. Galletti, A. A. Burkov, and S. Stemmer, *The surface states of strained thin films of the Dirac semimetal Cd₃As₂*, Phys. Rev. Mater. **3**, 064204 (2019).
7. D. A. Kealhofer, H. Kim, T. Schumann, M. Goyal, L. Galletti, and S. Stemmer, *Basal-plane growth of cadmium arsenide by molecular beam epitaxy*, Phys. Rev. Mater. **3**, 031201(R) (2019). Editors Suggestion.

Intrinsic Topological Superconductors for Next-Generation Quantum Systems

Susanne Stemmer, Leon Balents, Stephen Wilson, Andrea Young, University of California, Santa Barbara

Keywords: Topological superconductors; single crystals; topological materials

Research Scope

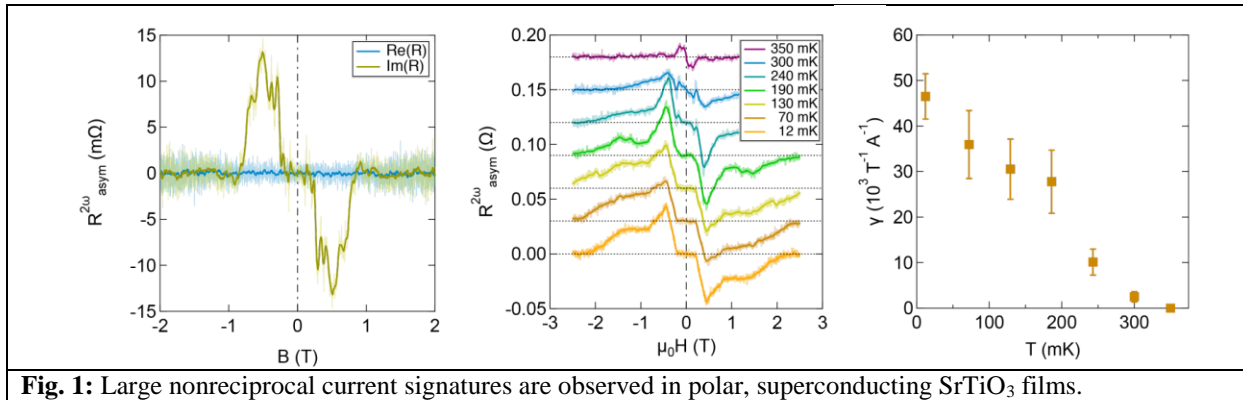
The drive to create robust, next generation quantum computing systems relies on the discovery and development of new materials capable of both hosting entangled electronic states and protecting them from rapid decoherence. Topological superconductors are an exciting frontier for realizing such protected states, but are exceedingly rare and many details remain controversial. Progress in topological band theory, recent advances in the synthesis of quantum materials and novel in-situ techniques that can detect the signatures of topological superconductors promise to accelerate the discovery of new candidate materials. Towards this objective, this project undertakes a coupled theoretical and experimental search for materials hosting topological superconductivity. Efforts focus on the prediction, growth, and characterization of topological superconductor candidates as well as the study of their exotic electronic properties. Promising new classes of materials are explored theoretically, complemented by high purity bulk crystal and tunable thin film synthesis of candidate materials and explored via novel, in-situ imaging techniques. Ultimately, the project looks to demonstrate new intrinsic topological superconductors as components for next-generation quantum devices.

Recent Progress

Synthesis of Topological Superconductor Candidate Materials: *Single crystal synthesis* focused on antiperovskites Dirac materials (such as Sr_3SnO), Sr_2RuO_4 , $\text{FeTe}_x\text{Se}_{1-x}$ and MnBi_4Te_7 . The Wilson group developed a novel, flux-based technique for large, high-quality single crystals of Sr_3SnO . Large crystals were characterized via magnetization and heat capacity measurements. Weak diamagnetism was observed, consistent with Landau diamagnetism; however, no superconductivity could be stabilized in single crystals. Experiments with polycrystalline samples determined that superconductivity appears only as a partial volume fraction of a metastable phase. The Wilson group also grew high quality Sr_2RuO_4 single crystals via high-pressure floating zone method. Using this technique, crystals can be grown without the need for excess RuO_2 during growth, yielding ultrapure single crystals that are currently being explored by the collaboration. The Wilson group also synthesized superlattices of MnBi_2Te_4 and Bi_2Te_3 that form within the material MnBi_4Te_7 . They are working to engineering dopants, such as Pd, to induce superconductivity within the Bi_2Te_3 spacing layers. Potential topological superconductivity in $\text{FeTe}_x\text{Se}_{1-x}$ alloys is an ideal materials platform for new detection schemes for topological superconductivity. Tuning the composition (x) in this system allows for the ground state to be tuned between and antiferromagnet (FeTe) and a bulk superconductor (FeSe). Recent work suggests that at $x=0.5$, a new superconducting phase emerges characterized by higher order

topology, in particular one where gapless helical edge modes appear on certain crystal boundaries protected by crystal symmetries. Because of the high $T_c \approx 14\text{K}$ and low interlayer bonding allowing for exfoliation, the crystals ideally suited to van der Waals heterostructuring and scanned probes. Wilson developed a process of producing uniform Fe concentrations through an iterated anneal-and etch process in which Fe is driven to the surface and removed by a chemical etch, leaving a nominally pristine bulk. This is an important advance because unreacted Fe is ferromagnetic and can lead to spurious magnetic signatures that are easily confused with unconventional superconductivity.

Development of Characterization Methods and Measurements: Superconductors that possess both broken spatial inversion symmetry and spin-orbit interactions exhibit a mix of spin singlet and triplet pairing. The Stemmer group focused on measurements of the superconducting properties of electron-doped, strained SrTiO_3 films. These films were previously shown to undergo a transition to a polar phase prior to becoming superconducting, making spin orbit coupling important. The Stemmer group found that that some films showed signatures of an unusual superconducting state, such as an in-plane critical field that is higher than both the paramagnetic and orbital pair breaking limits. Moreover, nonreciprocal transport, which reflects the ratio of odd vs. even pairing interaction, was observed (Fig. 1). These characteristics indicated that these films provide a tunable platform for investigations of unconventional superconductivity.



The central goal of the Young group is to detect thermal signatures of edge states in topological superconductors, providing direct evidence for protected energy transport in a topological superconductor, in a collaborative effort between single crystal synthesis, van der Waals assembly, and scanned probe thermometry. The Young group has patterned mesoscopic-thickness FeTeSe flakes into devices suitable for scanning probe thermometry measurements as well as mesoscopic transport measurements. **Error! Reference source not found.** Error! Reference source not found. shows a resistance trace in which a sharp transition at the expected superconducting T_C is evident, measured in an exfoliated flake ~ 50 nm thick. The superconducting transition does not reach zero resistance, due to high contact resistances and, potentially, mesoscopic phase separation

between superconducting and non-superconducting regions. To explore this further, the Young group has begun to perform nanoSQUID on tip

microscopy of these devices. This is a scanning tool capable of resolving deep submicron gradients in both magnetic field and local temperature.

Error! Reference source not found. **Error! Reference source not found.** **b** shows an atomic force micrograph of a patterned device with five electrical contacts and, at right, a patterned heater, designed to allow for controlled introduction of heat currents. Figures 2c-e show comparisons of topography, magnetic, and thermal images of this flake.

Notably, significant microscopic structure is evident in the magnetic and thermal images, consistent with only small pockets of

superconductivity amid a largely ferromagnetic matrix, with neither magnetic nor thermal contrast observed in thinner regions of the flake. These preliminary results point to significant inhomogeneity in the material, and are being investigated in more thoroughly annealed flakes.

Theory: Theoretical investigations focus on the response to magnetic fields and to thermal gradients, and how these may be used to prove their topological nature. To seek signatures of topological superconductivity in topological metals, the Balents group built a model for a planar junction between two intrinsically topological superconducting metals, and calculated the resulting Josephson effect. The Balents group is also building theoretical models for the effect of unconventional superconductors on phonon transport. They have developed formalism to show how electronic degrees of freedom can induce phonon Berry phases leading to observable effects on heat and sound propagation. They have developed a theory for unconventional superconductivity induced by saddle points in two-dimensional band structures. The new theory is more general and should apply also to intrinsic bulk (but quasi-two-dimensional) materials studied in the experiments described above.

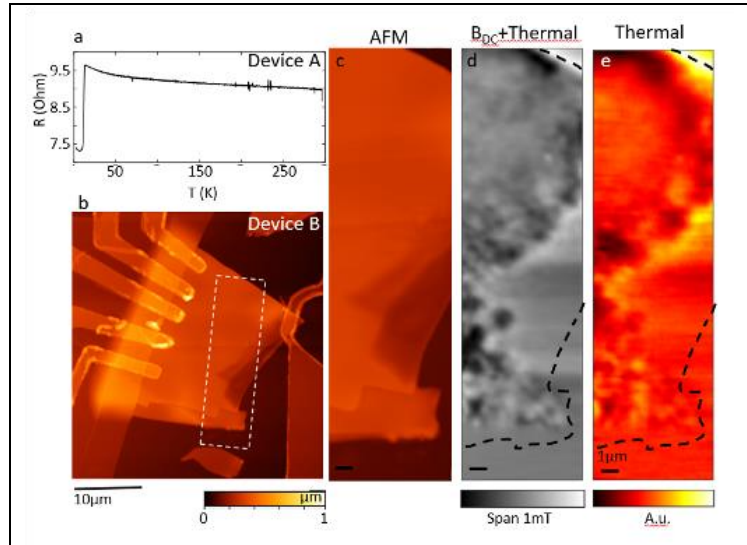


Fig. 2: Flake measurements. (a) $R(T)$ of a ~ 50 nm thick device showing a sharp superconducting transition. (b) Atomic force micrograph of a different device. (c) Section of the AFM image compared to (b) nanoSQUID image including both magnetic field and thermal contrast and (c) nanoSQUID image in a B-insensitive regime.

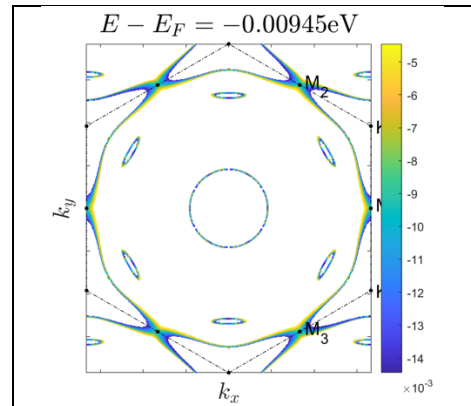


Fig. 3: Constant energy contour of band structure in CsV_3Sb_5 showing saddle point 9 meV from the Fermi energy, which can generate topological superconductivity.

Future Plans

The main focus in the experiments will be the optimization, characterization and tuning of the materials described above. Theory will be applied to materials synthesized in the Wilson and Stemmer groups.

Publications (2019-2020)

1. T. Schumann, L. Galletti, H. Jeong, K. Ahadi, W. M. Strickland, S. Salmani-Rezaie, and S. Stemmer, Possible signatures of mixed-parity superconductivity in doped, polar SrTiO₃ films, Phys. Rev. B **101**, 100503(R) (2020) (Rapid Comm.).

Exploring and Embracing Heterogeneity in Atomically Thin Energy Materials

Peter Sutter, Dept. of Electrical & Computer Engineering, University of Nebraska-Lincoln, Lincoln, NE 68588 (psutter@unl.edu); Eli Sutter, Dept. of Mechanical & Materials Engineering, University of Nebraska-Lincoln, Lincoln, NE 68588 (esutter@unl.edu)

Keywords: Cathodoluminescence, in-situ microscopy, Van der Waals crystals, heterostructures

Research Scope

Atomically thin semiconductors offer extraordinary opportunities for the manipulation of charge carriers, many-body optical excitations, quantum light emitters, and non-charge based quantum numbers. Confinement and reduced dielectric screening in these two-dimensional (2D) materials give rise to large characteristic energies so that many-body and quantum effects are important even at room temperature. Optical excitations in extended homogeneous areas have been investigated intensely, albeit mostly focusing on a limited set of materials, particularly transition metal dichalcogenides. Much less understood are light-matter interactions for other classes of 2D semiconductors, as well as effects that arise in heterogeneous materials, either near naturally occurring defects, impurities, edges and grain boundaries, or as a result of intentional interface formation in heterostructures. Addressing such systems experimentally involves significant challenges: *Understanding the atomistic growth mechanisms* of 2D semiconductors, so that novel systems with designed properties, specific ‘imperfections’, or controlled interfaces can be realized; and *probing of local excitations* at scales that match the relevant (micrometer to nanometer) length scales in heterogeneous materials. Here, we address these challenges by harnessing quantitative *in-situ* microscopy to study the growth of 2D and layered semiconductors and heterostructures, combined with local spectroscopic measurements of quasiparticles excited at the nanometer scale. An integral part of the research is the development of novel experimental approaches, both for *in-situ* microscopy of synthesis and for nanometer-scale spectroscopy. Experiments are guided and analyzed *via* computations of structure, chemistry, and excitation spectra. The particular materials focus is on group IV chalcogenides, a family of less explored 2D/layered semiconductors whose diversity in crystal structure and properties promises access to novel materials architectures and the discovery of phenomena that can support emerging technology needs.

Recent Progress

The combined probing of structure and optoelectronics with nanometer spatial resolution, a key capability developed under this program (Fig. 1), has been applied to nanostructures and heterostructures of group IV chalcogenide van der Waals semiconductors (MX, MX₂; M: Ge, Sn; X: S, Se). Correlated (scanning) transmission electron microscopy ((S)TEM), nanobeam electron diffraction, and an expanding suite of cathodoluminescence capabilities in STEM (STEM-CL)

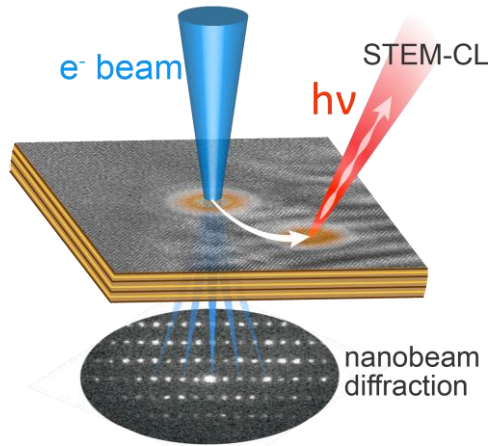


Figure 1: Combined nanobeam electron diffraction and STEM-CL on van der Waals materials and heterostructures.

have enabled advances in our understanding of novel van der Waals architectures and the discovery of interfacial phenomena in heterostructures.

i. Twisted van der Waals interfaces: Van der Waals stacks with variable interlayer twist have attracted interest as a platform for studying correlated electron phenomena supported by moirés with weakly dispersive electronic bands at specific twist angles. Such twisted layers have previously been realized only by micromechanical stacking. We demonstrated van der Waals nanowires as an unconventional system for obtaining precise interlayer twists (*Publication 2*). Using nanobeam electron diffraction along individual layered germanium monosulfide (GeS) nanowires, we discovered

a chiral structure caused by Eshelby twist due to an axial screw dislocation. STEM-CL identified variations in optoelectronic properties due to progressive changes in twist moiré registry along the nanowires. These results demonstrated an elegant alternative to mechanical stacking for realizing quantum materials based on twist moirés at van der Waals interfaces. Furthermore, *in-situ* microscopy combined with calculations allowed us to identify a process for synthesizing planar twisted van der Waals stacks. Our approach uses the growth of a 2D crystal with fixed azimuthal alignment to the substrate, followed by the solid-state transformation of this intermediate. Low-energy electron microscopy (LEEM) during growth of ultrathin orthorhombic SnS on trigonal SnS₂ showed that van der Waals epitaxy yields azimuthal order even for non-isotypic 2D crystals. Excess sulfur drives the spontaneous transformation of the few-layer SnS to SnS₂, whose orientation – rotated 30° against the underlying SnS₂ crystal – is defined by the intermediate rather than the substrate. Preferential nucleation of additional SnS on such twisted domains can repeat the process, paving the way for the realization of complex twisted stacks by bottom-up synthesis (*Publication 5*).

ii. Interfacial optoelectronics in novel van der Waals heterostructures: Major advances in the bottom-up synthesis of van der Waals heterostructures under this program have provided unique materials for probing optoelectronic phenomena at interfaces. The existence of several stable crystal phases with different chalcogen content (*e.g.*, SnS and SnS₂) formed the basis for new wrap-around heterostructures in which spontaneous phase separation produces a layered (SnS) core surrounded by a few-layer (SnS₂) shell, yielding interfaces with parallel and perpendicular van der Waals stacking (*Publication 3*). STEM-CL spectroscopy near such core-shell interfaces shows a type II band alignment with anisotropic charge separation. Spatially indirect interfacial absorption provides infrared sensitization, extending light absorption to photon energies far below those of the two constituent materials. Similar properties were realized in GeS-GeS_{2-x} core-shell structures, albeit with an amorphous shell. Here, the shell provides chemical protection that makes the encapsulated GeS van der Waals flakes long-term stable in air, in contrast

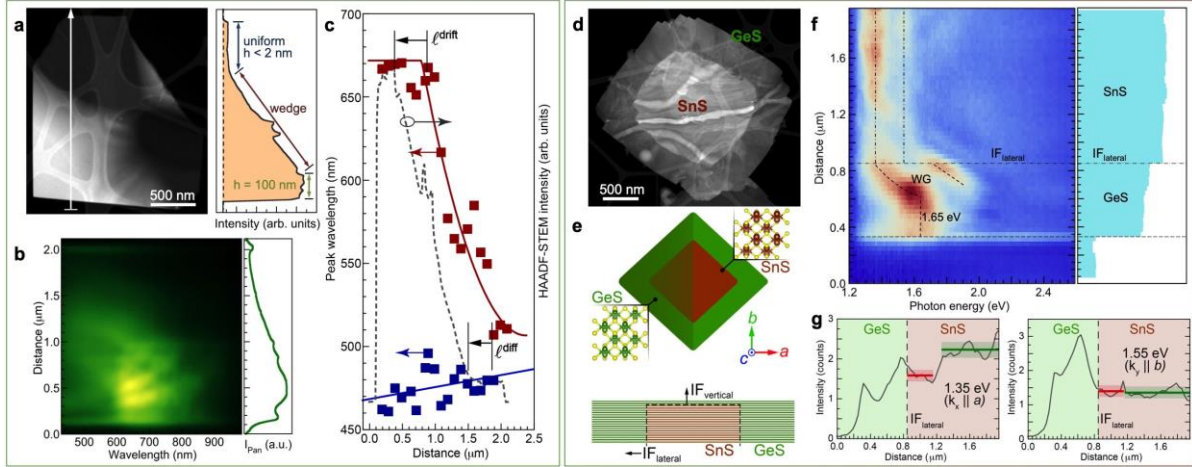


Figure 2: STEM-CL spectroscopy on GeS and GeS-SnS heterostructures. GeS-GeS_{2-x} core-shell crystals:
a. (Left) HAADF-STEM of a wedge-shaped GeS flake; (right) STEM intensity profile demonstrating the continuously varying thickness. **b.** Hyperspectral CL linescan across the wedge (line in a.), and corresponding integrated CL intensity profile. **c.** Fitted CL peaks as a function of position across the wedge, analyzed to extract the minority carrier (electron) diffusion length, ℓ^{diff} . **Valley physics in multilayer SnS-GeS lateral heterostructures:** **d.** HAADF-STEM of a SnS-GeS heterostructure. **e.** Schematic illustrating the lateral heterostructure between multilayer GeS and SnS. **f.** (Left) Hyperspectral STEM-CL linescan showing the luminescence across the lateral GeS-SnS interface (IF_{lateral}); (right) corresponding STEM intensity. **g.** CL intensity profiles at the energies of the X- and Y- valleys of SnS, showing a valley-selective luminescence quenching due to anisotropic electron transfer across the interface.

to exfoliated GeS that decomposes within hours (*Publication 4*). A type II core-shell interface again provides efficient charge separation, as demonstrated by STEM-CL. Nanometer-scale CL spectroscopy on wedge-shaped crystals allowed measuring the minority carrier diffusion length in the synthetic p-type GeS, yielding values $\ell^{\text{diff}} = 0.27 \mu\text{m}$, on par with reported diffusion lengths in the highest-quality chalcogenide semiconductors (Fig. 2a-c).

Going beyond the traditional vertical stacks and lateral heterostructures of 2D crystals, we demonstrated the integration of anisotropic layered Ge and Sn monosulfides into multilayer heterostructures with seamless lateral interfaces that intersect many individual layers (Fig. 2d, e). The anisotropic lattice mismatch at the lateral interfaces between GeS and SnS is accommodated by alloying and relaxed *via* dislocations. STEM-CL shows the characteristic light emission of joined high-quality van der Waals crystals. Using CL spectroscopy across the lateral interfaces, we discovered a valley-selective luminescence in the bulk SnS component that arises due to anisotropic electron transfer across the interface (Fig. 2f, g). The results demonstrate the ability to realize high-quality lateral heterostructures of multilayer van der Waals crystals that show fundamentally new behavior, *e.g.*, in valleytronics (*Publication 8*).

iii. Understanding synthesis through in-situ microscopy: Using *in-situ* LEEM, we established the fundamental growth mechanisms of group IV monochalcogenides that are of broad interest due to properties such as strongly bound excitons, ferroelectricity, and optically addressable valley spins. Few-layer crystals showing these properties have been challenging to obtain by exfoliation and synthesis. Real-time microscopy during growth identified the enhanced

reactivity due to an open surface structure as the origin of a fast vertical growth that hinders the synthesis of ultrathin crystals. We demonstrated several avenues for overcoming this challenge, *e.g.*, *via* surface passivation by excess chalcogens, and thus achieved unique few-layer crystals for exploring ferroelectricity, phonons, valley physics, *etc.* (*Publication 9*).

Future Plans

Combining *in-situ* microscopy of synthesis with nanometer-scale optoelectronic probes creates unique opportunities for exploring emerging phenomena in atomically thin energy and quantum materials. Building on our understanding of the fundamental growth processes, we are now able to create materials and engineered heterostructures that realize properties of interest for energy conversion and information processing, including ferroelectricity in small bandgap van der Waals semiconductors and novel photonic architectures. Continuing our focus on layered group IV chalcogenides, we will explore how phase-conversion, alloying, and phase separation produce novel heterostructure architectures, and study their interfacial light-matter interactions at the nanometer scale using STEM-CL spectroscopy and mapping. Fully addressing these opportunities also involves the development of spectroscopic microscopy techniques. For example, we will develop LEEM into a powerful tool for probing ferroelectric polarization; and we will realize new spectroscopy capabilities in STEM-CL to quantify valley polarization, excite and measure hybrid light-matter states, and characterize single photon quantum emitters in our anisotropic van der Waals crystals and heterostructures. Through these combined thrusts, we will realize the overarching goals of this program: A fundamental understanding of the ways in which defects and judiciously placed interfaces affect the interactions between light and many-body excitations, and its translation into robust materials platforms that harness imperfections for new functionality in energy conversion and information processing.

Publications

1. E. Sutter, J. Wang, and P. Sutter, *Nanoparticle-Templated Thickness Controlled Growth, Thermal Stability, and Decomposition of Ultrathin Tin Sulfide Plates*, *Chemistry of Materials* **31**, 2563 (2019).
2. P. Sutter, S. Wimer, and E. Sutter, *Chiral Twisted van der Waals Nanowires*, *Nature* **570**, 354 (2019).
3. P. Sutter, J. Wang, and E. Sutter, *Wrap-Around Core-Shell Heterostructures of Layered Crystals*, *Advanced Materials* **31**, 1902166 (2019).
4. E. Sutter, B. Zhang, M. Sun, and P. Sutter, *Few-Layer to Multilayer Germanium(II) Sulfide: Synthesis, Structure, Stability, and Optoelectronics*, *ACS Nano* **13**, 9352 (2019).
5. P. Sutter, R. Ibragimova, H.-P. Komsa, B.A. Parkinson, and E. Sutter, *Self-Organized Twist-Heterostructures via Aligned van der Waals Epitaxy and Solid-State Transformations*, *Nature Communications* **10**, 5528 (2019).
6. J. Sun, G. Giorgi, M. Palumbo, P. Sutter, M. Passacantando, and L. Camilli, *A Scalable Method for Thickness and Lateral Engineering of 2D Materials*, *ACS Nano* **14**, 4861 (2020).

7. Y. Huang, P. Sutter, E. Sutter, et al., *Universal Mechanical Exfoliation of Large-Area 2D Crystals*, Nature Communications **11**, 2453 (2020).
8. E. Sutter, J. Wang, and P. Sutter, *Lateral Heterostructures of Multilayer GeS and SnS van der Waals Crystals*, ACS Nano, in press (2020), DOI: 10.1021/acsnano.0c05978.
9. E. Sutter, J. Wang, and P. Sutter, *Surface Passivation by Excess Sulfur for Controlled Synthesis of Large, Thin SnS Flakes*, Chemistry of Materials, in press (2020). DOI: 10.1021/acs.chemmater.0c03297.

Dielectrics under Extreme Electric Fields: *In situ* studies on nanoscale mechanisms

Xiaoli Tan, Iowa State University, Materials Science and Engineering, Ames, IA

Geoff Brenneka, Colorado School of Mines, Metallurgical and Materials Engineering, Golden, CO

Keywords: *in situ* biasing TEM, dielectric breakdown, nanomaterials, oxides, point defects

Research Scope

Atomic and nanoscale defects, such as charged point defects, are suggested to be responsible for the electric breakdown in dielectrics which typically fail at 2~3 orders of magnitude below their intrinsic dielectric breakdown strengths in electric devices. In order to improve the dielectric strength of the next-generation materials for critical applications, a better understanding of the behavior of these defects in solid dielectrics under intense electric fields is needed. The scope of this project is to develop advanced techniques to characterize and study the generation and migration of defects under high electric fields *in situ* at nanoscales. This is in compliance with the goal of achieving higher energy efficiency in energy storage and distribution to meet the increasing demands in renewable energy consumption, which relies on ultimately the innovation of materials to operate reliably in extreme environments.^[1]

Under this project, we explore the potentials of the *in situ* biasing TEM technique to study responses of dielectric oxides to extreme electric fields at the nanoscale level. Enabled by the newly designed Hysitron PI95 specimen holder, we can apply electric fields up to the intrinsic strength of most dielectrics to different nanomaterials so as to observe the premature dielectric breakdown processes as well as identify the defect kinetics and mechanisms with μ s temporal resolution. Samples are coated on a heavily doped Si wedge substrate which serves as one electrode. The *in situ* holder uses a W probe with tip radius readily below 50 nm which is capable to move along the front edge of the Si wedge to serve as the other electrode. For thin film types of materials, the probe tip induces local strong electric field at pre-selected areas of the specimen to confine the breakdown region (Fig. 1). Below, we show briefly our findings on electrically induced directional crystallization in amorphous TiO₂, conductive filaments characterization in CuO_x films, field strength dependent breakdown mechanisms in TiO₂ single nanocrystals, and electron beam induced amorphization in electrically stressed BaTiO₃ nanocrystals.

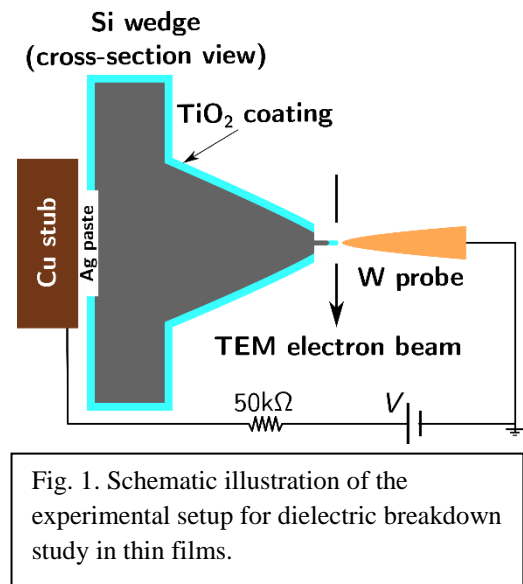


Fig. 1. Schematic illustration of the experimental setup for dielectric breakdown study in thin films.

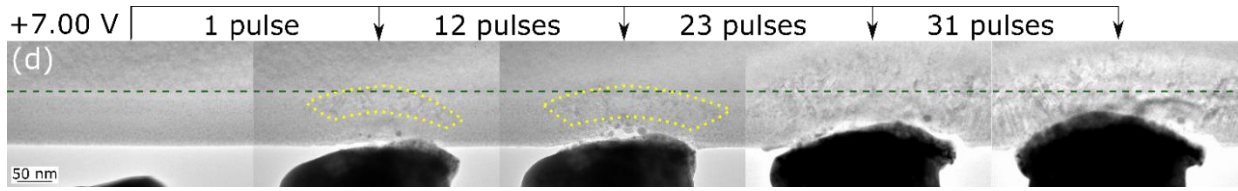


Fig. 2. Successive expansion of the field-induced structural transformation zone upon applying a series of square pulses. The green-dashed line indicates the Si (upper)/TiO₂ (lower) interface. The early-stage new phases are highlighted within the yellow-dotted lines.

Recent Progress

Using sol-gel deposition, we prepared amorphous TiO₂ (“a-TiO₂”) thin films on the Si wedge. Upon the application of 7V short pulses (100μs duration), a crystalline region forms at the Si/a-TiO₂ interface and gradually expands upon the application of additional bias pulses. Preferred growth orientation of rutile TiO_{2-x} with respect to the Si substrate is observed. Under a reversed polarity of the electric field, the amorphous to crystalline transition initiates near the W/a-TiO₂ interface, showing a polarity-dependent crystallization process. The crystalline region is found to be composed of sub-stoichiometric rutile TiO_{2-x} and the Magnéli phase Ti₃O₅. We associate the TiO₂ crystallization process with the electrochemical reduction of TiO₂ at the anode side, polarity-dependent oxygen migration, and Joule heating. The experimental results are supported by our phase-field modeling.

By using cathodic reduction of Cu(II) tartrate solution, we electrodeposited copper oxide thin films on Si wedge substrate. For two types of copper oxides (CuO and Cu₂O), dynamic conductive path formation and dissolution under intense fields are noticed. Formation of Cu₄O₃ phase is observed in the CuO film where the electric field strength is highest upon the application of electric bias as the resistance of CuO is dropping. By placing the W probe tip in several different parts of a Cu₂O film, we find that the decrease in resistivity of Cu₂O film is more extensive and occurs in an area whose size depends on the level of current compliance.

Next, we focused our work on dielectric behavior of individual nanocrystals. The TiO₂ colloidal nanocrystals were coated on the Si wedge in a process similar to Langmuir-Blodgett coating and then cleaned and sintered to a larger size (Fig. 3). As the intensity of applied

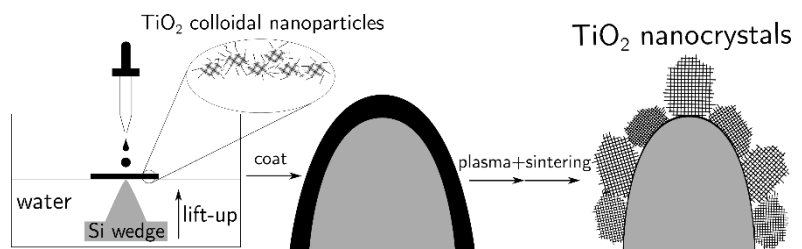


Fig. 3. Schematic illustration of the experimental setup for dielectric breakdown study in nanocrystals.

electric field on the nanocrystal increases, rutile-to-anatase phase transition (Fig. 4), local amorphization and melting (Fig. 5), or ablation are identified as the corresponding breakdown

processes based on synchronized electrical and structural characterizations. The field intensity thresholds of different behaviors are found to be related to the probe tip position and the duration of the applied bias relative to the time of charged defects accumulation. Such intensity-dependent dielectric response of crystalline oxides suggests that the initiation of premature breakdown in nanocomposite dielectrics can be suppressed through a tight control over the interface between nanocrystals and the matrix to mitigate or eliminate field modifiers.

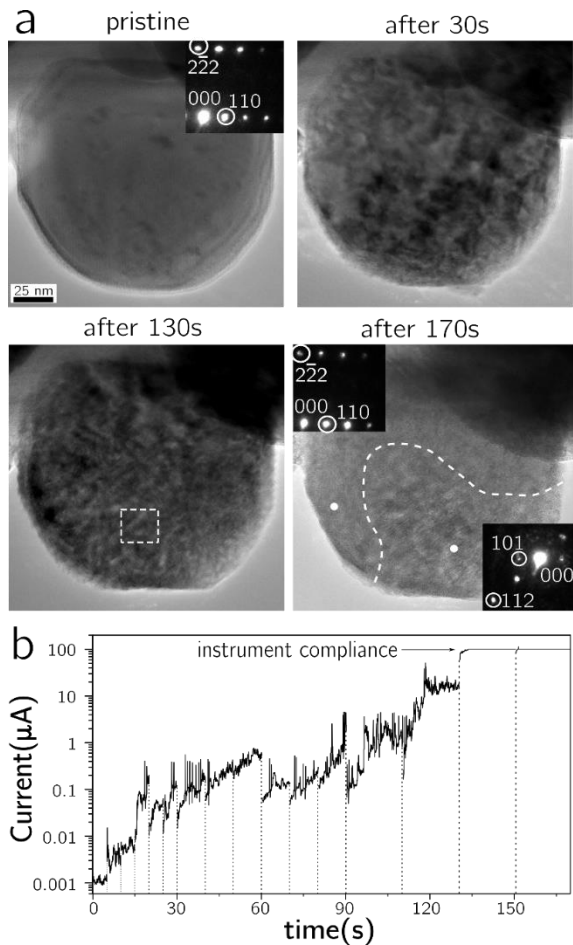


Fig. 4. Progressive dielectric breakdown and phase transition in a TiO_2 nanocrystal. (a) TEM micrographs of the nanocrystal after constant bias for different times. (b) Recorded current-time profile of the nanocrystal under the constant bias.

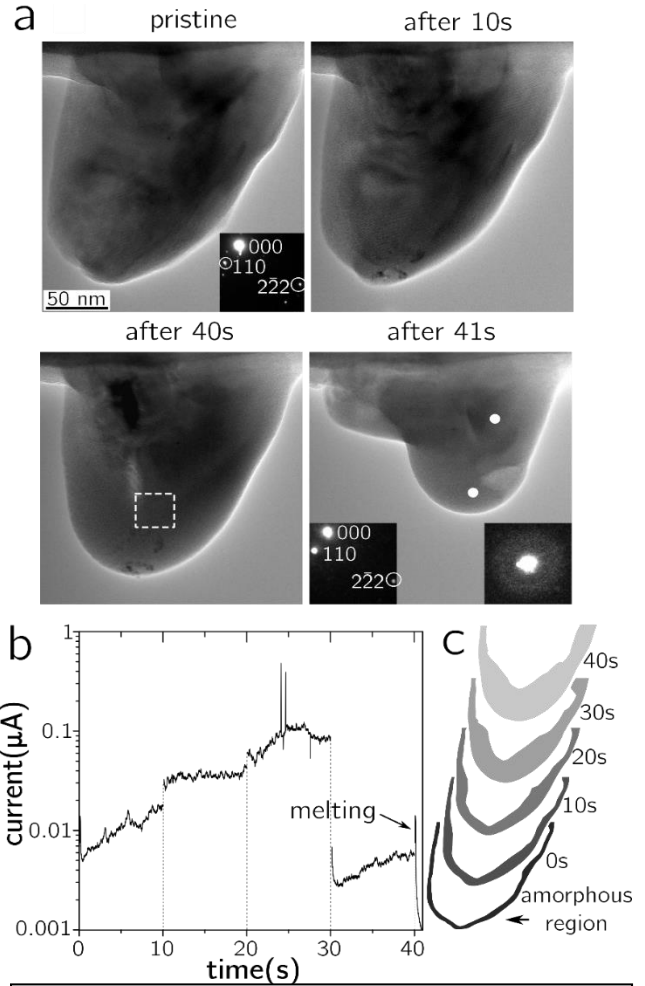


Fig. 5. Partial amorphization and melting of a TiO_2 nanocrystal. (a) TEM micrographs of the nanocrystal showing the morphology change under bias. (b) Recorded current-time profile under the constant bias.

In a similar way, we loaded BaTiO_3 perovskite nanocrystals on the Si wedge. We find in BaTiO_3 nanocrystals that formation of oxygen vacancies due to electrical stressing makes the oxide prone to amorphization under electron beam illumination in TEM. The same amorphization process is also observed in BaTiO_3 nanocrystals annealed in reduced atmosphere, suggesting that accumulation of oxygen vacancies caused either by electric stressing or chemical reduction can affect the structural stability of BaTiO_3 nanocrystals upon high energy radiation. The resistivity of the

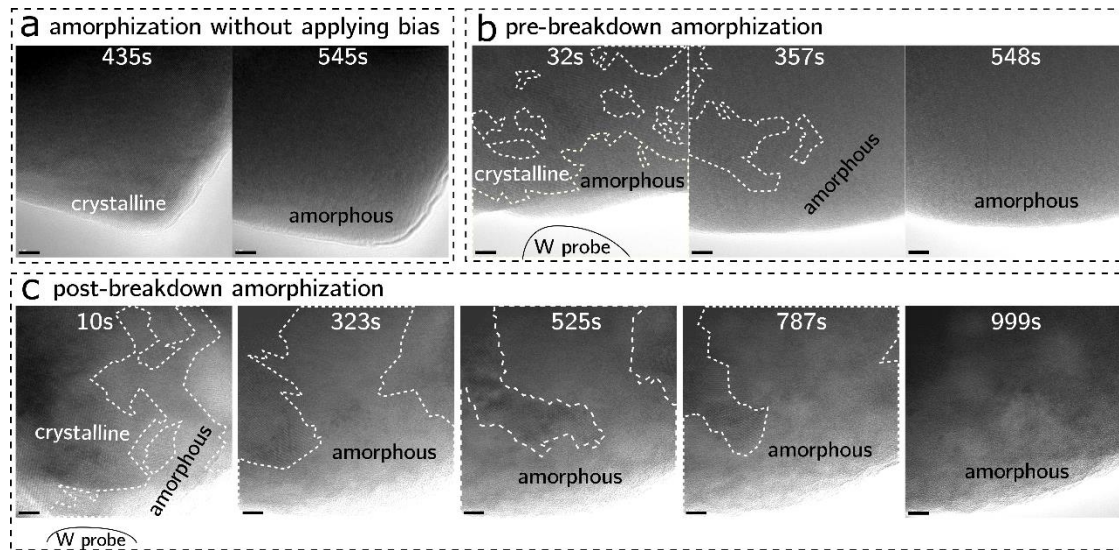


Fig. 6. Time-lapse TEM micrographs showing the amorphization process in BaTiO₃ nanocrystals after different treatments. (a) Annealed in argon atmosphere with high oxygen deficiency. (b) Applied with a constant bias of 2V for 5s. (c) After dielectric breakdown introduced by applying a constant bias at 25V for 5s to the nanocrystal. The electron beam dose rate is 2.09×10^4 e/(nm²·s). Scale bar: 5nm.

nanocrystal, on the other hand, seems not to be affected by the amorphization process, at least in the early stage. Electric stressing tends to induce clustering of oxygen vacancies in perovskite oxides^[2] and leads to an inhomogeneous amorphization process in contrast to the homogeneous process in oxygen deficient BaTiO₃ nanocrystal (Fig. 6). Electrostatic charging from the electron beam on the insulating nanocrystals is proposed to create a local electric field that drives the out-diffusion of oxygen and is accountable for the amorphization process. This finding suggests that oxygen vacancies should be monitored and controlled closely to ensure long term structure stability of the material and the extended service life of the device for future applications of perovskite nanocrystals in extreme environments.

Future Plans

The dielectric strength of materials is affected heavily by dopant type and concentration. In the remaining period of the project, we will focus on the dielectric behavior of donor and acceptor doped BaTiO₃ nanocrystals. By directly placing the doped nanocrystals on the Si wedge substrate, we will use the *in situ* TEM technique to evaluate the effects of doping on breakdown.

References

1. J. Wadsworth, G. W. Crabtree, R. J. Hemley, R. Falcone, I. Robertson, J. Stringer, P. Tortorelli, G. T. Gray, M. Nicol, and J. Lehr, S. W. Tozer, T. Fitzsimmons, J. S. Vetrano, C. L. Ashton, S. Kitts, C. Landson, B. Campbell, G. Gruzalski, D. Stevens, *Basic Research Needs for Materials under Extreme Environments*, Report of the Basic Energy Sciences Workshop on Materials under Extreme Environments, (2008).
2. J. F. Scott, and M. Dawber, *Oxygen-vacancy ordering as a fatigue mechanism in perovskite ferroelectrics*, Applied Physics Letters **76**, 3801 (2000).

Publications

1. X. Tian, G. L. Brennecka, and X. Tan, *Structural Instability in Electrically Stressed, Oxygen Deficient BaTiO₃ Nanocrystals*, *Advanced Functional Materials*, accepted, 2020. DOI: 10.1002/adfm.202004607.
3. X. Tian, S. Yazdanparast, G. L. Brennecka, and X. Tan, *In Situ Transmission Electron Microscopy Study of Conductive Filament Formation in Copper Oxides*, *IEEE Transactions on Device and Materials Reliability*, published online, 2020. DOI: 10.1109/TDMR.2020.3015398.
2. X. Tian, G. L. Brennecka, and X. Tan, *Direct Observations of Field-Intensity-Dependent Dielectric Breakdown Mechanisms in TiO₂ Single Nanocrystals*, *ACS Nano* **14**, 8328 (2020).
4. X. Tian, C. Cook, W. Hong, T. Ma, G. L. Brennecka, and X. Tan, *In Situ TEM Study of the Amorphous-to-Crystalline Transition during dielectric Breakdown in TiO₂ Film*, *ACS Applied Materials & Interfaces* **11**, 40726 (2019).
5. X. Tian, T. Ma, L. Zhou, G. L. Brennecka, and X. Tan, *In Situ TEM Study of the Transitions Between Crystalline Si and Nonstoichiometric Amorphous Oxide Under Bipolar Voltage Bias*, *Journal of Applied Physics* **125**, 245304 (2019).

Probing Majorana States in Topological-Superconductor Proximity Systems

Stuart Tessmer

Department of Physics, Michigan State University, East Lansing, MI 48824

Dale Van Harlingen

Department of Physics, University of Illinois at Urbana-Champaign, Urbana, IL 61801

Alex Levchenko

Department of Physics, University of Wisconsin, Madison, Madison, WI 53706

Research Scope

The primary goals of the projects involve the creation and detection of Majorana states in topological-superconductor proximity systems. Moreover, understanding the physics of the topological insulator (TI)/superconductor interface is key for all of the proposed projects. Working as a close collaboration between experiment and theory, we are advancing three interconnected studies: Probing Majorana States in Josephson-Junction Devices; Electronic and Magnetic Imaging of MF States; Development of Scanning Majorana Microscopy.

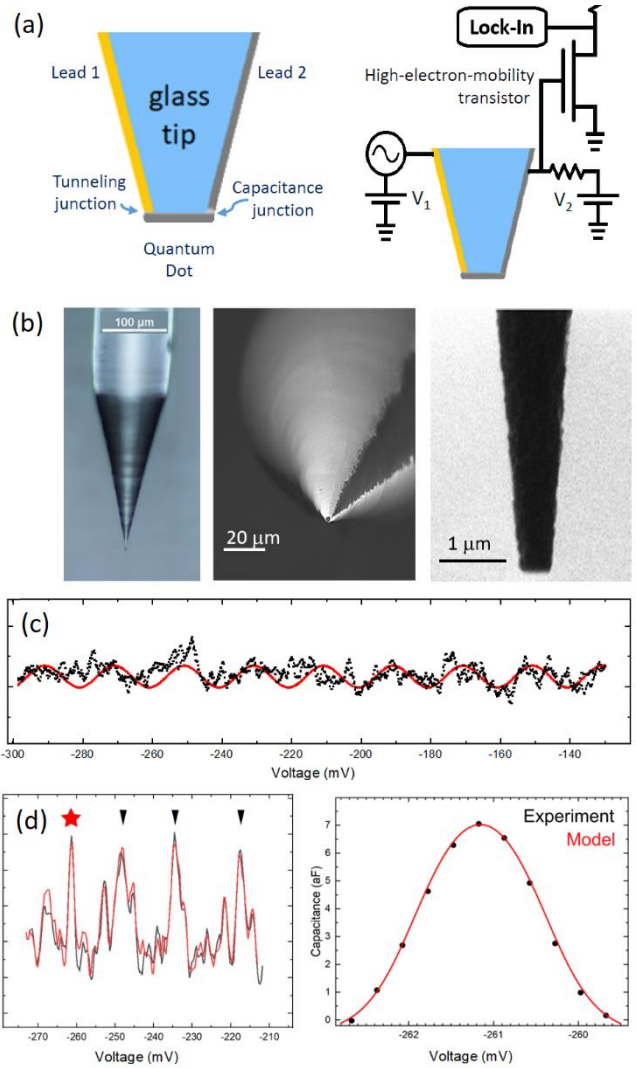
Recent Progress

Development of Scanning Majorana Microscopy

Majorana bound state candidates can be identified in experiments by the emergence of the zero-energy resonances. However, a critical challenge of these measurements is to exclude the other false-positive contributions to zero-bias peaks that are ubiquitous in condensed matter systems. In addition to tunneling conductance signatures of Majorana states, theory predicts that full counting statistics could provide unambiguous identification of these elusive states. Of particular use is a study of a mesoscopic device consisting of a quantum dot (QD) coupled to a Majorana bound state and two symmetric normal leads [1]. The Keldysh path-integral approach was used to compute the frequency dependence of the cumulants $C_n(w)$ of the current fluctuation flowing through the QD. The most remarkable property of cumulants is that they exhibit plateaus corresponding to the universal sequence of values $\{C_1(w), C_2(w), \dots, C_8(w)\} = \{1/2, 1/4, 0, -1/8, 0, 1/4, 0, -17/16\}$ in the frequency range $w < \min\{\Gamma, \kappa^2/\Gamma\}$, where $\Gamma(\kappa)$ is tunnel coupling between the leads (Majorana mode) and the QD. The sequence of universality is governed by $C_n(0) = E_{n-1}(1)/2$ where $E_n(x)$ is the Euler polynomial. Interestingly this result is independent of the microscopic parameters such as the QD energy level and QD-MF coupling strength. The measurement of such cumulants has the potential to uniquely identify the presence of the Majorana modes, excluding false-positive signatures in the tunneling transport.

We are developing a new scanning probe microscope based on this theoretical insight: the Scanning Majorana Microscope (SMM). Fig. 1 shows a schematic of the instrument, consisting of a quantum dot and two electrical leads fabricated onto a glass tip. The counting statistics of electrons entering the dot can be measured, similar to the operation of a scanning SET microscope. However, by employing a capacitance-based single-electron detection method, the technique only requires one tunneling lead which is protected from mechanical contact with the

Figure 1. (a) Scanning Majorana Microscope schematics. (b) Optical and SEM images of the probe tip. (c, d) Capacitance measurement versus voltage across the dot, V_2-V_1 . Part (c) shows a roughly periodic charging pattern superposed with its dominant Fourier component. Part (d) shows similar data at an expanded scale. The sharp peaks are highly reproducible. The fit to the right shows a well-isolated peak (star) compared to the shape expected for single-electron resonances. These data were acquired in a top loading helium-3 cryostat at a temperature of 280 mK.



surface. In this way the microscope allows the quantum dot wavefunctions to hybridize with surface states, including candidate Majorana states, without compromising the single-electron detection circuit. Hence this microscope represents a tool for detecting Majoranas that can reach beyond other experimental probes. As shown in the figure, the capacitance characteristics demonstrate that we can detect single electrons. Moreover, we have shown that single-electron detection is robust; similar capacitance data are observed before and after allowing electron tunneling from the apex of the tip to a conducting sample. We have applied for a patent for this method.

Scanning SQUID Microscopy Imaging

We have continued to use the technique of scanning SQUID Microscopy, which we helped pioneer

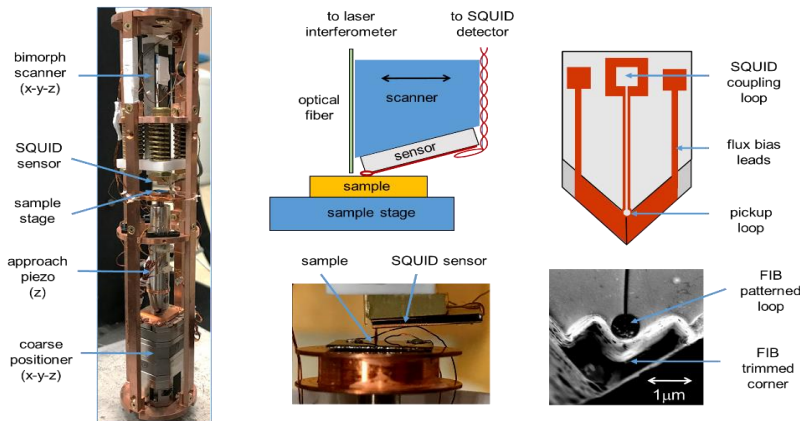


Figure 2. Scanning SQUID Microscope designed for operation at ultralow temperatures, showing details of the scanning stage and the custom superconductor pickup coil coupled to a dc SQUID detector.

[2], to image Josephson vortices that support Majorana fermions in S-TI-S (superconductor-topological insulator-superconductor) Josephson junctions in a magnetic field [3,4]. Prior to the shutdown of our labs due to COVID, we had installed our SQUID scanning stage into a wet He-3 system and verified operation of the laser interferometry that is used to monitor the location of the SQUID probe and its

distance from the sample surface. Most of the attention has been on sensor development, a challenging component of our system since we require spatial resolution not standardly achieved in SSM detectors. We developed a technique based on electron-beam lithography and FIB (focused ion beam etching) to fabricate superconducting pickup coils with submicron dimensions at the corner of a crystal, designed to allow the sensor to be located close to the sample, as shown in Figure 2.

When were not able to continue experiments, we carried out extensive simulations of the spatial distribution of supercurrents in the S-TI-S junctions to determine the expected location and signatures of the Majorana states. These will valuable for designing our sensors and interpreting SSM imaging data.

Semiclassical Theory for Superconducting and Topological Proximity Effects

Experimentally, Nb/Bi₂Se₃ nanostructures were probed cryogenically with scanning tunneling microscopy. We observed clear spectroscopic features of the topologically-protected surface states of the Bi₂Se₃ leaking into the superconducting material [5]. This section describes the theoretical development of a semiclassical theory for the description of superconductivity in multi-band metals that is applicable to the experimental system, Project (2), below.

We developed semiclassical theory that covers both systems hosting correlated electronic states as well as topological materials. The approach is based on deriving Eilenberger equations with general boundary conditions at heterostructure interfaces. We revealed the connection between our theory and the circuit theory of Andreev reflection and extended it to superconducting junctions of arbitrary nature. In particular, our approach allows to account for competing interactions and consider spatially inhomogeneous problems of superconducting state with coexisting order parameters. We used this formalism to consider two types of problems.

For Project (1), we considered the Josephson effect between two multiband superconductors with competing superconducting and magnetic interaction. As a particular example, we studied a proximity circuit between two disordered extended s-wave superconductors allowing for the coexistence between superconductivity and spin-density-wave orders. The intra- and inter-band disorder-induced scattering was treated within the self-consistent Born approximation. We calculated the spatial profile of the corresponding order parameters on both sides of the interface with a finite reflection coefficient and used our results to evaluate the local density of states at the interface as well as critical

supercurrent through the junction as a function of phase or applied voltage. Our methods are particularly well suited for describing spatially inhomogeneous states of superconductors where e.g. controlled structural disorder can be created by an electron irradiation. For Project (2), we revealed dual nature of superconducting and topological

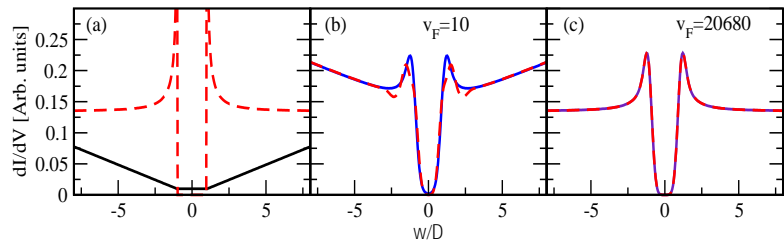


Figure 3. Panel (a) shows density of states for the Fu-Kane model (solid black line) and for the standard BCS model (dashed red line). For comparison, panels (b,c) show the density of states for our full model with two hybridization couplings $\gamma=0.5\Delta$ (solid lines) and $\gamma=2\Delta$ (dashed red lines) whose strength is measured in units of superconducting gap Δ . These panels differ by a choice of Fermi velocity in the effective band model.

proximity effects by studying the hybridization mechanism between corresponding surface states. We found that not only superconducting correlations can be induced into topological insulator, but the reverse effect occurs as well when Dirac surface states leak into the adjacent superconductor. To describe this physics, we considered experimentally relevant geometry of superconducting droplets deposited on the surface of the topological insulator. To determine an effective properties of topological surface states we integrated out superconducting degrees of freedom in the effective model that enables us to determine renormalized density of states. Conversely, by integrating over the topological insulator we find an effective density of states in the superconductor that reveals linearly dispersing behavior at energies above the superconducting coherence peaks. We find that this effect is extremely sensitive to the strength of hybridization and details of the band structure.

Future Plans

With respect to scanning Majorana Microscopy, our plan for the coming year is to apply the SMM method to probe Majorana candidates in topological insulator/superconductor samples, including Josephson junctions and vortex geometries. These studies have been delayed significantly by the COVID disruptions.

With respect to Scanning SQUID Microscopy Imaging, our initial plan for the coming year is to complete the Josephson vortex imaging measurements that have been considerably delayed by the disruption of lab access during COVID. In addition, we will target two development projects in the next year: (1) to install the SSM in a dry dilution refrigerator, which we believe will be necessary to track the Majorana fermion states in braiding and hybridization experiments, and (2) to incorporate a SET (single-electron transistor) onto the pickup coil of our SSM to enable simultaneous charge sensing designed to readout the parity of the Majorana states bound to the Josephson vortices. Figure 4 shows the design of the hybrid SSM/SET sensor.

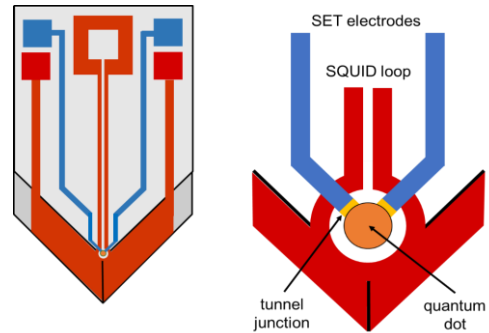


Figure 4. Hybrid SSM/SET detector for simultaneous magnetic imaging of Josephson vortices and charge imaging of the parity of Majorana bound states bound to them.

References

- [1] Dong E. Liu, Alex Levchenko, and Roman M. Lutchyn, *Majorana zero modes choose Euler numbers as revealed by full counting statistics*, Phys. Rev. B **92**, 205422 (2015).
- [2] L. N. Vu, M. S. Wistrom, and D. J. Van Harlingen. *Imaging of vortices in superconducting networks and clusters by scanning SQUID microscopy*. Appl. Phys. Lett. **63**, 1693-1695 (1993).
- [3] C. Kurter, A. D. K. Finck, Y. S. Hor, and D. J. Van Harlingen, *Evidence for an anomalous current-phase relation in topological insulator Josephson junctions*. Nature Comm. **6**, 7130 (2015).
- [4] S. S. Hegde, Y. Wang, E. Huemiller, G. Yue, D. J. Van Harlingen, and S. Vishveshwara, *A topological Josephson junction platform for creating, manipulating, and braiding Majorana bound states*, <http://arxiv.org/abs/1907.02935v1> (2019).
- [5] (2) N. Sedlmayr, E.W. Goodwin, M. Gottschalk, I. M. Dayton, C. Zhang, E. Huemiller, R. Loloee, T. C. Chasapis, M. Salehi, N. Koirala, M. G. Kanatzidis, S. Oh, D. J. van Harlingen, A. Levchenko, S. H. Tessmer, *Dirac surface states in superconductors: a dual topological proximity effect*, arXiv:1805.12330 (2020).

Publications

- (1) A. A. Kirmani, Maxim Dzero, Alex Levchenko, *Quasiclassical circuit theory of contiguous disordered multiband superconductors*, Phys. Rev. Research 1, 033208 (2019).
- (2) Nicholas Sedlmayr, E.W. Goodwin, Michael Gottschalk, Ian M. Dayton, Can Zhang, Erik Huemiller, Reza Loloee, Thomas C. Chasapis, Maryam Salehi, Nikesh Koirala, Mercouri G. Kanatzidis, Seongshik Oh, D.J. van Harlingen, Alex Levchenko, Stuart Tessmer, *Dirac surface states in superconductors: a dual topological proximity effect*, arXiv:1805.12330 (2020).
- (3) E.W. Goodwin, Michael Gottschalk, Reza Loloee, Alex Levchenko, Stuart Tessmer, *Strong-coupling scanning quantum dot microscope*, Review of Scientific Instruments (in preparation).
- (4) Nicholas Sedlmayr and Alex Levchenko, *STM signatures of hybridized superconductor and topological insulator surface states in an inverse proximity effect*, Solid State Communications, special issue on Spintronics (in preparation).

Tools for and Applications of 4D STEM to Functional Materials

Paul M. Voyles and Dane Morgan, Department of Materials Science and Engineering, University of Wisconsin-Madison

Keywords: 4D STEM, neural networks, transition metal dichalcogenides, Heusler alloys, ferroelectrics

Research Scope

4D STEM is a powerful and rapidly developing method for characterizing the structure and functional properties of materials.¹ In it, a probe is scanned across a sample to provide spatial sampling while a high speed pixelated camera acquires a convergent beam electron diffraction (CBED) pattern at every position to provide reciprocal space sampling. The resulting data sets are large, rich, and often noisy. They can be analyzed to create bright-field, dark-field, or synthetic images of the sample, to measure local strain fields or ferroic distortions, or to measure internal electric and magnetic fields.¹

This project supports development of mathematical and software tools for analyzing large 4D STEM data sets and applications to characterization of the structure and functional properties of materials, especially involving point defects. In the past two years, tools we have developed include convolutional neural networks (CNNs) for directly extracting local TEM sample thickness from atomically-resolved 4D STEM data and tensor singular value decomposition (SVD), a fast, effective method for denoising 4D STEM data. We have applied 4D STEM to study the geometry of WS₂ multilayer mesostructures with interlayer twists governed by the cone-shaped morphology of the crystals, not by a central screw dislocation, and to study the lattice distortions and ferroelectric polarization in hexagonal Heusler alloys, a new class of functional materials.

Recent Progress

4D STEM Methods

We have developed convolutional neural networks (CNNs) for direct determination of a property of interest about the sample from 4D STEM data.^C We selected TEM sample thickness as the easiest property for a first attempt, since it has the greatest influence on the CBED patterns. We also determined thickness from patterns averaged over only a single atomic column, rather than the unit cell averaging used in similar previous.² We used multislice simulations to generate labeled data for SrTiO₃ [100] as a function of thickness, then augmented that data by adding randomly-generated Poisson noise, rotations, center shifts, shears, and scale shift distortions.

Figure 1 shows the performance of two different types of CNNs. One is a classification network (c-CNN), which assigns each pattern to a 2 nm wide range of thickness (the class). The other is regression network (r-CNN), which assigns each pattern a real-valued thickness, based on

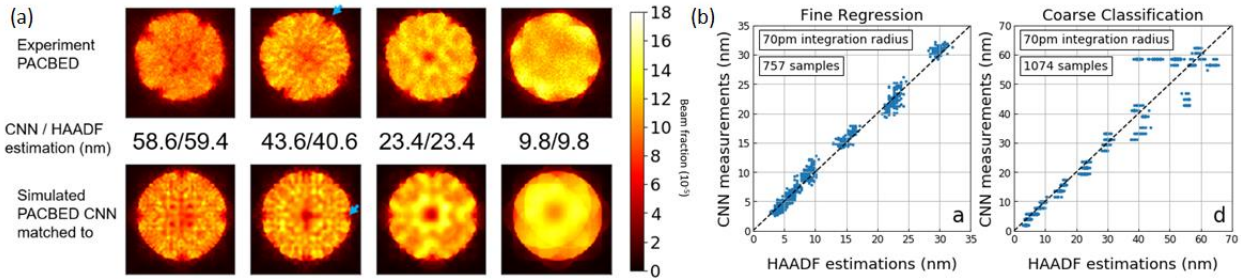


Figure 1: CNN analysis of 4D STEM data. (a) Example column-resolved PACBED patterns compared to the matches from simulated training data selected by the classification CNN. (b) Performance of the regression and classification CNNs as a function of local sample thickness estimated from quantitative HAADF STEM.

interpolation between thicknesses in the training data set. Figure 1(a) shows example matches between experimental and simulated CBED patterns for the c-CNN. Figure 1(b) shows the CNN-derived thickness versus the thickness independently determined from quantitative HAADF STEM. The networks perform well, with root mean square deviation from the HAADF thickness of 1.0 nm for thicknesses up to 35 nm. CBED simulations and network training are computationally intensive, but the CNNs execute on a single pattern in ~ 1 ms, making real-time feedback to the microscope operator possible.

As direct electron cameras increase in speed and lower electron doses are sought to avoid beam damage to sensitive materials, 4D STEM data sets grow noisier and noisier. However, the size of 4D STEM data poses challenges to state-of-the-art denoising schemes that depend on non-local methods (see, *e.g.* Ref. 3). Non-local methods render the data into “patches”, which are overlapping subsets of the data, which explodes the data size, rendering processing of even a few GB 4D STEM datasets impractically slow. We have collaborated with Anru Zhang’s group to developed tensor SVD as an approach to denoising 4D STEM datasets.^A Tensor SVD estimates a low-rank representation of a the 4D STEM data, making it similar in spirit to the widely-used principle component analysis (PCA) approach. Unlike PCA, which works only for 2D matrices, tensor SVD works with matrices (tensors) of any size and shape, which allows tensor SVD to make use of structure in the data in both (x, y) and (k_x, k_y) , leading to better denoising performance. Figure 2 that tensor SVD outperforms other commonly used and state-of-the-art approaches, quantified by peak signal to noise ratio (PSNR), a suitable image quality measure for Poisson-noise corrupted data. Tensor SVD can be executed in GB-scale datasets in a few minutes on a desktop computer.

Figure 3(a)-(h) show examples of tensor SVD denoising of experimental 4D STEM data on a SrTiO_3 [100] test sample and a LiZnSb Heusler ferroelectric thin film. Both the reconstructed ADF images and the single CBED patterns are significantly improved, although this primarily reveals the lower quality of the LiZnSb TEM sample. In particular, the arcs of the objective aperture

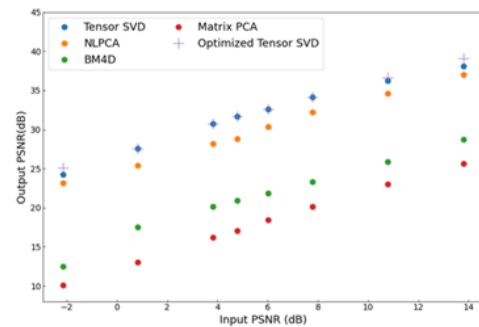


Figure 2: Denoising performance of various algorithms for a simulated SrTiO_3 [100] 4D STEM data set corrupted by Poisson noise.

edges outside BF disk are clearly visible in Figure 3(d) but not in Figure 3(b). Tensor SVD also improves more complicated signals derived from 4D-STEM data. Figure 3(i)-(l) show the recently-developed symmetry STEM signal,⁴ for the case of a 180° rotation. SrTiO₃ has 180° rotation symmetry on all the atomic column sites, as reflected in the image computed from noiseless simulations (Figure 3(l)), but with corrupting noise artifacts appear as lower computed symmetry on the Sr sites (Figure 3(j)). The denoised results (Figure 3(k)) recover the correct pattern of symmetries.

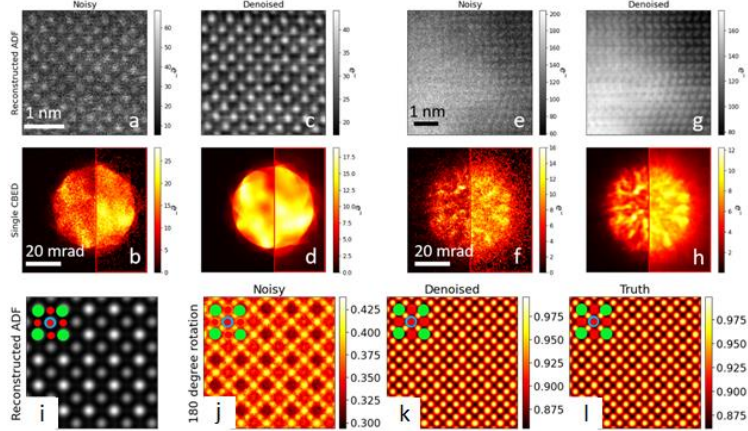


Figure 3: 4D STEM denoising with tensor SVD. Experimental data on (a)-(d) SrTiO₃, (e)-(h) LiZnSb, showing a reconstructed ADF image and CBED pattern before and after denoising. The right half of each CBED is shown a square root intensity. (i)-(l) Symmetry STEM signals for simulated SrTiO₃ and a 180° rotation, showing artifacts in the noisy data that are removed with denoising.

Materials Applications

We have worked with Song Jin's group to understand the structure of WS₂ and WSe₂ twisted, mesostructures they observed in samples fabricated by chemical vapor deposition.^B The morphological interlayer twist in these structures is large and highly variable, in strong contrast to the small twists achievable in Eshelby twist structures.⁵ As shown in Figure 4, we used 4D STEM to show that the lattice orientation of the WS₂ crystal exhibits the same interlayer twist as the morphology. The atomic moiré patterns arising from the twist (Figure 4(d)-(f)) create novel optical second harmonic generation,^B and are expected to create other properties.

The origin of the twist in these structures is a small protrusion from the substrate, visible as a bright feature in the center of Figure 4(a). The protrusion nucleates the crystal, which then grows in a cone shape draped over the protrusion. The geometry of the cone determines both the twist angle and screw dislocation crystallography of the spiral, with a shaper cone angle resulting in a larger interlayer twist. Controlled introduction

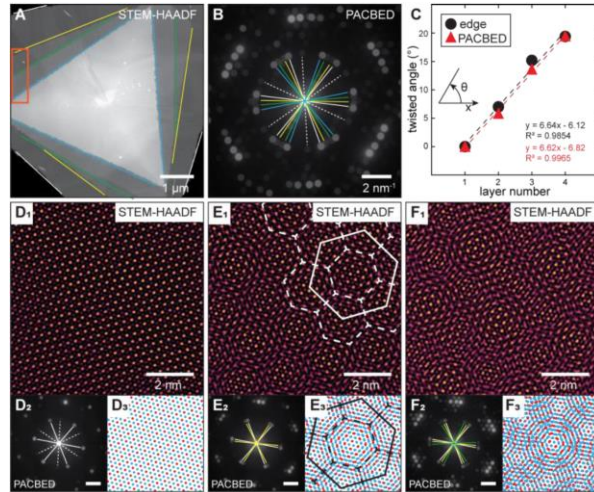


Figure 4: (A) HAADF image of a twisted WS₂ plate (B) Summed PACBED collected from the red rectangular region in (A). (C) Twist angles measured by morphology and diffraction as functions of the layer number, showing highly correlated linear relationships. (D1-F1) High-resolution HAADF images collected from the 1-, 2-, and 3- layer areas in in (A). The images were high-pass filtered for better visualization. (D2-F2) PACBED collected from areas corresponding to (D1-F1). (D3-F3) Moiré patterns corresponding to (D1-F1) using WS₂ atomic models (W in red, S in blue).

of protrusions offers an avenue for tailoring the twist angle of the resulting structures. Thus, this growth method offers a clean, *in situ* path to synthesis of twisted transition - metal dichalcogenide structures.

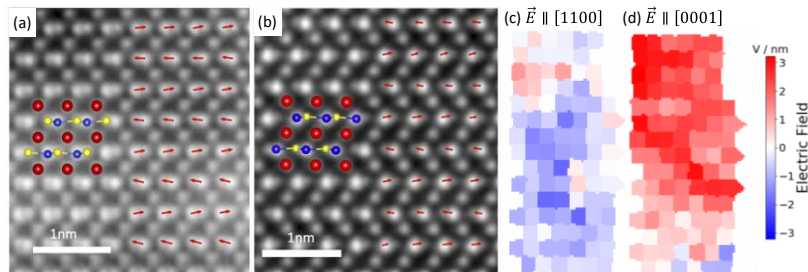


Figure 5: High precision HAADF STEM images of buckling distortions of (a) LaPtSb and (b) LaAuGe. (c) and (d) 4D STEM COM images of the internal electric field along the [1100] and [0001] directions in the LaPtSb.

Hexagonal Heusler alloys with the chemical

formula ABC and the LiGaGe structure type (space group $P6_3mc$) can exhibit buckling of the BC (0001) planes which creates a polar distortion of the crystal structure. If the material is semiconducting, the buckling has been predicted to create hyperferroelectric materials which can maintain high polarization in the face of large depolarizing fields. If the material is metallic, the buckling has been predicted to create a polar metal. We have studied both types of buckled hexagonal Heuslers. LiZnSb is a hyperferroelectric^E and LaPtSb and LaAuGe are polar metals.^G Figure 5 shows the structure of LaPtSb and LaAuGe films. The polar buckling has a mean value of 22 pm for LaPtSb and 18 pm for LaAuGe. Figure 5(c) and (d) show 4D STEM center of mass images of the electric field of the LaPtSb, averaged over a unit cell of the crystal to reduce the effect of the nuclear charges. Naïvely, mobile charges in a polar metal should screen the intrinsic field, but that does not seem to be the case. The average field is ~ 2 V/nm and is maintained even when the entire dataset is averaged together.

Future Plans

Under separate support, we are developing an ultrafast direct electron camera, capable of data acquisition at up to 120,000 frames per second and ~ 2.5 pA / pixel. Installation has been substantially delayed by COVID-19 disruptions, but is now anticipated by mid-November. In its last six months, this project will support integration of the camera with our 4D-STEM acquisition system and characterization of the camera performance for 4D STEM. Farther in the future, we plan to use the new camera for time-resolve ptychographic imaging experiments on defects in twisted and pristine transition metal dichalcogenide materials and functional Heusler and half Heusler alloy thin films and membranes.

References

1. Ophus, C. Four-Dimensional Scanning Transmission Electron Microscopy (4D-STEM): From Scanning Nanodiffraction to Ptychography and Beyond. *Microsc. Microanal.* **25**, 563–582 (2019).
2. Xu, W. & Lebeau, J. M. A deep convolutional neural network to analyze position averaged convergent beam electron diffraction patterns. *Ultramicroscopy* **188**, 59–69 (2018).
3. Yankovich, A. B. *et al.* Non-rigid registration and non-local principle component analysis to improve electron microscopy spectrum images. *Nanotechnology* **27**, 364001 (2016).
4. Krajnak, M. & Etheridge, J. A symmetry-derived mechanism for atomic resolution imaging. 1–7 (2019).
5. Liu, Y. *et al.* Helical van der Waals crystals with discretized Eshelby twist. *Nature* **570**, 358–362 (2019).

Publications

10 most relevant publications out of the 14 supported by this project in 2019 and 2020.

- A. Chenyu Zhang, Rungang Han, Anru R. Zhang, Paul. M. Voyles, *Denoising Atomic Resolution 4D Scanning Transmission Electron Microscopy Data with Tensor Singular Value Decomposition*, (submitted)
- B. Yuzhou Zhao, Chenyu Zhang, Daniel D. Kohler, Jason M. Scheeler, John C. Wright, Paul M. Voyles, Song Jin, *Super-twisted spirals of layered materials due to non-Euclidean surfaces*, Science (to be published)
- C. Chenyu Zhang, Jie Feng, Luis Rangel DaCosta, Paul. M. Voyles, *Atomic Resolution Convergent Beam Electron Diffraction Analysis Using Convolutional Neural Networks*, Ultramicroscopy **210**, 112921 (2020). DOI: 10.1016/j.ultramic.2019.112921
- D. Estiaque H. Shourov, Ryan Jacobs, Wyatt A. Behn, Zachary J. Krebs, Chenyu Zhang, Patrick J. Strohbeen, Dongxue Du, Paul M. Voyles, Victor W. Brar, Dane D. Morgan, Jason K. Kawasaki, *Semi adsorption-controlled growth window for half Heusler FeVSb epitaxial films*, Phys. Rev. Mat. **4**, 073401 (2020) DOI: 10.1103/PhysRevMaterials.4.073401 ArXiv: 2003.05971
- E. Dongxue Du, Patrick J. Strohbeen, Hanjong Paik, Chenyu Zhang, Konrad Genser, Karin M. Rabe, Paul M. Voyles, Darrell G. Schlom, Jason K. Kawasaki, *Control of polymorphism during epitaxial growth of hyperferroelectric candidate LiZnSb on GaSb (111)B*, J. Vac. Sci. Tech. B **38**, 022208 (2020). DOI: 10.1116/1.5145217
- F. Yizhan Wang, Yeqi Shi, Ziyi Zhang, Corey Carlos, Chenyu Zhang, Karishma Bhawnani, Jun Li, Jingyu Wang, Paul M. Voyles, Izabela Szlufarska, Xudong Wang, *Bioinspired Two-Dimensional Growth of Monocrystalline Oxide Nanosheets*, Chemistry of Materials **31**, 9040 (2019). DOI: 10.1021/acs.chemmater.9b03307
- G. Dongxue Du, Amber Lim, Chenyu Zhang, Patrick J. Strohbeen, Estiaque H. Shourov, Fanny Rodolakis, Jessica L. McChesney, Paul Voyles, Daniel C. Fredrickson, Jason K. Kawasaki, *High electrical conductivity in the epitaxial polar metals LaAuGe and LaPtSb*, APL Materials **7**, 121107 (2019). DOI: 10.1063/1.5132339
- H. Zefeng Yu, Chenyu Zhang, Paul M. Voyles, Lingfeng He, Xiang Liu, Kelly Nygren, Adrien Couet, *Microstructure and microchemistry study of irradiation-induced precipitates in proton irradiated ZrNb alloys*, Acta Mat. **178**, 228 (2019). DOI: 10.1016/j.actamat.2019.08.012
- I. Aidan Combs, Jason Maldonis, Jie Feng, Zhongnan Xu, Paul Voyles, Dane Morgan, *Fast approximate STEM image simulations from a machine learning model*, Adv. Struct. Chem. Im. **5**, 2 (2019) DOI: 10.1186/s40679-019-0064-2
- J. Patrick Strohbeen, Dongxue Du, Chenyu Zhang, Estiaque Shourov, Fanny Rodolakis, Jessica McChesney, Paul M. Voyles, Jason Kawasaki, *Electronically enhanced layer buckling and Au-Au dimerization in epitaxial LaAuSb films*, Phys. Rev. Mat. **3**, 024201 (2019). DOI: 10.1103/PhysRevMaterials.3.024201

Visualizing emergent phenomena in topological and quantum materials

Weida Wu

Department of Physics and Astronomy, Rutgers University, Piscataway, NJ, 08854

Keywords: MFM, topological insulators, domain walls, antiferromagnets, chiral edge states

Research Scope

The objective of this proposal is to visualize emergent topological quantum phenomena such as chiral spin texture, antiferromagnetic domain walls and chiral edge states to understand the fundamental mechanisms. Combining magnetic imaging and other complementary techniques such as *in-situ* transport, the PI will investigate magnetic domains, domain walls and chiral edge states in magnetic topological insulators, surface magnetism and possible surface spin-flop transition, and chiral spin texture in two-dimensional ferromagnets.

Recent Progress

- *Magnetic imaging of domain walls in the antiferromagnetic topological insulator MnBi₂Te₄*

The control of domain walls or spin textures is crucial for spintronic applications of antiferromagnets. Despite many efforts, it has been challenging to directly visualize antiferromagnetic domains or domain walls with nanoscale resolution, especially in magnetic field. In a recent work,¹ we report magnetic imaging of domain walls in several uniaxial antiferromagnets, the topological insulator MnBi₂Te₄ (MBT) family, using cryogenic magnetic force microscopy (MFM). The MBT family was predicted and confirmed to be an antiferromagnetic TI that may host QAH and axion-insulator states in thin films with odd and even numbers of septuple layers (SLs) respectively.¹⁻⁵ Our MFM results reveal higher magnetic susceptibility inside the domain walls than in domains. Domain walls in these antiferromagnets form randomly with strong thermal and magnetic field dependence. The direct visualization of these domain walls and domain structures in the magnetic field will not only facilitate the exploration of intrinsic topological phenomena in antiferromagnetic topological insulators but will also open a new path toward control and manipulation of domain walls or spin textures in functional antiferromagnets.

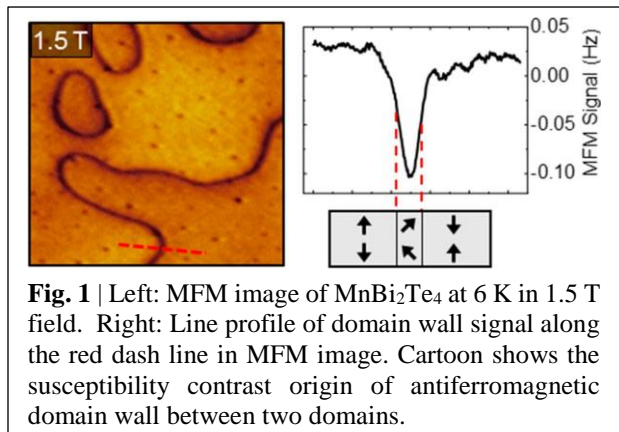


Fig. 1 | Left: MFM image of MnBi₂Te₄ at 6 K in 1.5 T field. Right: Line profile of domain wall signal along the red dash line in MFM image. Cartoon shows the susceptibility contrast origin of antiferromagnetic domain wall between two domains.

- *Robust A-Type Order and Spin-Flop Transition on the Surface of the Antiferromagnetic Topological Insulator MnBi₂Te₄*

Recent transport measurements on exfoliated thin flakes provide compelling evidence for these predictions,^{4,5} suggesting gapped topological surface states. On the other hand, recent high-resolution angle-resolved photoemission spectroscopy (ARPES) studies reveal gapless (or small

gap) surface states below the antiferromagnetic ordering temperature, suggesting a surface relaxation of the A-type order and/or the formation of nanometer-sized magnetic domains.⁶⁻⁹ The domain structure of MnBi_2Te_4 was revealed by imaging of antiferromagnetic domain walls by our MFM studies.¹ The observed domain size is on the order of $10\ \mu\text{m}$, excluding the speculated nanometer-size domain scenario.⁶ In this work, we present microscopic evidence of the persistence of uniaxial A-type antiferromagnetic order to the surface layers of MnBi_2Te_4 single crystals using magnetic force microscopy.¹¹ Our results reveal termination-dependent magnetic contrast across both surface step edges and domain walls, which can be screened by thin layers of soft magnetism. The robust surface A-type order is further corroborated by the observation of termination-dependent surface spin-flop transitions, which have been theoretically proposed decades ago. Our results not only provide key ingredients for understanding the electronic properties of the antiferromagnetic topological insulator MnBi_2Te_4 , but also open a new paradigm for exploring intrinsic surface metamagnetic transitions in natural antiferromagnets.

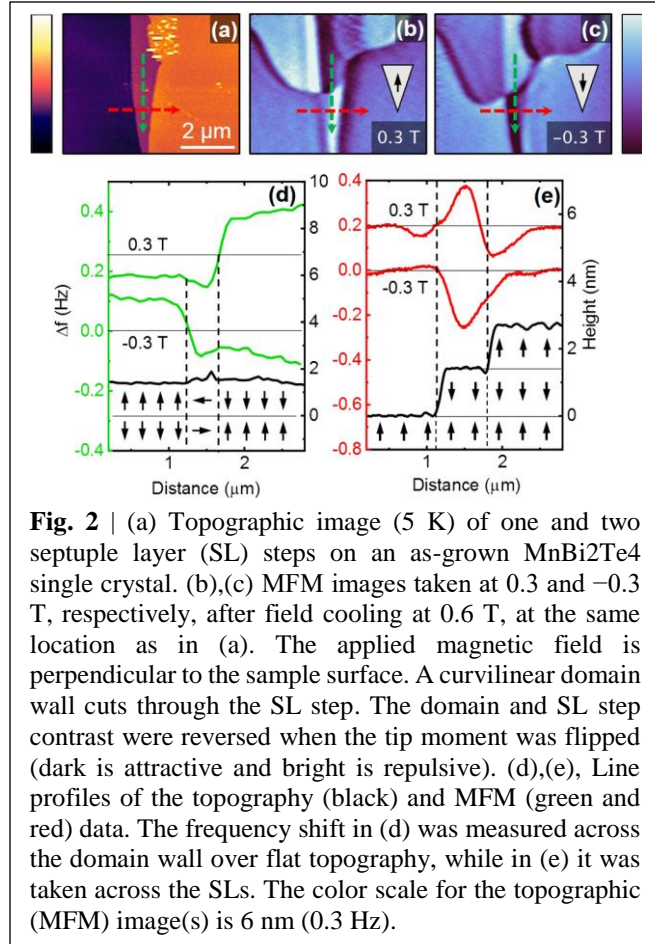


Fig. 2 | (a) Topographic image (5 K) of one and two septuple layer (SL) steps on an as-grown MnBi_2Te_4 single crystal. (b),(c) MFM images taken at 0.3 and $-0.3\ \text{T}$, respectively, after field cooling at 0.6 T, at the same location as in (a). The applied magnetic field is perpendicular to the sample surface. A curvilinear domain wall cuts through the SL step. The domain and SL step contrast were reversed when the tip moment was flipped (dark is attractive and bright is repulsive). (d),(e), Line profiles of the topography (black) and MFM (green and red) data. The frequency shift in (d) was measured across the domain wall over flat topography, while in (e) it was taken across the SLs. The color scale for the topographic (MFM) image(s) is 6 nm (0.3 Hz).

- *Spin chirality fluctuation in 2D ferromagnets with perpendicular magnetic anisotropy*

Non-coplanar spin textures with scalar spin chirality can generate an effective magnetic field that deflects the motion of charge carriers, resulting in a topological Hall effect (THE). However, spin chirality fluctuations in two-dimensional ferromagnets with perpendicular magnetic anisotropy have not been considered so far. In a recent work, we reported evidence of spin chirality fluctuations by probing the THE above the Curie temperature in two different ferromagnetic ultrathin films, SrRuO_3 and V-doped Sb_2Te_3 .¹¹¹ The temperature, magnetic field, thickness and carrier-type dependence of the THE signal, along with Monte Carlo simulations, suggest that spin chirality fluctuations are a common phenomenon in two-dimensional ferromagnets with perpendicular magnetic anisotropy. Our results open a path for exploring spin chirality with topological Hall transport in two-dimensional magnets and beyond. This work was published in Nature Materials.

- *Giant topological Hall effect in correlated oxide thin films*

Strong electronic correlations can produce remarkable phenomena such as metal-insulator transitions and greatly enhance superconductivity, thermoelectricity or optical nonlinearity. In correlated systems, spatially varying charge textures also amplify magnetoelectric effects or electroresistance in mesostructures. However, how spatially varying spin textures may influence

electron transport in the presence of correlations remains unclear. In collaboration with M. Bibes' group at CNRS, we demonstrate a very large topological Hall effect (THE) in thin films of a lightly electron-doped charge-transfer insulator, $(\text{Ca,Ce})\text{MnO}_3$.^{IV} Magnetic force microscopy reveals the presence of magnetic bubbles, whose density as a function of magnetic field peaks near the THE maximum. The THE critically depends on carrier concentration and diverges at low doping, near the metal–insulator transition. This work was published in Nature Physics.

- *Two-channel anomalous Hall effect in SrRuO_3*

The Hall effect in SrRuO_3 thin films near the thickness limit for ferromagnetism shows an extra peak in addition to the ordinary and anomalous Hall effects. This extra peak has been attributed to a topological Hall effect due to two-dimensional skyrmions in the film around the coercive field; however, the sign of the anomalous Hall effect in SrRuO_3 can change as a function of saturation magnetization. In collaboration with Robinson's group at UK, the PI and his student reported Hall peaks in SrRuO_3 in which volumetric magnetometry measurements and magnetic force microscopy indicate that the peaks result from the superposition of two anomalous Hall channels with opposite sign.^V These channels likely form due to thickness variations in SrRuO_3 , creating two spatially separated magnetic regions with different saturation magnetizations and coercive fields. The results are central to the development of strongly correlated materials for spintronics.

- *Seeing is Believing: Visualization of Antiferromagnetic Domains*

Understanding and utilizing novel antiferromagnetic (AFM) materials has been recently one of the central issues in condensed matter physics, as well as in materials science and engineering. The relevant contemporary topics include multiferroicity, topological magnetism and AFM spintronics. The ability to image magnetic domains in AFM materials is of key importance for the success of these exciting fields. While imaging techniques of magnetic domains on the surfaces of ferro-(ferri)magnetic materials with, for example, magneto-optical Kerr microscopy and magnetic force microscopy have been available for a number of decades, AFM domain imaging is a relatively new development. In a recent review article, the PI and colleagues review various experimental techniques utilizing scanning, optical, and synchrotron X-ray probes to visualize AFM domains and domain walls, and to unveil their physical properties.^{VI} We also discuss the existing challenges and opportunities in these techniques, especially with further increase of spatial and temporal resolution.

Future Plans

Magnetic imaging of antiferromagnetic domain walls and surface magnetism

The PI and his students will continue explore the magnetic imaging of antiferromagnetic domain walls in other topological antiferromagnets using the susceptibility contrast mechanism established by the PI's group. The PI and his students will also explore the surface spin-flop transitions in other A-type antiferromagnets, which would have substantial impact on spintronic devices using antiferromagnetic thin films.

Magnetic imaging of QAH systems and chiral edge states

The PI and his students will investigate ferromagnetic domain behaviors in magnetic TIs, using VT-MFM with *in situ* high magnetic/electric field capabilities. The ultimate goal is to visualize

one-way conduction of chiral edge states in these fascinating systems. Another direction is to investigate Axion insulators in magnetic TI heterostructure to explore the Axion physics.

Design and development of an ultra-low temperature MFM

The PI was awarded a DURIP grant to develop a He3 temperature MFM with 14 T magnet. However, the DURIP grant doesn't provide personnel support. With BES renewal support, the PI and his student are designing the scanner head to be integrated with the He3 refrigerator. The delivery of cryostat and magnet is delayed 3-4 months by the impact of COVID-19 pandemic. The PI and his student will construct and perform preliminary cryogenic tests before the arrival of He3 refrigerator with 14 T magnet.

References

1. Otrokov, M. M. *et al.* Prediction and observation of the first antiferromagnetic topological insulator. *Nature* **576**, 416–422 (2019).
2. Otrokov, M. M. *et al.* Unique Thickness-Dependent Properties of the van der Waals Interlayer Antiferromagnet MnBi₂Te₄. *Phys. Rev. Lett.* **122**, 107202 (2019).
3. Gong, Y. *et al.* Experimental realization of an intrinsic magnetic topological insulator. *Chin. Phys. Lett.* **36**, 076801 (2019).
4. Deng, Y. *et al.* Quantized anomalous Hall effect in intrinsic magnetic topological insulator MnBi₂Te₄. *Science (80-.)*. **367**, 895–900 (2020).
5. Liu, C. *et al.* Robust axion insulator and Chern insulator phases in a two-dimensional antiferromagnetic topological insulator. *Nat. Mater.* **19**, 522–527 (2020).
6. Chen, Y. J. *et al.* Topological Electronic Structure and Its Temperature Evolution in Antiferromagnetic Topological Insulator MnBi₂Te₄. *Phys. Rev. X* **9**, 041040 (2019).
7. Hao, Y.-J. *et al.* Gapless surface Dirac cone in antiferromagnetic topological insulator MnBi₂Te₄. *Phys. Rev. X* **9**, 041038 (2019).
8. Li, H. *et al.* Dirac surface states in intrinsic magnetic topological insulators EuSn₂As₂ and MnBi₂Te₄. *Phys. Rev. X* **9**, 041039 (2019).
9. Swatek, P. *et al.* Gapless Dirac surface states in the antiferromagnetic topological insulator MnBi₂Te₄. *Phys. Rev. B* **101**, 161109 (2020).

Publications (supported by BES in recent 2-year)

^I Paul M. Sass, Wenbo Ge, Jiaqiang Yan, D. Obeysekera, Junjie Yang, and Weida Wu, *Magnetic imaging of domain walls in the antiferromagnetic topological insulator MnBi₂Te₄*, *Nano Letters*, **20**, 2609 (2020).

^{II} Paul M. Sass, Jinwoong Kim, David Vanderbilt, Jiaqiang Yan, and Weida Wu, *Robust A-type order and spin-flop transition on the surface of antiferromagnetic topological insulator MnBi₂Te₄*, *Phys. Rev. Lett.*, **125**, 037201 (2020).

^{III} Wenbo Wang, Matthew W. Daniels, Zhaoliang Liao, Yifan Zhao, Jun Wang, Gertjan Koster, Guus Rijnders, Cui-zu Chang, Di Xiao, Weida Wu, *Spin chirality fluctuation in two-dimensional ferromagnets with perpendicular magnetic anisotropy*, *Nature Materials*, **18**, 1054–1059 (2019).

^{IV} Lorenzo Vistoli, Wenbo Wang, Anke Sander, Qiuxiang Zhu, Blai Casals, Rafael Cicheler, Agnès Barthélémy, Stéphane Fusil, Gervasi Herranz, Sergio Valencia, Radu Abrudan, Eugen Weschke, Kazuki Nakazawa, Hiroshi Kohno, Jacobo Santamaria, Weida Wu, Vincent Garcia, and Manuel Bibes, *Giant topological Hall effect in correlated oxide thin films*, *Nature Physics*, **15**, 67–72 (2019).

^V Graham Kimbell, Paul M. Sass, Bart Woltjes, Eun Kyo Ko, Tae Won Noh, Weida Wu, Jason W. A. Robinson, *Two-channel anomalous Hall effect in SrRuO₃*, *Phys. Rev. Mater.*, **4**, 054414 (2020).

^{VI} Sang-Wook Cheong, Manfred Fiebig, Weida Wu, Laurent Chapon, and Valery Kiryukhin, *Seeing is Believing: Visualization of Antiferromagnetic Domains*, *npj Quantum Materials*, **5**, 3 (2020).

Machine Learning-Enabled Advanced Electron Tomography for Resolving Chemical Inhomogeneity and Materials Dynamics

Huolin Xin, Department of Physics and Astronomy, University of California, Irvine, CA

Keywords: machine learning, artificial intelligence, electron tomography, fast and statistical imaging.

Research Scope

The development of lithium-ion batteries (LIB) is one of the key innovations in the past several decades that have revolutionized many aspects of our lives and changed how we interact with machines and the environment. However, building safe, high-energy, long cycle-life and low-cost batteries is still a grand challenge for the research community. Many of the long-standing issues in the field are due in part, if not entirely, to the lack of characterization tools to resolve the electrode materials' failure modes and degradation mechanisms. Although conventional (scanning/) transmission electron microscopy (S/TEM) has proven effective at imaging battery electrode materials at high spatial resolution in two dimensions, the technique remains unable to fully characterize 1) chemical heterogeneity at the atomic scale in three dimensions (3D); and 2) how electrode materials grow and transform during electrochemical reactions or under external stimuli in real time, at nano- and atomic-scale resolution, and in 3D.

The central goal of this Early Career project is to develop machine learning-enabled 1) low-dose and chemically sensitive atomic-resolution electron tomography (ET) as well as 2) high temporal resolution electron nanotomography. This project will result in three-dimensional imaging of atomic species, bonding, and electronic structures at the single-atom scale as well as unprecedented sub-10-second temporal resolution for probing battery materials' transformation dynamics. When realized, this technique will offer a significant improvement in ET's capability in imaging chemistry as well as temporal resolution compared to the state of the art and will offer opportunities to directly visualize unseen transformations of electrode materials in energy storage devices during electrochemical reactions. It also will enable us to address three of the five Transformative Opportunities defined in the 2015 DOE-BESAC reports "Beyond Ideal Materials and Systems: Understanding the Critical Roles of Heterogeneity, Interfaces, and Disorder?," "Revolutionary Advances in Models, Mathematics, Algorithms, Data, and Computing," and "Exploiting Transformative Advances in Imaging Capabilities across Multiple Scales," as well as the Grand Challenge, "How do we characterize and control matter away—especially very far away—from equilibrium?"

This project aims to use this advanced 3D imaging technology to reveal novel phenomena related to the dynamic evolution of the surfaces and interfaces in compositionally complex oxide electrodes as well as alkaline metal anodes. Fundamental descriptions of interfaces' energy,

structure, chemistry, and mechanical/functional behavior are sought to help uncover characteristics that improve the electrodes' performance in order to devise ways to optimize their performance and design rules for future development.

Future Plans

To achieve the ambitious project goals within a 5-year funding period, we will combine the PI's strength in machine learning and *in situ* ET and imaging technique development as well as ready access to state-of-the-art transmission electron microscopes and detectors at the PI's institution. Specifically, in the next two years, we will develop novel tomography acquisition schemes and algorithmic development using deep learning-based machine learning methods to enable fast, low-dose, and statistically significant electron tomography and to push the boundary of chemically sensitive electron tomography. The methods developed will first be tested on dose-resistant materials, such as multielement rock salt/spinel oxides. Once proven effective, we will apply them to dose-sensitive materials such as multielement catalysts, compositionally complex layered oxide materials, and alkaline electrodes.

Transport and Imaging of Mesoscopic Phenomena in Novel Low-Dimensional Materials

Yacoby, Amir - Harvard University, yacoby@physics.harvard.edu
Jarillo-Herrero, Pablo – MIT, pjarillo@mit.edu

Project Scope

Layered materials offer a new playground for exploring novel physics in reduced dimensions. In particular, they allow exploring interacting electron physics in new regimes unexplored previously. Our focus in this proposal is to use innovative methods to fabricate ultra-low disorder graphene and other novel 2D materials devices, in conjunction with ultra-sensitive scan probe, local tunneling, and capacitance methods, as well as low-temperature electronic transport techniques in order to explore new and spatially varying mesoscopic phenomena in graphene and TMD devices and heterostructures.

Recent Progress

In this talk we will focus on two new regimes of graphene multilayers where interactions play a crucial role. The first is the exploration of hydrodynamic flow in single layer graphene near the charge neutrality point studied using a scanning Nitrogen Vacancy magnetometer and the second is the observation interaction physics in correlated moiré heterostructures. Below we elaborate in detail on each topic:

Imaging Viscous Flow of the Dirac Fluid in Graphene. Manuscript published in Nature

The electron-hole plasma in charge-neutral graphene is predicted to realize a quantum critical system whose transport features a universal hydrodynamic description, even at room temperature. This quantum critical “Dirac fluid” is expected to have a shear viscosity close to a minimum bound, with an inter-particle scattering rate saturating¹ at the Planckian time $\hbar/(k_B T)$. While electrical transport measurements at finite carrier density are consistent with hydrodynamic electron flow in graphene, a clear demonstration of viscous behavior at the charge neutrality point remains elusive. In this work, we directly image viscous Dirac fluid flow in graphene at room temperature via measurement of the associated stray magnetic field. Nanoscale magnetic imaging is performed using quantum spin magnetometers realized with nitrogen vacancy (NV) centers in diamond. Scanning single-spin and wide-field magnetometry reveals a parabolic Poiseuille profile for electron flow in a high-mobility graphene channel near the charge neutrality point, establishing the viscous transport of the Dirac fluid. This measurement is in contrast to the conventional uniform flow profile imaged in a metallic conductor and also in a low-mobility graphene channel. Via combined imaging-transport measurements, we obtain viscosity and scattering rates, and observe that these quantities are comparable to the universal values expected at quantum criticality. This finding establishes a nearly-ideal electron fluid in charge-neutral, high-mobility graphene at room temperature. Our results pave the way to study hydrodynamic transport in quantum critical fluids relevant to strongly-correlated electrons in high- T_c superconductors. This work also highlights the capability of quantum spin magnetometers to probe correlated-electronic phenomena at the nanoscale.

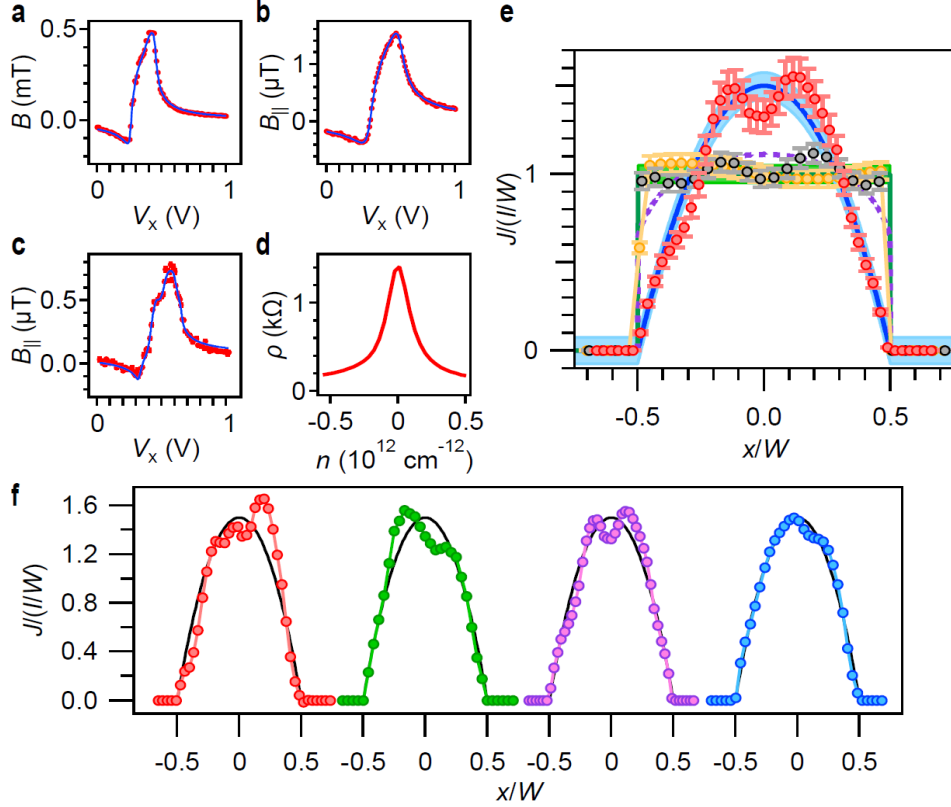


Fig. 1 Scanning magnetometry of the projective stray field $B_{||}$ measured with **a**, the Pd channel, **b**, the low-mobility graphene device, and **c**, a standard (hBN-encapsulated) graphene device at the CNP. Horizontal axis is the piezo voltage that drives the scanning probe in the x -direction. Lines: $B_{||}$ from reconstructed current density J_y . **d**, Transport measurement of resistivity ρ vs. carrier density n for hBN-encapsulated graphene device, same as in **c**. The standard graphene device is set to the CNP by tuning the gate voltage to achieve maximal resistivity. Data for the Pd channel is measured with optically-detected magnetic resonance (ODMR) and a sourced current of 1 mA. Data for the low-mobility and standard graphene devices are measured with spin-echo AC magnetometry (Details of the measurement technique described in Methods). A source-drain voltage $V_{sd}=50$ mV is applied for the low-mobility device and 5.8 mV for the standard device. The width is $1 \mu\text{m}$ for the low-mobility and standard graphene devices and 800 nm for the Pd channel. Pd channel is 30 nm thick and $100 \mu\text{m}$ long. All the graphene devices measured in this work have lengths $\geq 5 \mu\text{m}$. For all devices, scanning magnetometry is performed at a y position near the mid-point along the length of the channel. For graphene devices, we ensure the y position of the scan is within $1 \mu\text{m}$ of the longitudinal mid-point via atomic force microscopy with the diamond probe. **e**, Reconstructed current density $J_y(x)$. J_y is normalized by the average charge carrier flux I/W , where $I = \int dx J_y(x)$ is the total flux and W is the width of the channel. The spatial coordinate x is normalized by W and centered on the channel. Red points: graphene at the CNP. Gray points: Pd channel. Orange points: low-mobility graphene. Error bars correspond to the relative deviation of J_y that generates $2\chi^2$, where χ^2 is the cost function. Blue (green) lines: ideal viscous (uniform) flow with 5% error band. Purple dashed curve: current profile of non-interacting electrons with diffusive boundary condition and momentum-relaxing mean free path $l_{mr} = 0.625W$, which corresponds to the maximum possible curvature for a non-interacting flow (see Supplementary Information²⁶). **f**, Current profile at the CNP from four different standard hBN-encapsulated graphene devices. Second profile from left is for current of $20 \mu\text{A}$ and is measured with ODMR, whereas other profiles have current $\lesssim 2 \mu\text{A}$ and are measured with spin-echo AC magnetometry.

Moiré superlattices, as exemplified by magic-angle twist bilayer graphene, have emerged as a powerful platform to study electron correlations and (spontaneous) symmetry breaking in a controllable way. Despite the extremely active studies, the correlated phenomena examined have been so far focused on correlated insulating, superconducting, and ferromagnetic states. Our recent experimental work discovered emergent ferroelectricity in graphene-based moiré heterostructures, a surprising but welcome addition to this rich set of phenomena.

Ferroelectric materials exhibit an electrically-switchable electric dipole, which is usually formed by spatial separation between the averaged centers of positive and negative charge within the unit cell. Based on this, it is difficult to imagine graphene, a material composed only of carbon atoms, exhibiting ferroelectricity. However, in this work, we indeed realize switchable ferroelectricity in Bernal-stacked bilayer graphene sandwiched between two hexagonal boron nitride (BN) layers (Fig2.a-b). By introducing a moiré superlattice potential (via aligning bilayer graphene with the top and/or bottom BN crystals), we observe prominent and robust hysteretic behavior of the graphene resistance with an externally applied out-of-plane electric field (Fig2.c-d). Our systematic transport measurements reveal rich and striking response as a function of electric field and electron filling, not previously observed in any 2D systems, and beyond the framework of conventional ferroelectrics. We further directly probe the ferroelectric polarization through a nonlocal monolayer graphene sensor. Our results suggest an unconventional, odd parity electronic ordering in the bilayer graphene/BN moiré system. This emergent moiré ferroelectricity may pave the way for ultrafast, programmable, and atomically thin carbon-based memory devices. This work is currently in press in Nature.

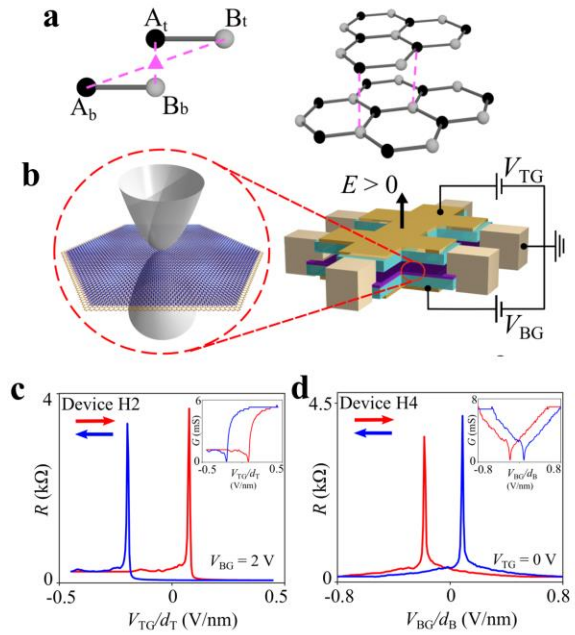


Fig. 2: Emergent ferroelectricity in bilayer graphene-BN moiré superlattices. **a**, Lattice structure of Bernal bilayer graphene. **b**, Schematic of a bilayer graphene-BN moiré device. **c-d**, Hysteretic resistance switching behavior with the gating field in two representative devices.

Future Plans - Our research effort for the next years will focus on the following topics:

1. Imaging electron compressibility in twisted bilayer graphene devices
2. Exploring magnon transport in quantum Hall phases of twisted bilayer graphene
3. Imaging magnetism and current flow in twisted bilayer graphene devices.
4. Measuring chemical potential and compressibility in correlated moiré systems
5. Measuring thermodynamic properties (e.g. entropy and magnetization) of correlated moiré systems.

Publications from DOE supported research – past 2 years

1. Di S. Wei, Toeno van der Sar, Seung Hwan Lee, Kenji Watanabe, Takashi Taniguchi, Bertrand Halperin, Amir Yacoby, “*Electrical generation and detection of spin waves in a quantum Hall ferromagnet*”, *Science* **362**, 229 (2018).
2. Tony X. Zhou, Joris J. Carmiggelt, Lisa M. Gächter, Ilya Esterlis, Dries Sels, Rainer J. Stöhr, Chunhui Du, Daniel Fernandez, Joaquin F. Rodriguez-Nieva, Felix Büttner, Eugene Demler, Amir Yacoby, “*A Magnon Scattering Platform*”, [arXiv:2004.07763](https://arxiv.org/abs/2004.07763).
3. Mark J. H. Ku, Tony X. Zhou, Qing Li, Young J. Shin, Jing K. Shi, Claire Burch, Huiliang Zhang, Francesco Casola, Takashi Taniguchi, Kenji Watanabe, Michael Fogler, Philip Kim, Amir Yacoby, Ronald L. Walsworth, “*Imaging viscous flow of the Dirac fluid in graphene*”, *Nature* **583**, 537 (2020).
4. D. Nandi, B. Skinner, G. H. Lee, K.-F. Huang, K. Shain, Cui-Zu Chang, Y. Ou, S.-P. Lee, J. Ward, J. S. Moodera, P. Kim, B. I. Halperin, and A. Yacoby, “*Signatures of long-range-correlated disorder in the magnetotransport of ultrathin topological insulators*”, *Phys Rev. B*, **98**, 214203 (2018).
5. Z. Zheng, Q. Ma, Z. Bi, S. de la Barrera, M.-H. Liu, N. Mao, Y. Zhang, N. Kiper, K. Watanabe, T. Taniguchi, J. Kong, W.A. Tisdale, R. Ashoori, N. Gedik, L. Fu, S.-Y. Xu, and P. Jarillo-Herrero, “*Unconventional ferroelectricity in moiré heterostructures*”. *Nature* (in press, 2020)
6. Y. Cao, D. Rodan-Legrain, O. Rubies-Bigordà, J.M. Park, K. Watanabe, T. Taniguchi, and P. Jarillo-Herrero, “*Tunable correlated states and spin-polarized phases in twisted bilayer–bilayer graphene*”. *Nature* **583**, 215 (2020).
7. M. Yankowitz, Q. Ma, P. Jarillo-Herrero, and B.J. LeRoy, “*Van der Waals heterostructures combining graphene and hexagonal boron nitride*”. *Nature Reviews Physics* **1**, 112 (2019).
8. J.I.-J. Wang⁺, L. Bretheau⁺, D. Rodan-Legrain, R. Pisoni, K. Watanabe, T. Taniguchi, and P. Jarillo-Herrero. “*Tunneling spectroscopy of graphene nanodevices coupled to large-gap superconductors*”. *Phys. Rev. B* **98**, 121411(R) (2018).
9. Y. Yang, S. Fang, V. Fatemi, J. Ruhman, E. Navarro-Moratalla, K. Watanabe, T. Taniguchi, E. Kaxiras, and P. Jarillo-Herrero, “*Enhanced Superconductivity and Suppression of Charge-density Wave Order in 2H-TaS₂ in the Two-dimensional Limit*”. *Phys. Rev. B* **98**, 035203 (2018).
10. R. Frisenda, E. Navarro-Moratalla, P. Gant, D. Pérez De Lara, P. Jarillo-Herrero, R. V. Gorbachev, and A. Castellanos-Gomez, “*Recent progress in the assembly of nanodevices and van der Waals heterostructures by deterministic placement of 2D materials*”. *Chemical Society Reviews* **47**, 53 (2018).

Probing Correlated Superconductors and Their Phase Transitions on the Nanometer Scale

Ali Yazdani

Department of Physics

Princeton University, Princeton, NJ 08544

Grant #: DE-FG02-07ER46419

Program Monitors: Dr. Jane Zhu

Reporting Period: September 2018-September 2020

Research scope:

Studies of correlated and topological quantum states of matter are at the forefront of research in condensed matter physics. Superconductivity in these systems continues to be among the most exciting topics — from the recent discovery in magic-angle twisted bilayer graphene (MATBG) near correlated insulating phases— to continued interest in realization of Majorana fermions in various platforms for topological superconductivity. Understanding how superconductivity emerges from correlated normal or insulating phases — long considered in heavy fermions and high-T_c cuprate superconductors — is now a critical question in understanding properties of electrons in two-dimensional (2D) moiré lattices realized in twisted bilayer graphene (TBLG). If correlations play a key role in superconductivity of this system, its structure lends promise that a chemically pristine platform can extend our understanding of superconductivity beyond that of cuprates, heavy fermions, and iron pnictide. Similarly, demonstrating topological superconductivity in new compounds and finding ways to probe the non-Abelian properties of Majorana zero modes (MZMs) or the chiral Majoranas they host, are currently among the most studied topics in condensed matter physics.

This program builds on our previous advances in spectroscopic techniques with the scanning tunneling microscopy (STM) on cuprates and heavy fermions systems to understand the properties of novel insulating and superconducting phases of 2D materials. The application of these techniques, in addition to those recently developed with density-tuned STM spectroscopy, is being applied to understand many key questions concerning the electronic correlation, topology, and superconductivity of MATBG and related 2D systems. Unlike other novel, bulk unconventional superconductors, where angle-resolved photoemission spectroscopy (ARPES) or neutron scattering techniques have provided rich spectroscopic information to understand the nature of those states, the device-based structure of MATBG and other 2D systems makes STM's spectroscopic techniques easier to apply than other methods. Under this program, we are also exploring the properties of monolayers of WTe₂, which has been discovered to be both a topological insulator and a superconductor depending on the doping level. This system provides a unique opportunity to create hybrid structures in which the two phenomena may be combined to create topological superconducting phases. Finally, we are developing a new capability to perform atomic force microscopy (AFM) techniques for device-like structures at millikelvin temperatures. AFM measurements will make it possible to examine complex devices with insulating and conducting regions and provide new types of measurements for probing the correlated insulating phases in 2D materials proposed in this program.

Highlights of breakthroughs under the DOE grant in last two years:

- Demonstration of spectroscopic signatures of strong electronic correlation in magic-angle graphene (Nature 2019).
- Discovery of a cascade of transitions between the correlated electronic states of magic-angle twisted bilayer graphene (Nature 2020)
- Direct visualization of multi-channel topological boundary modes in a quantum Hall valley system (Nature 2019).

Recent Progress:

Fabrication of MATBG samples for high resolution STM studies

The first important technical breakthrough in the proposed program has been the development of the in-house capability to fabricate MATBG devices that are specifically designed for STM studies. While the transport studies can work with stacks of buried MATBG structures, development samples with MATBG exposed, which are of sufficient cleanliness for high-resolution STM studies, has taken considerable time and effort. The first generation of the samples (Figure 1) allowed us to perform high resolution imaging of the moiré superlattice in MATBG samples, with which we were able to demonstrate the presence of two peaks in the density of states of this system associated with its valence and conduction flat bands (Fig. 1d). In these experiments, we were also able to characterize the local strain in this moiré lattice and show that when this is taken into account, we can fully understand the non-interacting spin particle density of states of MATBG. This non-interacting description accurately explains the properties of this system, when its two flat conduction and valance bands are either fully occupied or completed empty.[1]

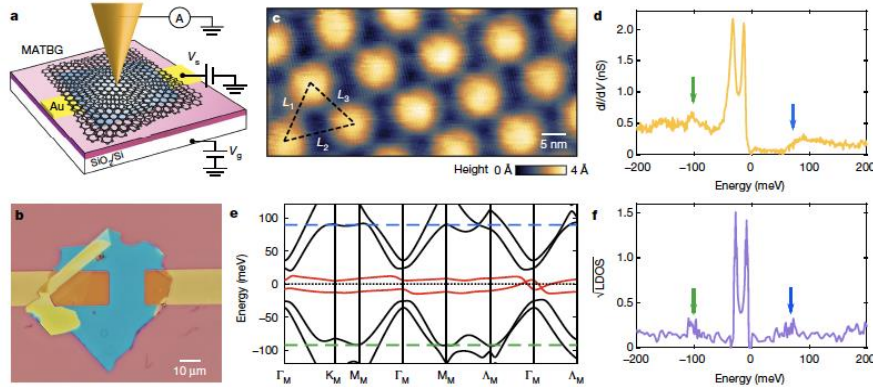


Figure 1. a) Schematic of typical device and, b) an optical picture of it. c) atomic scale image of moiré pattern in a MATBG device. d) electronic band structure using lattice parameter from c. e) STM spectra showing peaks in DOS for the flat bands. f) calculation of DOS for the lattice parameters that are extracted from STM measurements.

Signature of strong electronic correlations and cascade of electronic transitions in MATBG

Along with the development of the MATBG device-like structures, we have also developed the capability to perform density-tuned scanning tunneling spectroscopy (DT-STs) of the MATBG system in these devices. The remarkable opportunity afforded by the 2D material platform is that in situ electrostatic tuning can be used to study their electronic properties as a function of carrier density tuned by the gate. DT-STs of MATBG has revealed a wealth of important information on

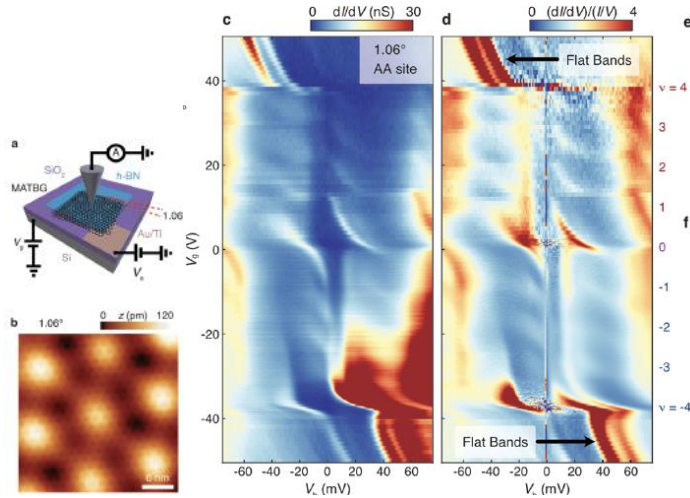


Figure 2. Density-tuned STM/STS measurements of MATBG. a) Device schematic. b) high resolution STM image of MATBG resolving atomic structure of the top layer, and moiré superlattice. Such measurements allow us to locally characterize angle and strain. c-d) DT-STC measurements showing a cascade of transition for MATBG at each integer filling. These features can be analyzed to extract bandwidth of the system when the flat bands are full (or empty) $V_g > 40V$ as well as the strength of the interactions at partial filling. $-40V < V_g < 40V$.

the nature of electronic correlations in this system. In a paper published in Nature in 2019, we reported that when the flat bands of MATBG are tuned to be partially filled, sharp density of states associated with the flat bands of this system (Fig. 1d) develop substantial broadening (see Figure 2c and discussion below).[1] This broadening is a direct consequence of a strong Coulomb interaction in this system, which cannot be captured by the mean field models of such an interaction. Exact diagonalization of a Hubbard-like model of MATBG carried out on small clusters confirms that a strong correlation can indeed give rise to such broadening features in STM spectroscopy measurements. This broadening signals the importance of correlation is significant as it shows that MATBG is a correlated system at all partial filling of its flat bands, not just when corresponding correlated insulating phases have been discovered in this system. They show that superconductivity emerges in this system in the presence of such strong correlations, thereby strongly suggesting that it has an unconventional pairing mechanism.

Following this work, with improvement in device quality (image in Fig. 2b), in a second Nature paper that appeared earlier in 2020, we showed that despite the broadening, DT-STC measurements (Fig.2c-d) show a sequence of sharp features in spectroscopy that could be further analyzed. These features, that correlate with integer filling of the valence and conduction flat band, indicate a cascade of transitions in the spectroscopic properties of this system, and demonstrate the interplay between the strong correlation and quantum degeneracies of this system. By including the spin and valley degrees of freedom in the electronic description of electronic interactions of MATBG in Hubbard-like modes, we elucidated an understanding of these findings. The underlying reason for these transitions is due to a rather sharp change in the chemical potential of this system at each integer filling of its flat bands — signaling the role spin and valley play in determining electron addition and removal in the system. The outcome of this analysis was to recognize that such measurements can provide a direct means to measure the strength of electron-electron interaction strength in MATBG at partial filling of its flat bands. The remarkable discovery is that we showed that this strength is estimated to be about 23meV, which far exceeds the bandwidth of this system, thereby quantitatively establishing MATBG as a strongly correlated system.

Visualizing a topological edge mode of a quantum Hall liquid and new microscopy techniques:

In other efforts during the last two years, we have also extended our use of STM to directly visualize quantum Hall states to visualize a spontaneously formed topological edge mode that

emerges at the interface between two valley polarized quantum Hall phases formed on the surface of Bi at high magnetic field. These experiments (published in Nature in 2019 [3]) are the first of their kind to show the development of such edge states emerging from closing and reopening a topological gap that can be spatially mapped with the STM. They also establish a new type of Luttinger liquid in which electron conduction in such channels along the edge is protected due to valley symmetry of the associated quantum Hall phases. We explored the physics of this problem in collaboration with Prof. Siddharth Parameswaran (University of Oxford, UK) in a theoretical paper.[4]

Finally, as part of this program we will also augment our arsenal of STM/STS techniques with the application of high-resolution imaging of their properties with cryogenic non-contact AFM. We are developing a millikelvin AFM (tuning fork Q-plus with both AFM/STM modes), which will be integrated with our versatile modular ultra-high vacuum (UHV) scanning probe system that is capable of studying gated devices. The instrument itself was developed under this program; the details, including its design, methods of construction, testing, and performance, have recently been published.[5] The AFM module for this instrument has also been designed and we are in the process of fabricating and testing the components.

Future plans:

Our plans moving forward will focus on the following key ideas:

1. Our work on MATBG will focus on understanding the nature of superconducting phase with high resolution spectroscopy. We will determine how the correlated normal phase of this system (as described in this report) transforms into the superconducting phase.
2. We have developed a new technique for probing topological phases with finite a Chern number using DT-STs spectroscopy. Application of this technique to MATBG will reveal a sequence of very exciting Chern phases that we are currently exploring.
3. An AFM module will be built and tested with our millikelvin instrumentation.
4. We have carried out some measurements on WTe_2 samples, probing their electronic properties with DT-STs. These are challenging experiments as WTe_2 has to be protected with a monolayer of BN after fabrication. This work is being carried out in collaboration with Prof. Wu at Princeton.

Publications supported by the DOE-BES (2019-2020):

In addition to publications directly related to DOE-BES projects, the DOE funding supports the instrumentation in our lab that has also assisted other projects. The publications from these projects benefiting from DOE support are also included in the list below (marked as partially supported by DOE).

1. Y. Xie, B. Lian, B. Jäck, X. Liu, C.-L. Chiu, K. Watanabe, T. Taniguchi, B. A. Bernevig, and A. Yazdani, “Spectroscopic signatures of many-body correlations in magic-angle twisted bilayer graphene,” Nature **572**, 101-105 (2019).
2. D. Wong, K. P. Nuckolls, M. Oh, B. Lian, Y. Xie, S. Jeon, K. Watanabe, T. Taniguchi, B. A. Bernevig and A. Yazdani, “Cascade of transitions between the correlated electronic states of magic-angle twisted bilayer graphene,” Nature **582**, 198-202 (2020).

3. M. T. Randeria, K. Agarwal, B. E. Feldman, H. Ding, H. Ji, R. J. Cava, S. L. Sondhi, S. A. Parameswaran, and A. Yazdani, “Interacting multi-channel topological boundary modes in a quantum Hall valley system,” *Nature* **566**, 363-367 (2019).
4. K. Agarwal, M. T. Randeria, A. Yazdani, S. L. Sondhi and S. A. Parameswaran, “Topology and symmetry-protected domain wall conduction in quantum Hall nematics,” *Phys. Rev. B* **100**, 16, 165103 (2019). (Partial support by DOE.)
5. D. Wong, S. Jeon, K. P. Nuckolls, M. Oh, S. C. J. Kingsley and A. Yazdani, “A modular ultra-high vacuum millikelvin scanning tunneling microscope,” *Review of Scientific Instruments* **91**, 023703 (2020).
6. R. V. Mishmash, A. Yazdani, and M. P. Zaletel, “Majorana lattices from the quantized Hall limit of a proximitized spin-orbit coupled electron gas,” *Physical Review B* **99**, 11, 115427 (2019). (Partial support by DOE.)

Spin-polarized scanning tunneling microscopy and spectroscopy of iridium-oxides

Ilija Zeljkovic, Boston College

Keywords: spin-polarized STM, iridates, antiferromagnetic ordering, magnetic transition.

Research Scope

A complicating factor in unraveling the interplay between magnetism, electronic correlations and chemical doping in complex oxides lies in the inhomogeneous nature of these systems prone to phase separation upon doping. The overarching aim of this project is to use spectroscopic imaging spin-polarized scanning tunneling microscopy (SP-STM) to simultaneously visualize atomic-scale magnetic and electronic structure in these materials, initially focusing on doped iridium-based oxides (iridates) Sr_2IrO_4 and $\text{Sr}_3\text{Ir}_2\text{O}_7$.

While it is well-established that the undoped parent state of many iridates hosts an antiferromagnetically (AF) ordered spin-orbit Mott phase, the evolution of the AF order with doping and its relationship to the local electronic structure remains difficult to extract. Specific objectives of our project include: (1) visualizing the evolution and collapse of the AF order as a function of charge carrier doping and temperature, (2) elucidating the relationship between the inhomogeneous electronic structure and the AF order at the nanoscale, and (3) searching for new spin- and pseudospin-ordered phases.

The comprehensive experimental approach we aim to establish here will provide a foundation to the SP-STM studies of other families of complex oxides in which spin, charge and orbital degrees of freedom intertwine to create new states of matter.

Recent Progress

1) Preparation of robust spin-polarized STM tips

We prepare spin-polarized STM tips from a bulk Cr wire ($\sim 1 \text{ mm}^2$ cross-section), by electrochemically etching the wire in NaOH solution, and annealing it in UHV to remove oxidation layer from the tip's surface. Prior to performing experiments on a material of interest, we characterize each tip on top of the surface of a UHV-cleaved single crystal of Fe_{1+y}Te (Fig. 1). If the tip is spin-polarized, the well-known diagonal double-stripe AF order with $2a_0$ period will be observed in STM topographs of Fe_{1+y}Te [1]. To achieve sufficient spin sensitivity and atomic resolution, we typically modify the tip *in-situ* by fast scanning over Fe impurities and/or

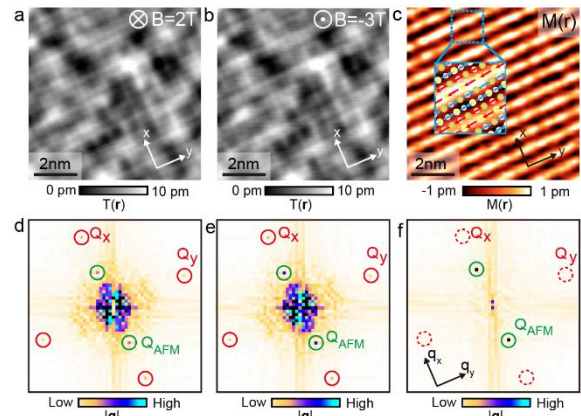


Fig. 1. STM topographs of Fe_{1+y}Te measured at (a) 2T and (b) -3T. (d,e) Fourier transforms (FTs) of the topographs in (a,b). Green circles in (d-f) denote peaks arising from the AF order. (c) Spin-resolved magnetic contrast map $M(\mathbf{r})$ obtained by subtracting (a) and (b). (f) FT of $M(\mathbf{r})$ map in (c).

pulsing the tip with several Volt bias on top of Fe_{1+y}Te . This results in a rearrangement of the atoms at the tip's apex, and likely in the tip picking up one or more excess Fe atoms from the Fe_{1+y}Te surface. To check that the tip's spin polarization can be changed by varying the direction of magnetic field B , we acquire STM topographs with different B applied perpendicular to the sample surface (Fig. 1(a,b)). By subtracting the topographs acquired at different B (negative sign denotes the reversal of field direction), we get a spin-resolved magnetic contrast $M(\mathbf{r})$ map (Fig. 1(c)). Its Fourier transform (FT) shows primarily the AF ordering peaks (Fig. 1(f)), consistent with the two topographs being taken over an identical field-of-view with only tip polarization being different, and the structural information being subtracted out.

2) Imaging melting of the antiferromagnetic order in a doped Mott insulator Sr_2IrO_4

The AF Mott insulator has been of particular interest as the low-temperature ground state of numerous transition metal oxides. Charge carrier doping can gradually suppress this insulating state, a process theoretically expected to lead to inherent phase separation. Consistent with this picture of doped Mott insulators, spatially inhomogeneous electronic states, varying

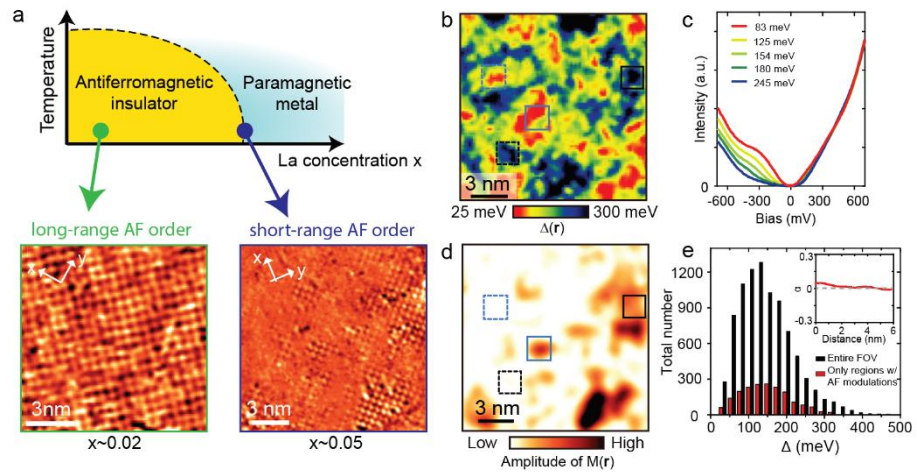


Fig. 2. (a) Phase diagram of $(\text{Sr}_{1-x}\text{La}_x)_2\text{IrO}_4$, and representative $M(\mathbf{r})$ maps away and near insulator-to-metal transition. (b) Spectral gap map and (c) average dI/dV spectra binned by gap size. (d) Amplitude of $M(\mathbf{r})$ maps denoting local intensity of the AF order. (e) Histograms of the gap size and (inset) cross-correlation between the AF order and the gap size, showing a weak cross-correlation.

on nanometer length scales, have been observed in several systems [2, 3]. However, a major experimental failing over the past few decades has been the inability to measure how the AF order evolves over the same length scales, and what is its relationship to the single-particle gap (charge gap) closing as the Mott state is tuned away from half filling.

We apply SP-STM to visualize periodic spin-resolved modulations originating from the AF order in a Mott insulator $(\text{Sr}_{1-x}\text{La}_x)_2\text{IrO}_4$, and study these as a function of La doping concentration x (Fig. 2). We find that near the insulator-to-metal transition (IMT), the long-range AF order melts into a fragmented state with short-range AF correlations. Importantly, we discover that the short-range AF order is locally uncorrelated with the observed spectral gap magnitude [4] (Fig. 2(b-e)). This strongly suggests that the short range AF correlations are unlikely to be the culprit behind inhomogeneous gap closing and the emergence of V-shaped “pseudogap” regions (red regions in the gapmap in Fig. 2(b)) near IMT.

3) Investigating magnetic “memory” in iridates

One of the crucial questions in inhomogeneous magnetic systems remains what sets the distribution of magnetic domains, and to what extent the domains are robust to thermal cycling through the magnetic transition. We focus on $(\text{Sr}_{1-x}\text{La}_x)_3\text{Ir}_2\text{O}_7$ near the AF transition at $x\sim 3\%$, where nanoscale AF puddles are clearly distinguishable (Fig. 3(a)). Similarly to procedure in Fig. 1, we acquire a spin-resolved magnetic contrast map $M(\mathbf{r})$. Then, we track an identical area of the sample as a function of temperature (Fig. 3(a-d)). We warm up the sample to ~ 10 K, where the AF signal appears to be gone, and cool it back down to ~ 5 K. Our first observation is that the average intensity of the AF modulations quickly lowers with temperature, and bounces back up upon cooling down the sample again (Fig. 3(f)). In sharp contrast to the rapid evolution of the AF order, we find that the spectral gapmap over the same region of the sample shows almost no change (Fig. 3(g,h)), thus corroborating our previous conclusion that the two observables are not spatially correlated.

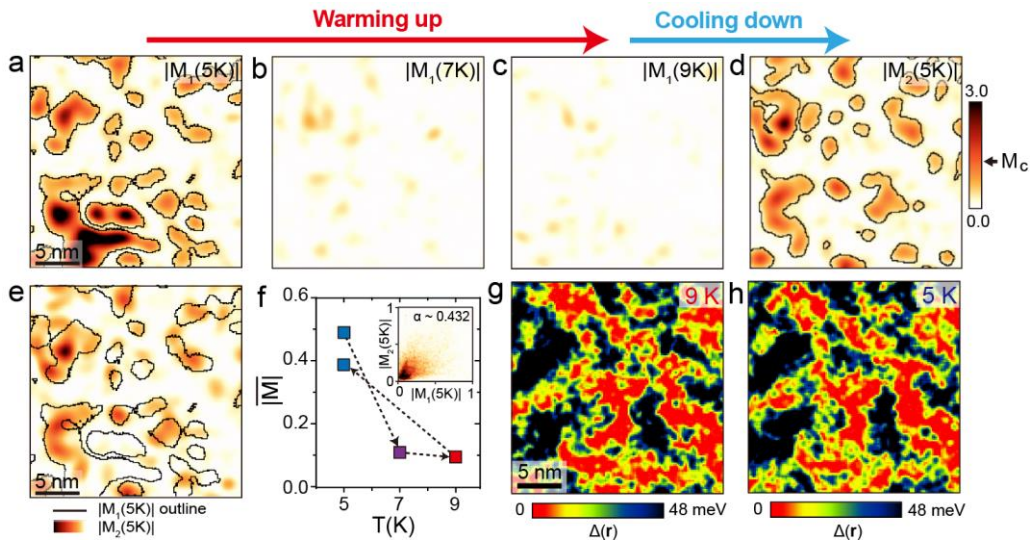


Fig. 3. The AF texture evolution during thermal cycling. (a-d) Evolution of the $|M(\mathbf{r})|$ maps (local intensity of the AF order map) as a function of temperature, acquired over an identical field-of-view in the $x\sim 3.4\%$ $(\text{Sr}_{1-x}\text{La}_x)_3\text{Ir}_2\text{O}_7$ sample. The AF-ordered puddles are outlined by black lines in (a,d). (e) The outline of AF puddles before thermal cycling on top of the AF intensity map after thermal cycling. (f) The average AF intensity from $|M(\mathbf{r})|$ maps as a function of temperature. The gap map over the same area as (a-d) at (g) 9 K and (h) 5 K, showing nearly identical gapmaps despite a dramatic change between $M(\mathbf{r})$ maps in (c,d). Red regions in (g,h) represent metallic puddles within an insulating matrix.

Surprisingly however, the comparison of $M(\mathbf{r})$ maps before and after thermal cycling shows a pronounced difference (Fig. 3(a,d)). This can be visualized by overlaying the two maps on top of each other (Fig. 3(e)). While there are some similarities and the cross-correlation is still substantial (inset in Fig. 3(f)), we can clearly observe new puddles forming and disappearing. This suggests multiple stable configurations of the low-temperature AF state, and prompts future experiments on the origin of this change.

Future Plans

We will proceed to investigate to what extent chemical substitutions are responsible for the inhomogeneous distribution of the AF order in iridates. To do so, we will image other defects and dopants not immediately seen from STM topographs, such as Ir site defects and La substitutions in subsurface SrO planes. We will also investigate the AF distribution as a function of other types of chemical substitutions. For example, we will explore substituting Ir for Ru, which in contrast to the expected electron doping by La at the Sr site, effectively hole dopes the system. Finally, we will investigate if the AF-ordered puddles in this system exhibit scale-invariant texture, as seen in other inhomogeneous correlated electronic states, such as the charge-ordered phase in cuprates [5].

References

1. Enayat M, Sun Z, Singh UR, Aluru R, Schmaus S, Yaresko A, Liu Y, Lin C, Tsurkan V, Loidl A, Deisenhofer J, Wahl P. *Real-space imaging of the atomic-scale magnetic structure of $Fe_{1+y}Te$* . Science **345**, 653 (2014).
2. Qazilbash MM, Brehm M, Chae B-G, Ho P-C, Andreev GO, Kim B-J, Yun SJ, Balatsky A V., Maple MB, Keilmann F, Kim H-T, Basov DN *Mott Transition in VO₂ Revealed by Infrared Spectroscopy and Nano-Imaging*. Science **318**, 1750 (2007).
3. Battisti I, Bastiaans KM, Fedoseev V, la Torre A de, Iliopoulos N, Tamai A, Hunter EC, Perry RS, Zaanen J, Baumberger F, Allan MP. *Universality of pseudogap and emergent order in lightly doped Mott insulators*. Nature Physics **13**, 21 (2017).
4. Zhao H, Manna S, Porter Z, Chen X, Uzdejczyk A, Moodera J, Wang Z, Wilson SD, Zeljkovic I. *Atomic-scale fragmentation and collapse of antiferromagnetic order in a doped Mott insulator*, Nature Physics **15**, 1267 (2019).
5. Phillabaum B, Carlson EW, Dahmen KA *Spatial complexity due to bulk electronic nematicity in a superconducting underdoped cuprate*. Nature Communications **3**, 915 (2012) .

Publications

He Zhao, Sujit Manna, Zach Porter, Xiang Chen, Andrew Uzdejczyk, Jagadeesh Moodera, Ziqiang Wang, Stephen Wilson and Ilija Zeljkovic, *Atomic-scale fragmentation and collapse of antiferromagnetic order in a doped Mott insulator*, Nature Physics **15**, 1267 (2019)

Emerging Functionality in Transition-Metal Compounds Driven by Spatial Confinement

Jiandi Zhang, Department of Physics and Astronomy, Louisiana State University

Keywords: High-resolution STEM/EELS, Interfacial phenomena, Collective excitations, Multiferroic, Magneto-electric coupling

RESEARCH SCOPE: The broken symmetry at an interface and spatial confinement in heterostructures can drive reconstruction of the lattice, charge, or spin, thus generating fascinating properties that are fundamentally different from their parent materials. Advances in atomically resolved electron microscopy and spectroscopy have allowed researchers to “visualize” the atomic structure, the chemical identity, and the bonding character between the atoms. In this project, we have come together as a team aiming at understanding and predicting new properties of interfaces at the atomic level. The group at LSU and UTK/ORNL carry out material growth, modification, and properties characterization. High-end electron microscopy/spectroscopy and theoretical studies are undertaken through the collaboration with Dr. Yimei Zhu’s group at BNL and Prof. Sokrates Pantelides’s group at Vanderbilt University, respectively.

Recent Progress:

- **Interface-induced magnetic polar metal phase in complex oxides [1]**

Polar metals are extremely rare as the polar structural constraints favor insulating over metallic phase. Structurally polar oxides in nature have empty valence d-orbital and while electron doping can create metallicity, removes the polar structure. This dichotomy restricts metals from adapting a polar structure. Moreover, no polar metals are known to be magnetic due to their empty d-orbital. Here taking advantage of interfacial coupling, we reported for the 1st-time the realization of a magnetic polar metal in a BaTiO₃(BTO)/SrRuO₃(SRO)/BaTiO₃ heterostructure grown on SrTiO₃ (STO) in (001), shown schematically in Fig. 1(a). Atomically resolved scanning transition electron microscopy (STEM) reveals induced non-centrosymmetry arising from polar distortions of Ru atoms in 3 u.c. SRO sandwiched between BTO layers. The annular bright field (ABF) images are shown in Fig. 1(b) with the polar distortion indicated schematically below the image [Fig. 1(c)]. Figure 1(d) is a plot of the measured distortions across the interfaces for 3-u.c. SRO between BTO (9/3/10). As shown in Figs. 1(e-g), electrical transport and magnetization measurements reveal that this heterostructure possesses a metallic phase with high conductivity and ferromagnetic ordering with high saturation moment as compared with a

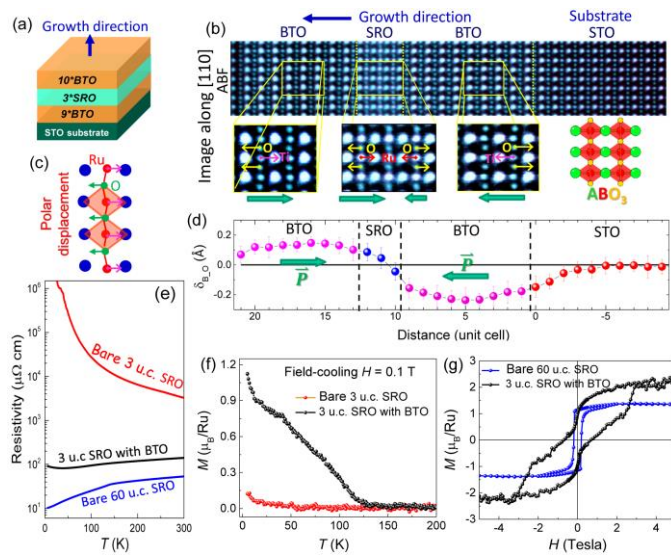


Fig. 1: (a) Schematic of the designed heterostructure. (b) Inverted ABF-STEM cross section image of the heterostructure with enlarged ABF-STEM images showing polar distortions in the BTO and SRO blocks. Green arrows indicate polar direction. (c) Schematic view of polar displacements in SRO. (d) Variation of polar displacements δ_{B-O} across the whole film. The polar displacements, δ_{B-O} , refer to relative displacements between B site cations and O anions. (e) T -dependence of longitudinal resistivity ρ , (f) T -dependence and (g) field-dependence of magnetization M for the BTO-sandwiched 3 u.c. SRO as compared with non-polar, bare 3 u.c. and 60 u.c. SRO films.

non-polar, bare 3 u.c. SRO film on STO. The bare 3 u.c SRO film is insulating and almost non-magnetic [Fig 3(e-f)]. The non-polar 60 u.c. SRO films (bulk), is metallic but has a much smaller M - H hysteresis loop than the BTO-sandwiched 3 u.c. SRO. The high conductivity in the SRO layer can be attributed electrostatic carrier accumulation induced by the BTO layers. Density-functional-theory (DFT) calculations through our collaboration with Pantelides's group at Vanderbilt University provide insights into the origin of the observed properties of the thin SRO film. Polar distortions are found to be responsible for the emergent ferromagnetism, revealing the intrinsic structural property relationship.

- **Spontaneous magnetic reversal in oxide films [2]**

Local change on atomic scale in structure and composition at interface can trigger new interactions which are absent in bulk. We have found that a new magnetic coupling appears at the interface of half-metallic $\text{La}_{2/3}\text{Sr}_{1/3}\text{MnO}_3$ films grown on a diamagnetic insulating SrTiO_3 (001) substrate (LSMO/STO), which governs the macroscopic properties of the entire monolithic thin film. Although the effect stems from the interface, it propagates to regions far beyond it. The STEM electron energy loss spectroscopy (EELS) and density-functional-theory (DFT) are employed to elucidate the physics. STEM-EELS reveals altered interfacial composition, subtle lattice distortions, and oxidation-state changes. Magnetic measurements combined with DFT calculations demonstrate that a unique form of antiferromagnetic exchange coupling appears at the interface, generating a novel exchange-spring-type interaction that results in a remarkable spontaneous magnetic reversal of the entire ferromagnetic film, and a total inverted magnetic hysteresis, persisting above room temperature. Results from electron-spectroscopy data show that interfacial oxidation states are not consistent with nominal charge counting. The STEM measurements provided tractable guidelines for theoretical calculations to help further understand how the structure and composition gradient can exhibit this type of peculiar magnetic interactions. DFT-calculated electrostatic potential is flat in both sides of the interface, indicating the absence of polar mismatch and of charge accumulation at the interface. This work exemplifies that it is possible to manipulate the macroscopic properties using interface driven interactions on microscopic scale.

- **Exchange bias and inverted hysteresis in monolithic oxide films [3]**

We uncover a previously unseen part of the phase diagram of a monolithic epitaxial thin film of LSMO on SrTiO_3 , which exhibits inverted hysteresis, spontaneous magnetic reversal, and exchange bias due to a structural gradient in the oxygen-octahedral network. The atomic-scale structure is determined using STEM in high angle annular dark field (HAADF) and ABF imaging modes [1, 3]. Varying the growth conditions, we have mapped the phase diagram of this material and discovered that at a specific oxygen pressure and above a critical thickness, a complex magnetic behavior appears. Atomic-scale characterization shows that this peculiar magnetism is closely linked to a continuous structural gradient that creates three distinct regions within the monolithic film, each with a different magnetism onset. We found that large Mn-O bond angle leads to lower Curie temperature, opposite to that expected from the standard double exchange model. Another important observation was the dependence of the exchange bias on the LSMO film thickness and oxygen pressure during growth. This study illustrates the importance of the octahedral geometry, pointing to the importance of coupling atomically controlled growth with STEM atomic imaging.

- **Probing the interfacial symmetry using rotational second-harmonic generation [4]**

Atomically resolved electron microscopy and spectroscopy is revolutionizing our ability to “see” the structure and composition of an interface. Yet, a significant challenge remains: *how to directly*

measure the electronic properties of the buried interface? Rotational second-harmonic generation (RSHG) is a powerful nonlinear optical technique for probing electronic symmetry originating from broken symmetry at the interface. Here we characterize the novel electronic properties at a buried interface due to the broken symmetry, using epitaxially grown high-quality LSMO thin films on SrTiO₃ (STO) (001) substrates, whose properties has been reported previously [3]. The unusual 4-fold anisotropy in RSHG originates from the buried interface, indicating that the interface symmetry cannot be higher than C₂, while both the film and substrate have C_{4v} symmetry. Given the STEM images and the RSHG results, it is possible to create an interface structural model whose symmetry is as low as C₁ [4]. Combining STEM and RSHG opens up a new world for determining interface symmetry, which has the possibility to extend to magnetic symmetry.

- **Phase transitions and magneto-electric (ME) coupling of epitaxial heterostructures [5]**

Pb(Fe_{0.5}Nb_{0.5})O₃/Ni_{0.65}Zn_{0.35}Fe₂O₄ (PFN/NZFO) multilayer heterostructures were grown and the structure and morphology characterized via XRD SAED, STEM and piezoresponse force microscopy (PFM) and then correlated to the measured dielectric, ferroelectric, magnetic, and ME properties. Fig. 2(a) is a cross-sectional TEM image of a (001) - oriented heterostructure where the PFN and NZFO layers appear as dark and bright bands, respectively. PFM measurements reveal the monodomain structure and polarization switching behavior. These nanostructures show well-saturated polarization (~ 52 μC/cm²) and magnetization (~ 62 emu/cm³) at RT. The magnetic and ferroelectric transitions occur well above RT. These heterostructures exhibit relaxor behavior and undergo a 2nd-order ferroelectric phase transition. Magnetodielectric measurements show significant variation of capacitance with increasing static magnetic field indicating strong coupling between the magnetic and electrical order parameters at RT (Fig. 2(b)). The observed ME coupling is attributed to various coupling mechanisms: (i) strain developed at different interfaces due to the inverse piezo electric/magnetic effect, (ii) spin exchange between the multiferroic (PFN) and magnetic (NZFO) layers, (iii) charge coupling at the interface, and (iv) strong strain transmission due to epitaxial growth and well defined sharp interfaces. The RT characteristics make them suitable as candidates for ultra-low power memory, spintronics, and different multifunctional (micro)nanoscale device applications.

Future Plans:

- **Nature of magnetic ordering in structural confined SrRuO₃ (SRO)**

SRO is often considered as an itinerant ferromagnet in bulk [Rev. Mod. Phys. **84**, 253 (2012)] while both magnetism and metallicity disappears simultaneously in ultra-thin film limit. However, we found recently that ferromagnetic (FM) order appears without metallicity. Also, in SRO-CaRuO₃ (CRO) heterostructures, the FM persists down to one unit

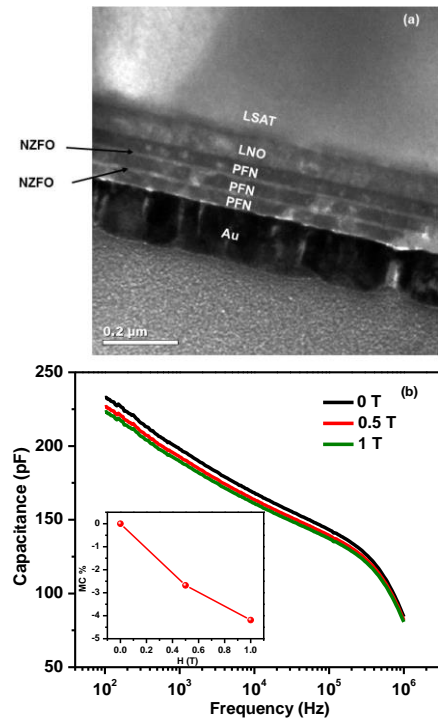


Fig. 2: (a) Cross-sectional high resolution TEM image (b) Frequency dependent parallel capacitance at different static magnetic field of PFN/NZFO/PFN/NZFO/PFN heterostructures at room temperature.

cell, evidencing prominent role of structural distortion and spatial confinement. The grand question remains as how localized and itinerant moments behave in SRO in cubic and orthorhombic octahedral network. We grow SRO-CRO superstructures with different thickness and stacking sequences to understand the interrelationship between magnetic and lattice structures. Especially, we will exploit electron magnetic chiral dichroism with STEM to produce a real-space map of magnetization with subnanometer resolution [see Nano Lett. **12**, 2499(2012)], thus allowing to reveal the spin density of states (DOS) distribution at interface from Ru and possible from O sites [PRB **100**, 054413 (2019)]. Complemented by theoretical modeling based on experimental determination of lattice structure as well as spin DOS we aim at understanding the nature of magnetism by systematically changing the structure.

- **Interface electron and lattice dynamics with STEM low electron energy loss spectroscopy**

Two important excited states in dimensionally confined materials are the lattice phonons and the electronic plasmons. Recent advances in valence electron loss spectroscopy (VEELS) developed by TEM community have offered the opportunity to probe interface collective excitations such as interface phonons and plasmons. We have also developed a surface EELS with energy- and momentum-mapping and solid expertise in measuring phonon and plasmon dispersion with electron beams and neutrons. The collaborations with BNL and ORNL give us access to the newest and highest resolution STEM and the theory group at Vanderbilt has calculated in detail the loss spectra in STEM [PRB **92**, 125147 (2015)], and can apply to the study of interface phonon and plasmon. We will develop test systems to critically examine our ability to measure and understand interfacial phonons and plasmons. We will use the FeSe/SrTiO₃ system (enhanced superconductivity in a single layered FeSe) as our test system, since we already know the structure, phonons, and plasmons. With our surface EELS, we reported that the ~90 meV Fuchs-Kliewer STO phonons penetrate into the FeSe film [PRB **94**, 081116(R) (2016)] and strongly couples with the electrons in FeSe layer [PRB **97**, 035408 (2018); PRL **122**, 066802 (2019)]. Prof. Pantelides collaborating with the electron microscopy group at ORNL reported an interfacial layer of Ti_{1+x}O₂ layer between the FeSe and SrTiO₃, which is key to the enhanced superconductivity. Knowing the lattice structure, they can calculate the vibrational energies, so we can probe vibrational energies layer by layer in this system, testing the capabilities of VEELS.

- **Interface electronic, magnetic and structural symmetries of interfaces**

Nonlinear optical techniques, specifically second harmonic generation (SHG) is important to characterize and contrast the symmetry of the electrons and spin states at the interface with the structure determined with STEM. When the materials being investigated are centrosymmetric (vast majority of complex oxides), the nonlinear signal comes from the regions of broken symmetry at the interface. We have constructed a UHV cryo-cooled sample system for in-situ studies of surfaces and interfaces. We have shown that the electronic symmetry at LSMO/SrTiO₃ (001) interface is different from the crystal symmetry [*J. Phys. Chem. C.*, **119**, 2300 (2019)]. We want to expand this capability to a broader range of materials such as SRO heterostructure that host magnetism, superconductivity and 2D electron liquid. Direct simultaneous access to the electronic and structural symmetry is our goal.

- **Optical control of magnetoelectric coupling and non- contact domain engineering**

Multiferroic magnetoelectric (MF-ME) materials, exhibit simultaneous ferroelectric and magnetic behaviors and permit control and switching of the magnetic order parameter via an electric field and electric polarization. Ferroelectric/multiferroic materials can also exhibit a photovoltaic effect, where control of the domain structure can modify the photocurrent of these materials. Therefore,

as the ferroelectric and magnetic domains are coupled in ME materials, illumination can modify both the ferroelectric and magnetic domain structures. This could lead to non-contact engineering of ferroelectric and magnetic domain structures and tuning of ME coupling by light. Using our new optical delivery system equipped on our TEM/STEM/EELS, we will explore the effect that light has on ferroelectric and magnetic domain structure and ME coupling of $\text{Bi}_{0.9}\text{La}_{0.1}\text{FeO}_3$ thin films (single-phase room temperature ME material). Complementary PFM scanning probe measurements under optical illumination will also be compared.

References:

- 1) Meng Meng, Zhen Wang, Saurabh Ghosh, Mohammad Saghayezhian, Rongying Jin, Yimei Zhu, Sokrates T. Pantelides, Jiandi Zhang, E.W. Plummer, and Hangwen Guo, *Interface-induced Magnetic Polar Metals in Correlated Oxides*, *Nature Commun.* **10**, 5248 (2019).
- 2) M. Saghayezhian, S.Z. Kouser, Z. Wang, H. Guo, R. Jin, Jiandi Zhang, Y. Zhu, S.T. Pantelides, E.W. Plummer, *Atomic-scale determination of spontaneous magnetic reversal in oxide heterostructures*, *Proceedings of the National Academy of Sciences*, **116**, 10309 (2019).
- 3) M. Saghayezhian, Zhen Wang, Hangwen Guo, Rongying Jin, Yimei Zhu, Jiandi Zhang, E. W. Plummer, *Exchange Bias and Inverted Hysteresis in Monolithic Oxide Films by Structural Gradient*, *Phys. Rev. Research* **1**, 033160 (2019).
- 4) Kun Zhao, Joel E. Taylor, Louis H. Haber, Jiandi Zhang, E. W. Plummer, and Mohammad Saghayezhian, *Probing the interfacial Symmetry Using Rotational Second-harmonic Generation in Oxide Heterostructures* *Journal Physical Chemistry C*, **123**, 23000 (2019).
- 5) Dhiren K. Pradhan, Shalini Kumari, Venkata S. Puli, Dillip K. Pradhan, Ashok Kumar, Sergei V. Kalinin, Rama K. Vasudevan, Ram S. Katiyar, Philip D. Rack, *Exploring Phase Transitions and Magnetoelectric Coupling of Epitaxial Asymmetric Multilayer Heterostructures* *Journal of Materials Chemistry C*, 2020, DOI:10.1039/D0TC02924F.

Publications (2019-2020, 10 most relevant):

1. "Visualizing quantum phenomena at complex oxide interfaces: An atomic view from scanning transmission electron microscopy," H. Guo, M. Saghayezhian, Z. Wang, Y. Zhu, Jiandi Zhang, and E.W. Plummer, *Frontiers of Physics*, **15**, 13401 (2020). [DOI.org/10.1007/s11467-019-0942-z](https://doi.org/10.1007/s11467-019-0942-z)
2. "High-Resolution Laser-Induced Graphene. Flexible Electronics Beyond the Visible Limit," M.G. Stanford, C.Z. Zheng, J.D. Fowlkes, I.N. Ivanov, P.D. Rack, and J.M. Tour, *ACS Appl. Materials & Interfaces* **11**, 11902 (2020). <https://doi.org/10.1021/acsami.0c01377>
3. "Probing the Interfacial Symmetry Using Rotational Second-Harmonic Generation in Oxide Heterostructures," K. Zhao, J.E. Taylor, L.H. Haber, Jiandi Zhang, E.W. Plummer, and M. Saghayezhian, *Journal of Physical Chemistry C*, **123**, 23000 (2019). [DOI.org/10.1021/acs.jpcc.9b05974](https://doi.org/10.1021/acs.jpcc.9b05974)
4. "Interface-induced magnetic polar metal phase in complex oxides," M. Meng, Z. Wang, A. Fathima, S. Ghosh, M. Saghayezhian, J. Taylor, R. Jin, Y. Zhu, S.T. Pantelides, Jiandi Zhang, E.W. Plummer, H. Guo, *Nature Communications*, **10**, 5248 (2019). [DOI.org/10.1038/s41467-019-13270-7](https://doi.org/10.1038/s41467-019-13270-7)
5. "Atomic-scale determination of spontaneous magnetic reversal in oxide heterostructures," M. Saghayezhian, S. Kouser, Z. Wang, H. Guo, R. Jin, Jiandi Zhang, Y. Zhu, S.T. Pantelides, and E.W. Plummer, *Proceedings of the National Academy of Sciences*, **116**, 10309 (2019). [DOI.org/10.1073/pnas.1819570116](https://doi.org/10.1073/pnas.1819570116)
6. "Exchange bias and inverted hysteresis in monolithic oxide films by structural gradient," M. Saghayezhian, Z. Wang, H. Guo, R. Jin, Y. Zhu, Jiandi Zhang, and E.W. Plummer, *Physical Review Research*, **1**, 33160 (2019). [DOI.org/10.1103/PhysRevResearch.1.033160](https://doi.org/10.1103/PhysRevResearch.1.033160)

7. "Surface and interface properties of $\text{La}_{2/3}\text{Sr}_{1/3}\text{MnO}_3$ thin films on SrTiO_3 (001)," L. Chen, Z. Wang, G. Wang, H. Guo, M. Saghayezhian, Z.L. Liao, Y. Zhu, E.W. Plummer, and Jiandi Zhang, *Phys. Rev. Materials* **3**, 044407 (2019). [DOI.org/10.1103/PhysRevMaterials.3.044407](https://doi.org/10.1103/PhysRevMaterials.3.044407)
8. "Rumpling and Enhanced Covalency at SrTiO_3 (001) Surface," M. Saghayezhian, R. Sani, S. Mojtaba, Jiandi Zhang, and E.W. Plummer *J. Phys. Chem. C* **123**, 8086 (2019). [DOI.org/10.1021/acs.jpcc.8b07452](https://doi.org/10.1021/acs.jpcc.8b07452)
9. "Pulsed Laser-Assisted Helium Ion Nanomachining of Monolayer Graphene-Direct-Write Kirigami Patterns," C. Zhang, O. Dyck, D.A. Garfinkel, M.G. Stanford, A.A. Belianinov, J.D. Fowlkes, and P.D. Rack, *Nanomaterials* **9**, 1394 (2019). <https://doi.org/10.3390/nano9101394>
10. "Low-Temperature Charging Dynamics of the Ionic Liquid and Its Gating Effect on $\text{FeSe}_{0.5}\text{Te}_{0.5}$ Superconducting Films," Cheng Zhang, Wei Zhao, Sheng Bi, C.M. Rouleau, J.D. Fowlkes, W.L. Boldman, Genda Gu, Qiang Li, Guang Feng, and P.D. Rack, *ACS Appl. Materials & Interfaces* **11**, 17979 (2019). <https://doi.org/10.1021/acsami.9b02373>

***AUTHOR INDEX
AND
PARTICIPANT LIST***

Bakaul, Saidur	46	Lev, Benjamin	133
Balents, Leon.....	185	Levchenko, Alex	199
Balke, Nina.....	3	Li, Jun.....	51
Balsara, Nitash	8	Li, Junjie.....	62
Batson, P. E.	69	Li, Lian.....	137
Biedron, Sandra.....	74	Liang, Zhixiu.....	51
Borisevich, Albina.....	3	Lupini, A. R.	26, 31, 41
Brahlek, Matt.....	36	Maksymovych, Petro	3, 36
Brennecka, Geoff	194	Manoharan, Hari C.....	18
Camden, Jon P.....	76	Martinez-Ramón, Manel	74
Chan, Emory	56	Masiello, David J.	76
Chandrasekhar, Venkat	81	McIntyre, Paul.....	13
Chen, Hanning	177	Meng, Y. Shirley	142
Chisholm, M. F.	31, 41	Meyhofer, Edgar	169
Chiu, Wah	13	Miao, Jianwei (John).....	146
Clark, Bryan K.	124	Minor, Andrew	8
Crozier, Peter A.....	86	Morgan, Dane.....	204
Cui, Yi.....	13	Narang, Prineha.....	26
Dionne, Jen.....	13	Nelson, C. T.	31, 41
Dumitrescu, Eugene	36	Nowack, Katja C.	151
Dyck, Ondrej.....	26	Orenstein, Joseph	18
Ercius, Peter	56	Oxley, M. P.	31, 41
Filler, Michael A.	91	Pan, Xiaoqing.....	155
Flannigan, David J.	96	Pantelides, Sokrates T.	160
Flatté, Michael E.	105, 115	Petford-Long, Amanda K.....	46
Fu, Xuewen	62	Phatak, Charudatta	46
Fuchs, Gregory D.....	101, 105	Prendergast, David	8
Garlow, Joseph.....	21	Ralph, Daniel C.....	105
Ginger, David S.....	110	Raschke, Markus B.	165
Goldhaber-Gordon, David.....	18	Reddy, Pramod.....	169
Gupta, Jay A.....	115	Ross, Frances M.	91
Halasz, Gabor.....	36	Ruan, Chong-Yu	173
Han, Myung-Geun.....	21	Solares, Santiago D.	177
Hong, Xia	120	Stemmer, Susanne.....	181, 185
Hua, Chengyun.....	36	Sutter, Eli	189
Huang, Pinshane Y.....	124	Sutter, Peter.....	189
Jarillo-Herrero, Pablo.....	215	Tan, Xiaoli.....	194
Jesse, Stephen.....	26	Tao, Jing.....	51, 62
Jiang, Xi	8	te Velthuis, Suzanne G. E.	46
Johnston-Halperin, Ezekiel	105	Tessmer, Stuart.....	199
Kalinin, S. V.....	31, 41	Van Harlingen, Dale.....	199
Kastner, Marc	18	Vasudevan, Rama.....	3
Kawakami, Roland.....	115	Voyles, Paul M.....	204
Konstantinova, Tatiana	62	Wang, Lin-Wang.....	56
Lai, Keji.....	128	Wilson, Stephen	185
Lawrie, Ben	36	Wu, Lijun	62

Wu, Weida.....209
Xin, Huolin.....213
Yacoby, Amir.....215
Yazdani, Ali219
Yoon, Mina26
Young, Andrea185
Zeljko, Ilija.....224
Zhang, Jiandi.....228
Zheng, Haimei.....56
Zhu, Yimei21, 62
Zuckermann, Ronald.....8

Name	Organization	Email Address
Bakaul, Saidur	Argonne National Laboratory	sbakaul@anl.gov
Balke, Nina	Oak Ridge National Laboratory	balken@ornl.gov
Balsara, Nitash	Lawrence Berkeley National Laboratory	nbalsara@berkeley.edu
Batson, Philip	Rutgers University	batson@physics.rutgers.edu
Biedron, Sandra	University of New Mexico	biedron@unm.edu
Bolin, Trudy	University of New Mexico	tbolin@unm.edu
Camden, Jon	University of Notre Dame	jon.camden@nd.edu
Chan, Emory	Lawrence Berkeley National Laboratory	EMChan@lbl.gov
Chandrasekhar, Venkat	Northwestern University	v-chandrasekhar@northwestern.edu
Chen, Julian	Los Alamos National Laboratory	chen_j@lanl.gov
Chi, Miaofang	Oak Ridge National Laboratory	chim@ornl.gov
Clark, Bryan	University of Illinois, Urbana Champaign	bkclark@illinois.edu
Crozier, Peter	Arizona State University	crozier@asu.edu
Cui, Yi	Stanford University/SLAC	yicui@stanford.edu
Ercius, Peter	Lawrence Berkeley National Laboratory	percus@lbl.gov
Fazio, Mariana	University of New Mexico	marianaafazio@gmail.com
Flannigan, David	University of Minnesota	flan0076@umn.edu
Flatté, Michael	University of Iowa	michael_flatte@mailaps.org
Fuchs, Gregory	Cornell University	gdf9@cornell.edu
Gersten, Bonnie	DOE-BES	bonnie.gersten@science.doe.gov
Ginger, David	University of Washington	dginger@uw.edu
Goldhaber-Gordon, David	Stanford University	goldhaber-gordon@stanford.edu
Gupta, Jay	The Ohio State University	gupta.208@osu.edu
Han, Myung-Geun	Brookhaven National Laboratory	mghan@bnl.gov
Hong, Xia	University of Nebraska, Lincoln	xia.hong@unl.edu
Horwitz, Jim	DOE	james.horwitz@science.doe.gov
Hua, Chengyun	Oak Ridge National Laboratory	huac@ornl.gov
Huang, Pinshane	University of Illinois, Urbana Champaign	pyhuang@illinois.edu
Hurd, Alan	Los Alamos National Laboratory	ajhurd@lanl.gov
Jesse, Stephen	Oak Ridge National Laboratory	sjesse@ornl.gov
Jiang, Xi	Lawrence Berkeley National Laboratory	xijiang@lbl.gov
Johnston-Halperin, Ezekiel	The Ohio State University	johnston-halperin.1@osu.edu
Kalinin, Sergei	Oak Ridge National Laboratory	sergei2@ornl.gov
Kastner, Marc	Stanford/SLAC	mkastner@mit.edu
Kawakami, Roland	The Ohio State University	kawakami.15@osu.edu
Kerch, Helen	USDOE	helen.kerch@science.doe.gov
Kortan, Refik	DOE-BES	refik.kortan@science.doe.gov
Lai, Keji	University of Texas at Austin	kejilai@physics.utexas.edu
Lapano, Jason	Oak Ridge National Laboratory	lapanojm@ornl.gov
Lawrie, Ben	Oak Ridge National Laboratory	lawriebj@ornl.gov
Lee, Ho Nyung	Oak Ridge National Laboratory	hnlee@ornl.gov
Lev, Benjamin	Stanford University	benlev@stanford.edu

Levchenko, Alex	University of Wisconsin, Madison	levchenko@physics.wisc.edu
Li, Yanbin	Stanford University	yanbinli@stanford.edu
Li, Junjie	Brookhaven National Laboratory	jli@bnl.gov
Li, Lian	West Virginia University	lian.li@mail.wvu.edu
Lupini, Andrew	Oak Ridge National Laboratory	arl1000@ornl.gov
Maksymovych, Petro	Oak Ridge National Laboratory	maksymovychp@ornl.gov
Manoharan, Hari	Stanford University / SLAC / SIMES	manoharan@stanford.edu
Maracas, George	DOE-BES	george.maracas@science.doe.gov
Masiello, David	University of Washington	masiello@uw.edu
McIntyre, Paul	SLAC National Accelerator Laboratory	pcm1@slac.stanford.edu
Meng, Shirley	University of California, San Diego	shmeng@ucsd.edu
Meyhofer, Edgar	University of Michigan	meyhofer@umich.edu
Miao, John	University of California, Los Angeles	miao@physics.ucla.edu
Minor, Andrew	UC Berkeley and LBNL	aminor@lbl.gov
Nowack, Katja	Cornell University	kcn34@cornell.edu
Orenstein, Joseph	University of California, Berkeley	jworenstein@lbl.gov
Oxley, Mark	Oak Ridge National Laboratory	oxleyp@ornl.gov
Pai, Yun-Yi	Oak Ridge National Laboratory	yunyip@ornl.gov
Pan, Xiaoqing	University of California, Irvine	xiaoqin@uci.edu
Pantelides, Sokrates	Vanderbilt University	pantelides@vanderbilt.edu
Pasupathy, Abhay	Brookhaven National Laboratory	apn2108@columbia.edu
Pechan, Michael (Mick)	DOE-BES	michael.pechan@science.doe.gov
Petford-Long, Amanda	Argonne National Laboratory	petford.long@anl.gov
Phatak, Charudatta	Argonne National Laboratory	cd@anl.gov
Raschke, Markus	University of Colorado	markus.raschke@colorado.edu
Reddy, Pramod	University of Michigan	pramodr@umich.edu
Reigelsperger, Lucas	ORISE	lucas.reigelsperger@orau.org
Rohnke, Brandon	DOE-BES	Brandon.Rohnke@science.doe.gov
Ross, Frances	Massachusetts Institute of Technology	fmross@mit.edu
Ruan, Chong-Yu	Michigan State University	ruanc@msu.edu
Schwartz, Andy	DOE	Andrew.Schwartz@science.doe.gov
Sefat, Athena	DOE-BES	athena.sefat@science.doe.gov
Sennett, Michael	DOE-BES	michael.sennett@science.doe.gov
Settersten, Tom	DOE-BES	thomas.settersten@science.doe.gov
Solares, Santiago	The George Washington University	ssolares@gwu.edu
Stemmer, Susanne	University of California, Santa Barbara	stemmer@mrl.ucsb.edu
Sutter, Peter	University of Nebraska, Lincoln	psutter@unl.edu
Sutter, Eli	University of Nebraska, Lincoln	esutter@unl.edu
Tao, Jing	Brookhaven National Laboratory	jtao@bnl.gov
te Velthuis, Suzanne	Argonne National Laboratory	tevelthuis@anl.gov
Tessmer, Stuart	Michigan State University	tessmer@msu.edu
Thiyagarajan, Thiyaga	DOE-BES	p.thiyagarajan@science.doe.gov
Tian, Xinchun	Iowa State University	xctian@iastate.edu

Van Harlingen, Dale	University of Illinois, Urbana-Champaign	dvh@illinois.edu
Vasudevan, Rama	Oak Ridge National Laboratory	vasudevanrk@ornl.gov
Vetrano, John	DOE-BES	john.vetrano@science.doe.gov
Voyles, Paul	University of Wisconsin, Madison	paul.voyles@wisc.edu
Wang, Lin-Wang	Lawrence Berkeley National Laboratory	lwwang@lbl.gov
Wilson, Lane	DOE	Lane.Wilson@science.doe.gov
Wu, Weida	Rutgers University	wdwu@physics.rutgers.edu
Wu, Lijun	Brookhaven National Laboratory	ljwu@bnl.gov
Xin, Huolin	University of California, Irvine	huolinx@uci.edu
Yacoby, Amir	Harvard University	yacoby@g.harvard.edu
Yazdani, Ali	Princeton University	yazdani@princeton.edu
Zeljko, Ilija	Boston College	ilija.zeljko@bc.edu
Zhang, Jiandi	Louisiana State University	jiandiz@lsu.edu
Zhang, Minghao	University of California, San Diego	miz016@eng.ucsd.edu
Zheng, Haimei	Lawrence Berkeley National Laboratory	hmzheng@lbl.gov
Zhou, Lin	Ames Laboratory	linzhou@ameslab.gov
Zhu, Jane	DOE-BES	jane.zhu@science.doe.gov
Zhu, Yimei	Brookhaven National Laboratory	zhu@bnl.gov